

# DEVELOPMENT OF A PEDESTRIAN LEGFORM TO ASSESS SENSORS USED IN ACTIVE PEDESTRIAN PROTECTION SYSTEMS

**James Manning**

TRL

United Kingdom

Paper Number 07-0271

## ABSTRACT

This paper reports on the development of a new legform to test contact sensors of active safety systems that could be used to deploy pedestrian protection systems. To test the systems accurately a test tool is required with properties that are as close as possible to human responses. Current legforms were not designed to test sensors, but were designed to assess passive protection by imparting a concentrated force to selected parts of the vehicle. Due to the characteristics of the legform it is believed that the bumper sensor threshold could be set too high, causing a late deployment or even preventing the active system from deploying. The possibility of serious or life threatening head injuries occurring could be increased if the active system does not deploy as intended.

To achieve a better force distribution on the bumper sensors, the revised impactor needs to be as biofidelic as possible. Data on the mechanical properties of human bone and flesh have been researched and materials selected to provide the most realistic response during a vehicle to pedestrian impact. The purpose of the impactor is to assess contact sensor technology that could be used in active safety pedestrian systems to distinguish an impact between a vehicle and a pedestrian and a vehicle and another object. The paper reviews the legform design specification in terms of its requirements and biofidelity data. Through finite element modelling, the use and limits of the test tool with regard to bumper reference height and the use of an upper body mass are discussed.

## INTRODUCTION

With the advent of active safety systems, vehicles are now being fitted with devices to improve the protection offered to pedestrians and other vulnerable road users should they be involved in an impact with a vehicle. These active systems can take the form of pop-up bonnets or A-pillar airbags for example. The method of detection of the pedestrian or other vulnerable road user can be by contact sensors, pressure sensors, infra-red sensors (to name just a few), or a combination of these. The detection systems are usually fitted into the bumper region of the vehicle as this is generally the first

point of contact and thus provides the greatest time to determine if deployment should occur or not.

The design and use of active safety pedestrian systems has come about through the requirement for greater levels of pedestrian protection and thus the requirement for pedestrian 'friendly' vehicles. It is hoped that with these systems the number of pedestrians that are killed or seriously injured will reduce. However, to develop and to test the effective deployment of these devices it is important that the properties of the test tool are closely matched to those of the human being. This will provide the most realistic response for the impactor and will provide a more realistic loading characteristic of the bumper and the detection system.

## IMPACTOR DEVELOPMENT

### Age Selection

Stats 19 pedestrian accident statistics for a period of five years (1997-2001 inclusive) were analysed to highlight which age group was at the highest risk. The Stats19 data displays the information in terms of age of the casualty. It was decided that the statistics could be divided into two main group areas, these being Child and Adult. The child group included the casualties of 0-17 years old and the adult group included casualties of 18-99 years old.

If all severities of injury and both sexes are considered then the number of child casualties is greater than the number adult casualties by less than 1% with approximately 10,026 children and 9,937 adults injured on average per annum (Figure 1). However, this includes slight injuries and although these are of concern the pedestrians that require greatest consideration are the killed and seriously injured casualties. If the total casualties are split into fatal, serious and slight injury categories then the data shows that the adult group makes up approximately 59% of the killed and seriously injured pedestrians. The data suggests that the adult group is an appropriate focus for the development of the new test tool. If the data statistics are split between male and female sexes in the adult category then the males represent approximately 61% of the adult population for the killed and seriously injured pedestrians. The

Stats19 data analysis would suggest that an adult male pedestrian is at most risk of being killed or seriously injured by being involved in an impact with a vehicle.

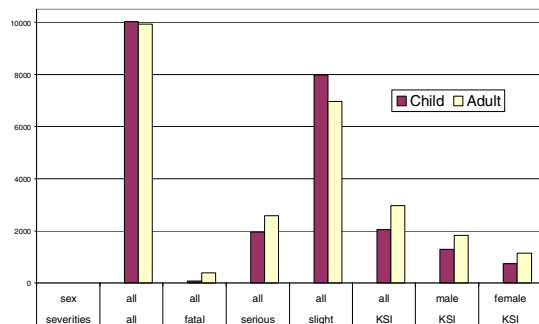


**Figure 1. Pedestrian accidents average per annum for child and adult groups (1997-2001 inclusive).**

The adult group was selected as the most common. Although the group had been determined the respective 'age' of the impactor had not. This was necessary as it would be used to determine the material properties of the bone. It is known that bone properties reach a peak and then deteriorate with increasing age. Consequently, it was believed that if the properties of the impactor bone were set to those of an elderly person the impactor could be too weak and result in otherwise pedestrian-friendly vehicles being inappropriately assessed. Similarly if the materials were set to those of a young adult (18-20 year old) the bone could be at its strongest and would therefore not truly represent the population. It was decided to design the impactor with the biomechanical properties of a 50-59 year old male. This age bracket will provide a middle position between the old and the young.

### Size selection

Current pedestrian legform impactors are representative of a 50<sup>th</sup> percentile human leg. A concern is that the height of the 50<sup>th</sup> percentile male may not represent the worst case impact configuration in regard to testing the deployment of active safety systems. For example, child or small adult pedestrians may impart a smaller load upon the sensors and the system may not register an impact with a human and may not deploy. If shorter pedestrians and consequently shorter legforms were used then it is likely that an upper body mass would be required to provide a realistic human body response. It is also likely that the pelvis of the human would contact with the bumper or bonnet leading edge of the vehicle.

Alternatively, the worst case may be a tall elderly person, with longer and potentially weaker limbs –

the breaking load required to cause fracture in a lateral impact might be less than for other sized pedestrians. A lower breaking load would suggest that a lower force signal would be recorded by the sensors. There is a general debate as to the 'true worst case'; however, it is believed that protection should be afforded to all potential impact casualties. The initial development of the legform concentrated on a 50<sup>th</sup> percentile male with the intention that a larger family of the impactors be developed to cover all relevant casualty sizes. The 50<sup>th</sup> percentile provides a good representation of the population and thus, although it may not be classified as the worst case size, the largest proportion of the pedestrian population will be covered by this size. The intention to develop a 'family' of different sizes would also prevent optimisation of active safety systems to protect only one size of pedestrian.

### Finite Element Modelling

With the development of any pedestrian impactor legform it is important to consider the requirement of an upper body mass for the impactor. In actual impacts the mass of the thorax of the human will contribute to the direction of travel. In an impactor the upper body mass may not be necessary for impacts where the vehicle bonnet leading edge does not contact the upper region and pelvis of the legform or where the vehicle does not impact above the centre of gravity of the leg. Impacting above the centre of gravity of the leg would cause the legform to be overridden, which is not believed to be realistic. In impacts with humans, if the impact is above the centre of gravity of the leg but below the centre of gravity of the human, the upper body mass will still cause the body to 'wrap-around' the vehicle.

For children and smaller adults it is possible that the pelvis region of the body will interact with the vehicle bumper or bonnet leading edge. It was decided that the legform would be based on a 50<sup>th</sup> percentile male, therefore it was important to assess whether the impactor would require an upper body mass for impacts with vehicles that could potentially be fitted with active safety systems.

A finite element modelling (FE) study was performed and two models were set-up in the LS-DYNA code. The first model featured an adapted Hybrid III dummy and the second model consisted of the right leg of the Hybrid III dummy model; both were placed in a standing position and put in front of a vehicle model. The Hybrid III 50<sup>th</sup> percentile model is an occupant dummy and consequently is designed to be used in a seated position. It was necessary to modify the model to allow it be orientated in a standing position. The

standing model is shown in Figure 2. The knee, ankle and hip joints were rotated to provide a standing dummy. The right leg was straight with the left leg rotated at the hip to provide a realistic walking action with the foot off the ground. It was considered unlikely that the pedestrian would be struck whilst having both feet on the ground and both legs straight. Friction between the pedestrian's shoe and the ground was modelled using a spotweld. (The term spotweld is used in FE modelling and enables the user to define a point to have a pre-determined failure load, in this model once the predetermined load was reached the foot and legform would be free to move). The right arm of the dummy model was placed in a raised position to remove any interference between the arm and the bumper or bonnet leading edge.

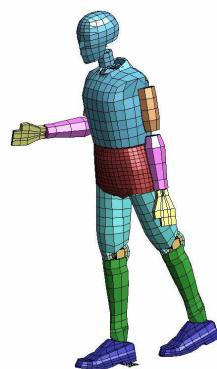


**Figure 2. The modified Hybrid III 50th percentile 'pedestrian' dummy model.**

To create a separate legform model that could be used to evaluate the need for an upper body mass the modified Hybrid III 'pedestrian' model was further modified. All sections except the first struck leg (right leg) were deleted from the model (Figure 3). The friction generated by the spotweld in the 'pedestrian' model was removed.

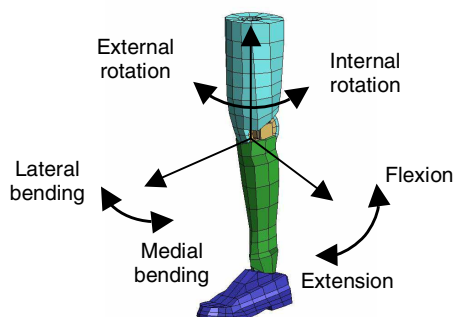


**Figure 3. The legform model from the modified Hybrid III 'pedestrian' dummy model.**

To replicate the knee joint and to enable it to respond in a humanlike manner the knee was

remodelled. The knee was modelled with a spherical joint that consisted of three degrees of freedom. For the lateral and medial directions the knee joint was set to have a plastic response with a stiffness of 200Nm. The lower leg is able to move further in flexion than in extension thus the knee joint was set to have 100 degrees of motion in flexion and 30 degrees in extension. The neutral (standing position) was set at zero degrees.

The 'pedestrian' model and the legform model were impacted by a model of a generic pedestrian-friendly vehicle. To model the vehicle, rigid steel plates were used for the bumper and bonnet with low density foam mounted on the surface. The chassis of the vehicle was represented by rigid plates and springs. These were attached to the rear of the bonnet and the bumper and were given a stiffness of 5kN/m to represent a generic stiffness of a pedestrian-friendly vehicle. The motion of the plates was constrained in all directions except for the direction of travel of the vehicle. Additional mass was added to the rigid plates and distributed to represent the mass of a real vehicle. The bonnet leading edge was inclined at 50 degrees to the horizontal and the bonnet 15 degrees to the horizontal. The vehicle was given an initial velocity of 11.1m/s.

To assess the legform impactor capabilities it was necessary to model the impacts with vehicles of differing bonnet leading edge and bumper top heights. A small study of the heights of a range of vehicles was performed. Table 1 shows the test matrix that was defined for each of the models to provide an assessment of the range of vehicles available.

**Table 1.**

**Matrix of vehicle dimensions used in the models**

| Height (mm)         |                 |                    |
|---------------------|-----------------|--------------------|
| Bonnet leading edge | Bumper top edge | Bumper bottom edge |
| 1000                | 800             | 500                |
| 1000                | 700             | 400                |
| 900                 | 650             | 350                |
| 850                 | 600             | 300                |
| 800                 | 550             | 250                |
| 700                 | 500             | 200                |
| 700                 | 450             | 150                |
| Undefined           | 400             | 100                |

To simulate off-road vehicles the bumper top edge height was set at heights of 700 and 800mm above ground. For the sports car range a bumper top height was set at 400mm with no bonnet contact

defined. The bumper lead was set at 100mm in all model cases.

The two models are shown in Figure 4 immediately prior to impact.

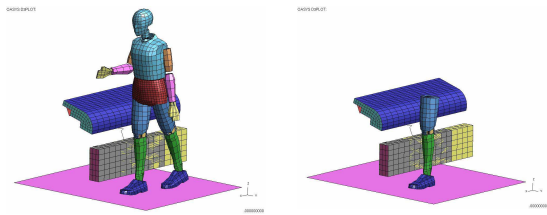


**Figure 4. The ‘pedestrian’ and legform models immediately prior to impact.**

The results of the model runs showed that the impact in the region of the legs was essentially complete by 25ms. After this time the pedestrian had ‘wrapped around’ the vehicle and contacted the bonnet top. It was found that good correlation occurred – in terms of legform kinematics and force on the bumper surface – between the ‘pedestrian’ and legform models for bumper top heights between 450 and 650mm (Figure 5).

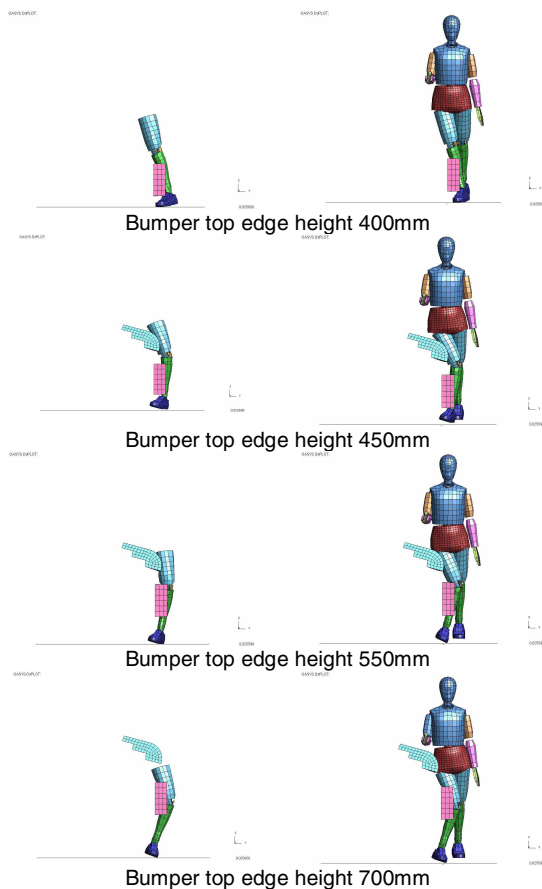


**Figure 5. The legform and ‘pedestrian’ model animations with different bumper top edge heights.**

Bumper top edge heights below 450mm exhibited rotation in the legform model on impact with the bumper. The rotation resulted in the anterior surface of the legform contacting the vehicle model. This was not seen in the ‘pedestrian’ model and was considered to be an unrealistic representation. At bumper top heights greater than 650mm it was noted that the bonnet top was impacting directly with the pelvis of the ‘pedestrian’ model and thus passed directly over the top of the legform model. This is again believed to be unrealistic; at heights such as these the impactor is likely to require an upper body mass to realistically represent impacts with humans.

Although the kinematics of the legform and the ‘pedestrian’ model differed significantly at bumper top edge heights below 450mm and heights above 650mm the model kinematics were considered good between these values. A slight additional rotation about the z-axis of the leg was noted to occur in the legform model that was not noted in the ‘pedestrian’ model. This was believed to be due to the foot altering the inertial properties of the leg due to it not being restrained from rotation at the pelvis. To reduce the possible rotation in the actual legform it was decided that the front section of the foot be removed and the weight added to the heel. The correct legform mass and inertia will be retained without the foot causing it to rotate.

The study into the impact performance of the legform model and the ‘pedestrian’ model indicated that physical testing with a single 50<sup>th</sup> percentile legform impactor without an upper body mass would be appropriate with car front profiles that have bumper top edge heights between 450mm and 650mm. Although the modelling suggests that sports cars (whose bumper top edge heights may be below 450mm and are more likely to be fitted with active systems) may not be able to be tested with the legform, the modelling needs to be verified and validated with physical testing.

### **Biomechanical Property Research**

**Bone Property Research** - To provide a definitive value for the biomechanical properties of human flesh and bone that would cover all sections of the population would be impossible. It is known that the bone properties, for example, change with increasing age. Peak bone strength is reached at an age of approximately 20-29 years, after which the bone strength will gradually reduce. Yamada [1] quotes that the strength of the femur long bone will deteriorate by approximately 17% by the age of 70-79 years from its peak value. The Yamada data shows that the strength of the femur long bones in the selected age group of 50-59 years will be

approximately 8% less than the 20-29 year old group.

In addition to the bone properties varying as the person grows older, it is also reported that the bone properties can vary between people of the same age. Environmental conditions, diet, fitness levels and illnesses are all contributory factors that will affect the strength of the human bones and will contribute to the bones being different for each individual. To provide data that can be used to estimate the strength of human long bones the average values for each age group can be used.

There has been a large amount of research completed into the strength of the human bones. However, the method of testing these bones has often been performed slightly differently in terms of how the specimen is treated prior to testing (whether it is fresh, dried, previously frozen etc) and whether it has been tested dynamically or quasi-statically. Also, the section and direction of the bone tested will affect the output of the results. It was not possible within the scope of this development project to conduct biomechanical testing of human long bones. The research data previously collected together by Yamada [1] has been widely used and acknowledged and for these reasons it was considered to be suitable for use in developing and determining the bone strength that would be used in the legform. One aspect that distinguishes the Yamada data is that all of the specimens used in the research were fresh and unembalmed.

It can be assumed that most impacts between pedestrians and vehicles result in a perpendicular loading to the long bones of the human leg. Due to the perpendicular loading direction the bending properties of the bone material are considered. Yamada reports on the bending breaking load of intact specimens of the femur and tibia that are supported under their ends and loaded with a compression tester with a head of 20mm diameter. The results from the bending breaking load tests performed by Yamada are shown in Table 2.

**Table 2.**  
**Bending breaking load (kg) of human wet long bones [1]**

| Bone   | Age Group |         |         |         |         | Adult Average |
|--------|-----------|---------|---------|---------|---------|---------------|
|        | 20-39yr   | 40-49yr | 50-59yr | 60-69yr | 70-89yr |               |
| Femur  | 277±11    | 252±5   | 240±9   | 238±6   | 218±11  | 250           |
| Tibia  | 296±11    | 257±11  | 248±5   | 244±9   | 234±9   | 262           |
| Fibula | 45±2      | 41±4    | 40±3    | 38±2    | 34±2    | 40            |

The data shown in Table 2 is for long bones tested in the anteroposterior direction. Most impacts between vehicles and pedestrians are likely to occur in the lateral direction. However, Yamada noted that “...there is no significant difference in the ultimate strength or in the bending breaking load between the anteroposterior and the lateromedial directions”. The properties listed in Table 2 were therefore used for determining the material specification for lateromedial loading.

Yamada also reports data for the fibula, which is the bone adjacent to the tibia. It is possible to stand without the fibula being present as it provides little support in the standing position. Its main role is to provide support as the leg twists; without a fibula this motion would not be possible. The bending load required to break the fibula is approximately six times smaller than that of the tibia; the ultimate deflection of the fibula is approximately 37% greater than that of the tibia (Table 3). The fibula can therefore be said to have little contributory effect on the performance of the legform in bending due to it having a larger deflection and significantly lower bending breaking load than the stronger tibia. It was decided that the fibula would not be included in the design of the legform.

**Table 3.**  
**Ultimate deflection (mm) of human wet long bones, approximated for lateromedial direction**

| Bone   | Age Group |         |         |         |         | Adult Average |
|--------|-----------|---------|---------|---------|---------|---------------|
|        | 20-39yr   | 40-49yr | 50-59yr | 60-69yr | 70-89yr |               |
| Femur  | 16.0      | 14.8    | 13.8    | 13.3    | 12.5    | 14.4          |
| Tibia  | 13.0      | 12.0    | 11.2    | 10.9    | 10.1    | 11.7          |
| Fibula | 21.1      | 19.0    | 18.1    | 17.3    | 15.3    | 18.6          |

The data for the ultimate deflection of the human wet long bones was originally provided by Yamada in the anteroposterior direction. Yamada found that the ultimate deflection in the anteroposterior direction was approximately 30% less than the ultimate deflection in the lateromedial direction for the tibia. The actual difference was not recorded for the femur and fibula but was stated to be similar to the tibia conversion factor. Table 3 shows the ultimate deflection of the human wet long bones adjusted from the anteroposterior direction to the lateromedial direction.

The properties highlighted in Tables 2 and 3 were used in selecting the material that would be used for the bone sections of the legform. The material selected for the bones is an epoxy filled glass fibre cylinder, which is calculated to have properties

similar to the required values discussed above. Both the femur and tibia will be manufactured from the same type of material. To achieve the different performance criteria of the femur and tibia the internal dimensions of the material will be altered. In addition to good stiffness performance, the failure mode of the material is known to be similar to that of bone with little deflection and creep before fracture occurs.

**Flesh Property Research** - The lower limb of the human consists of the femur, tibia, fibula, ankle and foot bones, numerous muscles, tendons, nerves, veins and fat etc. A legform with individual muscles and tendons would result in a complex device. For the purpose of this legform it was decided that individual muscles and tendons would not be required. For the development of the test tool the 'flesh' will consequently consist of all parts of the human leg apart from the bones and the skin. The bones and the skin are considered separately.

It was found that the biomechanical properties of bone altered with age and it was found that the properties are different even between people of similar ages. It was considered that this would also be the case for the flesh. If the human that was impacted by a vehicle was fit and healthy it is likely that the muscles would be stronger and would need to be represented by a potentially more dense material. On the other hand should the human that is being impacted be of a relatively weak build they will have less muscle mass and consequently the material required to represent the flesh would need to be less dense. In this instance the term dense refers to the amount of muscle compared to the amount of fat and vice versa and not the material property.

Research has previously been performed on the density of human fat and muscle. Human fat is known as adipose tissue and has an approximate density of  $0.92\text{g/cm}^3$  (Table 4). The density of muscle is found to have a greater range than that of the adipose tissue. It is assumed that the difference could be due to the assessment methods and the specimens tested could well have been obtained from people of differing levels of fitness. The density of was found to be approximately  $1.08\text{g/cm}^3$  (Table 4). As the human leg consists of a combination of muscle and adipose tissue the required density of the legform will be within the range of  $0.9\text{g/cm}^3$  and  $1.08\text{g/cm}^3$ . Cross-sections of the human leg show that the majority of the soft tissue is muscle, rather than adipose tissue. For this reason the material for the flesh was selected with a density towards the higher end of the range (approximately  $1.03\text{g/cm}^3 - 1.06\text{g/cm}^3$ ).

**Table 4.**

**Comparison of the densities of adipose tissue and muscle**

| Source         | Adipose Tissue<br>(Extracted human fat) | Muscle/rest of body          |
|----------------|---|------------------------------|
| Ref [2]        | 0.940                                   | 1.082                        |
| Ref [3]        | 0.918                                   | 1.100                        |
| Ref [4]        | 0.948                                   | 1.090                        |
| Ref [5]        | 0.901                                   | 1.061                        |
| Ref [6]        | 0.900                                   | 1.100                        |
| Ref [7]        | 0.900                                   | 1.060                        |
| <b>Average</b> | <b>0.918g/cm<sup>3</sup></b>            | <b>1.082g/cm<sup>3</sup></b> |

For pedestrian impacts it is assumed that the person is impacted whilst the weight is directly above one straight leg (on the struck side) with the non-struck leg off the ground. Immediately prior to the impact between a vehicle and a pedestrian it is assumed that the majority of pedestrians will become aware of the impending impact. The awareness of the impending impact is likely to cause the pedestrian to tense the muscles in the leg due to the shock of an impact occurring. In the few impacts where the pedestrian is not aware of the impending impact some of the leg muscles will be tensed anyway as part of the natural walking or running motion. Consequently the material selected for the flesh of the legform will represent the human leg in its tensed state. It was considered necessary to evaluate the hardness of human flesh in the tensed state as this would contribute to achieving a material with humanlike responses.

To measure the hardness of flesh, people were selected that were approximately 50<sup>th</sup> percentile in height and who were in a good level of health and fitness. A handheld Instron Shore 'A' Durometer (Figure 6) was used to measure the flesh hardness.



**Figure 6. The Instron Shore S1 Durometer hardness tester with the Shore 'A' indenter.**

The hardness value is determined by the level of penetration of the indenter into the material. If the indenter does not penetrate the material the recorded value will be 100 and if the indenter penetrates the material completely the recorded hardness value will be 0. The Shore 'A' scale was used as this is used to measure the hardness of soft rubbers and plastics.

Each person was tested with the Durometer hardness tester a number of times to provide an average value. Repeating the tests reduced the possibility of anomalous results through the user applying different levels of pressure when using the durometer. Figure 7 shows the procedure used to measure the hardness the legs of the volunteers.



**Figure 7. The Shore Durometer hardness tester in use on one of the volunteers.**

The hardness of the leg was assessed in both the relaxed and tensed states. Although the whole leg was tested (624 points) on one of the volunteers, the calf and thigh muscles were considered to provide the most relevant results. Along the front of the tibia (shin region) the results would be influenced by the limited amount of flesh between the indenter and the bone.

A summary of the results of the hardness testing of the calf and thigh muscles of the volunteers in both the relaxed and tensed states is shown in Table 5. The hardness was found to be approximately 10A for the muscles in the relaxed state compared to approximately 14A for the muscles in the tensed state.

**Table 5.**

**A summary of the results of the Durometer hardness testing of the volunteers (Shore ‘A’)**

| Person      | Relaxed |       | Tensed |       |
|-------------|---------|-------|--------|-------|
|             | Calf    | Thigh | Calf   | Thigh |
| Volunteer 1 | 9.64    | 10.04 | 15.17  | 15.17 |
| Volunteer 2 | 8.89    | 15.09 | 14.26  | 16.90 |
| Volunteer 3 | 11.98   | 9.13  | 12.89  | 13.69 |
| Volunteer 4 | 9.48    | 9.12  | 11.63  | 13.28 |
| Average     | 10.42   |       | 14.13  |       |

The front of the tibia of volunteer 1 was tested to investigate what influence the bone being close to the surface had on the hardness value. It was found that the hardness in this region increased to approximately 20 – 25A, but this would not be representative of the hardness of the lateral aspect

of the lower limb, which is the most likely bumper contact point in a pedestrian impact. As a result the material specification for the flesh was between 14 and 15 on the Shore ‘A’ scale, along with a density between 1.03g/cm<sup>3</sup> – 1.06g/cm<sup>3</sup>.

Based on the results of the hardness testing and the analysis of the density of the flesh (muscles and adipose tissue) many flesh materials were considered, including soft rubbers and different composition polyurethanes. Figure 8 shows a selection of the materials that have been considered for this application.



**Figure 8. A selection of some of the materials considered for use in making the flesh.**

Finally a polyurethane material was selected for the flesh that has a density in the required range and a hardness of approximately 15A on the Shore ‘A’ scale.

**Skin Property Research** – The skin of the legform impactor will have three roles.

- To act in compression as the skin of the human would
- To provide protection to the legform as it impacts with the vehicle to make it more robust, and
- The skin layer will be sufficiently thick to represent the clothing that the pedestrians will be wearing.

The human skin layer ranges in thickness from 0.5-4.0mm depending upon the location [8]. The skin layer selected for the legform is a neoprene material that has a thickness of approximately 3mm.

**Knee Ligament Research** - The knee consists of many tendons and ligaments. Depending upon whether the leg is in its straight position or in its bent position some of the ligaments will be relaxed and some will be tense. If the knee ligaments are damaged, for example in an impact with a vehicle, then the casualty can have problems walking in the future. Ligament damage can lead to many disabilities and can require a long time for healing and rehabilitation [9].

Similarly to the bone and flesh material, the strength of the knee ligaments has been the subject of considerable debate. The ligaments in the current EEVC WG17 legform impactor have an approximate stiffness of 400-500Nm. It has been discussed that this stiffness is higher than the ligaments of the average person and it has been suggested that the stiffness of the ligaments should be nearer to 200Nm. It is unclear whether this stiffness takes into consideration the effects of muscle tension. It was therefore decided that a ligament of approximately 250-300Nm would be used for the initial legform impactor. This range is above that used in the FE modelling, however, once bending ligament stiffness has been agreed by biomechanical groups, it will be possible to adjust the stiffness to the required limit.

The initial design of the ligament is shown in Figure 9. The rounded design allows impacts from different angles to be assessed. The stiffness of the ligament would be altered to represent the stiffness of the human ligaments in the different impact configurations. This allows the active safety systems to be tested in many different impact configurations. For example, the impact to the human could be from the rear where the stiffness in the ligaments would be different to the stiffness in the ligaments if the impact was from the front.



**Figure 9.** The shape of the ligament will provide an opportunity to tests at different impact angles.

### Anthropometric Measurements

It was decided that the legform impactor would represent a 50<sup>th</sup> percentile male. The measurements for a 50<sup>th</sup> percentile male were obtained from anthropometric data. For the development of ATD's that are used in vehicles the UMTRI anthropometric data is used. However, the UMTRI measurements are taken with a seated occupant. The leg shape of a seated occupant is different to that of a pedestrian hence the Adultdata [10] source was used.

A volunteer was measured and the results compared with the 50<sup>th</sup> percentile anthropometric data. It was found that the tibia and knee of the volunteer were within approximately 2-3mm of the measurements for the 50<sup>th</sup> percentile male. The

femur length of the volunteer was found to be slightly longer than that of the 50<sup>th</sup> percentile male; however, this was not considered to cause concern as the femur section of the impactor would be moulded to the length applicable to position the hip end for mounting to the propulsion system. The anthropometric data was also used to compare the circumference of the volunteer and the 50<sup>th</sup> percentile male. The human leg is not a perfect circle but in order to evaluate the approximate differences between the radiuses of the leg measurements the legs were assumed to be of circular cross-section.

Table 6 shows a comparison of the measurements of the circumference of the volunteer's leg and the mean adult data.

It was found that the radius of the leg of the volunteer was approximately 1.3mm smaller than the approximate radius of a 50<sup>th</sup> percentile male. As the leg of the volunteer was used it was necessary to increase the approximate radius of the legform. The skin layer selected for the legform has a thickness of approximately 3mm. This skin layer will increase the radius of the legform and will also provide a small allowance for the thickness of the clothing that the pedestrian would be wearing.

**Table 6.**

**Comparative measurements for the circumference of the 50th percentile male data and the volunteer (mm)**

| Position     | Adult mean data | Approx Radius | Volunteer data | Approx Radius | Difference |
|--------------|-----------------|---------------|----------------|---------------|------------|
| Thigh top    | 590.6           | 94.01         | 578.0          | 92.01         | -2.01      |
| Thigh bottom | 375.0           | 59.69         | 379.0          | 60.33         | 0.64       |
| Knee crease  | 382.2           | 60.84         | 365.0          | 58.10         | -2.74      |
| Knee cap     | 385.0           | 61.29         | 373.0          | 59.38         | -1.91      |
| Knee below   | 360.3           | 57.35         | 335.0          | 53.33         | -4.03      |
| Calf max     | 380.8           | 60.62         | 374.0          | 59.54         | -1.08      |
| Talus        | 244.4           | 38.90         | 250.0          | 39.80         | 0.89       |
| Above talus  | 226.0           | 35.98         | 224.0          | 35.66         | -0.32      |
| Average      |                 |               |                |               | -1.32      |

### Position of the Bone

The position of the bone within the legform is important to provide a realistic human response. During an impact between a vehicle and a human leg the vehicle bumper will compress the flesh (muscles etc.) and then contact the femur or tibia bones. If the bone is incorrectly positioned in the legform, as the vehicle compresses the flesh material it will contact the bone earlier or possibly later than would occur in impacts with pedestrians. To investigate the position of the bones within the

leg, cross-sections of the leg were sourced from the Visible Human Project® [11], [12].

The Visible Human Project® consists of detailed cross-sections of a male and female. The male was transversely sliced in 1mm slices with a total of approximately 1871 slices. The male cadaver was sliced with the foot placed in a downwards position. The slice that represents the base of the heel is approximately slice 1790. This translates to an approximate subject height of 1790mm, which is greater than a 50<sup>th</sup> percentile male. However, it was assumed that the bone position relative to the outer layer of skin would be approximately the same for each human subject. Therefore, by measuring the bone position of the Visible Human cadaver and applying a correction factor to take into account for the differences in cross-sectional width and depth of the leg (between 50<sup>th</sup> percentile male and the Visible Human cadaver) the bone could be positioned in the 50<sup>th</sup> percentile male legform impactor.

Measurements of the cross-sectional position of the bone in the leg of the Visible Human male cadaver were taken at 20mm intervals along the length of the leg. The cross-sectional images were downloaded and opened in photo-editing software. The pixel number relative to the outer edge of the flesh was recorded and the corresponding point on the outer surface of the bone. The pixel numbers were then adjusted to represent a dimension calculated from the number of pixels/cm. The measurements were recorded for the front of the leg flesh to the front of the bone and similarly for the rear of the leg. The cross-section dimensions were also measured from the left side of the leg to the bone and similarly for the right side. The cross-sectional width and depth of the bone was also measured (Figure 10).

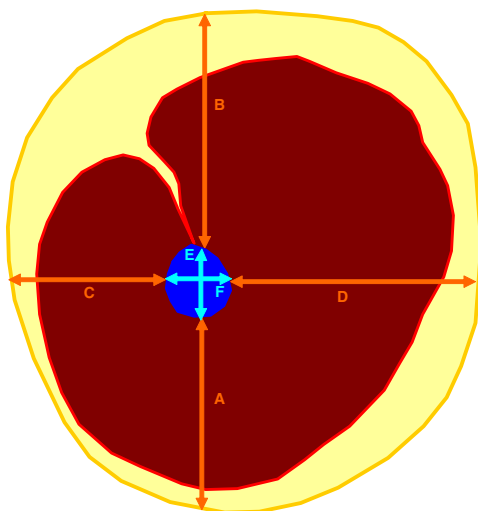


**Figure 10. Schematic of a cross-section of the human leg showing the measurements recorded.**

The dimensions that were calculated from the Visible Human male cadaver were plotted to check for any erroneous results. These would be highlighted by a misshaped profile. Figure 11 shows the front view profile of the legform.

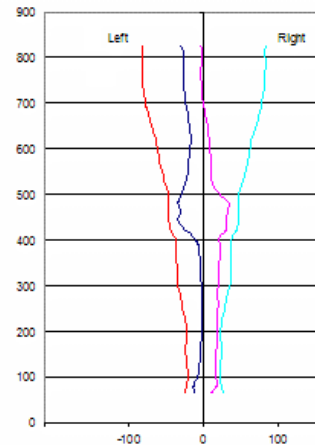


**Figure 11. Front profile of the Visible Human male leg created from measurements of the leg.**

The bones of the human leg, especially the femur are not straight. It was considered that constructing realistically shaped bones would make the build process very complex and increase the material costs. The shape of the bones would also influence the flight profile of the legform during its propulsion into the vehicle as off-centre masses (due to the shape) would cause the legform to rotate prior to impact, which is an undesirable action. It was therefore decided that the bones for the legform would be manufactured straight. This would have an influence on the position of the bone within the flesh. By using a straight bone the legform impactor would become easier to use as the bone could be removed from the legform and replaced with greater ease. To position the bone as accurately as possible it was considered that the tibia bone, knee region and bottom of the femur were the most important as these were more likely to be impacted by the vehicle.

In addition to positioning the bone within the legform the dimension of the bones themselves needed consideration. It was possible using the same methods as before for obtaining the cross-sectional dimensions of the leg to measure the bone of the Visible Human male cadaver. The femur and tibia bones do not have a perfectly circular cross-section (the tibia has a kite shaped cross-section). Both bones are longer in depth than they are in width at their mid-span position and vice versa at the ends of the bones. The average dimensions of the bones are shown in Table 7. The 'approximate average diameter' is an average of the depth and width values.

**Table 7.**

**Average values for measurements of the cross-sections of the femur and tibia bones**

| Bone  | Average depth | Average width | Approximate average diameter |
|-------|---------------|---------------|------------------------------|
| Femur | 26.26mm       | 30.23mm       | 28.29mm                      |
| Tibia | 23.70mm       | 27.17mm       | 25.44mm                      |

To retain ease of use and to minimise manufacturing costs it was decided that the bones would be manufactured with a circular cross-section. For the prototype legform the outer diameter of each bone was set to be 30mm as this sized outer diameter was more readily available. The internal diameter was altered to achieve the required bone properties discussed earlier. Although the human femur and tibia bones were found to have different average diameters it was considered that if the outer diameters of the bones were kept the same then it would be possible to insert and remove the bones from either end of the impactor should the bone fracture during its use. The outer diameter (and thus wall thickness) will be reviewed once initial component testing has been completed.

### Impactor Foot

It was found during the finite element modelling that the legform rotated slightly at the point of impact which was noted not to occur in the full 'pedestrian' model. The rotation was partly believed to be caused by the foot of the impactor. The front section of the foot was believed to cause the impactor to be unbalanced during the free flight. Consequently, the front of the foot was removed on the legform impactor. By removing the front of the foot section it was intended that it would remove the rotational inertia effects about the longitudinal axis of the lower limb that it caused. This will be confirmed during the full testing of the legform. To retain the foot mass and the inertia effects in the direction of impact, the mass of the foot section removed will be replaced at the heel of the impactor close to the centreline of the bone.

## LEGFORM IMPACTOR BUILD

### Shaping the Impactor

To replicate the human response it is not only considered necessary to have materials that replicate the human equivalent but also a legform that has a shape of the human leg. To create an exact replica of the leg of the selected volunteer it was decided that it should be moulded. Based on

advice from special effects and prosthetics manufacturers regarding the moulding process, it was decided to use a seaweed based extract known as alginate, which is safe to use on the skin and when mixed with water provides an excellent copy of the object being moulded. The alginate has a cure time of approximately 6-8 minutes from the time the water is added. The material needed to be sufficiently mixed and poured within this time.

A wooden box was constructed with steps inside to support the alginate when the volunteer's leg was removed (Figure 12). To achieve a realistic cast, it was necessary for the volunteer to stand with their leg in a straight stance and with the leg muscles tensed.

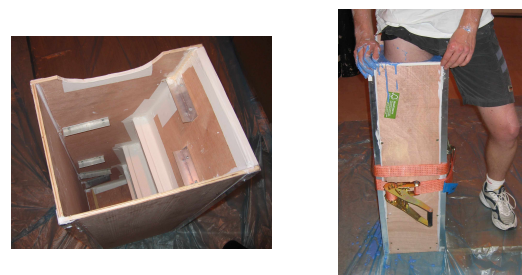


**Figure 12. The wooden box mould showing the support steps and moulding the leg of the volunteer.**

Prior to pouring the alginate the leg of the volunteer was covered with petroleum jelly to reduce the possibility of alginate moulding around the leg hairs. The petroleum jelly also acted as a release agent and enabled the volunteer to manoeuvre and slide their leg from the mould without damaging the delicate alginate (Figure 13).



**Figure 13. A top view of the alginate legform mould.**

The alginate mould is not permanent and therefore plaster casts of the leg were taken within a few hours of the alginate mould being created. The casts were made out of Plaster of Paris and although every attempt was made to remove the air bubbles from the mould as it was poured some surface bubbles were unavoidable. To achieve a smooth finish the legform was smoothed with wet and dry paper and the air bubbles were filled with plaster and filler. Figure 14 shows a side and front view of the plaster cast legform as it was removed

from the mould, prior to the finishing and smoothing process. Throughout the finishing process the plaster leg was checked to ensure that it was dimensionally accurate.



**Figure 14. A side and front view of the plaster legform as it was removed from the mould.**

It was not possible during moulding of the leg of the volunteer to mould higher than the crotch area. Consequently the legform cast was shorter than required and did not have a hip section. To mould this section of the volunteer would be very complex. It was decided that the top of the plaster legform could be extended to represent the top of the femur and thus the hip section. The profile of the top of the legform was copied and transferred onto sheets of fibreboard. These were cut out and fixed together to create a separate mould (Figure 15). Plaster of Paris was poured into the mould and once cured was removed. The hip section required some refinishing work prior to being attached to the legform itself.



**Figure 15. The mould for the top of the femur and hip section.**

In order to mould the flesh material, a lightweight, reusable fibreglass mould was made. The fibreglass mould was manufactured in two sections to make the removal of the flesh once it had been moulded much simpler. The surface of the fibreglass mould was smooth and followed the contours of the plaster legform exactly.

As discussed earlier in the paper, the femur and tibia bones are represented by straight cylinders. It was therefore necessary to mould the hollow section in the flesh where the bones would be inserted. To replicate the human leg as much as possible the position of the bone in the flesh was important. The straight bone complicates the accurate positioning of the bone slightly. However,

it was decided that the flesh material should be poured into the mould with a metal tube of the correct outside diameter to act as the bone. The metal tube was fixed to a base plate to prevent it from moving during the pouring process. The two halves of the fibreglass mould were then offered up to the tube. The vehicle impact is likely to occur in the tibia and knee regions. Consequently most effort was given to accurate positioning of the straight bone in this region. It was accepted that there would be some deviation from the ideal bone position at the ankle and top of the femur. The position of each half of the mould was then marked and secured in place. The metal tube was used as part of the moulding process only and was removed once the flesh material had cured. Figure 16 shows the two sections of the fibreglass mould and also shows the mould with the metal tube and flesh material during curing.



**Figure 16. The two sections of the fibreglass mould and the mould with the flesh during the curing process.**

Once cured it was possible to remove the legform flesh from the mould and with the metal tube in place the path of the bone in the leg flesh is clearly visible (Figure 17).



**Figure 17. A front and right side photograph of the flesh material. The metal tube used in the moulding process clearly shows the position of the bones.**

## Knee

The glass-fibre type material selected to represent the bones will fracture should the loads imposed on it be sufficient. The knee ligament is made from metal and thus it is important that the ligament does not impose unrealistic loads on the bone causing it fail prematurely. To overcome the possibility of premature failure and unrealistic stresses induced from the ligament, the ligament is mounted within a sleeve that fits onto the ends of the bones (Figure 18). The sleeves have been designed to support the ligament during its loading and to reduce the stress concentrations between the mating of the materials by having a tapered inner surface. The ligament is secured in the sleeves by the use of roll pins; once the test has been conducted and the entire bone removed from the flesh, the ligament can be removed and changed by removing the pins. The metalwork associated with the knee was kept to a minimum to reduce any effects it would have on the legform in replicating an impact between a vehicle and a pedestrian. The type and thickness of metal used for the sleeves, hip end and foot can be altered to produce the correct inertial effects and centre of gravity position for the legform.



**Figure 18. The ligament with sleeves attached. The femur and tibia bones are fitted into the ends of the sleeves.**

## FUTURE WORK

The legform impactor is currently at the stage of initial testing. The testing phase will involve component tests to evaluate the performance of the material against the required properties. Each of the components will also be tested to evaluate the repeatability and robustness characteristics. It is envisaged that the component tests used in the development phase will also be part of the certification process to ensure that all the components will respond as required. Following the successful completion of the component tests, full legform tests will be performed and the results compared with those from current impactors.

## Bone Material

The biomechanical properties of human long bones were found from data produced by Yamada [1]. To verify that the material selected for the bones

replicated the human bones, the material will be tested using a similar process to that of Yamada. Yamada used quasi-static loading to test the bending breaking load of wet long bones. To replicate this, the material will be tested in a Hounsfield loading machine with a round bar of diameter 20mm to act as the loading head. The deflection and load to cause failure will be recorded.

## Flesh Material

The flesh density has been measured as approximately 1.02-1.04g/cm<sup>3</sup> and so is within the range required for the flesh material. In addition during the moulding process to make each flesh, a small test sample will be poured and will be used to assess the hardness. To determine the robustness of the flesh material the flesh will be subjected to dynamic testing with bones that have a more elastic response than the selected bone material. This will identify the performance characteristics of the flesh.

## Knee Ligament

To achieve the desired knee ligament stiffness the selected material will be tested at a component level. This process will be used to certify a batch of ligaments prior to use to establish that each batch will be within a stated tolerance and will return consistent results.

## Whole System Testing

### Centre of gravity and moment of inertia -

Once the component testing is complete the legform will be tested as a whole system to evaluate the moment of inertia and the centre of gravity. If either of these aspects requires adjustment then it would be possible by altering the mass of the material at the hip end, knee and foot.

**Dynamic tests -** The tests will be conducted using simulated vehicle fronts of varying heights and stiffness and the impact speed will be varied. This test matrix will assess the legform's performance for a generic range of vehicles for which it is expected that this legform could be used and those vehicles to which the active safety systems are expected to be fitted. The dynamic testing will be used to confirm the free flight performance of the legform. A cradle specifically for the legform has been developed to support it during the launch phase and to reduce the possibility of rotation of the legform occurring.

In addition to the tests with the simulated vehicle fronts it is scheduled that full vehicle tests will be conducted with a vehicle that has an active safety

contact sensor system fitted. The response from the vehicle sensors for the legform impactor will be compared with the responses from current full legform pedestrian impactors. It is envisaged that apart from the alteration to the shape of the cradle to support the legform no other changes would need to be made to the current legform propulsion systems.

## SUMMARY

Active safety systems are being fitted to vehicles to improve the level of pedestrian protection. To develop and test these systems a test tool was required that had humanlike properties.

As part of the development of the test tool, research was completed into the properties of the femur and tibia bone, the flesh and the knee ligaments. Materials were selected that had the required properties and were expected to provide a realistic humanlike dynamic response.

Anthropometric data was used to select a suitable volunteer whose leg was moulded to provide an exact replica. The plaster cast of the volunteer was used to create a fibreglass mould from which the flesh material was moulded.

The legform is currently at the testing stage, whereby the robustness and repeatability of the test tool will be evaluated and the results used to validate the range of bumper heights for which the tool can be used.

## ACKNOWLEDGMENTS

The author of this paper would like to thank Helen Bateman for the work on the finite element modelling simulations and the legform development project team.

## REFERENCES

- [1] Yamada, H. and Evans, F.G. 1970. "Strength of Biological Materials". The Williams and Wilkins Company Baltimore.
- [2] Behnke A.R., Feen, B.G. and Welham, W.C. 1942. Journal of the American Medical Association, 118:495-498.
- [3] Rathbun, E.N. and Pace, N. 1945. "Studies on Body Composition.I. The Determination of Total Body Fat by Means of the Body Specific Gravity". Journal of Biological Chemistry, 158:667-676.
- [4] Keys, A. and Brozek, J. 1953. "Body Fat in Adult Man". Physiological reviews, 33:245-325.
- [5] Allen, T.H., Welch, B.E., Trujillo, T.T. and Robert, J.E. 1959. "Fat, water and tissue solids of the whole body less its bone mineral". Journal of Applied Physiology, 14:1009-1012.
- [6] Internet search for density of adipose tissue: <http://www.outsidemag.com/bodywork/mrfit/archives/199910/19991006.html>
- [7] Harrington, T.A.M., Thomas, E.L., Frost, G., Modi, N. and Bell, J.D. 2004. "Distribution of Adipose Tissue in the Newborn." Pediatric Research, 55:437-441
- [8] Tortora, G.J. and Grabowski, S.R. 1993. "Principles of Anatomy and Physiology" Seventh Edition. Harper Collins.
- [9] Yamamoto S, Saito A, Nagasaka K, Sugimoto S, Mizuno K, Tanaka E and Kabayama M (2003). "The strain-rate dependence of mechanical properties of rabbit knee ligaments" Proceedings of the 18<sup>th</sup> international technical conference on the Enhanced Safety of Vehicles, Nagoya, Japan, 19-22 May 2003: US Department of Transportation, National Highway Traffic Safety Administration (NHTSA),
- [10] Department of Trade and Industry. "Adultdata. The Handbook of Adult Anthropometric and Strength Measurements – Data for Design Safety".
- [11] Visible Human Project®, United States National Library of Medicine, National Institutes of Health. [http://www.nlm.nih.gov/research/visible/visible\\_human.html](http://www.nlm.nih.gov/research/visible/visible_human.html)
- [12] The NPAC/OLDA Visible Human Viewer website: <http://www.dhpc.adelaide.edu.au/projects/vishuman2/VisibleHuman.html>

# EVALUATION OF THE EFFECTS OF TEST PARAMETERS ON THE RESULTS OF THE LOWER LEGFORM IMPACTOR

**Sven Olav Siems**

Volkswagen AG

**Oliver Zander**

BAST – Bundesanstalt für Straßenwesen

**Peter Leßmann**

**Dirk-Uwe Gehring**

BGS – Böhme und Gehring GmbH

**Klaus Bortenschlager**

PDB – Partnership for Dummy Technology and Biomechanics

**Karl Barnsteiner**

BMW AG

**Leonard Ferdinand**

Dr. Ing. h.c. F. Porsche AG

**Markus Hartlieb**

DaimlerChrysler AG

**David Kramberger**

Audi AG

**Manfred Zeugner**

Adam Opel AG

Germany

Paper Number 07-0009

## ABSTRACT

The PDB, BAST and Opel conducted two test series to evaluate possible effects on the results obtained using the EEVC WG17 Lower Legform Impactor as a test tool for the assessment of pedestrian safety.

The reproducibility and repeatability of the test results were assessed using six legform impactors while keeping the test parameters constant. In the second series one impactor was used and the test parameters were varied to assess the effects on the readings of the legform. The test parameters were velocity, temperature, relative humidity, the point of first contact regarding the deviation in z-direction and the deviations of the pitch, roll and yaw angle.

The tests were performed using an inverse setup, i.e. the legform was hit by a guided linear impactor equipped with a honeycomb deformation element. This setup was chosen to be able to vary each single parameter while avoiding variations of the other test parameters at the same time. The test parameters were varied stronger than allowed in regulatory use in order to determine possible dependencies between the parameters and the readings which were acceleration, bending angle and shear displacement.

## INTRODUCTION

During the last years great progress was made in enhancing the pedestrian safety capabilities of

passenger cars. To improve current and future vehicles even more it is necessary to have testing equipment which enables the engineers to assess improvements even in small steps.

Therefore it is essential to know in detail about the performance of the testing equipment and the parameters that influences the performance.

For this purpose PDB, BAST and Opel designed a series of tests to research the performance of the EEVC WG17 Lower Legform Impactor. The test series were split into two steps. In the first step the repeatability and the reproducibility were addressed. In the second step effects produced by the propulsion system, e.g. point of impact and deviations of the angular orientation as well as environmental influences, e.g. temperature and humidity were addressed.

All tests had in common an inverse setup. That means that the legform in contrary to regular testing was attached to a fixture and was hit by a linear guided impactor. To simulate the impact on a bumper of a vehicle, the face of the impactor was equipped with an aluminum honeycomb deformable element. This setup was chosen to be able to precisely control the variation of the test parameters. Thus the effect on the performance of the legform could be evaluated in detail.

The velocity at the time of impact was chosen according to the regulatory test procedure to achieve similar kinematics in order to avoid discrepancies due to dynamic effects.

## TEST SETUP

As mentioned in the introduction the test setup was inverse as shown in Figure 1. The legform was attached to a frame using a hook, that was designed such that the legform releases itself when it starts to move due to the impact (Figure 2). In that way the influence of the fixture on the kinematics of the legform could be considered negligible.

The aluminum honeycomb had the dimension 250mm x 160mm x 60mm and a compressive strength of 75psi. The impact surface was covered with a layer of paper to prevent the neoprene skin of the legform from being cut by the honeycomb.

The impactor which was attached to a sled that runs on two tubes using linear ball bearings was accelerated by a hydraulic propulsion system. By using the guiding tubes the propulsion system did not affect the position and the orientation of the impactor. The Propulsion system was able to reproduce the speed within a close tolerance.



**Figure 1. Propulsion system with linear guided impactor.**



**Figure 2. Support system for the legform with release spring (left) and position of impactor relative to point of impact (right).**

The chosen point of impact was the midpoint of the cavity in the ligaments and the upper edge of the honeycomb on the impactor (Figure 2).

For this series of tests the ligaments, the foam and the honeycombs were taken from a single

batch each to minimize the influence of a possible variation of the material properties.

The determination of the influence of varying material properties on the performance of the legform could be an objective of a subsequent test series.

## PREPARATION AND CHECK OF THE LEGFORM IMPACTORS

For the assessment of the repeatability and reproducibility as well as for the parameter study all legform individuals used for the tests were inspected regarding

- no visible damages,
- weight,
- geometry,
- center of gravity (femur, tibia, assembly),
- passed static and dynamic certification test.

The center of gravity was corrected when needed as far as possible by adjusting the position of the weight in the tibia section.

This was done to ensure that the variation of the test results was not affected by readings of an impactor which could not be considered for regular testing due to failing a certification test or being out of the specification.

Before starting with the inverse impacts all legforms were certified by performing the static and dynamic tests as specified in [2]. Each legform was assigned to an individual set of foam and ligaments.

## ASSESSMENT

The assessment was performed by statistically evaluating the particular maxima of the measured data for the bending angle, the shear displacement and the tibia acceleration considering the mean value, the standard deviation, the absolute minimum and maximum, the minimum and maximum deviation from mean and the CV (coefficient of variation, i.e. standard deviation divided by the mean value in percent). For “acceptable” repeatability and reproducibility, respectively, the threshold of the CV is defined to be less than 5% [3]. Test equipment causing a CV higher than 5% is considered to be “not acceptable” for testing.

## TESTING

The testing was split into two steps. In the first step six legforms were used to assess the repeatability and the reproducibility of the lower legform while keeping the test parameters as constant as possible. In the second step only one legform was used to assess the influence of the different test parameters that could vary when

performing regular tests on vehicles. The test parameters which are supposed to affect the test results were identified to be

- the velocity at the time of impact,
- the point of first contact with respect to the z-direction,
- the orientation of the legform at the time of first contact, regarding pitch, roll and yaw angle,
- the temperature of the foam and
- the relative humidity of the foam.

### Repeatability and Reproducibility

The tests for assessing the repeatability and the reproducibility of the legform were performed using six individuals.

The test conditions were defined as follows:

- impactor velocity – 11.1m/s,
- point of impact – mid of ligaments,
- temperature – 21°C±1°C,
- rel. humidity – 30%-70% .

The series contained a total of 76 tests. The tests were distributed to the legforms according to Table 1.

**Table 1.**  
**Number of tests with the individual legforms**

| Legform #       | L1 | L2 | L3 | L4 | L5 | L7 |
|-----------------|----|----|----|----|----|----|
| Number of tests | 10 | 10 | 15 | 10 | 15 | 16 |

**Results** – The first tests confirmed that the chosen setup was convenient to produce readings comparable to those obtained in tests with a vehicle. Figure 3 shows typical responses of the three sensors produced with the inverse setup for an impact velocity of 11.1m/s.

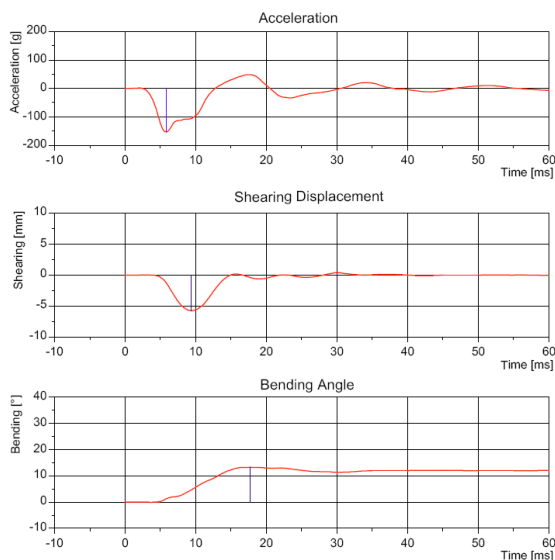


**Figure 3.** Typical readings of the legform sensors obtained with the inverse setup.

The bar graphs in Figure 4 give an image of the individual means for the three measurement locations of the legform whereas the graph in Figure 5 displays the three CV's for each legform.

The results of the statistical evaluation for the assessment of the reproducibility are listed in Table 2. The CV values from Table 2 are pictured in Figure 6.

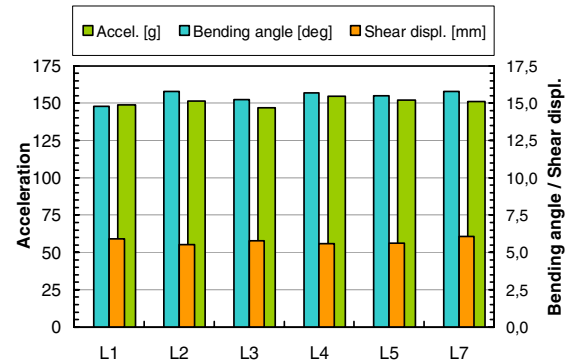


**Figure 4.** Mean values of bending angle, shear displacement and tibia acceleration of the legforms.

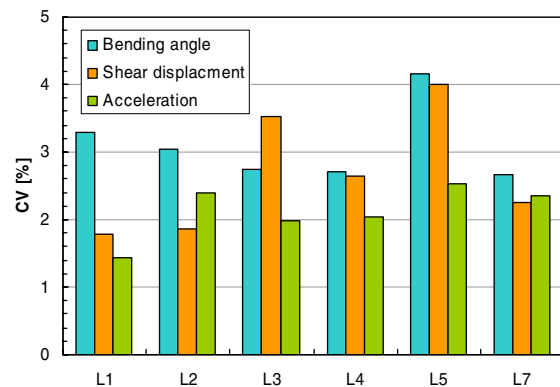


**Figure 5.** Coefficient of variation with respect to repeatability over all tests of each legform.

**Table 2.**  
**Results of the reproducibility study in engineering units (EU) and %.**

|                    |      | Bending angle | Shear displ. | Accel. |
|--------------------|------|---------------|--------------|--------|
| Mean               | [EU] | 15.47         | 5.76         | 150.64 |
| Standard deviation | [EU] | 0.58          | 0.26         | 3.98   |
|                    | [%]  | 3.76          | 4.50         | 2.64   |
| Minimum absolute   | [EU] | 14.00         | 5.20         | 140.90 |
| Maximum absolute   | [EU] | 16.70         | 6.30         | 159.90 |
| Max dev. from mean | [EU] | 1.47          | 0.56         | 9.74   |
|                    | [%]  | 9.47          | 9.70         | 6.47   |
| CV                 | [%]  | 3.76          | 4.50         | 2.64   |

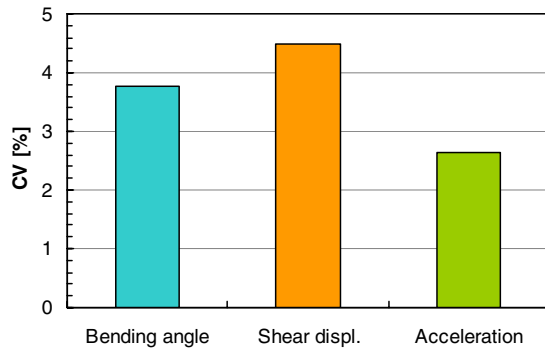


**Figure 6. Coefficient of variation with respect to reproducibility over all tests.**

**Analysis** – The analysis of the means shows no significant behavior of one of the legforms which can be covered by the measurements even if the standard deviations of the individuals differ considerably.

With regard to the mentioned CV threshold of 5% for an acceptable repeatability all legforms fulfilled this criterion. In this context it is important to keep in mind that the test parameters had to be within narrower than the regulated corridors. It can be observed that the legforms differ with respect to their overall performance. The wider spread readings of legform #5 in comparison to the other five legforms could not be explained by the influence of test parameters that were outside the defined limits or setup failures.

Looking at the three measures the tibia acceleration shows the best repeatability followed for the majority of the legforms by the shear displacement. The bending angle seems to be the least predictable measurement.

The result of the data evaluation regarding reproducibility with CV's below the threshold could be expected due to the fact that all individual CV's were acceptable and the means didn't differ that much. But it is also evident that deviations of almost ten percent from the overall mean are possible without any observable indication for the particular cause.

### Parameter study

For a better understanding of the influence of the different test parameters on the performance of the legform this parameter study was conducted. The assessment was carried out using one single legform.

If not intentionally varied the values for the six parameters were set to the same values and the same limits, respectively, as in the repeatability and reproducibility test series.

In detail the corridors for the variation of the test parameters were set as follows:

- impactor velocity –  $\pm 0.5\text{m/s}$  from  $11.1\text{m/s}$  (6 tests),
- point of impact –  $\pm 5\text{mm}$  and  $\pm 10\text{mm}$  from mid of ligaments (6 tests each),
- orientation – pitch, roll and yaw angle  $\pm 5^\circ$  (6 tests each)
- temperature –  $16^\circ\text{C}$  –  $24^\circ\text{C}$  (6 tests),
- rel. humidity –  $10\%$  –  $70\%$  (12 tests),
- time between subsequent tests –  $0.5\text{h}$ ,  $1\text{h}$ ,  $2\text{h}$ ,  $4\text{h}$  and  $12\text{h}$  (16 tests).

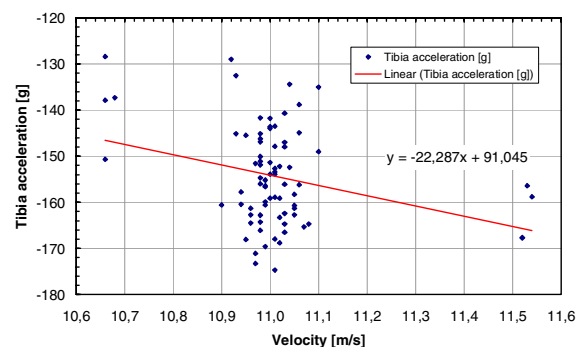
For the variation of the legform temperature and the relative humidity a climate chamber was used, that was capable to control both parameters at the same time.

**Results** – The following diagrams are the most significant from the complete matrix of results which contains the dependencies of the three measures from all the test parameters listed above. The dependencies were determined using a linear regression that was applied to the data. The data points are also shown as scatter plots to give an impression of their distribution.

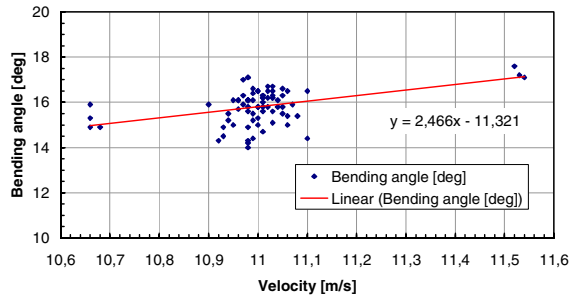
The Figures 7, 8 and 9 show the influence of the impact velocity on the tibia acceleration, the bending angle and the shear displacement. The dependency of the tibia acceleration from the temperature is shown in Figure 10, and the dependency of the bending angle from the point of impact in the z-direction in Figure 11.

Table 3 summarizes the outcome for those parameters that were identified to have a considerable influence on the test results to be produced with the legform. The results are given as a gradient of the linear regression and as a percentage with respect to the threshold of the particular measurement.

The results of a statistical evaluation are listed in Table 4. The values were calculated only for that subset of the data which was produced with the test parameters within the allowed corridors. To emphasize the CV values they are additionally depicted in the bar graph of Figure 12.



**Figure 7. Dependency of the tibia acceleration from the impact velocity.**



**Figure 8. Dependency of the bending angle from the impact velocity.**

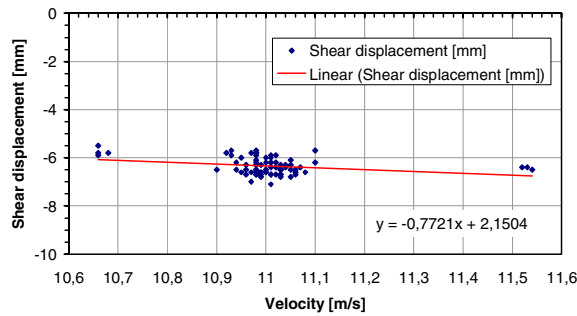


**Figure 9. Dependency of the shear displacement from the impact velocity.**

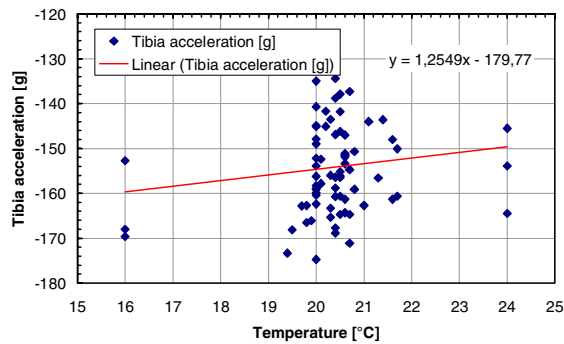


**Figure 10. Dependency of the tibia acceleration from the temperature.**

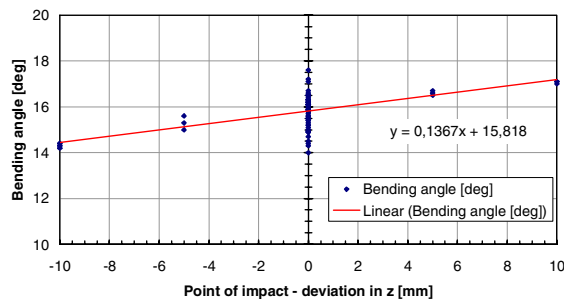


**Figure 11. Dependency of the bending angle from the point of impact.**

**Table 3. Dependency of the measurements from the test parameters.**

| Test parameter          | Bending angle | Shear displ. | Accel. |
|-------------------------|---------------|--------------|--------|
| Threshold [1]           | 15°           | 6mm          | 150g   |
| Velocity [EU/(m/s)]     | 2.47          | 0.77         | 22.30  |
| [%/(m/s)]               | 16.47         | 12.83        | 14.87  |
| Temperature [EU/°C]     | 0.06          | 0.03         | 1.25   |
| [%/°C]                  | 0.38          | 0.43         | 0.83   |
| Point of impact [EU/mm] | 0.14          | 0.03         | 0.03   |
| [%/mm]                  | 2.28          | 0.45         | 0.02   |

**Table 4. Evaluation of the repeatability based only on tests parameters within the allowed limits.**

|                          | Bending angle | Shear displ. | Accel. |
|--------------------------|---------------|--------------|--------|
| Mean [EU]                | 15.70         | 6.41         | 152.94 |
| Standard deviation [EU]  | 0.82          | 0,37         | 10.54  |
| [%]                      | 5.21          | 5.70         | 6.89   |
| Minimum absolute [EU]    | 14.00         | 5.70         | 129.00 |
| Maximum absolute [EU]    | 17.1          | 7.10         | 174.70 |
| Max. dev. from mean [EU] | 1.70          | 0.71         | 23.94  |
| [%]                      | 10.85         | 11.06        | 15.65  |
| CV [EU]                  | 5.21          | 5.70         | 6.89   |

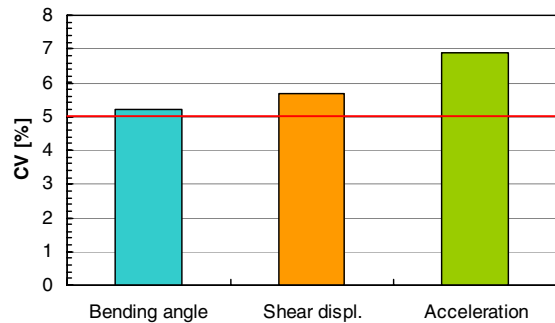


**Figure 12. Coefficient of variation based only on tests parameters within the allowed limits.**

**Analysis** – The comparison of all regressions showed that the impact velocity has the strongest effect on the performance of the legform. This influence could be expected and can be supposed to be even stronger for impacts on vehicles due to the quadratic dependency of the kinetic energy from the velocity.

There are small influences of the temperature on the tibia acceleration and of the point of impact on the bending angle. The variations of the pitch, roll and yaw angle had no significant effect on the performance just like the relative humidity.

The statistical evaluation of the data with respect to repeatability showed that the rating of the legform changed from “acceptable” to “not

acceptable” as a consequence of varying the test parameters over the full width of the allowed corridors. It can be assumed that the repeatability may be reduced even more, if there are coincident effects of more than one parameter which may lead to an increase or a decrease, respectively, of the measured signal due to a superposition of the effects. The latter should be the scenario occurring in the field.

## **CONCLUSIONS**

The repeatability and reproducibility study showed that there are systematic differences between the examined legforms regarding the individual performance. There are no considerable differences in the mean amplitudes but in the variation of the readings. A detailed inspection of all legforms didn't reveal any particular cause. According to the parameter study it is essential for testing with the legform to adjust first of all the impact velocity as close as possible to the nominal value in order to achieve a good repeatability. But also the sum of the minor influences can lead to an increase of the deviation.

## **REFERENCES**

- [1] DIRECTIVE 2003/102/EC OF THE EUROPEAN PARLIAMENT AND OF THE COUNCIL of 17 November 2003 relating to the protection of pedestrians and other vulnerable road users before and in the event of a collision with a motor vehicle
- [2] COMMISSION DECISION of 23 December 2003 on the technical prescriptions for the implementation of Article 3 of Directive 2003/102/EC of the European Parliament and of the Council relating to the protection of pedestrians and other vulnerable road users before and in the event of a collision with a motor vehicle (2004/90/EC)
- [3] ISO/TC22/SC12/WG5 N751, Calculation Methods & Acceptance Levels for Assessing Repeatability and Reproducibility (R & R), H. Mertz, WG 5 Chairman, Dec. 6, 2004

## **Relevance on Injury Causation of Vehicle Parts in Car to Pedestrian Impacts in different Accident Configurations of the Traffic Scenario and Aspects of Accident Avoidance and Injury Prevention**

**Otte Dietmar,**

Medical University Hannover  
Accident Research Unit  
Germany

**Huefner Tobias,**

Medical University Hannover  
Department of Trauma Surgery  
Germany  
Paper Number 07-0176

### **ABSTRACT**

This study is concerned with the analysis of pedestrian accidents and the corresponding analysis, which injuries are caused by what type of vehicle impact in different accident scenarios. The question is: to what extent can innovative driver assistance systems and measures in traffic environment help to avoid or completely prevent injuries of pedestrians. For this purpose, a total of n=1107 accidents documented in surveys in Hannover and Dresden involving passenger cars and pedestrians were examined and the injury situations shown. To this end, characteristic values such as driving and collision speed, injury severity MAIS and AIS of the individual injuries for different accident scenarios were regarded. For the identification of the relevant accident scenarios, classifications of the accident types were used and many of those represented in statistically representative accident material GIDAS (German in-Depth-Accident Study - 1) for the years 1995 to 2004 were filtered out. The study should be of assistance and support decision-making in the evaluation of future technical innovative measures for accident avoidance and thus injury reduction

### **INTRODUCTION AND TARGETS**

Pedestrian safety has been significantly improved over the past 30 years. Where in 1975 in a country like the Federal Republic of Germany (STBA - 2) still n = 3973 fatalities and n = 60033 casualties among pedestrians were registered, the number of fatalities at n = 686 and casualties at n = 33803 in the year 2005 clearly seems like an improved situation. Nevertheless it cannot be overlooked that in today's Europe of 27 different countries, there are still far more than 40 000 pedestrians killed in traffic annually. This requires manifold efforts of scientific research, which can no longer be limited exclusively to passive security like injury reduction, but must also aim at measures of active security for the avoidance of accidents as well. Also, the requirements postulated by the European Union commission in the year 2000 for all member states to halve the number of deaths within the next 10 years, constitutes a difficult target to reach until 2010

The aim had been to increase the protection of pedestrians by implementing different phases. All new vehicles have had to pass phase 1 of EEVC pedestrian tests after October 1<sup>st</sup>, 2005 and all new registrations of existing models by 2012. As part of this Directive, a feasibility test was also conducted to evaluate to what extent manufacturers would be able to comply with the full test criteria defined by the EEVC (EU commission - 3). If strong arguments were put forward, proving that manufacturers would not be able to design vehicles to comply, then active safety systems would be evaluated to assess whether they would be able to make up the difference in estimated casualty reductions as a result of relaxing the tests recommended by EEVC. After negotiation with the industry, the EU proposed a regulation, which would incorporate all the present requirements of phase 1 and revised requirements for phase II based on a feasibility study. A first phase set of test requirements (phase I) was applied to all new types of vehicles as from October 1<sup>st</sup>, 2005 and to all new vehicles placed on the market after December 31<sup>st</sup>, 2012. A second phase of tests (phase II), based on the results of a comprehensive study into the feasibility of the original requirements, will apply to all new types of vehicles from September 1<sup>st</sup>, 2010 and to all new vehicles by 2015. Additionally, the active safety system, brake assist, will be required in all new vehicles from July 1<sup>st</sup>, 2008. The use of new systems, such as collision avoidance, will be recognised as alternatives. The two ways to encourage manufacturers to dedicate more resources towards protection issues are through consumer demand and setting high crash test standards that are relevant to the real world.

This study deals with the analysis of traffic accidents involving pedestrians and filtering the accident scenarios frequently occurring during such accidents. It is to be determined, whether collisions between passenger cars and pedestrians cause less severe injuries at pedestrian crosswalks than, for instance, in case of collisions on free stretches of the road or at junctions and/or intersections, and, for example, if other sources of injury at the vehicle are responsible for the injuries. Particular attention is paid to the severely injured pedestrians.

Such questions require a differentiating methodology for multi-phase analysis and comprehensively documented accident data, such as they are available due to collections at the sites of accidents, GIDAS. These records contain information concerning injuries and vehicle deformations besides data referring to places and types of accidents. Beyond that, there are detailed descriptions concerning the origins of accidents and the sequence of the accidents based on questioning the persons involved and documentation of the environment of the scene of the accident. These supply information in connection with the technical accident reconstruction regarding the speed the vehicles were traveling at and the collision speed on the basis of recorded skid marks and final positions of the vehicles.

### CASE BASE AND METHODOLOGY

Since 1999 compilations have been conducted at the site of accidents, GIDAS (German in-Depth-Accident Studies, Otte - 4), at the medical university Hanover and the technical University of Dresden on behalf of the Federal Institution for roads, BAST, and the German Automotive industry FAT. The methodology is described by Brühning (1) and Otte (4). Based on a random sample, representative data processing can be done in connection with a statistic weighing of the data (Pfeiffer - 5). From a population of traffic accidents with personal injury documented by scientific teams in the years 1999 to 2005, accidents in which passenger cars and pedestrians were involved, were selected and for this sub-group the different accident scenarios were filtered. For this purpose, the classification according to accident types (FGSV - 6) and the recording of the environment of the accidents according to categories such as urban/rural, straight road/junction, with/without traffic lights, with/without line-of-sight obstructions was used. The analysis of the location and severity of the injuries was conducted based on the AIS- injury classification (American Association for Automotive Medicine - 7). The record of every accident contains a comprehensive reconstruction of the motion sequences of the vehicle and the pedestrian on the basis of a true-to-scale drawing based on an image created using 3-D-Laser technology showing the site of the accident and measured skid marks as well as the final positions of the vehicles (Otte -8). 1107 accidents with pedestrians constitute the basis of the analysis, of these 182 suffered an injury severity grade of MAIS higher than 2 (MAIS 3+). This corresponds to a portion of severely injured person of 16.4%.

For the identification of the relevant accident configurations, the accidents were now differentiated according to the origins of the accidents and the accident characteristics. For this purpose, the accident incidences for all pedestrians

(table 1) and for severely injured /killed pedestrians (table 2) in a collision with a passenger car were illustrated. Tables 1 and 2 show that accidents on straight roads without safety features are the most frequent more than 50 % and accidents at intersections with traffic lights at around 10% and without traffic lights at 14.4% of all and at 19% of severely injured pedestrians are the second most frequent, in each case for passenger cars traveling straight ahead and pedestrians traversing the road. Taken together, these constitute already about 70% of all collisions resulting in severely injured pedestrians. Almost 90% of all accidents with pedestrians occur in principle at 3 different locations:

- 1 - straight roads without safety feature
- 2 - intersections without traffic lights with passenger car traveling straight ahead
- 3 - intersections with traffic lights with passenger car traveling straight ahead

**Table 1.**  
**Pedestrian accident situation and locations**  
**(n=1107)**

| 70 % of cases                                 | total  | Movement of Pedestrian |                       |                        |                          |                         |                           |                 |                 |
|---|--------|------------------------|-----------------------|------------------------|--------------------------|-------------------------|---------------------------|-----------------|-----------------|
|   |        | contrary to car        | same direction as car | from left no obstruct. | from left with obstruct. | from right no obstruct. | from right with obstruct. | enter or aboard | others, unknown |
| total   | 100.0% | 9.0%                   | 3.2%                  | 16.8%                  | 13.9%                    | 24.4%                   | 22.6%                     | 3.7%            | 6.4%            |
| Movement of Car                               |        |                        |                       |                        |                          |                         |                           |                 |                 |
| intersection, no traffic light straight ahead | 14.4%  | 0.5%                   | 0.6%                  | 2.6%                   | 2.0%                     | 3.7%                    | 3.3%                      | 0.7%            | 0.9%            |
| intersection, no traffic light, turning left  | 2.5%   | 0.8%                   | 0.2%                  | 0.5%                   | 0.0%                     | 0.7%                    | 0.2%                      | -               | 0.1%            |
| intersection, no traffic light, turning right | 1.5%   | 0.3%                   | 0.1%                  | 0.3%                   | 0.1%                     | 0.7%                    | 0.0%                      | -               | -               |
| intersection, traffic light, straight ahead   | 10.8%  | 1.0%                   | 0.1%                  | 2.8%                   | 1.0%                     | 4.2%                    | 1.3%                      | 0.1%            | 0.3%            |
| intersection, traffic light, turning left     | 3.8%   | 0.8%                   | 0.2%                  | 1.5%                   | 0.1%                     | 1.1%                    | -                         | -               | 0.1%            |
| intersection, traffic light, turning right    | 1.5%   | 0.1%                   | -                     | 0.4%                   | -                        | 1.1%                    | -                         | -               | -               |
| curve   | 3.8%   | 1.2%                   | -                     | 0.3%                   | 0.6%                     | 0.9%                    | 0.8%                      | -               | 0.0%            |
| straight line, no crosswalk                   | 51.1%  | 3.8%                   | 1.4%                  | 6.4%                   | 9.0%                     | 9.1%                    | 15.1%                     | 2.9%            | 3.6%            |
| straight line, crosswalk no traffic light     | 2.8%   | -                      | -                     | 1.0%                   | 0.1%                     | 1.4%                    | 0.3%                      | -               | -               |
| straight line, crosswalk traffic light        | 0.4%   | -                      | -                     | 0.1%                   | 0.1%                     | 0.2%                    | -                         | -               | -               |
| others  | 7.3%   | 0.5%                   | 0.5%                  | 0.9%                   | 0.9%                     | 1.4%                    | 1.5%                      | 0.1%            | 1.5%            |

Particularly significant are these groups: pedestrians approaching from the right with line-of-sight obstructions (15.1%), intersections with traffic lights and "pedestrians approaching from the right without line-of-sight obstructions" (4.2%) and intersections without traffic lights and "pedestrians approaching from the right without line-of-sight obstructions" (3.7%). If also considers the special lower level conflict situations (about 1 %), then all the marked boxes of the table offer the frequent accident situations involving pedestrians.

If only accidents resulting in severely and fatal injured pedestrians are regarded, a near analogy with all accidents can be noticed, nearly the same incidences apply (table 2).

**Table 2.**  
**Accident situation and locations of pedestrians**  
**MAIS 3+ (n=182)**

|   | total  | Movement of Pedestrian |                       |                        |                          |                         |                           |      | enter or aboard | others, unknown |
|---|--------|------------------------|-----------------------|------------------------|--------------------------|-------------------------|---------------------------|------|-----------------|-----------------|
|   |        | contrary to car        | same direction as car | from left no obstruct. | from left with obstruct. | from right no obstruct. | from right with obstruct. |      |                 |                 |
| total   | 100.0% | 12.2%                  | 5.5%                  | 21.8%                  | 11.2%                    | 21.3%                   | 17.1%                     | 2.1% | 8.8%            |                 |
| Movement of Car                               |        |                        |                       |                        |                          |                         |                           |      |                 |                 |
| intersection, no traffic light straight ahead | 18.8%  | 1.3%                   | 1.2%                  | 4.3%                   | 0.6%                     | 6.5%                    | 4.1%                      | -    | 0.2%            |                 |
| intersection, no traffic light, turning left  | 1.3%   | 0.7%                   | 0.6%                  | -                      | -                        | -                       | -                         | -    | -               |                 |
| intersection, no traffic light, turning right | 0.7%   | 0.4%                   | -                     | -                      | -                        | 0.3%                    | -                         | -    | -               |                 |
| intersection, traffic light, straight ahead   | 12.0%  | -                      | -                     | 5.9%                   | 0.3%                     | 3.8%                    | 1.3%                      | -    | 1.0%            |                 |
| intersection, traffic light, turning left     | 1.9%   | 0.4%                   | -                     | -                      | 0.9%                     | 0.6%                    | -                         | -    | -               |                 |
| intersection, traffic light, turning right    | -      | -                      | -                     | -                      | -                        | -                       | -                         | -    | -               |                 |
| curve   | 4.7%   | 1.9%                   | -                     | 0.6%                   | 0.4%                     | 1.3%                    | -                         | -    | 0.4%            |                 |
| straight line, no crosswalk                   | 52.7%  | 5.6%                   | 2.3%                  | 9.5%                   | 8.1%                     | 7.3%                    | 10.7%                     | 2.1% | 7.1%            |                 |
| straight line, crosswalk no traffic light     | 0.7%   | -                      | -                     | 0.3%                   | -                        | 0.3%                    | -                         | -    | -               |                 |
| straight line, crosswalk traffic light        | 0.6%   | -                      | -                     | 0.6%                   | -                        | -                       | -                         | -    | -               |                 |
| others  | 6.7%   | 2.0%                   | 1.4%                  | -                      | 0.9%                     | 1.5%                    | 1.0%                      | -    | -               |                 |

A striking number of accidents happened to pedestrians approaching from the right of a driver with line-of-sight obstructions (proportion 15.1% of all, 10.7% of the severely injured/killed pedestrians). 20% of accidents were observed on straight line without any crosswalk when pedestrian was moving from left (9.5%) or from right with obstructions (10.7%)

### ACCIDENTS OF PEDESTRIANS AT INTERSECTIONS/JUNCTIONS WITH TRAFFIC LIGHTS FOR PASSENGER CARS CONTINUING STRAIGHT AHEAD

80% of all collision velocities of the passenger cars were found at these locations (figure 1) up to 32 km/h, the corresponding driving speeds at the point of the reaction of the driver were determined up to 49 km/h (figure 2). 58.5 % of the pedestrians were lightly injured, with degree of severity MAIS 1, 14.3 % suffered from injures of a severity above MAIS 2 (MAIS 3+).

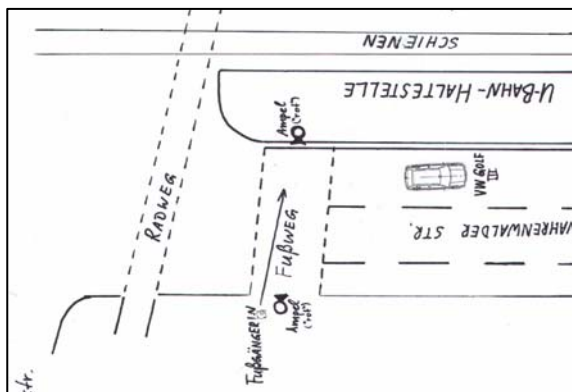


**Figure 1.** exemplary accident situation of this category

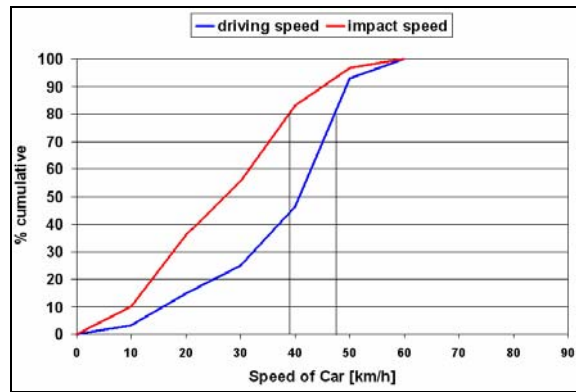


**Figure 2.** cumulative frequency distribution of the accidents as a function of collision speed and driving speed

Pedestrians under these collision conditions were injured at the head in 62.4% of the cases (figure 3). These injuries were particularly severe in 37.5 % of the cases (AIS 2+). A quarter of the injuries to the head (23.0%) originated from the impact of the head on the windshield, 10,3% from the impact of the head on the hood. At 49.8 % approximately half of all head injuries were caused by hitting the road surface.

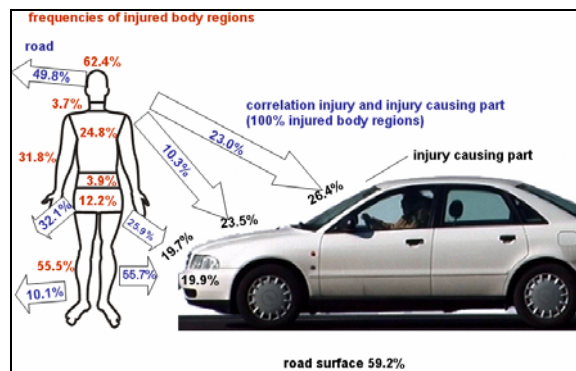


**Figure 3.** Frequency of injury of different areas of the body (100% all persons) with the corresponding proportions of the parts of the cars that have caused the injuries (100% all injured body regions).

In 55.5 % the legs were injured, in 56 % of the cases due to impact of the bumper. Injuries of the pelvis occurred in 12.2 % of the pedestrians, in 25.9 % of the cases they had been caused by the front edge of the hood, in 32.1% they were due to the secondary impact on the road surface. The windshield was the source of injury in 26.4% of all cases on these frequently seen accident situation category.

### ACCIDENTS OF PEDESTRIANS AT INTERSECTIONS/JUNCTIONS WITHOUT TRAFFIC LIGHTS FOR PASSENGER CARS CONTINUING STRAIGHT AHEAD

These are accidents where pedestrians step into the road in the area of a junction or intersection, which

has not been equipped with traffic lights or crossing aids (pedestrian crossing) (example figure 4).

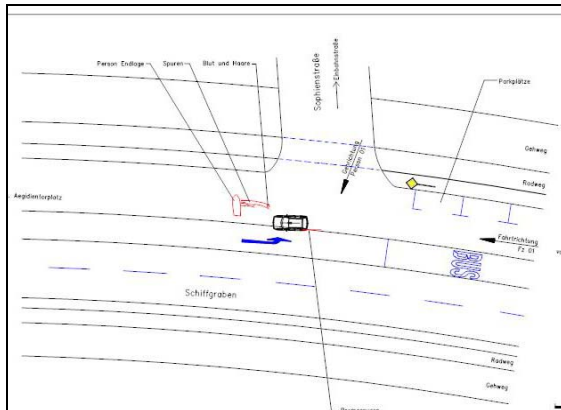


**Figure 4. exemplary accident situation of this category**

12.2% of the pedestrians involved in this situation suffered from severe injuries MAIS 3+ and 63.1 % were slightly injured (MAIS 1). 80% of all impact speeds could be registered with values of up to 32 km/h (figure 5).

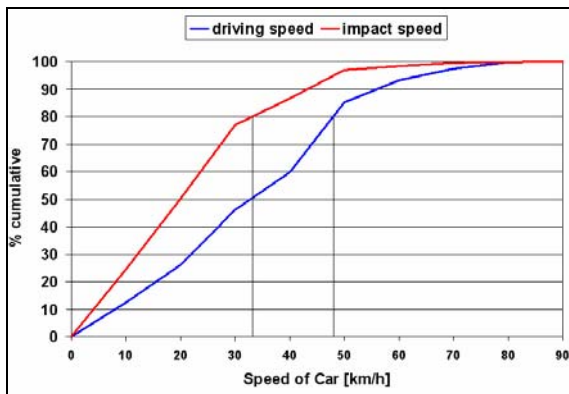


**Figure 5. cumulative frequency distribution of the accidents with collision speeds and driving speed**

52.8 % suffered from injuries to the head, of these approximately one third were severe, AIS 2+ (35 %). Injuries to the pelvis were recorded in 12.8 % of the cases and injuries to the legs in 63.8%, at 36% (AIS 2+) the latter were more frequently severe (figure 6).

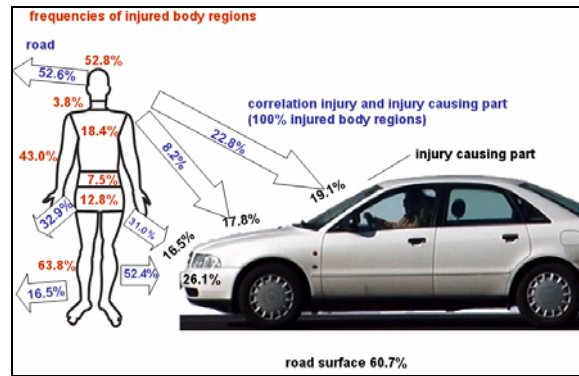


**Figure 6. Incidence of injuries to the different parts of the body (100% all persons) with corresponding proportions of the parts of the cars causing these injuries (100% all injured parts of the body)**

22.8% of the injuries to the head were caused by an impact on the windshield, which was responsible for the injuries of pedestrians in 19.1 % of the cases. A collision of the head with the hood turned out to be the cause of injuries in only 8.2 % of the cases, whereas 52.9 % of the injuries to the head could be attributed to an impact on the road surface. One third of the injuries to the pelvis (31 %) were caused by impacts with the front edge of the hood, another third (32.9%) by a secondary impact on the road surface.

### ACCIDENTS OF PEDESTRIANS ON STRAIGHT ROADS WITHOUT SAFETY ELEMENTS

These are accidents, where pedestrians without line-of-sight obstructions step onto the road not equipped with crosswalks of lighting signs coming from the right (example figure 7)

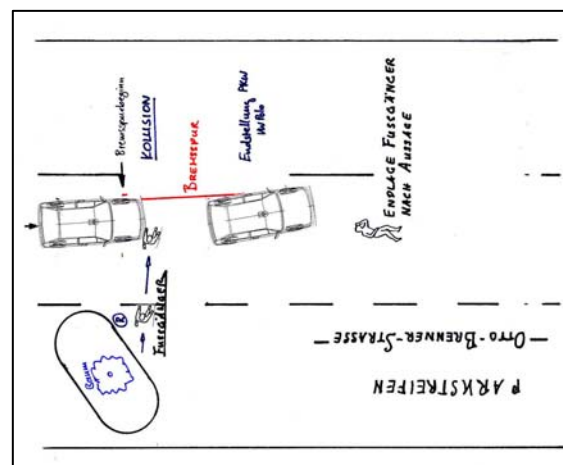


**Figure 7. exemplary accident situation of this category**

The 80-percent value of the collision speeds in these cases was situated up to 40 km/h (figure 8).

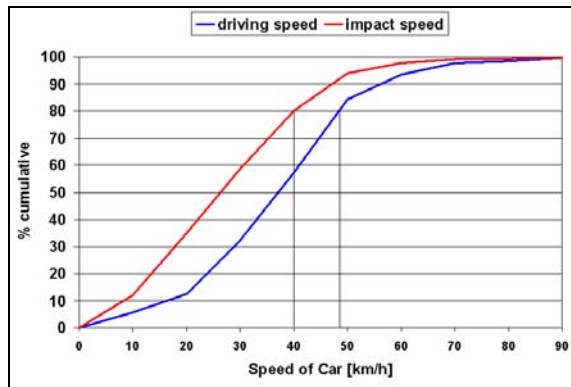


**Figure 8. cumulative frequency distribution of the accidents with collision speeds and driving speed**

11.1 % of the pedestrians were severely injured (MAIS 3+), 64.3 % were only slightly injured (MAIS 1). In 51.5 % of the cases the head was injured, in 70.1 % the legs and in 13.3 % the pelvis (figure 9). 39 % of the injuries to the head were severe (AIS 2+). Injuries to the legs were severe in only 24.6% of the cases and the injuries to the pelvis in 20.3%.

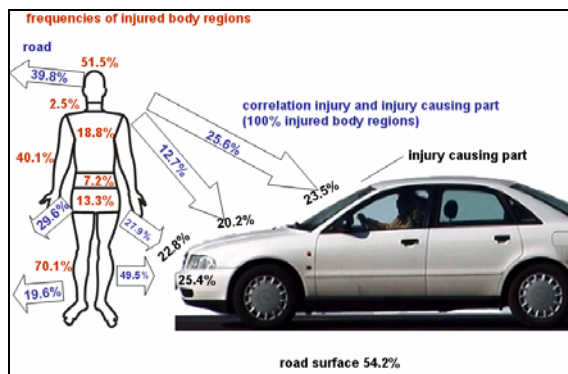


**Figure 9. Incidence of injuries to the different parts of the body (100% all persons) with corresponding proportions of the parts of the cars causing these injuries (100% all injured parts of the body)**

25.6 % of the injuries to the head resulted from an impact on the windshield, 20.2 % on the hood. An impact on the road surface was regarded as causal in only 39.8 % of the cases of an injury to the head. 27.9 % of the injuries to the pelvis were attributed to the front edge of the hood.

### RELEVANCY OF THE SOURCES OF INJURIES ON VEHICLES FOR DIFFERENT ACCIDENT SCENARIOS

No significant differences of the injury situations could be seen for different places in the traffic environment. For all accidents, whether on straight roads or at intersections/junctions, nearly the same frequency distributions concerning injury severity, the injured body parts and the car parts causing the

injuries apply. In all cases approximately 60 % of the pedestrians having collided with a car were slightly injured (MAIS 1), the proportion of severely injured pedestrians (MAIS 3+) was always 11 or 12 %, always about one fourth of the pedestrians suffering from head injuries had hit the windshield. These, however, were at 40 % more frequently severe (MAIS 2+) on straight roads without special crosswalks than at intersections/junctions (34% MAIS 3+). The proportion of head injuries caused by an impact with the windshield was highest - at 25,6 % - for this accident location as well. Injuries to the pelvis also occur more frequently for this accident location (18.8 % as opposed to 12%), but they are not more severe.

In order to determine, if the injury situation differs in those locations, where an increased measure of caution towards pedestrians is required, only accidents on crosswalks or places equipped with traffic lights were evaluated and compared to the accidents of places without crosswalks (figure 10). It turned out that in these cases 80 % of the collision speeds up to 33 km/h and of the driving speeds at 47 km/h were slightly lower than in comparison with other accident locations. Thus the resulting injuries were also significantly less severe.

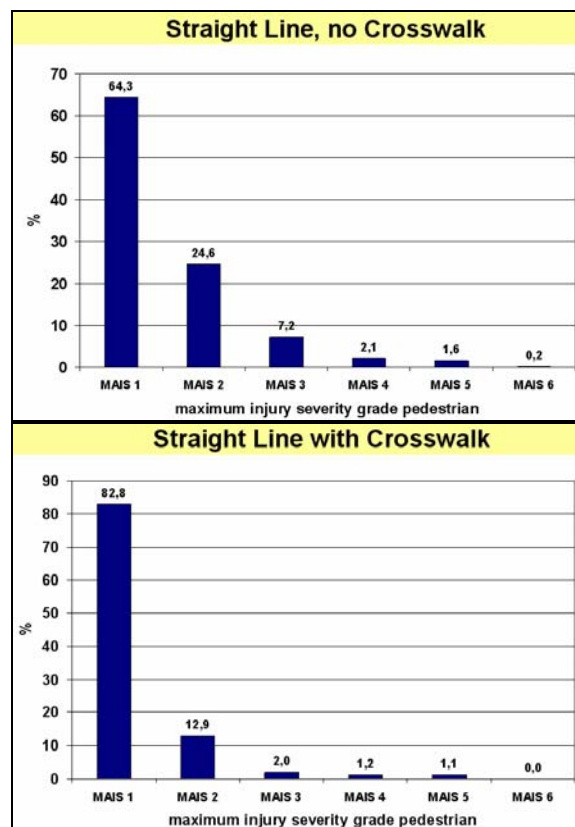


**Figure 10. Comparison of the frequency distributions of the severity of the injuries, MAIS, for accidents with pedestrians along straight stretches with and without crossings.**

For accidents at crosswalks a lower injury severity for nearly all parts of the body is discernible (figure

11), for the head (23.2 %, AIS 2+) as opposed to 39 % at locations without crossing, for the pelvis (7.0% as opposed to 20.3%, AIS2+) and for the legs (10.9% as opposed to 24.6%, AIS 2+). At crossings, 33 % of the injuries to the head have been caused by an impact on the windshield and 51 % of the injuries to the pelvis have been caused by the front edge of the hood. However, figure 11 shows no reduced potential for injuries for legs and pelvis resulted for accident situations with crosswalks.

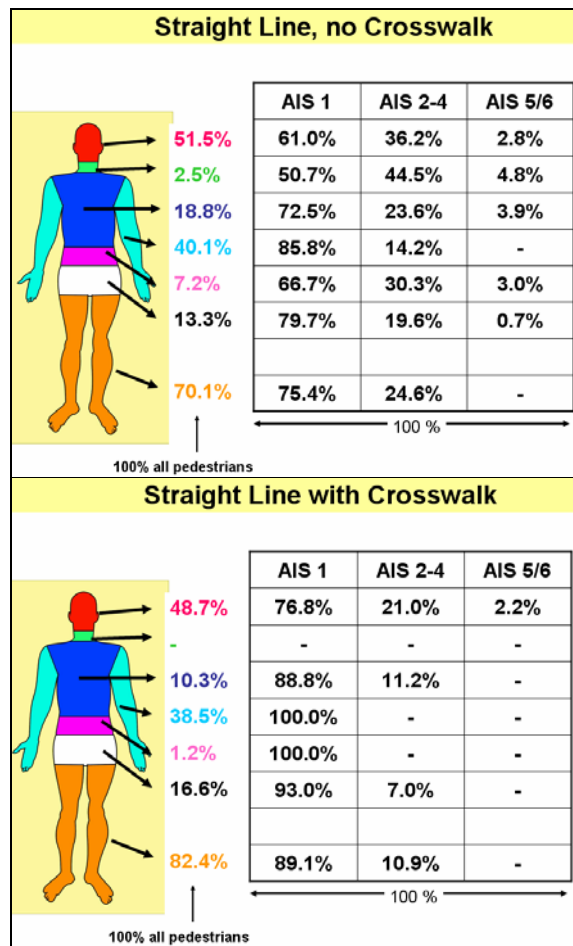


Figure 11. Frequencies of injured body parts and degrees of the severity of injuries MAIS at accident locations with and without crossing

Thus it seems that the measures on passenger cars undertaken lately for an optimized safety of pedestrians have been realized sufficiently extensively, as they are not influenced by the different accident scenarios and their differing incidences. As a rule, this is due to the fact that the pedestrian collides with the front of the car, which submits the person to pre-determined body kinematics of impact. Locally differing accident situations only result in differing impact velocities, if at all, and thus reduced severities of injuries, but as the study shows, these concern nearly exclusively the head, which mainly collides with the windshield, the defusing of which as a source of injury seems more than urgently required.

## POTENTIAL OF PREVENTING ACCIDENTS BY TECHNICAL DESIGN OF THE SITE OF ACCIDENTS AND INNOVATIVE AUTOMOTIVE ENGINEERING ASSISTANT

On closer inspection of accident locations frequently involving pedestrians it was proven that a special, design-engineered crossing for pedestrians, by markings on the road or traffic lights, significantly lower the resulting severity of injuries. Thus it seems that local conditions, which draw the attention of the driver, do constitute a safety-increasing effect for pedestrians. Still, other solutions and developments of automotive engineering are possible, which can transmit a risk signal of a possibly occurring collision to the driver at an early stage.

If the time elapsed between the response and the collision itself is regarded - it was possible to determine these from the accident data provided - a significant difference between accidents with traffic lights or crossings and without such devices was noticeable (figure 12). Thus the maximum time that had elapsed between response and collision was 2.4 seconds for traffic lights and 2.1 seconds for crossings, whereas for accidents without traffic lights or crossings maximum values of up to 4 seconds occurred. This seems to leave sufficient space for a reduction of the response time and the braking distance.

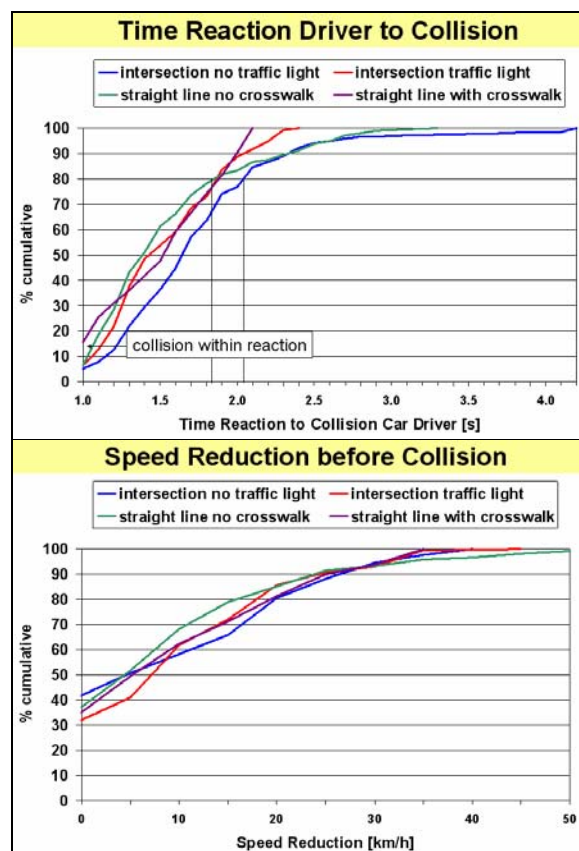
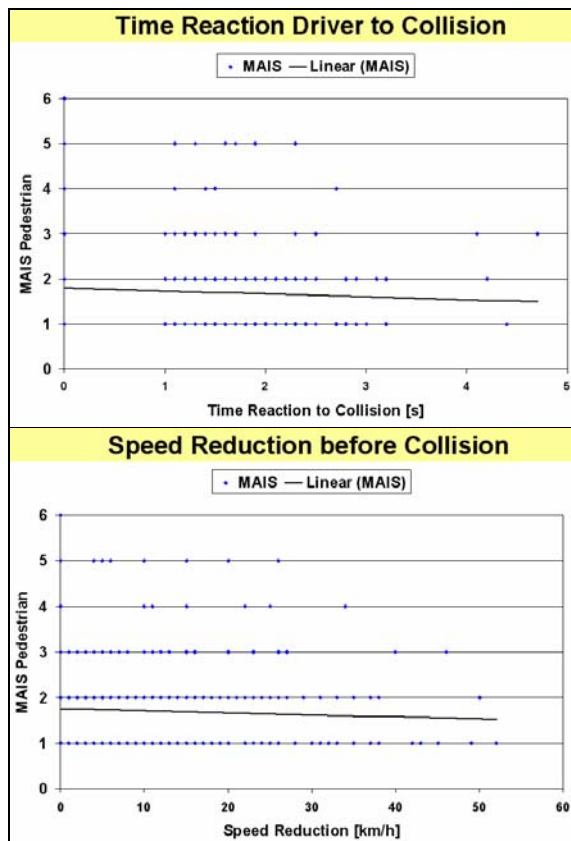


Figure 12. time duration from response to collision and corresponding reduction in velocity determined at the sites of accidents

90 % of all accidents at the sites of accidents investigated contained a reduction of the velocity of up to 25 km/h. The cumulative frequency distributions for the different sites of accidents show that this applies to all in nearly the same way. Approximately 40 % of the accidents do not contain a reduction in velocity before the impact. It could be shown that an increasing reduction of the velocity and a reduced [response] time were linked to a reduction of the resulting severity of injury, MAIS (figure 13).



**Figure 13. Correlation of severity of injury, MAIS, and time from response to collision as well as the resulting reduction in speed**

If it would be possible to implement measures resulting in a reduction of the response time by 0.3 seconds for instance, an extension of the braking distance and an impact velocity reduced by approximately 9 km/h would follow. This can be seen in figure 14, referring to the accident population investigated here, and based on the correlation of MAIS and collision speed, the injury severity could be reduced by nearly half a degree. For instance at 50 km/h with an expected degree of severity of injury MAIS 2 to then 41 km/h with a MAIS of 1,8 (0.2 MAIS – points).

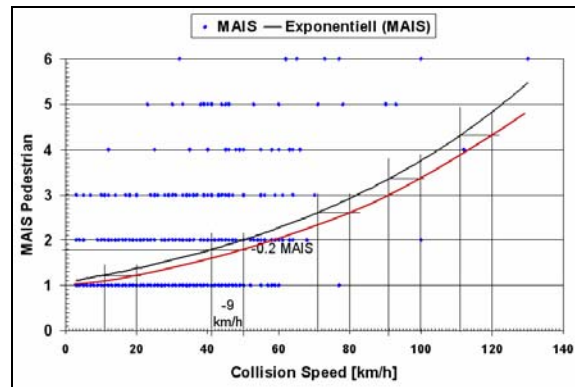


**Figure 14. Correlation of the injury severity of all pedestrian-car collisions with the collision speed of the car with exponential regression line and representation of the expected reduction potential with a response time shortened by 0.3 seconds**

## CONCLUSIONS

For this study, 1107 statistically representative accidents between cars and pedestrians collected in GIDAS (German-In-Depth-Accident-Study) were evaluated. From this population the most frequent accident situations for pedestrians involved in accidents with passenger cars were extracted. It turned out that 90 % of all collisions between cars and pedestrians occur in three major accident situations, at straight roads without safety features like crosswalks or special lighting systems, at intersections/junctions without traffic lights and at intersections/junctions with traffic lights. 20 % of all accidents occur at straight roads without any safety features for the pedestrian crossing the street from the left (9.5%) as well as with a line-of-sight obstruction for the driver of the passenger car when crossing the street from the right (10.7%). No clear difference could be shown in the injury situation of pedestrians having been hit by a car in different locations of the traffic environment; always approximately 60 % were slightly injured, MAIS 1, the proportion of MAIS 3+ was always between 11 and 12 %. This is following from the kinematics of the course of the collision is dominated by the position of the pedestrian in front of the car and the resulting bodily movement across the hood with subsequent sliding or flying phase. As these are largely collisions of the front end of the car with a pedestrian, the resulting injury based on the classical configuration of pedestrian and car consists or injury severity MAIS and injury frequency percentages nearly in the same manner, the differences are partly margin. The influence of accident locations is mainly focused to the speed level of the collision. Thus this study was able to show that for accidents occurring at locations with safety features for pedestrians, such as crossings or traffic lights, the distribution of injury severity occurring here resulted more frequently in slightly injured persons than for

locations without any safety features. The study also showed that at locations with crossing features, injuries to the head occur less frequently, and also legs and pelvis are less severely injured. In the course of the study it was shown that the time that elapsed from the moment of reaction until the collision lasted up to 2 seconds in 80 % of the cases, the speed reduction to the point of collision was up to 25 km/h in 80% of the cases; up to approximately 40% of the cars did not reduce speed until the collision. Thus a significant potential for further reductions of the collision speed can be made out. The study postulated that a reduction of the response time by 0.3 seconds, for instance, would result in a collision speed reduced by about 9 km/h for the car and that the expected injury severity for the accident population regarded could be reduced by about 10 % by using the AIS Scale as linear and carried out an exponential regression analysis on injury vs. speed relation. The study was thus able to confirm the expected potential of a brake assist system based on an analysis of accidents. In addition, the result of this study can support the evaluation of different accident scenarios involving pedestrians regarding the different technical assisting systems applicable. For instance, assistance systems that are constantly monitoring the driving situation ahead would be able to reduce response time in accidents involving pedestrians walking in the same or opposite direction facing the vehicle. This would cover 12% of all accidents involving pedestrians and 18% of all pedestrians injured MAIS 3+ as a target group. Also, for pedestrians crossing the road from the left, technical information systems seem sensible in order to reduce response times, as these constitute one third of all accidents involving pedestrians (31% of all and 33% of all MAIS 3+).

## LITERATURE

- [1] Brühning, E., Otte, D., Pastor, C.; 30 Jahre wissenschaftliche Erhebungen am Unfallort für mehr Verkehrssicherheit, Zeitschrift für Verkehrssicherheit 51, 175-181, 2005
- [2] StBA- Statistische Daten der Verkehrsunfälle in Deutschland 2005  
Stat. Bundesamt Wiesbaden, Fachserie P, Reihe 7, Verlag Metzler-Poeschel, 2006
- [3] Commission of the European Communities; Proposal for a Directive of the European Parliament and of the Council relating to the protection of pedestrians and other vulnerable road users in the event of a collision with a motor vehicle and amending Directive 70/156/EEC, Brussels, 2003
- [4] Otte, D.; The Accident Research Unit Hannover as Example for Importance and Benefit of Existing In Depth Investigations, SAE-Paper No. 940712, Proc. International SAE Congress, Detroit/USA, 1994
- [5] Pfeiffer, M., Schmidt, J.: Statistical and Methodological Foundations of the GIDAS Accident Survey System, 2<sup>nd</sup> ESAR Conference, Hannover, 2006
- [6] FGSV, Forschungsgesellschaft für Straßen- und Verkehrswesen: Erfahrungen mit dem dreistelligen Unfalltypenkatalog, Arbeitsgruppe Verkehrsführung und Verkehrssicherheit, Arbeitsausschuß Verkehrsunfälle, Arbeitspapier Nr. 24, 1990
- [7] American Association for Automotive Medicine: The Abbreviated Injury Scale - Revision 98, American Ass. f. Automotive Medicine., Morton Grove, Illinois (USA) 1998
- [8] Otte, D.; 3-D Laser systems for scaled accident sketches and documentation of the traces after traffic accidents as basis of biomechanical analysis, Ircobi Conference, 435-438, 2005

## APROSYS European In-Depth Pedestrian Database

CE Neal-Sturgess<sup>1</sup>, E. Carter<sup>1</sup>, R. Hardy<sup>2</sup>, R. Cuerden<sup>3</sup>, L. Guerra<sup>4</sup>, J. Yang<sup>5</sup>.

1 Birmingham Automotive Safety Centre (BASC)

2 Cranfield Impact Centre (CIC)

3 TRL Ltd Crowthorne

4 INSIA UPM

5 Chalmers University

Page No. 07-0177

### Abstract:

The EU FP 6 Integrated Project on Advanced Protection Systems (APROSYS) is exploring the relevance of vehicle pedestrian protection systems in the real world. A pedestrian injury database was compiled of in-depth information to permit reconstructions of the pedestrian/ cyclist/ vehicle/ground interactions.

The database consisted of 63 pedestrians cases and 7 cyclist cases. Results were obtained on: injury risk as related to impact speed; the locations of primary head impacts with vehicles; the proportion and frequency of ground impacts; and the over representation of elderly fatals with MAIS3. It is concluded that (i) the head impact locations for pedestrian protection need to be reviewed to include the windscreen, A pillars and scuttle areas, and (ii) a calibration of MAIS and ISS against fatality/non fatality for a large sample of pedestrians is necessary, with children / adults/elderly (>60 years of age) ranked separately.

## INTRODUCTION

In order to compile a number of detailed Vulnerable Road User (VRU) pedestrian and cyclist accident cases from around Europe containing sufficient detail for computer reconstruction work, an in-depth database (IDD) was developed in MS Access. The cases were compiled from five different sources from four different countries (the UK, Spain, Germany and Sweden).

## ANALYSIS

The database contents are summarised here and some of the variables are compared with the UK pedestrian accident epidemiology (1997 – 2001) [1] to gauge how well the reconstruction cases represented that population, since 90% of in-depth cases were pedestrian and 70% of the cases came from the UK. Some German In Depth Accident Study (GIDAS) data is also used for comparison for some variables not available

in the UK epidemiology. Despite the relatively small sample size, the database yielded some interesting observations on variables not available from the epidemiological studies – particularly concerning injury body region, severity and head impact location on the vehicle, and age versus injury outcome. Statistical tests were carried out where applicable to determine significance.

| Vulnerable Road User type | No. of in-depth cases | % of in-depth cases | % of total UK VRU accidents |
|---------------------------|-----------------------|---------------------|-----------------------------|
| Pedestrians               | 63                    | 90%                 | 66.5%                       |
| Cyclists                  | 7                     | 10%                 | 33.5%                       |

| Gender  | No. of in-depth cases | % of in-depth cases | % of total UK pedestrian accidents |
|---------|-----------------------|---------------------|------------------------------------|
| Male    | 39                    | 56%                 | 58%                                |
| Female  | 28                    | 40%                 | 42%                                |
| Unknown | 3                     | 4%                  | 0%                                 |

## Pedestrian Orientation

In the in-depth sample, 89% of the pedestrians were hit on either the right (41%) or left side (48%). The observation that most of the pedestrians in the sample were struck side-on is in agreement with the literature [2]

## Age

The age of the victim was known for 64 out of the 70 cases. Since the BASC cases were all fatal, they had a higher proportion of older pedestrians than the population (which includes all severity pedestrian accidents), but this was balanced by the other data sources which mostly provided serious but non-fatal cases. The frequency analysis of the in-depth sample resulted in the same mode [1] but found that it was over-represented in the older age categories (mainly due to the UK fatal contribution)

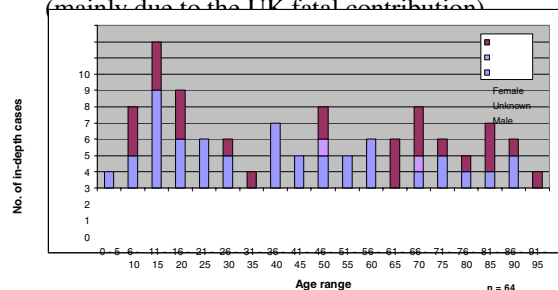


Figure 1- In-depth sample: Age of vulnerable road user

### Age vs. Severity

According to several studies and the UK pedestrian epidemiology, the chances that a pedestrian will receive fatal injuries from an accident increases with age. This pattern is less obvious but still apparent in the in-depth sample, Figure 2 for which fatal accidents were over-represented as explained previously.

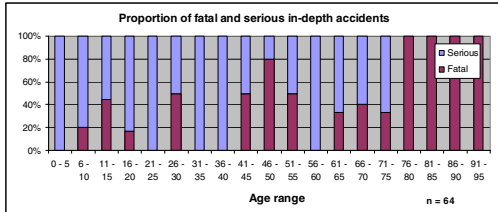


Figure 2- In-depth sample: Age vs. severity (proportion)

Table 3 – Age vs. severity (comparison with epidemiology)

|                   | Mode (all severities) | Mode (fatal) | Mode (serious) |
|-------------------|-----------------------|--------------|----------------|
| In-depth sample   | 11 – 15               | 81 – 90      | 11 – 20        |
| UK ped. accidents | 11 – 15               | 71 – 80      | 11 – 20        |

This comparison Table 3 shows the in-depth database to be a reasonably good representation of the epidemiology with respect to age vs. severity.

Table 4 – Age vs. severity (in-depth cases)

|                | Age (years) |        |     |     |      |
|----------------|-------------|--------|-----|-----|------|
|                | Mean        | Median | Min | Max | SD   |
| Fatal (n=27)   | 56.2        | 61.0   | 10  | 94  | 27.6 |
| Serious (n=37) | 34.5        | 28.0   | 5   | 75  | 22.1 |

In Table 4 the difference in mean age between serious and fatal accidents is 22.6 years. This difference is highly significant ( $p < 0.01$ ).

### Vehicle details

The year-of-manufacture frequency Figure 3 shows the distribution of ages of the vehicles involved. Although the average age is relatively low (1995), which is mainly a reflection of the age of the European fleet, half of the in-depth cases involve vehicles manufactured in 1997 or later, but with a large range.

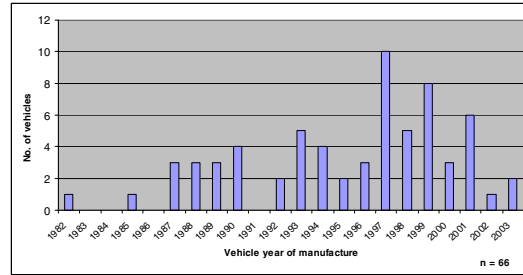


Figure 3 – In-depth sample: Vehicle year of manufacture

### Impact speed

Figure 4 below compares the in-depth sample impact speeds with those found in the GIDAS sample. The in-depth sample (mean impact speed of 40km/h) tended to have higher impact speeds than the GIDAS sample (approximate mean impact speed of 28 km/h). This is a consequence of having a disproportionate number of fatal and serious accidents, which are more likely to be the result of higher speed impacts.

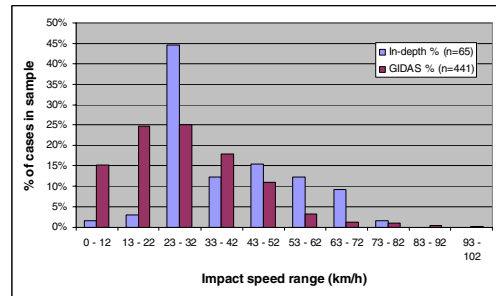


Figure 4 – Comparison with GIDAS data

### Impact speed vs. injury severity

Previous work [3] has established the significant relationship between impact speed and pedestrian injury severity. This relationship is presented for the current study using 3 different definitions of injury severity: fatal / non-fatal, MAIS (Maximum AIS) and ISS (Injury Severity Score).

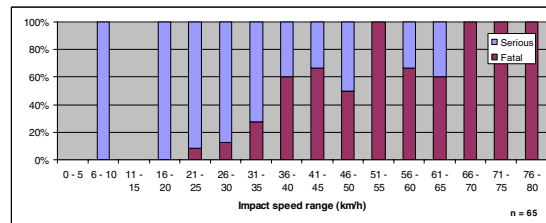


Figure 5 – In-depth sample: Impact speed vs. severity (proportion)

**Table 5 – Impact speed vs. severity**

|                       | Impact speed (km/h) |        |      |      |      | % of accid. at ≤ 40km/h |
|-----------------------|---------------------|--------|------|------|------|-------------------------|
|                       | Mean                | Median | Min  | Max  | SD   |                         |
| <b>Serious (n=39)</b> | 32.6                | 30.0   | 8.0  | 64.4 | 12.1 | 79%                     |
| <b>Fatal (n=26)</b>   | 49.3                | 49.1   | 25.0 | 75.6 | 13.3 | 31%                     |

The difference between the mean impact speeds for serious and fatal accidents is 15.9km/h. This difference is highly significant (p<0.01).

The approximate proportion of serious accidents occurring at impact speeds of less than 40km/h is  $0.79 \pm 0.13$  at a 95% confidence level (p<0.05). The approximate proportion of fatal accidents occurring at impact speeds of less than 40km/h is  $0.31 \pm 0.13$  at a 95% confidence level (p<0.05). The difference between these proportions is highly significant (p<0.01).

**Table 6 – Impact speed vs. MAIS (n=66)**

| MAIS              | Impact speed (km/h) |        |      |      |      | Accidents at ≤ 40km/h (%) |
|-------------------|---------------------|--------|------|------|------|---------------------------|
|                   | Mean                | Median | Min  | Max  | SD   |                           |
| <b>2 (n=24)</b>   | 30.3                | 28.0   | 20.0 | 56.3 | 9.0  | 88                        |
| <b>3 (n=23)</b>   | 44.8                | 49.0   | 8.0  | 70.8 | 16.8 | 39                        |
| <b>4 (n=7)</b>    | 46.3                | 40.2   | 22.5 | 75.6 | 17.1 | 57                        |
| <b>5 (n=11)</b>   | 42.8                | 41.0   | 27.4 | 62.8 | 10.3 | 46                        |
| <b>2-3 (n=47)</b> | 37.4                | 32.2   | 8.0  | 70.8 | 15.1 | 64                        |
| <b>4-5 (n=18)</b> | 44.1                | 40.6   | 22.5 | 75.6 | 13.4 | 50                        |

The difference between the mean impact speeds for MAIS 2-3 accidents and MAIS 4-5 accidents is 6.6km/h. This difference is not significant (p>0.05).

88% of MAIS 2 accidents occurred at speeds of less than or equal to 40 km/h. To extend this to the population with a 95% confidence level, the proportion of MAIS 2 accidents occurring at speeds ≤ 40km/h would be approximately between 75% and 100% (p<0.05). It can also be estimated that approximately 51% - 77% of MAIS 2-3 accidents would occur at speeds of ≤ 40km/h (p<0.05).

Due to the very low number of MAIS 4 accidents, both MAIS 4 and MAIS 5 accidents are presented together in Figure 6. The majority

(63%) of MAIS 2 cases were at impact speeds of between 21 and 30km/h. Less conclusively, the speed range mode for MAIS 3 cases was 31 – 40 km/h and for MAIS 4 – 5 cases, 62% were within a broader range of 31 – 50 km/h. The MAIS 2 distribution is more ‘normal’ and has a relatively low Standard Deviation (SD) of 9 whereas the MAIS 3 and MAIS 4-5 do not demonstrate a good normal distribution curve and have significantly spread (as shown in Table 6 above).

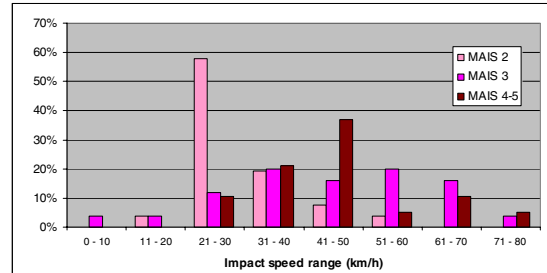


**Figure 6 – Impact speed vs. MAIS**

**ISS vs. impact speed**

The Injury Severity Score (ISS) was presented in 1974 [4] as a method of numerically describing the overall injury severity of patients with injuries to more than one area of the body. It could be argued that since pedestrian fatalities in particular are often caused by multiple injuries as opposed to one single injury, ISS would be a more meaningful representation of the severity of such accidents. In order to test this hypothesis with respect to the current study, the relationship between ranges of ISS scores and their corresponding impact speed was observed (Figure 7). Looking at each ISS range in Figure 7, a tendency to more normal distributions can indeed be seen than those for MAIS vs. impact speed.

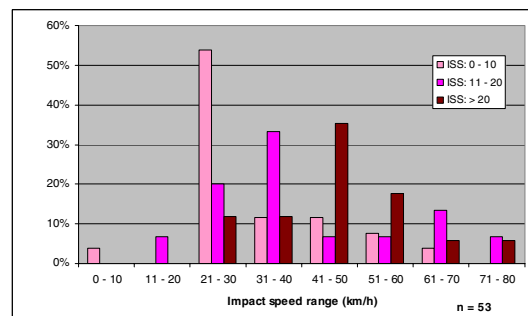


**Figure 7 – Impact speed vs. ISS**

### Probability of injury vs. impact speed

Figure 8 shows a comparison between injury severity and impact speeds for pedestrian injuries from studies spanning 26 years, from Ashton and Mackay [5] Anderson,[6] Hannover [7] and now the current study (APROSYS 2005). The curves drawn are for the relationship:

$$\text{Probability of Injury} \propto V^3$$

From Neal-Sturgess [8] where it is shown that pedestrian injuries can be correlated with impact speed using the concept of Peak Virtual Power.

The trends in the data show that the APROSYS results correlate well with the previous results for serious injuries. For fatal injuries, the APROSYS results are closer to the Hannover results for 2001, indicating that the impact speed for fatalities may be increasing slightly compared to that for the data from 1979 and 1995.

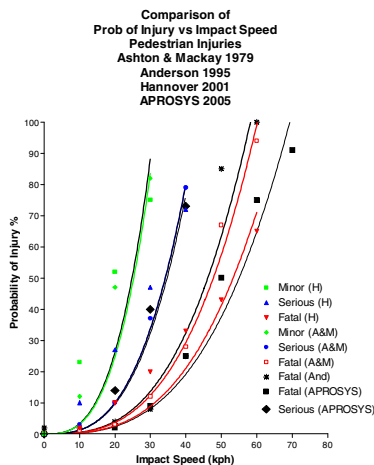


Figure 8 - Probability of injury vs. impact speed

### Vehicle braking

Table 7 – In-depth sample: vehicle braking (n=62)

|              | No. of cases (%) |
|--------------|------------------|
| Hard braking | 10 (16)          |
| Some braking | 26 (42)          |
| No braking   | 26 (42)          |

The braking behaviour of vehicles in the sample as presented in Table 7 is comparable with the

braking deceleration found in the GIDAS database.

### Injury severity

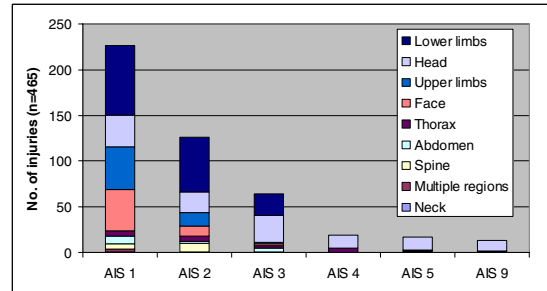


Figure 9 - No. of injuries at each level of severity

Table 8 – Gender vs. severity

| Gender        | Minor injuries (AIS 1, 2) | Serious injuries (AIS 3+) | All injuries |
|---------------|---------------------------|---------------------------|--------------|
| Male (n=39)   | 198 (78%)                 | 49 (19%)                  | 254          |
| Female (n=28) | 137 (71%)                 | 50 (26%)                  | 193          |
| Unknown (n=3) | 17 (94%)                  | 1 (6%)                    | 18           |
| Total (n=70)  | 352 (76%)                 | 100 (22%)                 | 465          |

The number of injuries of a given severity are shown in Figure 9, and the Gender breakdown in Table 8. Males had a mean of 6.5 injuries and females a mean of 6.7 injuries. The females in the sample tended to have more serious injuries, but this could have more to do with the fact that a higher proportion of VRU's over the age of 60 were female.

Table 9 – VRU type vs. severity

| VRU type          | Minor injuries (AIS 1, 2) | Serious injuries (AIS 3+) | All injuries |
|-------------------|---------------------------|---------------------------|--------------|
| Pedestrian (n=63) | 316 (75%)                 | 94 (22%)                  | 423          |
| Cyclist (n=7)     | 36 (86%)                  | 6 (14%)                   | 42           |

Cyclists had a mean of 5.8 injuries and pedestrians a mean of 6.6 injuries. Also, cyclist injuries tended to be less serious, although the sample size is too small to make inferences about the population.

An analysis of the IDD for ISS gave Figure 10 as shown below. It is to be expected that the injury severity will increase towards the upper right hand quadrant, but the clear demarcation shown here is probably an artifact of the small sample

size. Nonetheless there are only 1-3 (1-3/23) fatalities below an impact velocity of 32 km/h, which equates to 20 miles/h, and is in accord with Figure 8. Also it can be seen that there are no fatalities below an ISS of around 10. The threshold of an ISS of 16, which is supposed to equate to a 10% risk of fatality Robertson & Redmond, 1991[9] ; Seow and Lau, 1996 [10] is also shown, but here it coincides with a risk of  $8/23 = 35\%$  risk of fatality. There already is some concern in the literature that even for large sample studies ISS shows some sample bias Henary et.al [11], and here it seems that the normal large vehicle occupant sample ISS limit does not accord with these results.

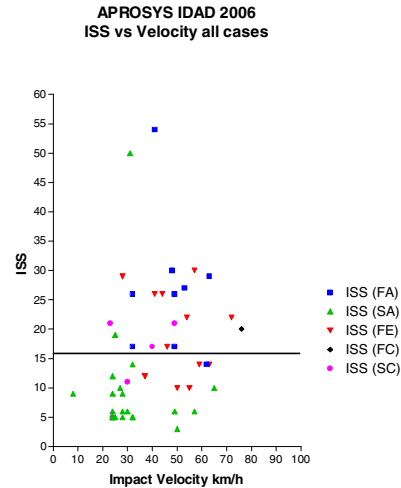


Figure 11.

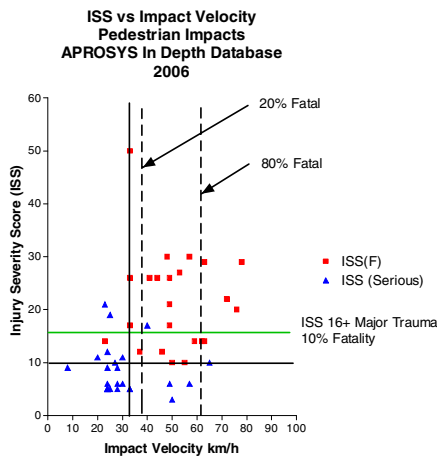


Figure 10.

The statistics are:

Fatals ISS: mean = 21.6 N=23

Standard deviation = 9.5

Serious ISS: mean = 8.1 N=19

Standard deviation = 4.6

These results are statistically significantly different  $p < 0.0014$ .

Examining the ISS scores for all types of case in the database child (<12 years old), adult fatal and serious, and elderly fatal and serious gives Figure 11. From Figure 11 it can be seen that the ratio of elderly fatalities below ISS = 16 is  $5/12 = 42\%$ , whereas the ratio of adult fatalities below ISS = 16 is  $1/9 = 11\%$ , which are in the same rank order as Henary et.al. [11] with 5/27 seniors and 0/28 adults respectively. Again the results are skewed here due to the nature of the sample.

### Injury severity by body region

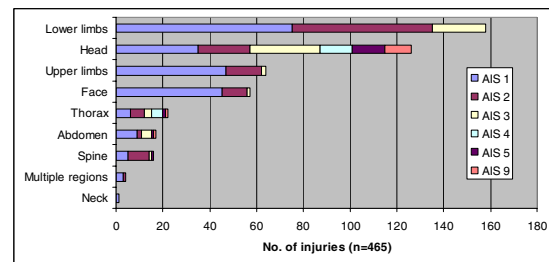


Figure 12– Injuries per body region (In-depth database 1997 - 2004)

The most frequently injured body regions are the head and lower limbs. However, a higher proportion of the head injuries are AIS 3+ compared with the lower limb injuries. In AIS and consequently in the current study, the face is treated as a separate body region. In a similar earlier study done at Hannover (Figure 20) [12] on accidents from 1985 - 1995, facial injuries are considered together with head injuries and consequently head injuries outnumber lower limb injuries. Accounting for this difference in methodology, the results are in agreement with the exception of the different relative proportion of injuries to the thorax and upper limbs in the two studies. This could be explained by the influence of the changing shape of vehicles on injured body regions since the earlier study.

The injury severity is also plotted against the contact zone on the vehicle in Figures 13 to 19 below. When reading these Figures, the table on the left hand side is the relative frequency of all

the injuries recorded in the database, whereas the numbers in the boxes on the arrows are the relative frequencies of injuries where the contact location was identified. There are a significant number of injuries recorded in the database for which no contact location was identified, hence the percentages are generally different.

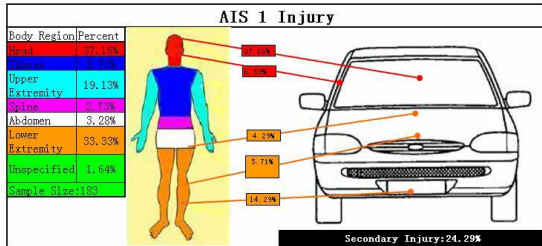


Figure 13.

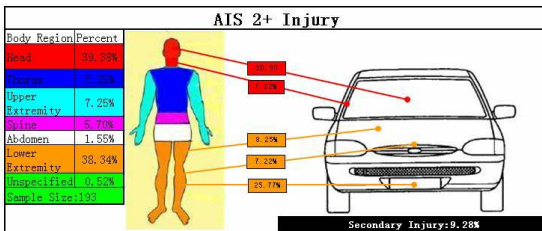


Figure 14.

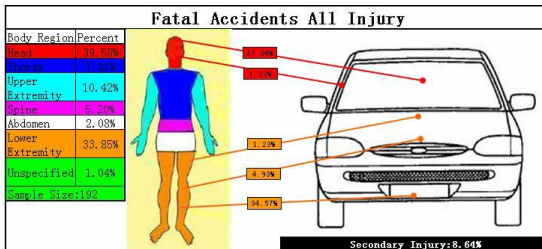


Figure 15.

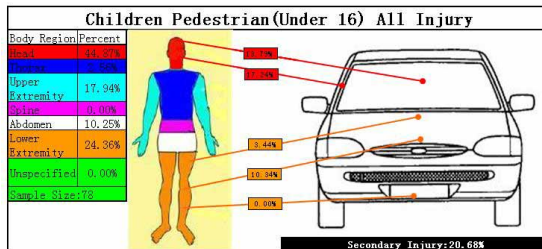


Figure 16.

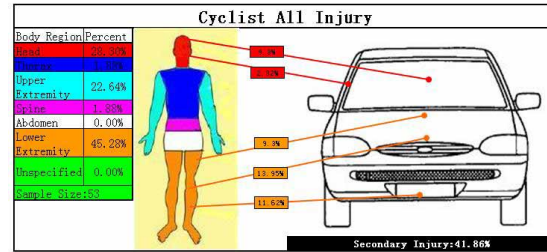


Figure 17.

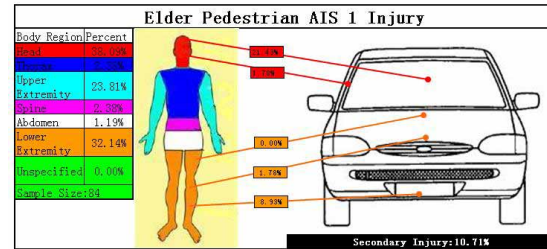


Figure 18.

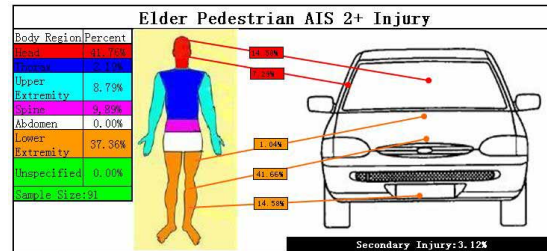


Figure 19.

The results from this study are compared to Otte and Pohlemann [13] Figure 20 below.

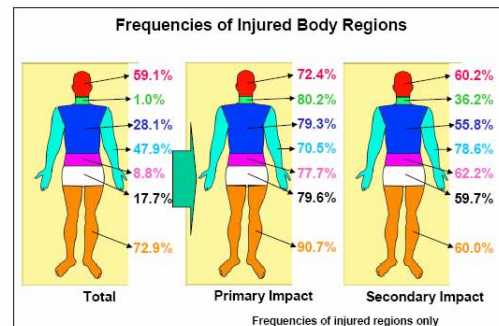


Figure 20.

From Figs. 13 to 19, and a comparison with Figure 20, it can be seen that the frequencies of the injuries to the body regions are broadly comparable in the two studies. The head and lower extremities are the most frequently injured regions, and the frequencies of the secondary impacts decrease as the severity of the injuries increase.

## Head impact location

The locations of head impacts for all the cases were plotted schematically on one standard vehicle – similar to the representation of Otte’s 1999 IRCOBI paper [7]. Head impact locations have been plotted in their relative positions as opposed to absolute positions for the sake of comparing accidents involving different shaped vehicles (i.e. a head impact occurring on the top left corner of the windscreen will be shown on the top left corner of the windscreen in the diagram regardless of what the WAD is).

As shown in Figure 21, the fatal head impacts occurred predominantly on and around the windscreen frame (A-Pillars and scuttle). The only impacts occurring in the centre of the windscreen were non-fatal. Of the 3 head impacts occurring on the bonnet away from the scuttle, all were non-fatal and 2 were children.

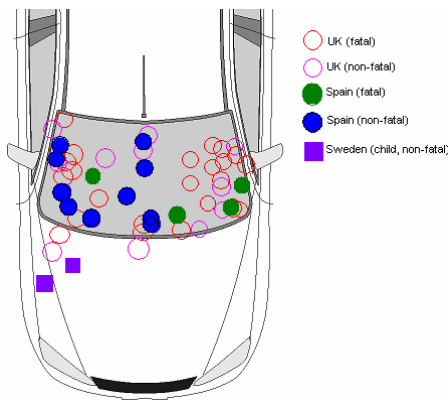


**Figure 21 – Head impact locations by severity and country.**

The head impact positions were also plotted and coloured according to which country the accident occurred in to see if impacts occurred on a certain side for left-hand and right-hand drive countries respectively - i.e. right-hand drive for UK, left-hand drive for Mainland Europe (Spain and Sweden) (Figure 21). There is a broad trend for more serious head strikes to occur on the side of the vehicle nearest the kerb.

## Secondary Impact

Of interest in this project is the significance of the secondary ground impact. This is a difficult parameter to assess, as the vast majority of pedestrian and cyclist collisions ultimately result in the victim lying on the ground. An analysis of

the database was conducted to see what evidence it contained, the results are shown below.

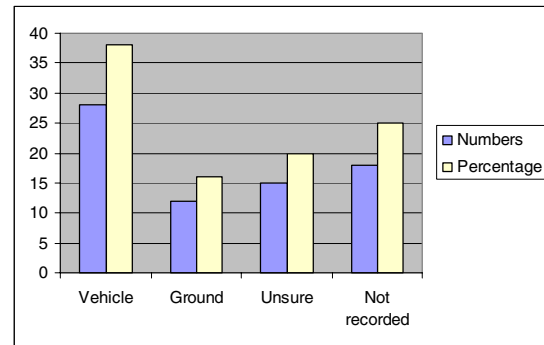


**Figure 22. Percentages of injury sources**

It is obvious from the Figure 22 that in 18 cases no information was recorded, and so there is a large margin of uncertainty. In this sample the percentage of the most serious injuries arising from the secondary ground impact are around 43% of the injuries ascribable to the vehicles. This is slightly lower, but of the same order as GIDAS, who give a percentage of around  $463/933 = 49\%$  of injuries caused by the secondary impact [13].

A summary table of the results displayed in Figs 13 to 19, is shown below:

| <b>Pedestrians</b>     |                         |                           |                        |
|------------------------|-------------------------|---------------------------|------------------------|
| <b>Injury Severity</b> | <b>Primary Impact %</b> | <b>Secondary Impact %</b> | <b>Ratio Pri./Sec.</b> |
| All                    | 68                      | 16                        | 4.25                   |
| AIS1                   | 68                      | 24                        | 2.8                    |
| AIS2+                  | 79                      | 9                         | 8.8                    |
| Serious ALL            | 62                      | 22                        | 2.8                    |
| Fatal All              | 80                      | 9                         | 8.9                    |
| Child All              | 45                      | 21                        | 2.1                    |
| Elderly All            | 78                      | 12                        | 6.5                    |
| Elderly AIS1           | 34                      | 11                        | 3.1                    |
| Elderly AIS2+          | 79                      | 3                         | 26.3                   |
| <b>Cyclists</b>        |                         |                           |                        |
| All                    | 48                      | 42                        | 1.1                    |

**Table 10.**

From table 10 it can be seen that in general for all categories of cases the secondary impacts are a larger proportion of the injuries for categories of lower injury severity. The primary impact

appears particularly important for the elderly victims. Secondary impacts appear more significant for children than adults, and particularly important for cyclists; although the sample for the cyclists is very small. However, caution is necessary when interpreting the frequency tables. A case by case analysis here (Table 11 below) shows that often the severity of the secondary impact is equal to the primary impact.

| Relative severity of primary and secondary impacts |          |                |                      |
|--|----------|----------------|----------------------|
| Case No in IDD                                     | Severity | MAIS in Impact | AIS Secondary Impact |
| BC001  | fatal    | 3              | 3                    |
| BP001  | fatal    | 3              | 3                    |
| BP002  | fatal    | 5              | 5                    |
| GC001  | serious  | 2              | 2                    |
| GC002  | serious  | 2              | 2                    |
| IP007  | serious  | 3              | 3                    |
| GP002  | serious  | 3              | 3                    |
| OC002  | serious  | 2              | 2                    |

Table 11.

### Elderly Fatal Pedestrians

The elderly cases were extracted to give Figure 23 shown below. From Figure 23 it is obvious that there are a large proportion of elderly casualties dying at low ISS scores (5/12). This should be compared to the study by Henary et.al [11] who reported 5/27 elderly deaths with ISS < 16. Following through on this possible anomaly it is necessary to consider the injury severities and frequencies in the various parts of the IDD, such as comparing the frequencies of adult and elderly of injury severity. The mortality rate for the elderly was almost three times that for the adults (100% cf. 37.5%), which again is similar to Henary et.al. [11], but here this was obviously influenced by the nature of the sample.

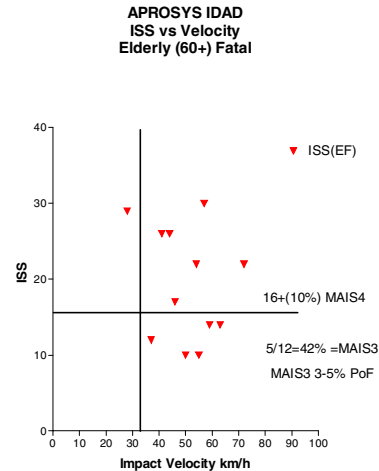


Figure 23.

From the IDD the Adult Fatal cases are as shown in the table below;

| Adult Fatal |             |      |     |
|-------------|-------------|------|-----|
| Vel. km/h   | Body Region | MAIS | ISS |
| 53          | H           | 3    | 27  |
| 48          | H           | 5    | 30  |
| 49          | H           | 3    | 17  |
| 62          | H           | 3    | 14  |
| 63          | H           | 5    | 29  |
| 41          | H           | 5    | 54  |
| 32          | T           | 4    | 17  |
| 49          | H           | 5    | 26  |
| 32          | H           | 5    | 26  |

Table 12.

Key for body region: H = Head, T = Thorax, S = Spine, P = Pelvis, E = Extremity.

From Table 12 it is evident that the proportions of the various injury severities are MAIS3 = 3/9 = 33%, MAIS4 = 1/9 = 11%, and MAIS5 = 5/9 = 66%. The body regions are Head 8/9 = 88%, and Thorax 1/9 = 11%. The table of Elderly Fatals is shown below:

| Elderly Fatal |             |      |     |
|---------------|-------------|------|-----|
| Velocity km/h | Body Region | MAIS | ISS |
| 54            | S/H         | 3    | 22  |
| 55            | P           | 3    | 10  |
| 37            | E           | 2    | 12  |
| 57            | S/H         | 5    | 30  |
| 72            | H           | 3    | 22  |

|    |     |   |    |
|----|-----|---|----|
| 28 | H   | 4 | 29 |
| 63 | H   | 3 | 14 |
| 41 | H   | 5 | 26 |
| 59 | E   | 3 | 14 |
| 46 | S/H | 3 | 17 |
| 50 | H   | 3 | 10 |
| 44 | H   | 5 | 26 |

Table 13.

From Table 13 it is evident that the proportions of the various injury severities are MAIS2 = 1/12 = 8%, MAIS3 = 7/12 = 58%, MAIS4 = 1/12 = 8%, and MAIS5 = 3/12 = 25%. Whereas the body regions are head (including cervical spine) 9/12 = 75%, extremities 2/12 = 16% and Pelvis 1/12 = 8%. A body region analysis for the elderly fatals gives Figure 28 shown below.

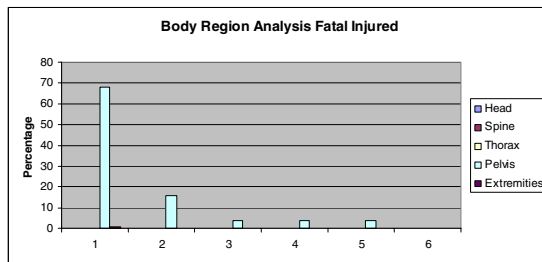


Figure 24.

From both Tables 12 and 13 and Figure 24 the body region overwhelming associated with the primary cause of death is the head. It is often thought that one of the confounding factors in elderly deaths after road traffic accidents (RTA's) is the length of stay in hospital, and hence the increased risk of secondary infection. To examine this the time-to-die was investigated, this is not necessarily the time in hospital, but it is believed to be an acceptable surrogate. Of the data in the database there were 15 instances of fatal injuries where the time to die was not recorded, which heavily reduced the number of valid entries; the valid entries are shown in Tables 14 and 15. Note that the numbers in these tables are not necessarily the same as in other categories of analysis, because the missing data may be either, gender, age, time to die, or ISS value. Two cases where the time-to-die was 100 and 150 days respectively were omitted from the analysis as they do not conform to the definition of death ( $\leq 30$  days) used for the rest of the analyses.

| Time to Die – Elderly (>60) |                       |           |           |           |
|-----------------------------|-----------------------|-----------|-----------|-----------|
| Days                        | 0                     | 2         | 13        | 14        |
| N                           | 6                     | 1         | 1         | 1         |
| MAIS (ISS)                  | 2<br>(12)             | 3<br>(10) | 2<br>(12) | 5<br>(26) |
|                             | 3xMAIS3<br>(22,14,17) |           |           |           |
|                             | 3xMAIS4<br>(29,21,24) |           |           |           |

Table 14.

| Time to Die - Adult (12<Y<60) |                       |        |
|-------------------------------|-----------------------|--------|
| Days                          | 0                     | 30     |
| N                             | 5                     | 1      |
| MAIS (ISS)                    | 3 (27)                | 4 (NC) |
|                               | 4                     |        |
|                               | 3xMAIS5<br>(30,54,26) |        |

Table 15.

There are too few entries to form significant conclusions, but it appears that, in this sample, the majority of the casualties were declared either dead at the scene or on arrival in the hospital. The elderly do show a number of intermediate stays in hospital, however the sample is small, whereas the adults show just one outlier at 30 days.

To compare the incidence of the injury severities in the IDD it is necessary to consider the frequencies of injury severities in a large population study. No large sample studies of pedestrians for the calibration of MAIS yet exist, therefore a study of CCIS Phase 6 & 7 1999 - 2005 (Neal-Sturgess and Hassan, BASC Report 2006 [14]) for vehicle occupants is taken as representative of large sample calibration of MAIS, as an example for comparison. It should be remembered that the injury data taken for the calibration of HIC i.e. Prasad-Mertz [15] is taken from vehicle occupant studies. In the study conducted here the cases were selected on the basis of belted passenger car occupants with a valid Estimated Test Speed (ETS) [a measure of impact speed], to maximize the sample size. The frequency table is as shown below:

Belted drivers in passenger cars – known ETS  
(kph)

| CCIS 1999 – 2005 |       |               |         |
|------------------|-------|---------------|---------|
| MAIS             | Fatal | Total Injured | % Fatal |
| 1                | 0     | 745           | 0.0     |
| 2                | 1     | 202           | 0.5     |
| 3                | 7     | 112           | 6.2     |
| 4                | 17    | 25            | 68.0    |
| 5                | 19    | 23            | 82.6    |
| 6                | 4     | 4             | 100.0   |
| Totals           | 48    | 1111          |         |

Table 16.

Further considering fatalities at a given MAIS value as a ratio of total fatalities, to account for frequency effects in a sample of fatalities, gives:

Belted drivers in passenger cars – known ETS  
(kph)

| CCIS Fatalities |       |                     |
|-----------------|-------|---------------------|
| MAIS            | Ratio | Percentage of Total |
| 1               | 0     | 0.0                 |
| 2               | 1/48  | 2.1                 |
| 3               | 7/48  | 14.6                |
| 4               | 17/48 | 35.4                |
| 5               | 19/48 | 39.6                |
| 6               | 4/48  | 8.3                 |
| Total           |       | 100.0               |

Table 17.

Comparing the significance of the frequency of the injury severities between the IDD and CCIS gives the following table:

| Significance levels CCIS vs IDD |                                     |  |
|---------------------------------|-------------------------------------|--|
| MAIS                            | Fatalities Adult                    | Fatalities Elderly   |
| 1                               | 0                                   | 0  |
| 2                               | 0                                   | Chi-square = 1.051 not significant.  |
| 3                               | Chi-square = 1.168 not significant. | Chi-square = 5.353<br><i>p</i> <= 0.025.<br>The distribution is significant. |
| 4                               | Chi-square = 1.240 not significant. | Chi-square = 2.08 not significant.   |
| 5                               | Chi-square = 0.300 not significant. | Chi-square = 0.436 not significant.  |
| 6                               | 0                                   | 0  |

Table 18.

From Table 18 it can be seen that for the categories of Elderly Fatalities the incidence of MAIS3 is very significant compared to the CCIS sample i.e. *p* < 0.025%.

## DISCUSSION

The in-depth database of pedestrian and cyclist developed for the reconstruction activity was analysed to assess whether or not it was representative of the European epidemiology. Data for which a reasonably direct comparison was possible included type, age and gender of the vulnerable road user, and also the relationship between age and severity. Cyclists were not well represented – only 7 cases were available which allowed few conclusions to be drawn about the characteristics of cycling accidents or injured cyclists. The younger age ranges (under 30) were represented in proportion with the epidemiology but the older age ranges were slightly over-represented (explained by the BASC contribution of all-fatal accidents and the higher proportion of older people in this category), male and female were well represented. When comparing age and severity, the general trend of increased age leading to increased risk of fatality could be seen to some degree in Figures 1 and 2. The difference in mean age of those seriously injured and those fatally injured was found to be statistically significant (Table 4). An assessment of the vehicles represented by the sample was more reflective of the fleet than any prevalence for a particular age or make of vehicle to be involved in a VRU collision. The average year of manufacture was 1995 but half the vehicles were 1997 or later.

The standing orientation of the pedestrian prior to impact was 89% stuck side-on – which agreed with the literature.[16] The in-depth sample impact speeds were presented and compared with those found in the GIDAS sample (Figure 4). The former tended to have higher impact speeds than the latter (mean of 40km/h and 28km/h respectively) - a consequence of having a disproportionate number of fatal and serious accidents which are more likely to be the result of higher speed impacts. The relationship between impact speed and injury severity was presented using 3 different definitions of injury severity: fatal / non-fatal, MAIS (Maximum AIS) and ISS (Injury Severity Score). The

difference between the mean impact speeds for serious and fatal accidents was highly significant. The MAIS vs. impact speed relationship, presented and discussed in detail in the main section, was found to be quite non-linear with an anomaly at MAIS 4. As expected, a better relationship was found between ISS and impact speed due to better suitability of this description of injury severity to the multiple injury nature of VRU accidents. There is a good correlation between the injury risk curves for serious injuries vs. impact speed derived from the current study and those from similar studies. For fatal injuries, the APROSYS results are closer to the 2001 study,[13] indicating that the impact speed for fatalities may be increasing slightly compared to that for the data from 1979 [5] and 1995 [6]. The mean impact speed of vehicles which braked before impact and those which did not was compared but no significant difference was found.

For each case, detailed injuries were recorded (total n=458). Lower limb injuries were most common followed closely by head injuries. Facial injuries were considered separately according to AIS protocol – if considered as one body region, the most common injury region would be the head as found by an earlier study [7]. Also interesting to note is that out of 458 injuries, only 1 was to the neck, AIS 1. Looking at AIS 4- 5 injuries only, the thorax is the next most significant region after the head, but including AIS 3 injuries, the upper limbs become the next most significant region after the head, followed by the thorax.

The head impact locations for all impacts were plotted schematically on one generic vehicle diagram, showing the positions of primary head impact relative to the windscreen, scuttle and A-Pillars for fatal and non-fatal impacts (Figure 21). The fatal head impacts occurred predominantly on and around the windscreen frame (A-Pillars and scuttle). The only impacts occurring in the centre of the windscreen were non-fatal. Of the 3 head impacts occurring on the bonnet away from the scuttle, all were non-fatal and 2 were children. The head impact positions were also plotted according to which country the accident occurred in the see if impacts occurred on a certain side for left-hand and right-hand drive countries respectively - i.e. right-hand drive for UK, left-hand drive for Spain and Sweden (Figure 21). All 13 non-fatal head impacts in Spain and Sweden were located on or

to the right of the windscreen centre-line, but the 3 remaining Spanish fatal head impacts did occur on the left side. The UK head impacts had only a slight skew towards the left side of the windscreen centre-line. Together, this does suggest that head impacts are slightly more common on the nearside of the vehicle.

The analysis of ground impact in this study, although subject to uncertainty due to the variables not being recorded in a number of cases, it was found that the injury severity from the ground impact was generally less frequent than the injury severity attributed to the vehicle, which is similar to recent analyses in the literature. However, a case by case study showed that the injury severity in the secondary impact can be similar to that in the primary impact. A recent study was conducted by Hannover University to address this specific issue [13]. Secondary injuries were found to be less severe - for example, 36% of the pedestrians received a head injury due to secondary impact compared with 43% due to primary impact, a greater proportion of which were AIS 2+. However, secondary impacts were still significant with over 2/3 (65%) of the pedestrians in the study received some kind of injury from the road. Both the Pedestrian Crash Data Study (PCDS) and the Pedestrian Injury Crash Study (PICS) conducted in the US [17-19] and Australia [20] found that most injuries caused by the environment (i.e. the road and roadside objects) were minor and that the more recent accidents involving newer cars had a much lower proportion of injuries caused by the road. A review of the literature by McLean et al [21] concluded that pedestrian injuries caused by impact with the environment were less severe than those caused by direct contact with the vehicle and in a later in-depth study of 77 cases by the same authors [22], analysis showed that while the environment was the most common cause of head injuries in general, it was not the cause of any serious head injuries (AIS 3+). Although this contradicts Otte's findings for all-severity head injuries (i.e. that the vehicle was the more common cause of head injuries in general), they are in agreement on the point that the vehicle was usually the cause of the serious head injuries. This agrees with earlier work by Ashton et al [23] that found that a head impact with the car is more likely to be the cause of significant brain injury to a pedestrian than contact with the road surface, although this does involve much older vehicle designs. This topic

is complex and requires further study, as the proportion of pedestrian/cyclist injuries from the ground (environment) represents the injuries that cannot be influenced by vehicle design, and so the base-line of injuries that cannot be reduced.

It is now generally acknowledged that the energy required to cause an injury reduces as a person ages Augenstein, 2001 [24], and older drivers are more vulnerable to injury in a crash. Their skeletal structures are more easily damaged, and the consequences of any assault are likely to be more serious compared with younger drivers (Dejeammes and Ramet, 1996 [25]; Evans, 1991 [26]; Mackay, 1989 [27]; Viano et al, 1989 [28]). The influence of osteoporosis particularly on females is now well established (Berthel, 1980 [29]). Dejeammes and Ramet, 1996 [25] concluded that the most elderly population could withstand a chest load of 5,000N, whilst the younger population could withstand a chest load of 8,000N. The implications of this are that older occupants may be several times more likely to sustain a life threatening chest injury (Padmanaban, 2001 [30]), and this can occur in a relatively moderate crash [24]. A study by Morris et.al AAAM 2002 [31] and Welsh et.al. 2006 [32]. found that skeletal injuries to the elderly were the major difference compared to a younger population, and that the major contact injuries were seat belt induced multiple rib fractures. This indicates the need for intelligent restraints and the BOSCOS project (Watson and Hardy 2006 [33]) aims to mitigate these age related injuries by bone scanning and automatic adjustment of restraints to compensate for increased fragility. Pedestrian-motor vehicle trauma affects all age groups, and the results from several epidemiological studies have indicated that the annual pedestrian mortality is substantially higher among seniors than any other age group (Aronson et al., 1984 [17]; Ashton et al., 1979 [23]; Harruff et al., 1998 [18]; Hoxie et al., 1994 [34]; Knoblauch et al., 1995 [19]; NHTSA, 2001 [35]; Oxley & Fildes, 1996 [36]). In addition to the increased exposure, a number of epidemiological studies have indicated that senior pedestrians also are more likely to get killed or severely injured once involved in a crash [37]. Kong et al. 1996 [38] conducted a retrospective review of 273 pedestrian victims from 1991 to 1994. They reported significantly ( $p < 0.05$ ) higher average ISS (11.6 vs. 8.8) and mortality (13 percent vs. 5 percent) for the senior (age  $\geq 60$  years), than for

the adult (age 16–59 years) victims. Kong's results were confirmed by Peng and Bongard 1999 [39]. The most recent statistics from NHTSA on the morbidity and mortality of various age groups of pedestrians indicate that the mortality for the senior (age  $\geq 60$  years) pedestrian victims in the United States during 2003 was approximately 12.9 percent, which was twice as high as for the corresponding adult (age 19–50 years) group (NHTSA, 2005 [40]). A recent study by Henary, Ivarsson, and Crandall [11] compares the morbidity and mortality of senior (age  $\geq 60$  years) and adult (age 19–59 years) pedestrian victims while controlling for other confounding factors that may influence this relationship. They used the NASS Pedestrian Crash Data Study (PCDS) database for a cross-sectional study to compare the outcome of senior (age  $\geq 60$  years) and adult (age 19 to 59 years) pedestrian victims. There were 352 pedestrian victims included in the study, of which 262 (74 percent) were adults and 90 (26 percent) were seniors. Compared to the adult victims, the seniors had a higher average ISS (23 vs. 16,  $p = 0.018$ ) and higher mortality (30 percent vs. 11 percent,  $p \leq 0.001$ ). The seniors were also more likely to have an ISS  $\geq 9$  (odds ratio = 2.72; 95 percent CI: 1.31–5.68) and to die (odds ratio = 6.68; 95 percent CI: 2.37–19.88). The results showed that mortality rate among subjects with an ISS  $\geq 16$  was 61 percent for the seniors compared to only 37 percent for the adults. Also, five out of the 27 seniors who died had ISS  $< 16$  while none of the 28 adults who died had ISS  $< 16$ . This finding is in agreement with what was previously reported, that ISS has a relatively low correlation with mortality in trauma victims over age 70 (Oreskovich et al., 1984 [41]). It was concluded that the adjusted age-dependent risks should be considered when calculating or projecting pedestrian morbidity and mortality.

In the study conducted here the “expectation” of cases with a MAIS3 in a random sample of fatalities in the CCIS analysis was 12%. Therefore, adjusting for frequency, in a random sample of 12 cases, only 17% of 12 = 2 cases should be evident with MAIS  $\leq 3$ . In the In-Depth APROSYS Database sample of elderly fatalities there are 8/12 = 75%, and so the MAIS  $\leq 3$  are very seriously over represented. Although this is a small sample, this highly significant degree of over representation is considered indicative that there are probably significant differences between the proportion of elderly pedestrian casualties who have died with only a MAIS3

injury, and a general vehicle occupant population. These statistics are broadly in agreement with the findings of Henary et.al. 2006. The consequences of this could be very significant, because **IF** MAIS3 or ISS = 9 is the relevant injury threshold level for fatalities in elderly pedestrian casualties, and a 15%tile is taken as reasonable (cf. HIC 1000 = 15%tile of MAIS4), then a level of HIC = 600 is more suitable for the elderly vulnerable road users (Prasad-Mertz [15]). Which casts doubt on the HIC levels chosen for the upcoming European Legislation (Phase 1: HIC = 1000 for 50% of bonnet area, and HIC = 2000 for 50% of the bonnet area, and Phase 2 possibly HIC = 1000 over the whole bonnet), which have been read-across from large sample vehicle occupant studies conducted by NHTSA, in terms of the possible relevance to elderly vulnerable road users in pedestrian impacts. Therefore a calibration of MAIS and ISS for a much larger sample of pedestrians is necessary, with the elderly (>60 years of age) ranked separately to the under 60's population, and the appropriate injury risk functions derived to see what are deemed to be the relevant HIC values for elderly vulnerable road users in pedestrian impacts.

## CONCLUSIONS

1. Cyclists were under-represented in the database, making it impossible to draw definitive conclusions on the characteristics of cyclist accidents or injured cyclists.
2. A better relationship was found between ISS (Injury Severity Score) and impact speed than between MAIS and impact speed, due to better suitability of this description of injury severity to the multiple injury nature of VRU accidents.
3. There was a good correlation of injury risk as related to impact speed between the cases in the In-depth database and previously published studies.
4. The locations of primary head impacts with vehicles lay principally on the windscreen, scuttle and A-pillar. Child head impacts were also identified in these regions.
5. Head impacts were identified as being slightly more common on the nearside of the vehicle (that is, nearest to the kerbside) regardless of which side of the road vehicles drive on.

6. The proportion of ground impacts found in this study were broadly comparable with the literature, the secondary impacts being generally associated with lower injury severity than injuries attributed to the vehicles. However, a case by case analysis showed that the severity of the secondary impact can be comparable to that of the primary impact.
7. There was a considerable over representation of elderly fatalities at MAIS3 than would be expected from population studies conducted on vehicle occupants, which again are similar to recent findings in the US.
8. It is concluded that a calibration of MAIS and ISS against fatality/non fatality for a much larger sample of pedestrians is necessary, with the elderly (>60 years of age) ranked separately to the under 60's population, and the appropriate injury risk functions derived to see what are deemed to be the relevant threshold injury values for elderly vulnerable road users in pedestrian impacts.

## REFERENCES

1. Carter, E., *APROSYS WP3.1.1 Accident Data: UK National epidemiological studies on pedestrian and cyclist accidents*. 2005.
2. Janssen, E.G. and J. Wismans. *Experimental and mathematical simulation of pedestrian-vehicle and cyclist-vehicle accidents*. in *10th ESV (Int. Tech. Conf. on Experimental Safety Vehicles)*. 1985. Oxford, UK.
3. Neal-Sturgess, C.E., G. Coley, and P. De Olivera. *Pedestrian injury - effects in impact speed and contact stiffness*. in *Vehicle Safety 2002*. 2002. London: IMechE.
4. Baker, S.P., et al., *The injury severity score: a method for describing patients with multiple injuries and evaluating emergency care*. *Journal of Trauma*, 1974. **14(3)**: p. p. 187-196.
5. Ashton, S.J. and G.M. Mackay. *Some Characteristics of the Population who Suffer Trauma as Pedestrians When Hit by Cars and Some Resulting Implications*. in *IRCOBI*. 1979.
6. Anderson, R.W.G., et al. *Vehicle Travel Speeds and the Incidence of Fatal Pedestrian Crashes*. in *IRCOBI*. 1995.

7. Otte, D. *Severity and mechanism of head impacts in car to pedestrian accidents*. in *IRCOBI (International Research Council On the Biomechanics of Impact)*. 1999. Sitges, Spain.
8. Neal-Sturgess, C.E.N., A *Thermomechanical Theory of Impact Trauma*. Proc. IMechE, Part D: J. of Automobile Div., 2002. **216**: p. p. 883-895.
9. Robertson, C. and A.D. Redmond, *The management of major trauma*. 1991, New York: Oxford University Press.
10. Seow, E. and G. Lau, *Who dies at A&E? The role of forensic pathology in the audit of mortality in an emergency medicine department*. Journal of Forensic Science International, 1996. **Vol. 82**: p. pp. 201–210.
11. Henary, B.Y., J. Ivarsson, and J.R. Crandall, *The influence of age on the morbidity and mortality of pedestrian victims*. Traffic Injury Prevention, 2006. **7**(2): p. 182 - 190.
12. Otte, D., *Pedestrian impacted by front of car*, in *Private communication from Accident Research Unit*. 1997, Medical University of Hannover: Hannover.
13. Otte, D. and T. Pohlemann. *Analysis and load assessment of secondary impact to adult pedestrians after car collisions on roads*. in *IRCOBI*. 2001.
14. Neal-Sturgess, C.E. and A.M. Hassan, *Calibration of AIS against fatality CCIS 1999-2005*. 2006, Birmingham Automotive Safety Centre.
15. Prasad, P. and H.J. Mertz. *The Position of the U.S. Delegation to the ISO Working Group 6 on the Use of HIC in the Automotive Environment*. in *SAE*. 1985.
16. Otte, D., *Pedestrian impacted by front of car*, in *Private communication from Accident Research Unit*. Medical University of Hannover. 1997.
17. Aronson, S.C., et al., *Traffic fatalities in Rhode island: Part IV the pedestrian victim*. Rhode Island Medical Journal, 1984. **Vol. 67**: p. pp. 485–489.
18. Harruff, R.C., A. Avery, and A.S. Alter-Pandya, *Analysis of circumstances and injuries in 217 pedestrian traffic fatalities*. Accident Analysis and Prevention, 1998. **Vol. 30**(No. 1): p. pp. 11–20.
19. Knoblauch, R., et al., *Older Pedestrian Characteristics for Use in Highway Design*. US Department of Transportation. DOT FHWA-RD-93-177., 1995.
20. Fildes, B.N., et al. *Older Driver Safety – A challenge for Sweden’s ‘Vision Zero’*. in *Proceedings of the Australian Transport Research Forum*. 2001. Hobart.
21. McLean, e.a., *PEDSPEED (1 & 2)*. 1994.
22. Anderson, R.W.G. and Maclean, *Vehicle design and speed and pedestrian injury*. 2001. [http://www.monash.edu.au/occe/roadsafety/abstracts\\_and\\_papers/110/110\\_revised.pdf](http://www.monash.edu.au/occe/roadsafety/abstracts_and_papers/110/110_revised.pdf).
23. Ashton, S.J., S. Bimson, and C. Driscoll, *Patterns of injury in pedestrian accidents*. Proc. American Association of Automotive Medicine, 1979. **Vol. 23**: p. pp. 185–202.
24. Augenstein, J. *Differences in Clinical Response between the Young and the Elderly*. in *Aging and Driving Symposium, Association for the Advancement of Automotive Medicine*. 2001. Des Plaines, IL.
25. Dejammes, M. and M. Ramet. *Aging Process and Safety Enhancements of Car Occupants*. in *Proceedings of Enhanced Safety in Vehicles Conference*. 1996. Melbourne, Australia.
26. Evans, L., *Traffic Safety and the Driver*. 1991, New York: Van Nostrand Reinhold.
27. Mackay, G.M. *Biomechanics and the Regulation of Vehicle Crash Performance*. in *Proceedings of 33rd AAAM Conference*. 1989. Baltimore, USA.
28. Viano, D., et al. *Involvement of Older Drivers in Multi-Vehicle Side Impact Crashes*. in *Proceedings of 33rd AAAM Conference*. 1989. Baltimore, USA.
29. Berthel, M., et al., *La Perte Minerale Ousseuse Liee a L’age*. *Medicine et Hygenie*, 1980. **38**: p. pp 1828-1831.
30. Padmanaban, J. *Crash Injury Experience of Elderly Drivers*. in *Proceedings of the Presentation at Aging and Driving Symposium, AAAM, Des Plaines, IL*. 2001. Southfield, MI.

31. Morris, A., et al. *An Overview of Requirements for the Crash Protection of Older Drivers*. in AAAM. 2002.
32. Welsh, R., et al., *Crash Characteristics and Injury Outcomes for Older Passenger Car Occupants*. Transportation Research, Special Issue, 2006: p. (Accepted for publication, in press).
33. Watson, J. and R. Hardy. *The BOSCOS System for Automotive Vehicles*. in *Design for Impact and Crashworthiness in Aerospace and Automotive Vehicle Structures*. 2006. Loughborough: IMechE.
34. Hoxie, R.E. and L.Z. Rubenstein, *Are older pedestrians allowed enough time to cross intersections safely?* Journal of American Geriatric Society, 1994. **Vol. 42:** p. pp. 241–244.
35. *Ageing and Transport: Mobility Needs and Safety Issues*, O.S.E. Group, Editor. 2001, OECD: Paris, France.
36. Oxley, J.A., et al. *Differences in traffic judgments between young and old adult pedestrians*. in *Proc. 40th AAAM*. 1996.
37. Leaf, W.A. and D.F. Preusser, *Literature Review on Vehicle Travel Speeds and Pedestrian Injuries*. 1999, U. S. Department of Transportation National Highway Traffic Safety Administration.
38. Kong, L.B., et al., *Pedestrian-motor vehicle trauma: An analysis of injury profile by age*. Journal of American College of Surgeons, 1996. **Vol.182:** p. pp. 17–23.
39. Peng, R.Y. and F.S. Bongard, *Pedestrian versus motor vehicle accidents: An analysis of 5,000 patients*. Journal of the American College of Surgeons, 1999. **Vol. 189:** p. pp. 343–348.
40. NHTSA, *Traffic safety facts 2003: A compilation of motor vehicle crash data from the Fatality Analysis Reporting System and the General Estimates System*. 2005.
41. Oreskovich, M.R., J.D. Howard, and M.K. Copass, *Geriatric Trauma: Injury patterns and outcome*. J Trauma, 1984. **Vol. 24:** p. pp. 565–572.

# DEVELOPMENT OF A BIOFIDELIC FLEXIBLE PEDESTRIAN LEGFORM IMPACTOR Type GT (FLEX-GT)

**Atsuhiko Konosu and Takahiro Issiki**

Japan Automobile Research Institute

**Masaaki Tanahashi and Hideki Suzuki**

Japan Automobile Manufacturers Association, Inc.

Japan

Paper Number 07-0178

## ABSTRACT

The Japan Automobile Research Institute and the Japan Automobile Manufacturers Association, Inc., have been developing a biofidelic flexible pedestrian legform impactor (Flex-PLI) since 2002, and its the latest version is called Flex-GT, and its prototype (Flex-GT-prototype) is developed in 2006. However, the Flex-GT-prototype is required further evaluation study on its biofidelity.

This study evaluated a biofidelity of Flex-GT-prototype, relationship to the human one using an FE Flex-GT-prototype model which has high fidelity to the actual one and a FE human model which has high biofidelity. This study result shows a good relationship between the Flex-GT-prototype model and the FE human model, especially under the 50 mm or 75 mm lift upped impact conditions.

## INTRODUCTION

A study designed to decrease the level of pedestrian injuries when crashing into a car (“study on pedestrian protection”) was initiated in the 1960s<sup>1),2)</sup>, and subsequently, test methods to evaluate the pedestrian protection performance of cars (“pedestrian protection test methods”) have been frequently discussed.

As a results, several pedestrian protection test methods are developed; the EEVC (European Enhanced Vehicle-safety Committee / European Experimental Vehicles Committee (former name)) Pedestrian Protection Test Method<sup>3),4)</sup>, ISO (International Organization for Standardization) Pedestrian Protection Test Method<sup>5)-7)</sup>, and the IHRA (International Harmonized Research Activity) Pedestrian Protection Test Method<sup>8)</sup>. In addition, thus far, regulations and technical standards based on these test methods (“technical standards for pedestrian protection”) have been examined by each organization, and the Japanese Technical Standards for Pedestrian Protection<sup>9)</sup>, the European Technical Standards for Pedestrian Protection<sup>10),11)</sup> and the Global Technical Standards (proposal) for Pedestrian Protection<sup>12)</sup> have been developed.

Moreover, in these pedestrian test methods and technical standards for pedestrian protection,

impactors imitating major human parts injured when impacting a car (e.g. head impactor and pedestrian legform impactor) are crashed into by a car (see Figure 1) and the pedestrian protection performance of the car is evaluated in terms of the degree of impact/loading levels on the impactors.

Basically, these impactors require a high level of biofidelity (equivalent deformation property under the load of a human body) and high injury evaluation ability (ability to properly evaluate injuries occurring in pedestrians). While the pedestrian legform impactor produced by TRL<sup>13)</sup> which was developed in the 1990s has been used in the EEVC Pedestrian Protection Test Method, European Technical Standards for Pedestrian Protection, and Global Technical Standards (proposal) for Pedestrian Protection, bone parts are made as a rigid body, and moreover, it is considered to be difficult to properly evaluate leg injuries due to the lack of biofidelity and insufficiencies in the measuring instruments incorporated.<sup>14)</sup>

Thus, currently, ECE/WP29/GRSP (“GRSP”) of the United Nations has focused its attention on “flexible pedestrian legform impactor”<sup>15)-19)</sup> which have a higher level of biofidelity than conventional impactors, enabling more accurate injury evaluation. As a results, GRSP established the Flexible Pedestrian Legform Impactor Technical Evaluation Subgroup<sup>20)</sup> under GRSP/INF-GR-PS (Informal Group on Pedestrian Safety) to conduct technical evaluation activities on these impactors.

In this article, we report on the status of the development of type GT (Flex-GT), which is the latest model of flexible pedestrian legform impactor.

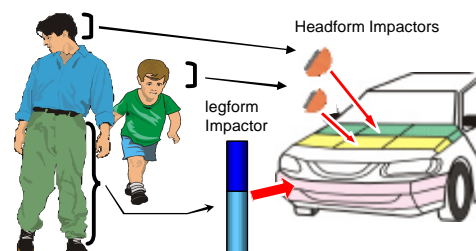


**Figure 1. Concept of the pedestrian protection test methods.**

# DEVELOPMENT OF FLEXIBLE PEDESTRIAN LEGFORM IMPACTOR TYPE GT

## Development of a prototype

The flexible pedestrian legform impactor type GT prototype (Type GT prototype) was developed in 2006 (February) (see Figure 2)<sup>21), 22)</sup>. In this version, a) the range of motion of the knee region, b) the light weight of the bone parts, as well as c) the biofidelity are improved. However, a validation of the biofidelity was not completely conducted, so it still needs to be validated.

Thus, to conduct additional validation for the biofidelity of this impactor, analysis with computer simulation was performed in this study.

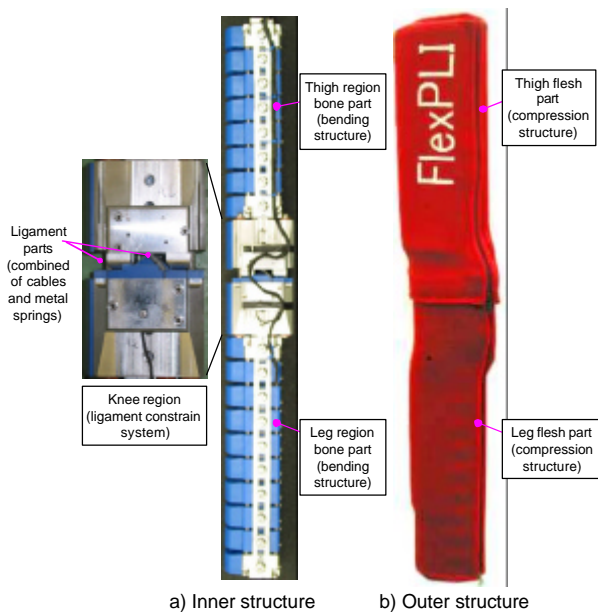


**Figure 2. Flexible pedestrian legform impactor type GT prototype (Flex-GT-prototype).**

## Methods

### Computer models

The computer models used in this study are shown in Figure 3. The computer models are broadly divided into three, including one imitating a human body (“human model”), one imitating the flexible pedestrian legform impactor type GT prototype (“Flex-GT-prototype model”) and one simply imitating a car (“simplified car model”).

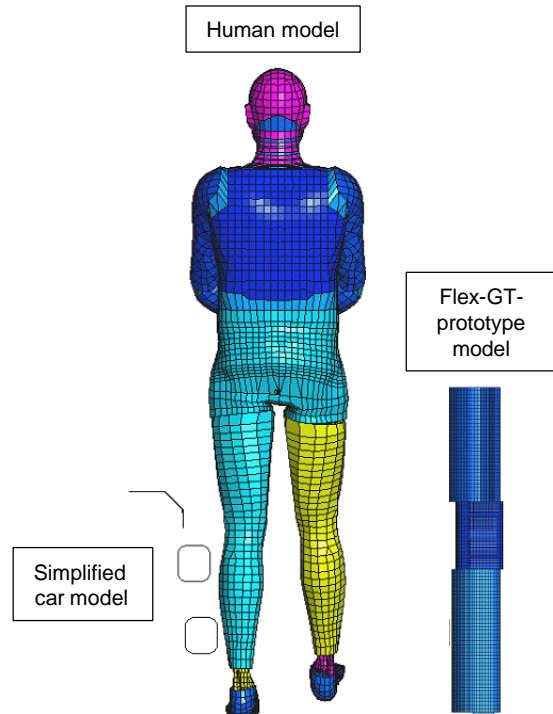


**Figure 3. Computer models used in this study (overview).**

**Human model** - The human model is structured based on the MRI (magnetic resonance imaging) scan data of a human body<sup>23), 24)</sup> with fidelic modeling of the inner cross-section structure of the bone part and the ligament structure of the knee region. The bone part of the knee region for this model was validated in detail using various donated body experiment data.

**Flex-GT-prototype model** - The Flex-GT-prototype model is structured based on the drawing of this impactor with detailed modeling of the structure of the bone part and knee region.<sup>25)</sup> This model was validated per part during the assembly stage, and has high fidelity to the actual impactor.

**Simplified car model** - The overview shape of the simplified car model is shown in Figure 4. The simplified car model is comprised of three parts including the bonnet leading edge part (“BLE”), the bumper part (“BP”) and the spoiler part (“SP”).

The structure of the simplified car is shown in Figure 5 - 7. BLE is made of deformable shell elements which can deform upon impact. In addition, the material properties of these elements are provided with the properties of automotive cold-rolled steel plate JSC270C (cold-rolled steel plate, tensile strength: 270 N/mm<sup>2</sup> and over, steel grade: C class).

On the other hand, BP and SP are made of rigid body elements, and the movable property is defined by the properties of the joint bond to each element (see Figure 6 and Figure 7).

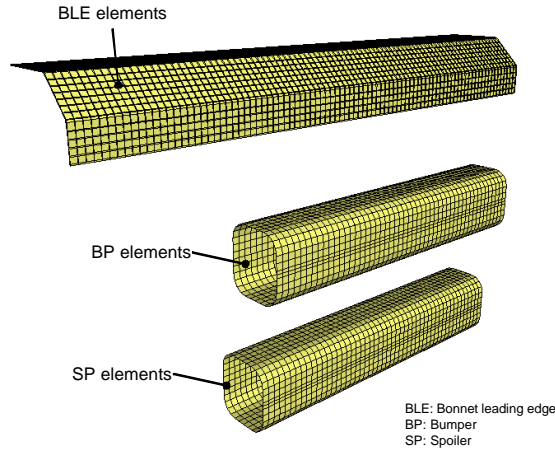


**Figure 4. Simplified car model (overview - oblique front projection drawing).**

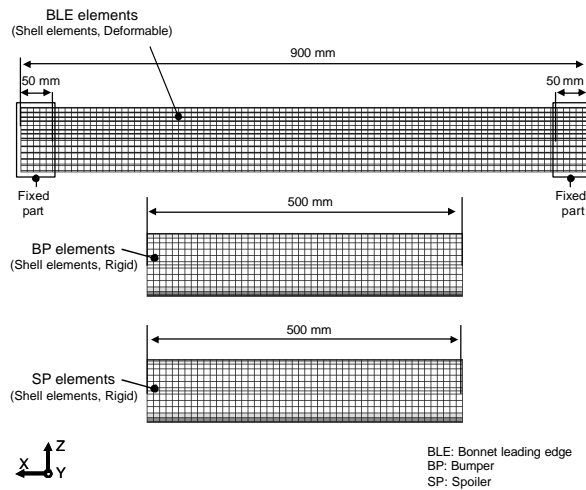


**Figure 5. Simplified car model structure (frontal view of the car).**

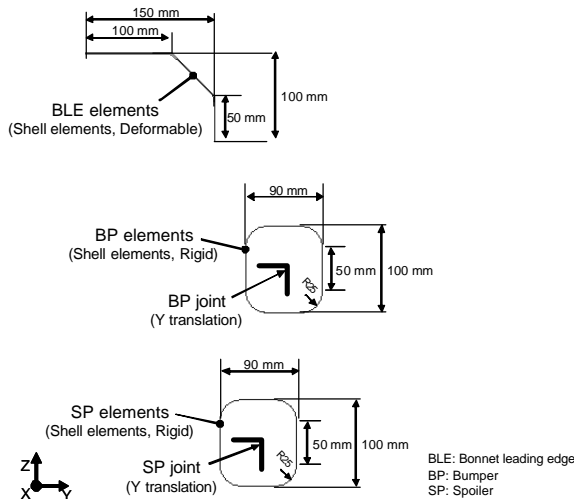


**Figure 6. Simplified car model structure (side view of the car).**

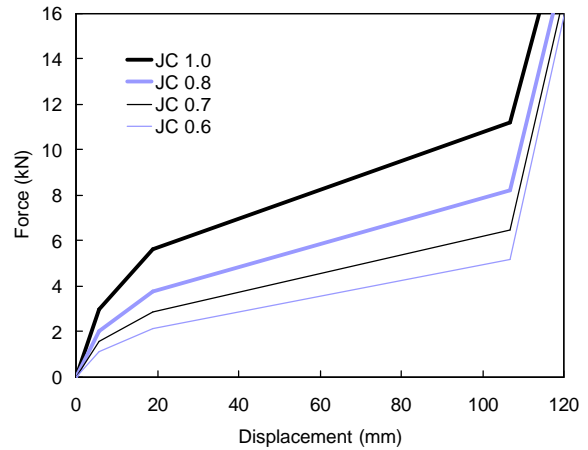


**Figure 7. BP and/or SP joint properties of the simplified car model (JC 0.6 – JC 1.0).**

### Setting conditions

In this analysis, several simplified car models made with varying stiffness and shapes were crashed into the human model and the Flex-GT-prototype model to compare the loading level of each model.

**Setting of the human model** - As for the human model, to find the correlation with the Flex-GT-prototype model, the model was set to output the load on the tibial part of the leg region and the knee medial collateral ligament (MCL) which are mainly taken as the subject of pedestrian lower limb protection (see Figure 8).

To simply compare the maximum output value on the tibia of the leg region and the knee collateral ligament, the setting of the bone parts fracture (except the fibula) and the setting of the breaking knee ligament parts in the human model are excluded.

As for the legs position of the human model, the initial crash side of the leg was set vertical to the ground, with the other leg casting out at 20 degrees in front of the pedestrian (see Figure 9). This setting is intended to simulate the pedestrian legform impactor impact condition (vertical to the ground, initial crash side of leg) and to prevent interfering with each other of leg.

In crash simulations with the simplified car model, as shown in Figure 10, BP and SP were placed on the leg for the initial crash and the other leg respectively. This is intended to prevent the entire BP and SP from moving backwards from the car due to the impact of the initial crash side of the leg, because it is difficult to imagine that the entire BP and SP backwards movement due to the impact of the initial crash side of the leg under an actual car crash condition.

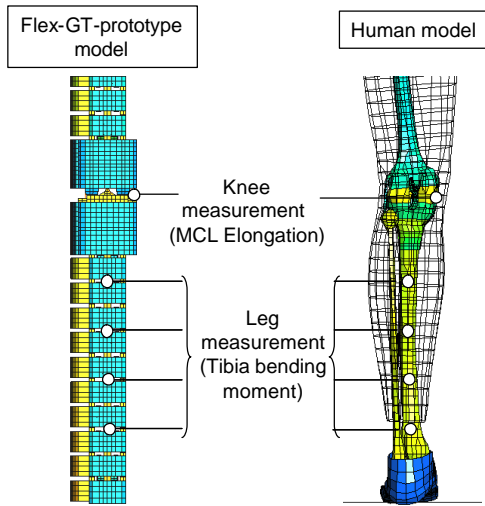


**Figure 8. Measurement points of the human model and the Flex-GT-prototype model**

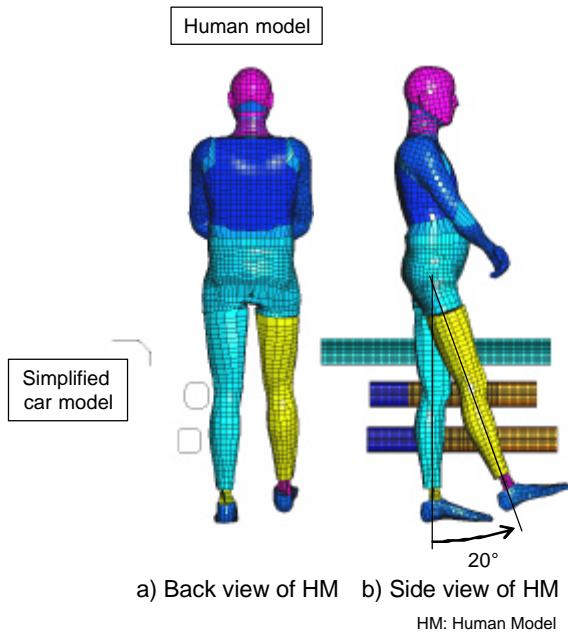


**Figure 9. Posture of the human model**

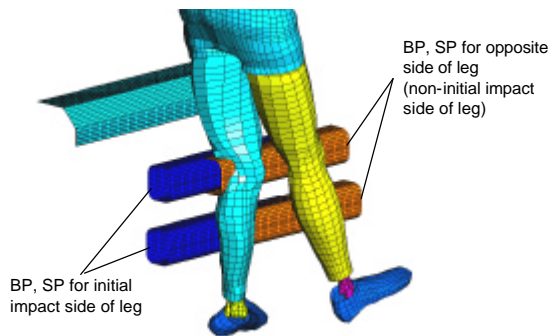


**Figure 10. Setting of the simplified car model for the human model**

**Setting of the Flex-GT-prototype model** - As for the Flex-GT-prototype model, the output setting is same of the human model case as mentioned above (see Figure 8). The front placement position of the Flex-GT-prototype model to the simplified car was set as the center of the car (Figure 11).

In this study, the tibia bending moment values were estimated from the strain values which were occurred in the bone part core part. However, this study did not using the conventional strain to bending moment conversion method (a method using the dynamic three-point leg bending test results) but simply used the three-point bending of the bone part core of leg. This is because the conventional method includes the effects of the inertial force of the bone parts and also includes the effect of the fixed conditions of the bone parts to the three-point bending equipments, which makes it difficult to obtain correct conversion values.

The bending moment conversion method is changed; “RCAL” is indicated in the graph title section to show the differences.

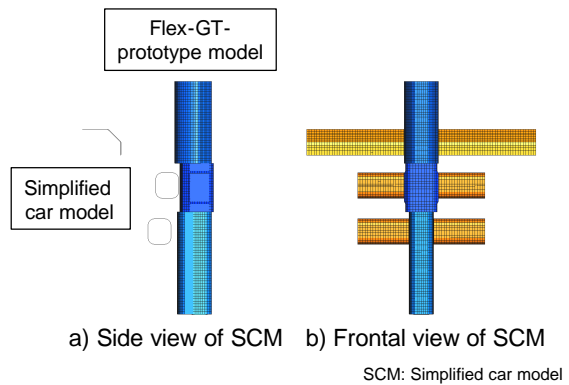


**Figure 11. Front placement position of the Flex-GT-prototype model to the simplified car model**

**Setting of the simplified car model** - The setting parameters of the simplified car model are shown in Table 1. The setting parameters are broadly divided into car stiffness and car shapes (see Figure 12 for the definition of car shapes).

As for car stiffness, BLE stiffness can be changed by altering the plate thickness of the shell elements comprising the car. BP and SP stiffness can be changed by altering the joint properties set for each element. As for car shapes, the shape of the car can be changed by altering the placement of each element.

If simplified car models are created by combining all the setting parameters of car stiffness and car shapes described in Table 1, 4,374 patterns of simplified cars can be created. However, because it takes tremendous time to create 4,374 patterns of

simplified cars and perform simulation analyses. In this study, therefore, using a design of experiment method (assignment of setting parameters using L18 orthogonal table), simulations for a total of 18 types of simplified cars representing all setting parameters were conducted (see Table 2).

**Table 1. Setting parameters of the simplified car model.**

| Parameter                        | Unit              | Level 1 | Level 2 | Level 3 |
|----------------------------------|-------------------|---------|---------|---------|
| K1 (BLE stiffness <sup>*</sup> ) | mm                | 0.4     | 0.6     |         |
| K2 (BP stiffness <sup>**</sup> ) | JC <sup>***</sup> | 0.7     | 0.8     | 1.0     |
| K3 (SP stiffness <sup>**</sup> ) | JC <sup>***</sup> | 0.6     | 0.8     | 1.0     |
| H1 (BLE height)                  | mm                | 650     | 700     | 750     |
| H2 (BP height)                   | mm                | 450     | 490     | 530     |
| H3 (SP height)                   | mm                | 250     | 270     | 350     |
| L1 (BLE lead)                    | mm                | 125     | 200     | 275     |
| L2 (SP lead)                     | mm                | -20     | 0       | 30      |

<sup>\*</sup> Stiffness is changed by steel plate thickness.

<sup>\*\*</sup> Stiffness is changed by joint characteristics.

<sup>\*\*\*</sup> JC: Joint characteristics

# BLE: Bonnet leading edge, BP: Bumper, SP: Spoiler

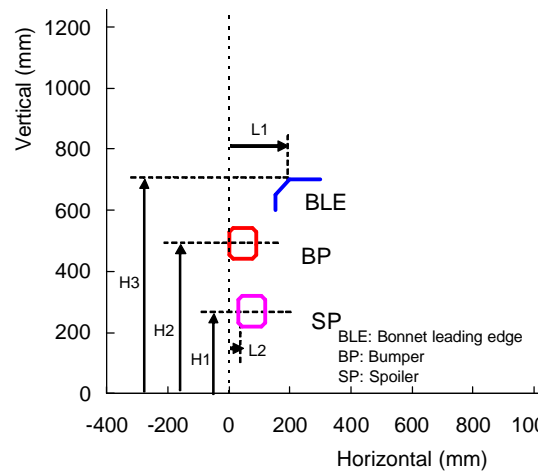


**Figure 12. Definition of the car shapes of simplified car models.**

**Table 2. Specifications of the simplified car models (total 18 types).**

| Simplified Car Model ID | K1 (BLE stiffness <sup>*</sup> ) mm | K2 (BP stiffness <sup>**</sup> ) JC <sup>***</sup> | K3 (SP stiffness <sup>**</sup> ) JC <sup>***</sup> | H1 (BLE height) mm | H2 (BP height) mm | H3 (SP height) mm | L1 (BLE lead) mm | L2 (SP lead) mm |
|-------------------------|-------------------------------------|--|--|--------------------|-------------------|-------------------|------------------|-----------------|
| S1                      | 0.4                                 | 0.7  | 0.6  | 650                | 450               | 250               | 125              | -20             |
| S2                      | 0.4                                 | 0.7  | 0.8  | 700                | 490               | 270               | 200              | 0               |
| S3                      | 0.4                                 | 0.7  | 1.0  | 750                | 530               | 350               | 275              | 30              |
| S4                      | 0.4                                 | 0.8  | 0.6  | 650                | 490               | 270               | 275              | 30              |
| S5                      | 0.4                                 | 0.8  | 0.8  | 700                | 530               | 350               | 125              | -20             |
| S6                      | 0.4                                 | 0.8  | 1.0  | 750                | 450               | 250               | 200              | 0               |
| S7                      | 0.4                                 | 1.0  | 0.6  | 700                | 450               | 350               | 200              | 30              |
| S8                      | 0.4                                 | 1.0  | 0.8  | 750                | 490               | 250               | 275              | -20             |
| S9                      | 0.4                                 | 1.0  | 1.0  | 650                | 530               | 270               | 125              | 0               |
| S10                     | 0.6                                 | 0.7  | 0.6  | 750                | 530               | 270               | 200              | -20             |
| S11                     | 0.6                                 | 0.7  | 0.8  | 650                | 450               | 350               | 275              | 0               |
| S12                     | 0.6                                 | 0.7  | 1.0  | 700                | 490               | 250               | 125              | 30              |
| S13                     | 0.6                                 | 0.8  | 0.6  | 700                | 530               | 250               | 275              | 0               |
| S14                     | 0.6                                 | 0.8  | 0.8  | 750                | 450               | 270               | 125              | 30              |
| S15                     | 0.6                                 | 0.8  | 1.0  | 650                | 490               | 350               | 200              | -20             |
| S16                     | 0.6                                 | 1.0  | 0.6  | 750                | 490               | 350               | 125              | 0               |
| S17                     | 0.6                                 | 1.0  | 0.8  | 650                | 530               | 250               | 200              | 30              |
| S18                     | 0.6                                 | 1.0  | 1.0  | 700                | 450               | 270               | 275              | -20             |

<sup>\*</sup> Stiffness is changed by steel plate thickness.

<sup>\*\*</sup> Stiffness is changed by joint characteristics.

<sup>\*\*\*</sup> JC: Joint characteristics

# BLE: Bonnet leading edge, BP: Bumper, SP: Spoiler

**Impact conditions** - A total of 18 types simplified car model were selected as mentioned above, and crashed into the human model and the flexible pedestrian leg impactor type GT prototype model (see Figure 13). The impact speed was set at 11.1 m/s defined in the current GTR proposal.

As for the impact height ( $H_i$ ) of the human model and the flexible pedestrian leg impactor type GT prototype model against the simplified cars, 25 mm above the ground as defined in the current GTR proposal.

In this study, as for the impact height for the flexible pedestrian leg impactor type GT prototype model, in addition to the base height of 25 mm (“base”), base + 50 mm, and base + 75 mm were also conducted.

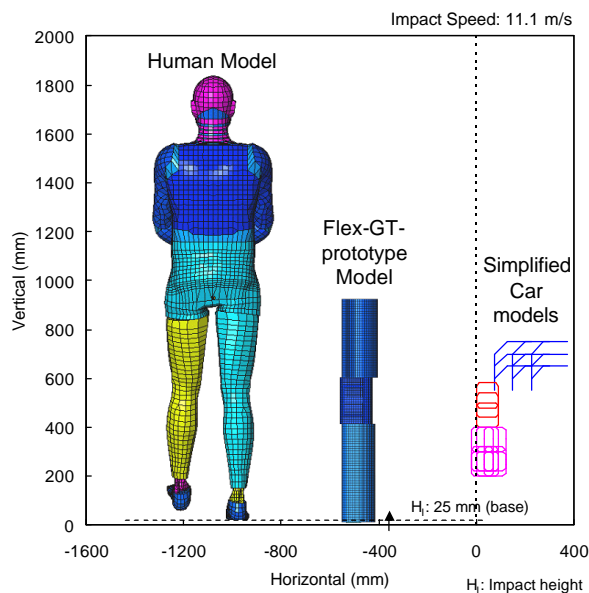


**Figure 13. Analysis conditions (image, impact height: 25 mm).**

### Simulation results

The results of the simulation are shown in Figure 14. This figure shows the relationship between the maximum bending moment occurring in the tibial part of the human model and the flexible pedestrian leg impactor type GT prototype model, as well as the maximum elongation occurring in the knee collateral ligament.

This figure indicates that the Flex-GT-prototype model output and Human model output has generally good relationship. Especially for the maximum bending moment occurring in the tibial part, the results for the impact height of the flexible pedestrian leg impactor type GT prototype model 50 mm higher than the base height best correlate with the output of the human model. As for the maximum elongation of

the knee medial collateral ligament, it was found that the results of impact height of the flexible pedestrian leg impactor type GT prototype model which was higher than 75 mm than the base height best correlate with the output of the human model.

Based on correlation coefficient obtained from each result, the tibial fracture evaluation point ( $R_{\text{tibia}}$ ), knee medial collateral ligament breaking evaluation point ( $R_{\text{MCL}}$ ) and total evaluation point ( $(R_{\text{tibia}} + R_{\text{MCL}})/2$ ) were calculated and the results are shown in the radar charts in Figure 15. As for total evaluation point, the results of the impact height of the flexible pedestrian leg impactor type GT prototype model 50 mm and 75 mm higher evaluation point (about 0.8) than the base height obtained equivalent evaluation points (about 0.6).

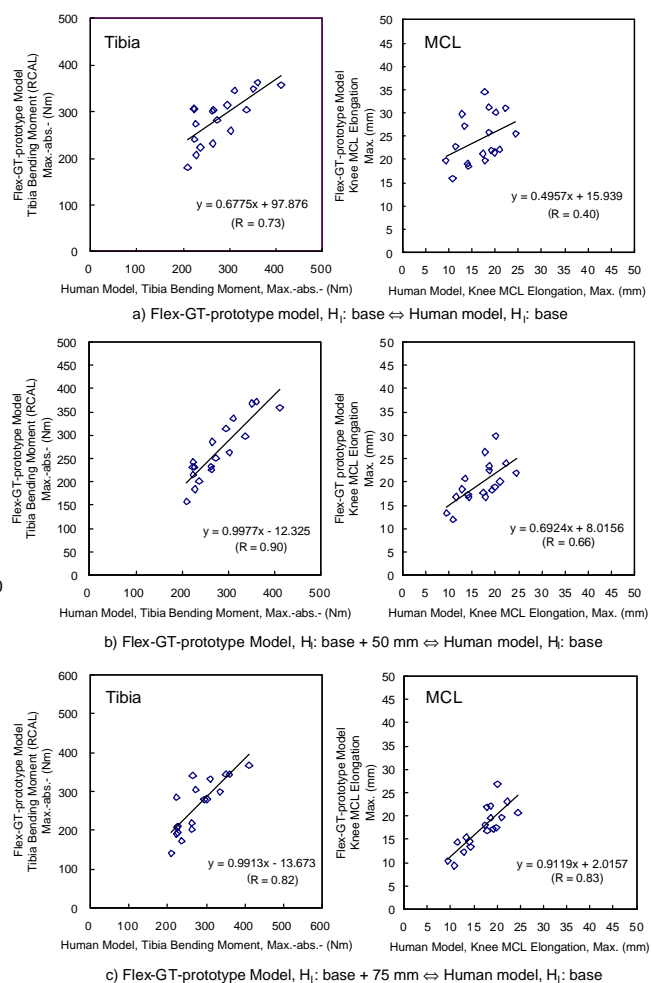


**Figure 14. Simulation results (output values and correlation coefficients).**

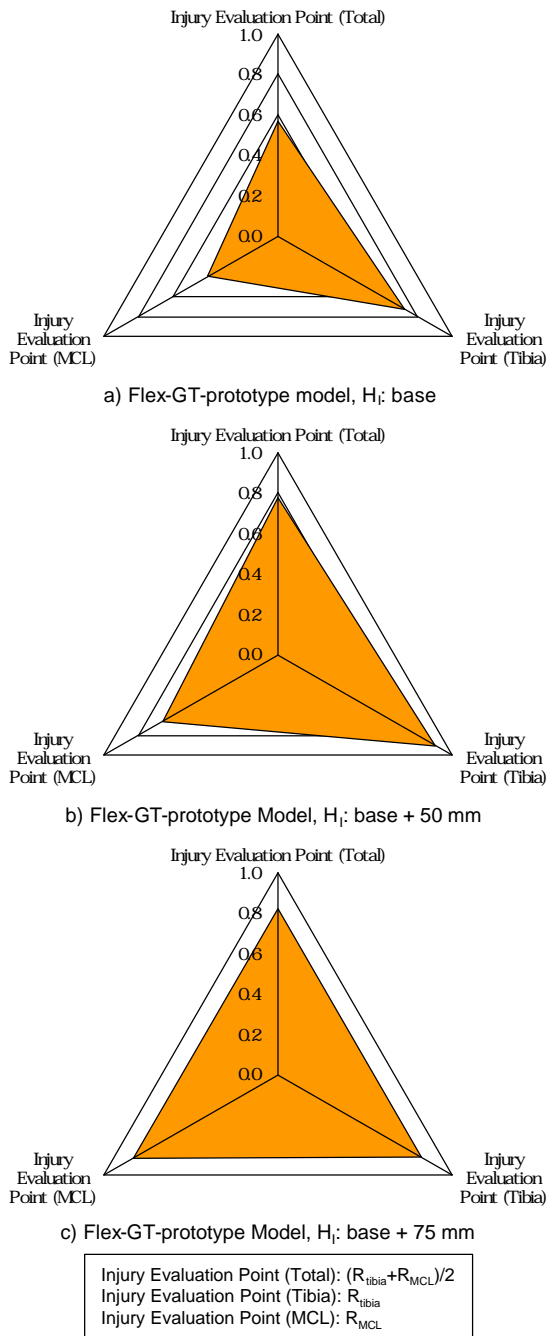


**Figure 15. Injury evaluation point.**

## DISCUSSION

From the results of this analysis, an impact height 50-75 mm higher than the base (25 mm) more correlated with the human model. One of the reasons for this is seemed as to be the effect of the presence or absence of the human upper body.

The human upper body has great inertia force because of its size in mass relative to the leg, which tends to stay relatively at the initial position even after the leg crashes into a car. Therefore, during impact with a car, the upper body tends to lift up the

leg overall (see Figure 16).

Figure 17 shows the difference in the knee joint position of the human model and the flexible pedestrian leg impactor type GT prototype (impact height: base) when the maximum bending moment occurs in the tibia in the leg region and when maximum elongation occurs in the knee medial collateral ligament. While in the human model, the knee joint position already rises approximately 20 mm on average when the maximum bending moment occurs in the tibia in the leg region, it only rises less than 5 mm on average in the flexible pedestrian leg impactor type GT prototype. In addition, while in the human model, the knee joint position rises approximately 60 mm on average when maximum elongation occurs in the knee collateral ligament, it rises only about 20 mm on average in the flexible pedestrian leg impactor type GT prototype.

It is highly possible that these differences cause the difference in the loading condition on the tibia and the knee medial collateral ligament, and it is suggested that changing the impact height of the pedestrian legform impactor have effects to correct these differences.

Moreover, the human upper body has the effect of inhibiting thigh movement due to its great inertia force (see Figure 18).

As mentioned above, the human upper body has great inertia force because of its size in mass relative to the leg, which tends to stay relatively at the initial position even after the leg crashes into a car. Therefore, during impact into a car, it inhibits thigh behavior to prevent the thigh from falling against the car. On the other hand, in the pedestrian impactor without an upper body, thigh behavior is not inhibited and the thigh easily falls against the car. These differences become factors which cause significant differences, particularly in the load on the knee collateral ligament.

As shown in Figure 19 and Figure 20, it is considered that shifting the impact position of the pedestrian legform impactor upwards especially facilitates rotation of the leg region of the pedestrian legform impactor, and as a result, the load occurring on the knee part has the same effect as in the human body.

Additionally, it has a chance that the difference in distribution of mass between the human body and the pedestrian legform impactor, while in the human body the bone part is very light in weight and a flesh part covers most of the mass, affects to the human and impactor differences. However, in the pedestrian legform impactor, it is difficult to reduce the mass of the bone part to be equivalent to that of the human body because of various limitations such as

incorporation of measuring sensors, endurance, and testability. Additionally, the presence or absence of the ankle joint may cause differences in load status.

However, to change the impactor specifications of the pedestrian legform impactor while meeting the basic specifications required for the pedestrian legform impactor (e.g. incorporation of measuring sensor, endurance, and testability) is very difficult. Moreover, to change the impactor specification has a high risk for the developments itself (unexpected issue will be happened). To keep the current specification of the impactor and to select best impact heights is therefore one of a good practical method.

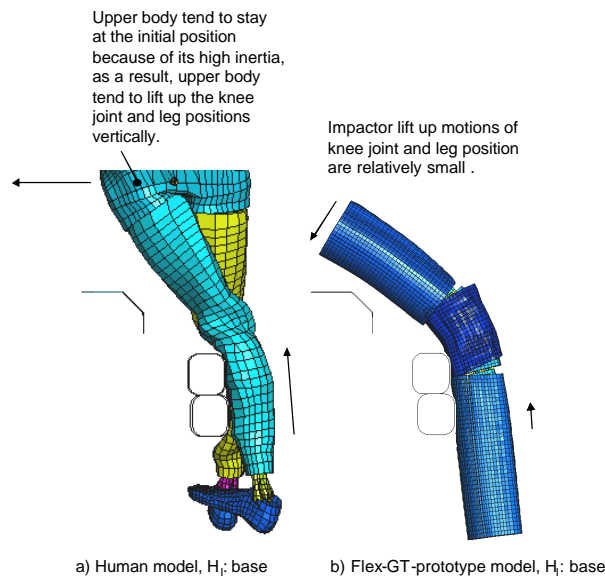
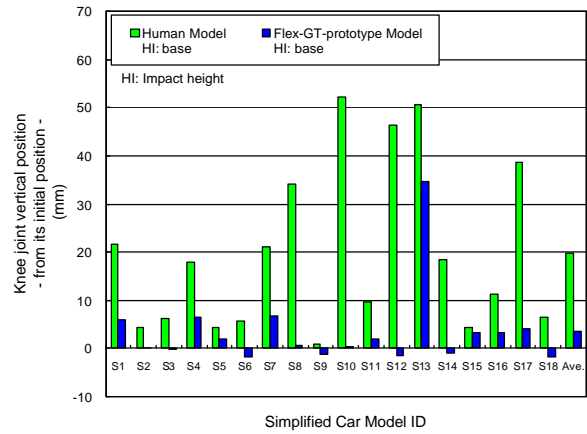
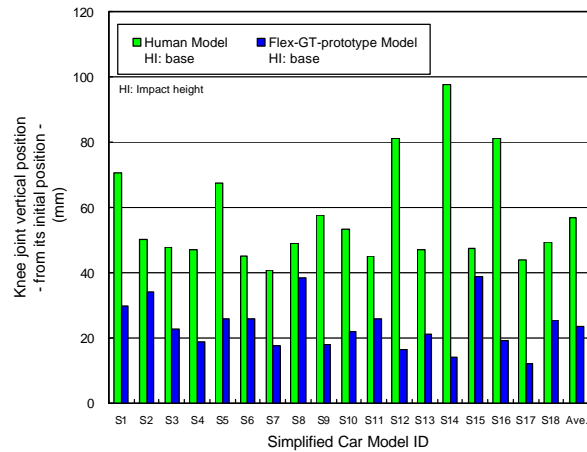


**Figure 16. Upper body effect (1) - Lifting up the lower limb.**



a) Tibia bending moment maximum timing



b) Knee MCL elongation maximum timing

**Figure 17. Difference in amount of rise of the knee position.**

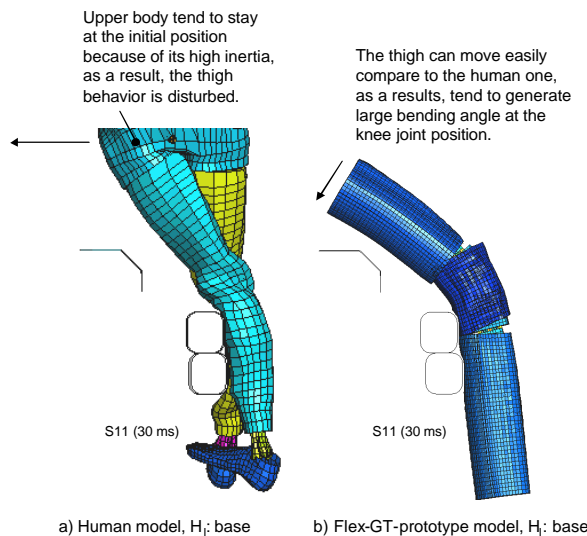


**Figure 18. Upper body effect (2) – Inhibition of thigh behavior.**

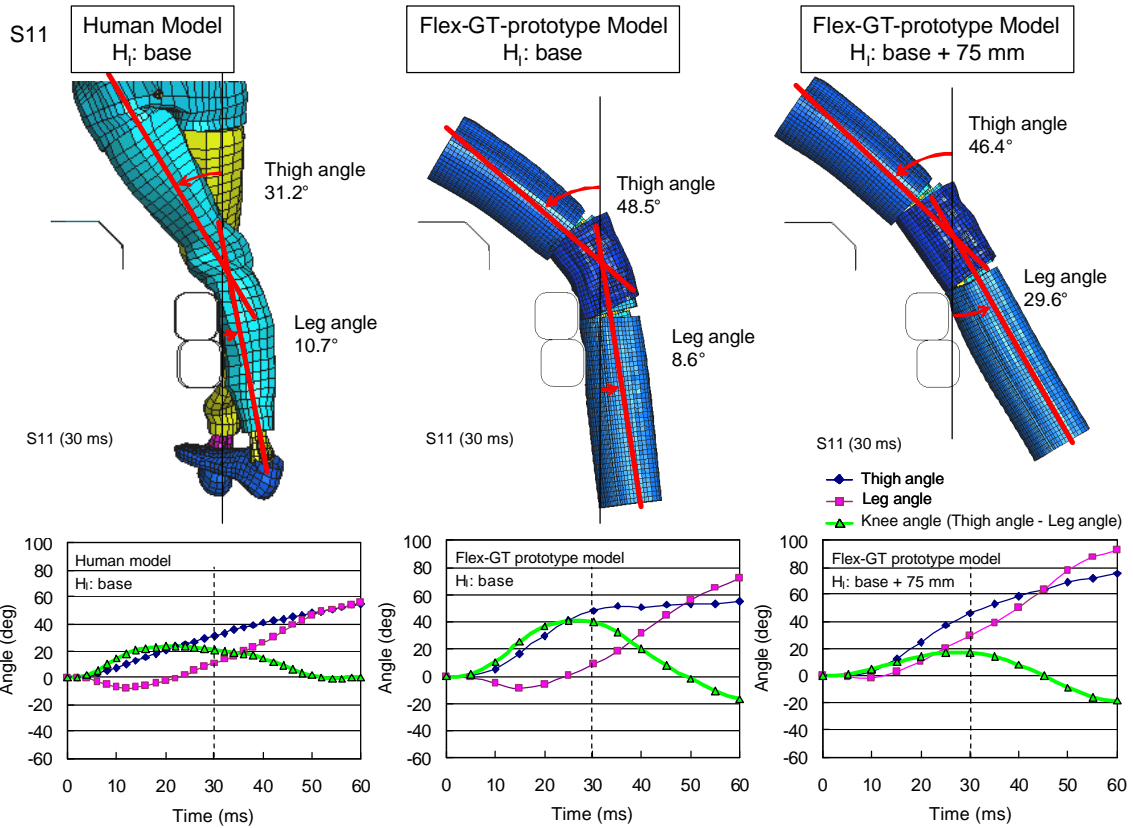


**Figure 19. Timely curves for the angle of the thigh, leg and knee (S11) , example.**

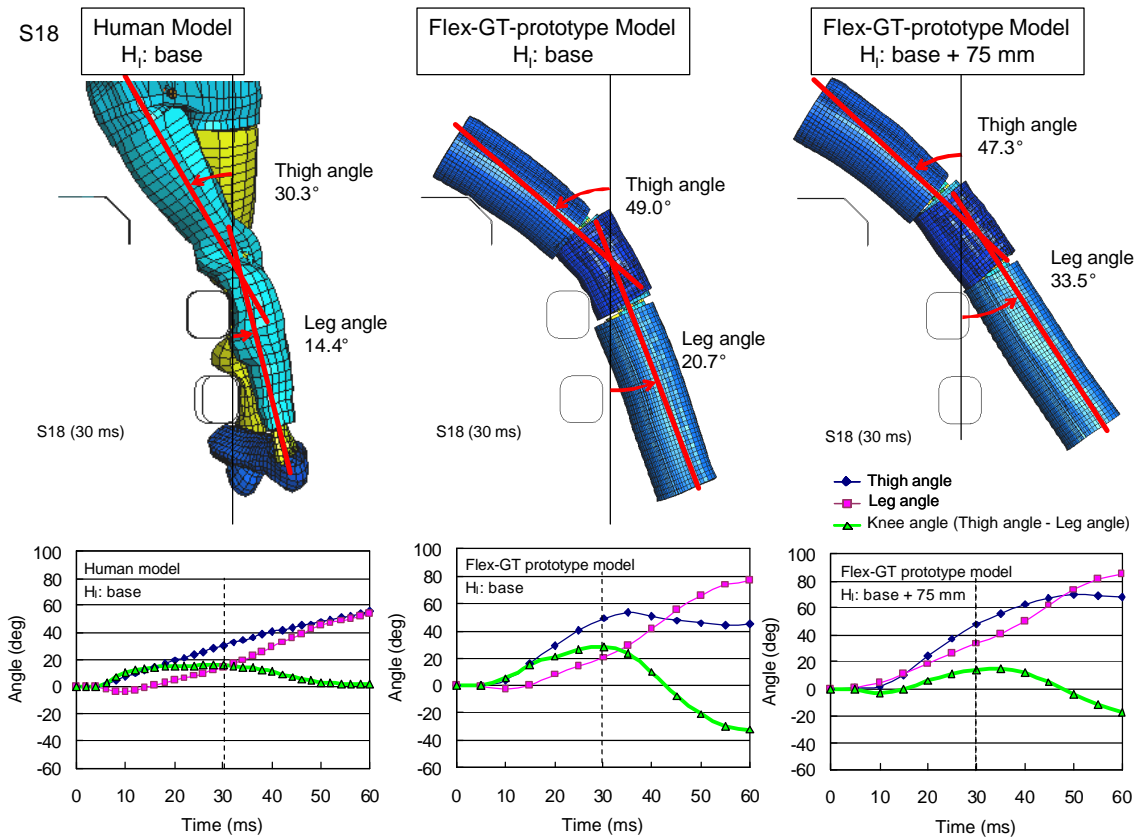


**Figure 20. Timely curves for the angle of the thigh, leg and knee (S18), example.**

## CONCLUSION

In this study, the biofidelity (correlation with the human body) of the flexible pedestrian legform impactor type GT prototype was verified using the Flex-GT-prototype model and the human model.

It was found that correlation with the human body becomes greater by increasing the impact height of the Flex-GT-prototype model by 50-75 mm.

As the main reason for this, it is believed that the human model has an upper body having great mass relative to the leg, affecting the rising of the knee position and the leg region position, and inhibiting thigh behavior, and the lack of these effects is simply corrected by raising the impact height.

Further analysis is required, however, to keep the current impactor specification with selecting a best impact height is one of a good practical method.

## ACKNOWLEDGEMENT

We would like to thank Honda R&D Co., Ltd. for their generous supply of a human model and valuable advice required for the analysis of this study.

## REFERENCES

- 1) Severy D.M.: Auto-Pedestrian Impact Experiments, Proc. 7th STAPP Car Crash Conference, pp. 345-373 (1963)
- 2) Ryan G.A. and McLean A.J.: Pedestrian survival, Proc. 9th STAPP Car Crash Conference, pp. 321-334 (1965)
- 3) European Experimental Vehicles Committee: EEVC Working Group 10 report - Proposals for methods to evaluate pedestrian protection for passenger cars (1994).
- 4) European Enhanced Vehicle-safety Committee: EEVC Working Group 17 report - Improved test methods to evaluate pedestrian protection afforded by passenger cars (1998).
- 5) ISO 11096: Road vehicles - Pedestrian protection - Impact test method for pedestrian thigh, leg and knee (2002).
- 6) ISO 14513: Road vehicles - Pedestrian protection – Head impact test method (2006).
- 7) ISO/FDIS 16850: Road vehicles - Pedestrian protection – Child head impact test method (2006).
- 8) Mizuno. Y.: Summary of IHRA Pedestrian Safety WG Activities - Proposed Test Methods to Evaluate Pedestrian Protection Afforded by Passenger Cars, Proc. 19th International Technical Conference on the Enhanced Safety of Vehicle, Paper Number 05-0138 (2005)
- 9) Ministry of Land, Infrastructure and Transport, Road Transport Bureau, Engineering and Safety Department, Engineering Planning Division, “Newly introducing pedestrian head protection standard to bonnets – Revision of safety standard of road trucking vehicles –”  
[http://www.mlit.go.jp/kisha/kisha04/09/090420\\_.html](http://www.mlit.go.jp/kisha/kisha04/09/090420_.html) (2004)
- 10) European Union: Directive 2003/102/EC of the European Parliament and of the Council of 17 November 2003 relating to the protection of pedestrians and other vulnerable road users before and in the event of a collision with a motor vehicle and amending Council Directive 70/156/EEC (2003)
- 11) European Union: 2004/90/EC - Commission Decision of 23 December 2003 on the technical prescriptions for the implementation of Article 3 of Directive 2003/102/EC of the European Parliament and of the Council relating to the protection of pedestrians and other vulnerable road users before and in the event of a collision with a motor vehicle and amending Directive 70/156/EEC (2004)
- 12) UN/ECE/WP29/GRSP: Proposal for a global technical regulation (gtr) on uniform provisions concerning the approval of vehicles with regard to their construction in order to improve the protection and mitigate the severity of injuries to pedestrians and other vulnerable road users in the event of a collision (gtr on pedestrian safety), ECE/TRANS/WP.29/GRSP/2006/2 (2006)
- 13)<http://www.trl.co.uk/store/legform-impactors.asp?pid=242>
- 14) UN/ECE/WP29/GRSP/INF-GR-PS: Information on the Flexible Pedestrian Legform Impactor (Flex-PLI) from J-MLIT Research, INF-GR-PS 106 (2004)
- 15) Konosu A. and Tanahashi M.: Development of a biofidelic pedestrian legform impactor: Introduction of JAMA-JARI legform impactor ver. 2002. Proc. 18th International Technical Conference on the Enhanced Safety of Vehicle, Paper No. 378 (2003)
- 16) Konosu A. and Tanahashi M.: Development of a Biofidelic Flexible Pedestrian Legform Impactor. Stapp Car Crash Journal, Vol. 47, pp. 459-472 (2003)
- 17) Konosu A. and Tanahashi M.: Development of a Biofidelic Flexible Pedestrian Leg-form Impactor (Flex-PLI 2004) and Evaluation of its Biofidelity at the Component Level and at the Assembly Level, Society of Automotive Engineers World Congress, SAE paper No. 2005-01-1879 (2005)
- 18) UN/ECE/WP29/GRSP/INF-GR-PS/Flex-TEG: General Information for the Flexible Pedestrian Legform Impactor - type G - (Flex-G), TEG-002 (2005)
- 19) UN/ECE/WP29/GRSP/INF-GR-PS/Flex-TEG: Information on the Flexible Pedestrian Legform Impactor GT Alpha (Flex-GT-alpha), TEG-021 (2006)
- 20)[http://www.unece.org/trans/main/wp29/wp29wgs/wp29grsp/pedestrian\\_FlexPLI.html](http://www.unece.org/trans/main/wp29/wp29wgs/wp29grsp/pedestrian_FlexPLI.html)
- 21) UN/ECE/WP29/GRSP/INF-GR-PS/Flex-TEG: Information on the Flexible Pedestrian Legform

- Impactor GT Alpha (Flex-GT-alpha), TEG-021 (2006)
- 22) UN/ECE/WP29/GRSP/INF-GR-PS/Flex-TEG: Evaluation Activities on Injury Assessment Ability of the Flexible Pedestrian Legform Impactor GT Alpha (Flex-GT-alpha), TEG-022 (2006)
- 23) Takahashi Y., Kikuchi Y., Mori F., and Konosu A.: Advanced FE Lower Limb Model for Pedestrians, Proc. 18th International Technical Conference on the Enhanced Safety of Vehicles, Paper Number 218 (2003)
- 24) Takahashi Y., Kikuchi Y., and Mori F.: Development of a Finite Element Model for the Pedestrian Pelvis and Lower Limb, Society of Automotive Engineers World Congress, SAE paper No. 2006-01-0683 (2006)
- 25) Issiki T., Konosu A., and Tanahashi T.: Development of An FE Flexible Pedestrian Leg-form Impactor (FLEX-GT-prototype) Model, Proc. 20th International Technical Conference on the Enhanced Safety of Vehicles, Paper Number 06-0179 (2007)

# THE STUDY ON DEVELOPING ACTIVE HOOD LIFT SYSTEM FOR DECREASING PEDESTRIAN HEAD INJURY

**Keun Bae Lee**

**Han Jo Jung**

**Han Il Bae**

HYUNDAI - KIA Motors

Korea

Paper Number 07-0198

## ABSTRACT

Active hood lift system has been developed to get more spaces for decreasing the head injury during pedestrian impact. This system is composed of detecting sensor, ECU where the algorithm is embedded and the pyro-type actuators which raise the hood. By this system, the rear part of the hood is raised up to approximately 120mm.

The test results of system operation are introduced for each three typical impact cases. In this test the system could detect the lower legform impactor from the other rigid pole and only in case of lower legform the actuator is deployed within the required operating time, 30ms.

To investigate the effects of this system on decreasing head injury, we have carried out the EURO NCAP child headform impact test in which the actuators are fully deployed and the rear part of the hood is initially lifted up to 115mm. Through this tests we could identify that the head injury could be reduced significantly at all target points

## INTRODUCTION

In order to satisfy the regulations on pedestrian head protection, passive protection measures, such as the stiffness modification of the hood itself and changes of engine room lay-out, have been frequently tried. Basically, pedestrian head injury would be reduced by the appropriate flexibility of the impact part on the hood. This, in turn, requires sufficient deformation space between hood outer skin and hard structure of the engine room. Generally, there are some limitations to fulfill this requirement by classical passive protection improvements mainly due to the strength regulations of hood itself and the difficulties of reducing the size of structures in engine room. To overcome this problem, the active measures, which lifts the hood before the head impacts the hood, are now

being widely studied [1][2].

The fundamental requirement of the active hood lift device is to classify the type of object in crash and, in turn, to differentiate between fire and non-fire case.

First of all, the system must satisfy the current and future regulations [3]. Therefore, we have considered the lower legform impact at a vehicle speed of 20km/h to 40km/h as a main hood lifting condition. The same adult legform of the EC directive 2003/102/EC was considered.

To cover the field stability especially for the case of 6 year old child pedestrian, we designed the lower impactor of small child which weighs typical weight of 6 year child leg, 3.7kg. This child lower legform was assumed to provide the real impact characteristics of the small child pedestrian. Therefore the algorithm should be made to send a pop-up signal when this impactor is detected.

In case of frontal impact against rigid wall, the engine room with a open hood would be deformed more and the occupants are exposed to more severe injury [4]. Therefore the system should differentiate this frontal/offset crash and avoid the activation. Adopting the membranes switch and wheel speed sensor, developed system could prevent this erroneous situation.

To ensure the proper operation for the various misuse case, we have considered as a most difficult case to classify the impact with rigid poles of which the diameter and mass are the same value of the child/adult legform.

## DEVELOPMENT OF THE ACTIVE HOOD LIFT SYSTEM

In the developed system, the data collected by the contact sensors, composed of two accelerometers and membrane switch is sent to the ECU where the algorithm decides the activation and non activation

case within the required time. The contact sensors consist of two accelerometer and membrane switch installed on bumper fascia. If the algorithm determines the event as a pedestrian or lower legform impact, the fire signal is sent to the pyro-type actuator and the rear part of the hood is lifted with the help of deployment of specially designed hood hinge.

**Determination of System Response Time**

As shown in Figure 1, the total response time (TRT) of the system which consists of triggering time and actuator deployment time should be less than the first contact time of head to the hood.

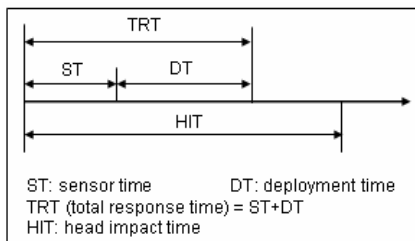
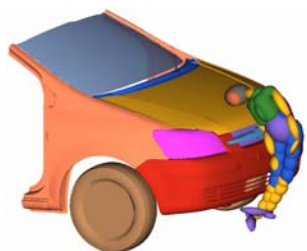
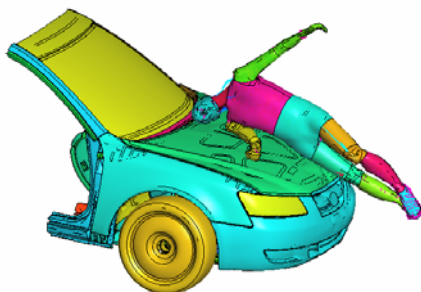


**Figure 1. System TTF (Time To Fire) requirement**

As shown in Figure 2, to calculate the head impact time (HIT), we have carried out a simulation of pedestrian impact at a vehicle speed of 40km/h for both cases of 6 year child and 50 %ile male human model. As a most severe case, the first contact time of 6 year child’s head was measured to 58msec in this simulation condition. Both child and adult pedestrians are initially in a walking posture.



Small sedan, 6yr child



Mid size sedan, 50%ile adult male

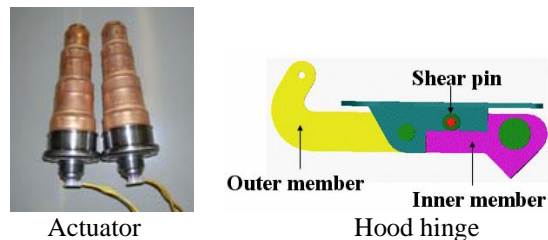
**Figure 2. CAE Simulation for pedestrian impact**

Typical deployment time of pyro-type actuator is approximately 30msec. Therefore, considering the system’s operational margin which depends on vehicles, the triggering time should be less than 15msec at a 40km vehicle speed.

**Verification Tests for Actuator Deployment Time**

As shown in Figure 3, pyro-type actuator is adopted to raise the hood rear part. This actuator, initially folded in radial direction, is deployed by the exploded gas pressure. Once the actuator is used, it could be changed easily with the new one by twisting and removing from the installed hole.

Hood hinge is newly modified to ensure the target stroke of actuator. As shown in Figure 3, this hood hinge is composed of inner/outer member and shear pin. When the actuator is deployed, the shear pin of the hinge is broken and the inner/outer member move upward as shown in Figure 4.



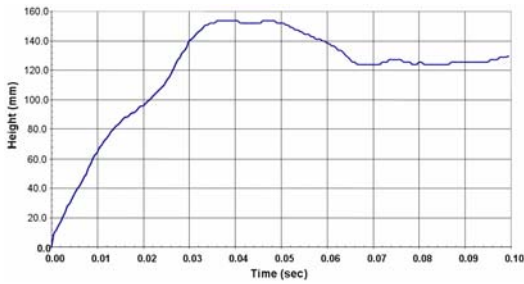
**Figure 3. Hood hinge and deployed actuator**

Figure 4 shows the test for actuator deployment. This test is carried out to confirm the appropriate operation of the hood lifting part. In this test, the actuator was forced to be activated by an ignition signal. The hood lifting displacement and actuator operation time are measured by the high speed camera.

As shown in Figure 5, the hood rear part is lifted up to the maximum value of 157mm. The operation time to reach the target displacement of hood, 115mm was less then the designed deployment time, 30msec. Through this test it is verified that the hood is fully lifted before the contact of 6 year child head to the hood, if the triggering time is less than 15msec.



**Figure 4. Test for actuator deployment**



**Figure 5. Time history of hood lifting displacement (at the hood hinge bracket point)**

**Tests to Generate Data for Algorithm Development**

As shown in Figure 6, the accelerometers are used as a main impact sensor. Because of the possibility of discrimination between rough road and impact with objects, two accelerometers are installed on the left/right bottom side of the bumper fascia. The main function of these sensors is to detect the impact with an object of a weight and stiffness equivalent to those of a pedestrian.

The sensing signal of the same object changes with the impact location and therefore the threshold value of metric used in the algorithm should be modified according to this impact location. In this study, the membrane switch, shown in Figure 6, is used to detect the impact location. Three membrane switches are attached on the bumper fascia front surface. Sixteen switch nodes are installed at each membrane switch as shown in Figure 7.

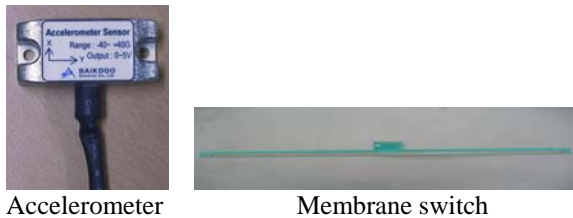


**Figure 6. Sensing system**

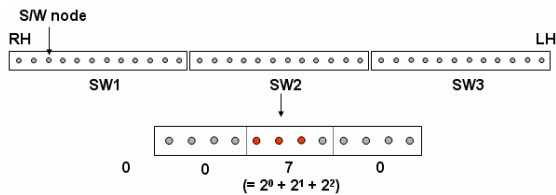


**Figure 7. Detecting impact location with membrane switch**

As previously mentioned, the impacts of the adult and 6 year child legform are considered as must-fire cases. On the contrary, thick and thin rigid pole, which have similar weight and diameter to the adult and child

legform respectively, are adopted as a must-not-fire cases as shown in Table 1.

**Table 1 Test matrix for sensing data**

|               | Target Objects                              |
|---------------|---|
| Must Fire     | Adult Legform (13.6kg)                      |
|               | Thin Pole with Foam (~Child Legform, 3.7kg) |
| Must Not Fire | Thick Rigid Pole (12.2kg)                   |
|               | Thin Rigid Pole (3.7kg)                     |
|               | Rough Road (Belgian)                        |
|               | Rough Road (Wave)                           |

The only difference between legform and rigid pole is the stiffness distribution of the object. There we assumed if the algorithm differentiates the impacts between these must and must-not fire conditions, the developed algorithm could cover most of the real fields misuse cases.

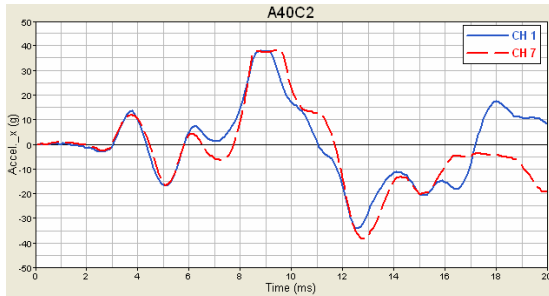
Figure 8 shows the test setup for adult legform impacts against vehicle bumper where several accelerometers and contact switches are installed. The sensing signals were saved within the notebook in real time.



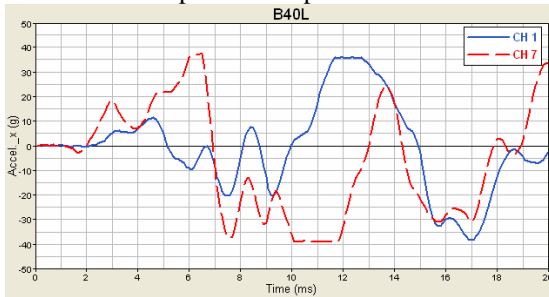
**Figure 8. Setup for sensing test (adult legform)**

The examples of obtained pulses for the impact legform are shown in Figure 9, where the fact that the pulse characteristics are affected by the bumper kinematics and impact location could be identified.

In order to choose the noise threshold value, the test was carried out on Belgian and wave load. In these cases acceleration larger than 7g was measured as shown in Figure 10. Therefore the algorithm would not start unless both of the 2 accelerations exceed this threshold value.



Impact at bumper center



Impact at bumper left

Figure 9. Acceleration pulse (adult legform)

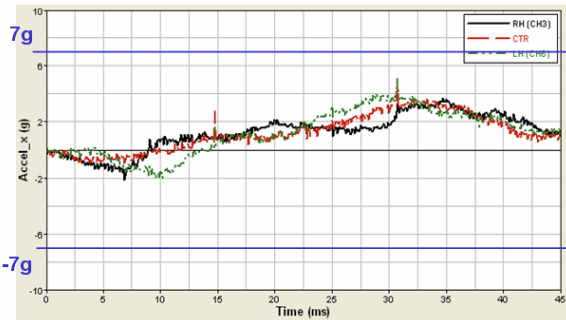


Figure 10. Acceleration pulse (Belgian road)

### Algorithm Development and Validation Test

The algorithm developed here is roughly introduced in Figure 11. The raw acceleration data is filtered and sampled. If this processed data exceeds a pre-defined threshold value and the contact switch is triggered, the algorithm starts. Then the impact location is detected and metrics are calculated until the time reaches the moment of deployment decision. The metrics are derived from the collected sensor signal to reflect distinctly the characteristics of the impact object. After the calculation of trigger thresholds (=metrics boundaries) and comparison between this value and metric, the decision of hood lifting is made. The trigger threshold values change with the impact location and vehicle speed.

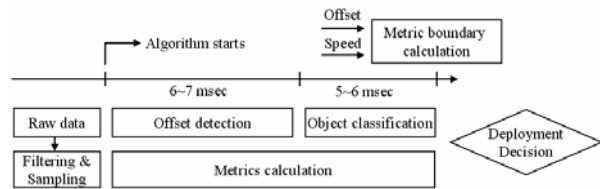


Figure 11. Setup for algorithm test

In order to confirm the algorithm performance, the system was tested with the use of wave form generator, where the sensing pulses were previously inputted. As shown in Figure 12, the input signals from wave form generator and contact switch are sent to the ECU and the algorithm determines the activation of system. If the firing signal is out from the ECU, two LED, assumed to be left/right actuators, would be lighted up. During this process, the input signals and the metrics used in the algorithm could be checked out with the oscilloscope and notebook computer, respectively. The system detected impact location of bumper fascia and discriminated the activation cases correctly for the typical five impact cases,

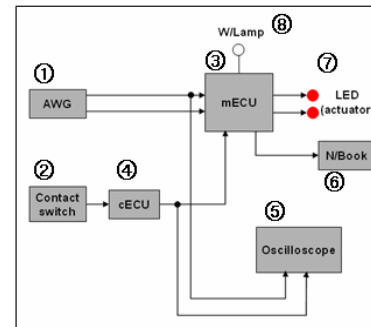
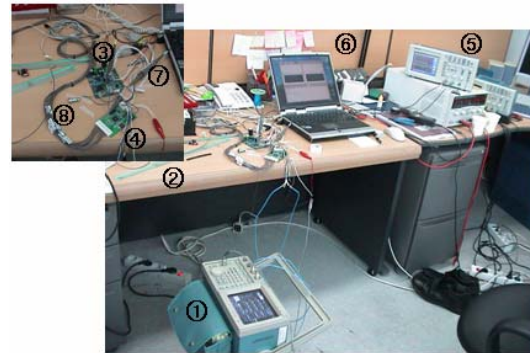


Figure 12. Setup for algorithm test

### Verification Tests of System Operation

To verify proper behavior of the system, three typical impact tests were performed. Impact objects and test conditions are shown in Table 2. The hood lift device was operated only in the case of adult legform impact. With the aid of high-speed camera, the total operation time, measured from the contact time between legform and bumper to the full deployment of actuator, was identified to be less than 50msec. Figure 13 shows the operation of the system for the legform impact.

**Table 2 Test matrix for system validation**

| Test items       | Impact velocity | Impact location | Results  |
|------------------|-----------------|-----------------|----------|
| Thin rigid pole  | 35km/h          | Left            | Not Fire |
| Thick rigid pole | 30km/h          | Right           | Not Fire |
| Adult legform    | 35km/h          | Center          | Fire     |



**Figure 13. Test of system operation**

### HEADFORM IMPACTOR TEST VERIFYING THE EFFECTIVENESS OF SYSTEM

In order to confirm the effects of the hood lifting device on the head injury reduction, the child headform impact tests of EURO-NCAP were conducted. As shown in Figure 14, five target points are selected, where, without hood lift device operation, the HPC value more than 1200 was measured.

Because proper operation of the lifting device was assured by the previous test, the headform was impacted against the initially lifted hood and the actuator was fully deployed. Figure 15 shows the test of headform impact on the projected hood point of the C3B (cowl top panel center).

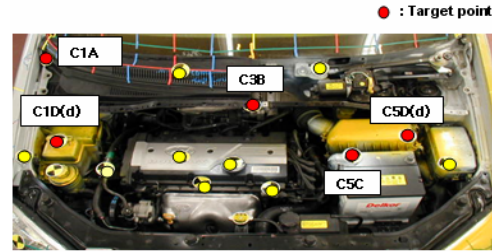
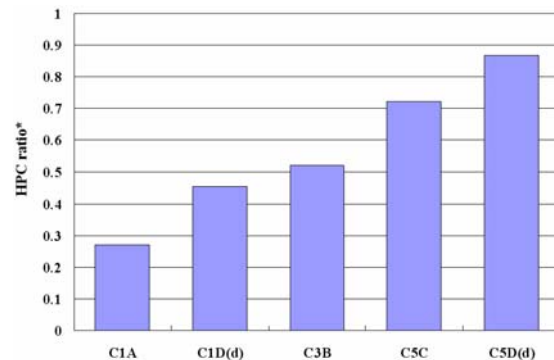


**Figure 14. Target points**



**Figure 15. Child headform impact test**

As shown in Figure 16, the improvement of the head injury could be confirmed with the operation of hood lift at all five points. However, due to the small initial space between hood skin and internal structure of engine room, the HPC value at some points were still more than target value of 1000. Therefore, in order to obtain the HPC value less than 1000, classical passive design improvements such as modification of hood structure and engine room layout should be considered simultaneously.



\*HPC ratio = HPC\_device / HPC\_no\_device

**Figure 16. Test results of headform impact**

In order to carry out an optimal design of the developed system at low cost, the simulation model of this device was developed. Figure 17 shows the comparison results of headform acceleration between test and simulation. The curve shape of simulation matches well with test results and peak values of acceleration are similar to each other.

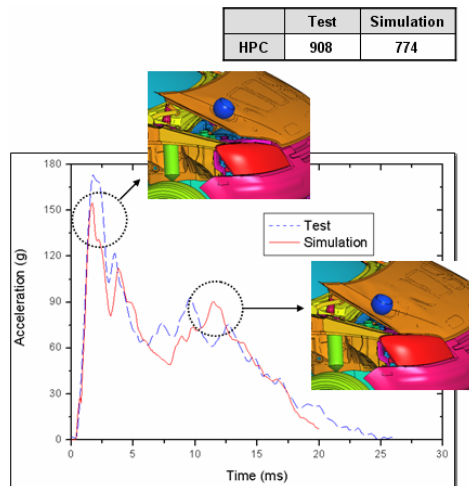


**Figure 17. Comparison between test and simulation results**

## CONCLUSIONS

Active hood lift system has been developed to get more spaces for decreasing the head injury during pedestrian impact. This system is composed of detecting sensor, ECU where the algorithm is embedded and the pyro-type actuators which raise the hood.

Through the development of this system, we could conclude this study as follows.

1) From the simulation of pedestrian impact at a vehicle speed of 40km/h for both cases of 6 year child and 50 %ile male human model, the first contact time of 6 year child's head was calculated to 58msec. Therefore, as a most severe case, the system operation time should be less than this time, 58msec.

2) The hood rear part is lifted up to the maximum value of 157mm. The operation time to reach the target displacement of hood, 115mm was less than the designed deployment time, 30msec. Hood is fully lifted before the contact of 6 year child head to the hood, if the triggering time is less than 15msec.

3) The total operation time of the system, measured from the contact time between legform and bumper to the full deployment of actuator, was identified to be less than 50msec.

4) With the aid of the developed hood lift system, it was confirmed that the pedestrian's head injury could be reduced significantly. However, in order to fulfill the HPC limits required by the regulation or EURO-NCAP

on pedestrian protection, the passive design/structural improvements should be also applied to the vehicles, especially for the small sedans, which show relatively small space between hood outer skin and hard structure of the engine room.

## REFERENCES

[1] R. Fredriksson, et al. 2001, "Evaluation of a New Pedestrian Head Injury protection System with a Sensor in the Bumper and Lifting of the Bonnet's Rear Part" 17<sup>th</sup> ESV Conference.

[2] K. Nagatomi, et al. 2005, "Development and Full-Scale Dummy Tests of a Pop-Up Hood System for Pedestrian Protection" 19<sup>th</sup> ESV Conference.

[3] Directive 2003/102/EC of the European Parliament and of the Council of 17 November 2003, Official Journal of the European Union, L 321/15

[4] Oliver Scherf. 2005, "Development and Performance of Contact Sensors for Active Pedestrian Protection Systems" 19<sup>th</sup> ESV Conference.

# **PREDICTION OF LOWER EXTREMITY INJURY RISKS DURING AN IMPACT ON MODERN CAR FRONTS WITH A FLEXIBLE PEDESTRIAN LEGFORM IMPACTOR AND THE PEDESTRIAN LEGFORM IMPACTOR ACCORDING TO EEVC WG 17**

**Oliver Zander**

**Bernd Lorenz**

Federal Highway Research Institute (BAST), Bergisch Gladbach, Germany

**Dirk-Uwe Gehring**

**Peter Leßmann**

BGS Böhme & Gehring GmbH, Bergisch Gladbach, Germany

Paper Number 07-0206

## **ABSTRACT**

A legform impactor with biofidelic characteristics (FlexPLI) which is being developed by the Japanese Automobile Research Institute (JARI) is being considered as a test tool for legislation within a proposed Global Technical Regulation on pedestrian protection (UNECE, 2006) and therefore being evaluated by the Technical Evaluation Group (TEG) of GRSP. In previous built levels it already showed good test results on real cars as well as under idealised test conditions but also revealed further need for improvement.

A research study at the Federal Highway Research Institute (BAST) deals with the question on how leg injury risks of modern car fronts can be revealed, reflected and assessed by the FlexPLI and how the impactor can be used and implemented as a legislative instrument for the type approval of cars according to current and future legislations on pedestrian protection. The latest impactor built level (GT $\alpha$ ) is being evaluated by a general review and assessment of the certification procedure, the knee joint biofidelity and the currently proposed injury criteria. Furthermore, the usability, robustness and durability as a test tool for legislation is examined and an assessment of leg injuries is made by a series of tests with the FlexPLI on real cars with modern car front shapes as well as under idealised test conditions. Finally, a comparison is made between the FlexPLI and the current european legislation tool, the legform impactor according to EEVC WG 17.

## **INTRODUCTION**

In its final report the EEVC Working Group 17 (2002) gave recommendations for the acceptance levels of shear displacement, bending angle and tibia acceleration for the EEVC legform to bumper test used for the european type approval within the first phase of the European Framework Directive (European Union, 2003) dealing with the protection of pedestrians and other vulnerable road users. Those acceptance levels were on the one hand based on cadaver tests (Kajzer, 1997) where

preloaded knee joints that were exposed to bending as well as shearing deformation showed the most common initial damage mechanisms at an average lateral bending angle from 15° on and at an average peak shearing force from 2,4 kN on. Those cadaver tests were reproduced by EEVC WG 17 in order to find a transfer function between cadaver output and impactor output. A lateral bending angle of 15° and 6 mm shear displacement based on a 4 kN shear force were considered to be appropriate acceptance levels. As for the lateral tibia peak acceleration on the other hand, WG 17 did not change the formerly proposed acceptance level of 150 g as they showed a good correlation between cadaver and impactor tests.

Konosu et al. (2001) analysed the influence of rigid bones on the estimation of leg injuries. From a bone bending effect on the bending angle as well as the acceleration varying with the impact conditions they concluded the need for a flexible legform impactor. Therefore, a flexible pedestrian legform impactor (FlexPLI) is being developed by the Japanese Automobile Research Institute and being evaluated by the Technical Evaluation Group (TEG) of GRSP. The present study gives a general review of the latest impactor built level and certification procedure and examines its usability, robustness and durability as a test tool for legislation by a series of tests on real cars with modern front shapes as well as under idealised test conditions.

## **DEVELOPMENT OF THE FLEX PLI**

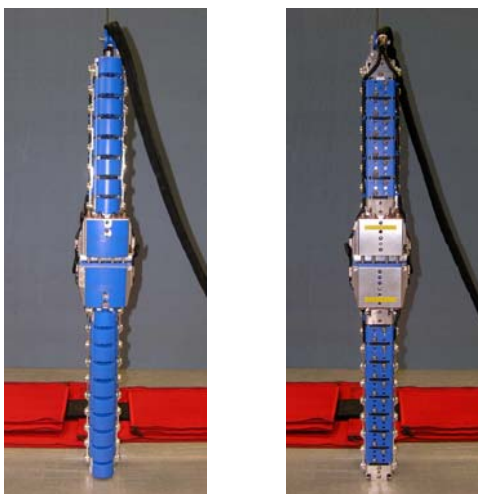
### **Flex-G**

A pedestrian legform impactor with biofidelic characteristics has been developed by the Japanese Automobile Research Institute (JARI) (Konosu et al., 2003) and showed first good results during real car tests in its version 2004 (Konosu et al., 2005). The Federal Highway Research Institute (BAST) gave an assessment of the impactor in its G-Level showing a good repeatability and reproducibility of test results under idealised test conditions on the one hand but revealing a need for further modification on the other hand (Zander et al., 2006). Tests at an impact speed of 40 km/h could only be performed on cars with modified front

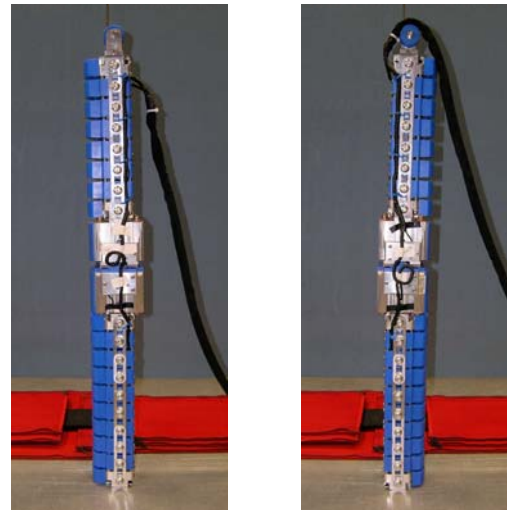
shapes. Even at reduced impact speeds the protection criteria could be met marginally only. Furthermore, an expansion of the limited measurement range that was already partially exceeded within those tests at reduced impact speeds was requested. Finally, the impactor was lacking a continuity between its different built levels - while the requirements for the Flex2004 could be met by a series production car, the same car exceeded the proposed Flex-G limits clearly (Imaizumi, 2005).

### Flex-GT $\alpha$

Those issues were addressed by JARI who developed the Flex-GT $\alpha$  in spring of 2006. The latest impactor built level has a higher knee bending angle limit and modified specifications to improve injury assessment ability. While the femur and tibia lengths remained the same, the locations of the centers of gravity were moved both towards the knee joint center. The overall impactor mass was reduced by 1,5 kg and is now 12,4 kg. This was mainly done by replacing most of the stainless steel housing by MC-nylon and aluminium. It has to be stated that regarding the weight and CoG characteristics the Flex-GT $\alpha$  differs more from the 50<sup>th</sup> AM leg than the previous impactor version. At the knee condyle longer knee springs were installed. Furthermore, the femur and tibia impact facing were brought in line with the knee by applying a thicker impact facing over the whole length of the impactor. Additionally, the bone core of both femur and tibia was made thinner and wider in order to obtain a smaller bending stiffness of the long bones. The knee size was changed in order to install longer springs for a higher knee bending limitation (+ 30%). Nine sets of knee ligaments were installed. The knee impact face was given a round shape. All measurement items, their positions and cables remained the same (Fig. 1-4).



Figures 1 and 2. Flex-GT $\alpha$  - impact view and left view.



Figures 3 and 4. Flex-GT $\alpha$  - front view and rear view.

Konosu (2006) justified the main changes between Flex-G and Flex-GT $\alpha$  with a better injury assessment ability. He stated a slightly smaller bending stiffness for the femur and tibia section of the Flex-GT $\alpha$  but still within the PMHS corridors developed by Ivarsson et al. (2004). The knee bending stiffness increased significantly but is still smaller than that of the rigid WG 17 lower leg impactor (Bhalla et al., 2003).

### REVIEW OF THE KNEE JOINT BIOFIDELITY AND LEG INJURY CRITERIA

In their 2001 study Konosu et al. reconsidered the injury criteria for the pedestrian subsystem legform with the rigid legform impactor. They took the results of dynamic PMHS tests performed by Kajzer et al. (1997) to obtain the human knee characteristics versus shearing and bending and applied a logistic analysis method (Nakahira et al., 2000) in order to produce an injury risk curve against the bending angle (Figure 5).

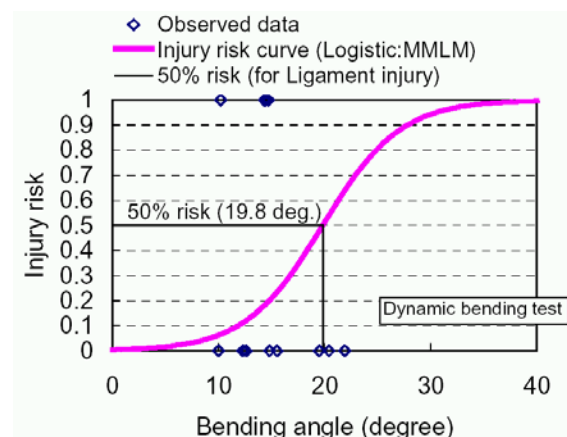
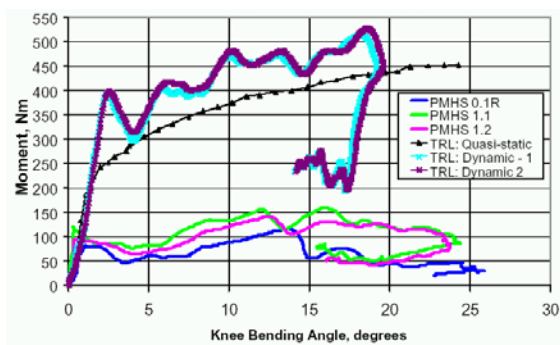


Figure 5. Injury risk curve and 50% injury risk against the bending angle (Konosu et al., 2001).

In an initial study for establishing pedestrian-impact lower limb injury criteria Kerrigan et al. (2003) found within PMHS knee bending and shear tests where the knee joint was isolated from the long bones and within femur and tibia bending tests a significantly lower average lateral failure bending moment for the knee joint than that reported in previous literature as well as that reported in the same study for the femur and for the tibia section. They concluded the importance of realistic boundary conditions and the need for the determination of a statistically valid impact threshold for the knee joint.

Bhalla et al. (2003) made a comparison between PMHS knee joint and mechanical knee joint tests and found a higher stiffness of the rigid EEVC WG 17 legform impactor and the POLAR II knee joint compared to the bending and shear loading stiffness of the PMHS knee, with much smaller differences between the POLAR II and the PMHS knee bending stiffness (Figures 6-8). They also found out pure shear of the knee joint being an extreme case not occurring in real world pedestrian accidents.



**Figure 6. Lateral knee bending stiffnesses of the EEVC WG 17 legform impactor compared to PMHS knee tests (Bhalla et al., 2003).**

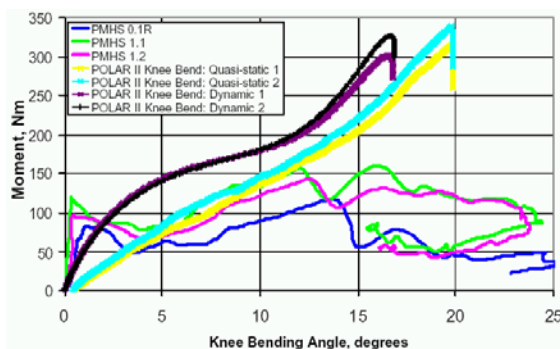


**Figure 7. Lateral knee bending stiffnesses of the POLAR II knee compared to PMHS knee tests (Bhalla et al., 2003).**

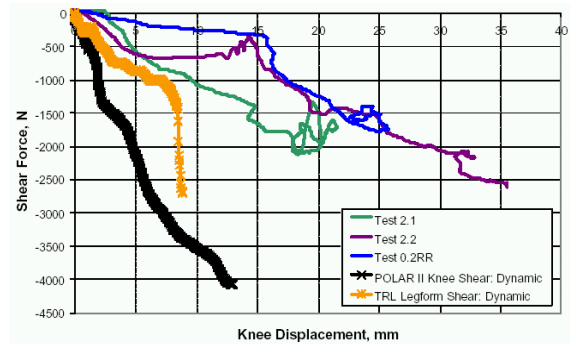


**Figure 8. Lateral shear stiffnesses of the EEVC WG 17 legform impactor and the POLAR II knee compared to PMHS tests (Bhalla et al., 2003).**

Bose et al. (2004) were analysing the response of the pedestrian knee to the pedestrian impact loading environment in order to determine injury thresholds and to validate computational models and mechanical legform impactors. They tested isolated PMHS knee joints in dynamic lateral-medial valgus loading (4 point bending and 3 point bending and shearing tests) replicating a vehicle-pedestrian impact at 40 km/h with the medial collateral ligament (MCL) as the only major load bearing knee structure being injured in the experiments. They found out a first peak bending moment between about 90 Nm and 150 Nm but assumed a knee shear force of zero within the 4-point pure bending tests. Thus, the four-point bending tests had a moment-shear ratio of infinity. The 3-point bending and shearing tests resulted in peak bending moments between 50 Nm and 80 Nm when inducing a knee angulation rate of 1°/ms and between 230 Nm and 270 Nm when increasing the proportion of the shear force acting at the knee.

Ivarsson et al. (2004) used the 4-point bending results from Bose to develop force-displacement and moment-displacement corridors with localized injury thresholds for the 50<sup>th</sup> AM femur, tibia and knee when being subjected to latero-medial bending at rates characteristic of the pedestrian impact loading environment. The study resulted in a 50% risk of femur fracture at a bending moment of 447 Nm and a 50% risk of tibia fracture at a bending moment of 312 Nm (Figures 9 and 10).

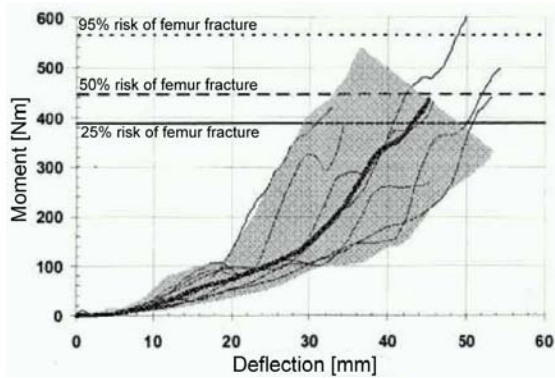


**Figure 9. Moment-deflection corridors for the 50<sup>th</sup> percentile male femur subjected to dynamic latero-medial loading with the point of load application at mid-span (Ivarsson et al., 2004).**

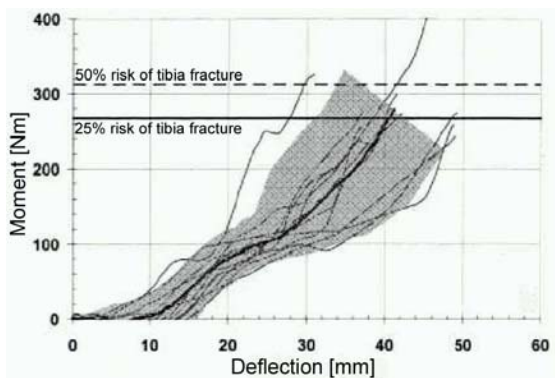


**Figure 10. Moment-deflection corridors for the 50<sup>th</sup> percentile male tibia subjected to dynamic latero-medial loading with the point of load application at mid-span (Ivarsson et al., 2004).**

For injuries occurring at the time of the first local moment peak Ivarsson et al. found a 50 % risk of MCL injury in dynamic valgus bending of the knee at a bending moment of 117 Nm or a knee bending angle of 13,9°; for injuries occurring at the time of the maximum moment the 50 % risk of MCL injury was at 134 Nm or 18,2° (Figures 11 and 12).

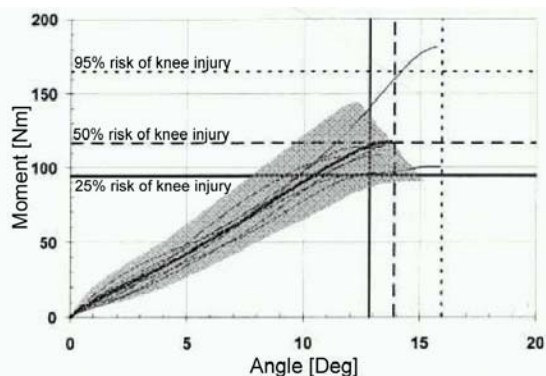


**Figure 11. Moment-angle response corridor for the 50<sup>th</sup> percentile male knee subjected to dynamic 4-point valgus bending for injuries occurring at the time of the first local moment peak (Ivarsson et al., 2004).**

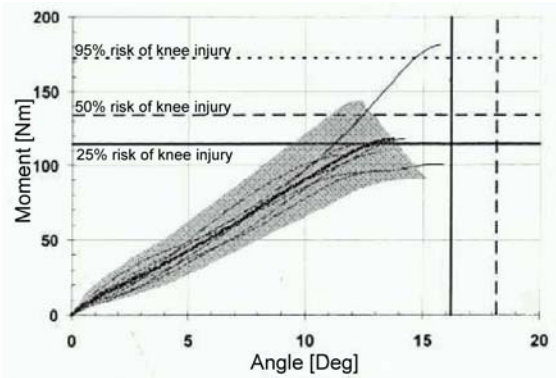


**Figure 12. Moment-angle response corridor for the 50<sup>th</sup> percentile male knee subjected to dynamic 4-point valgus bending for injuries occurring at the time of the maximum moment (Ivarsson et al., 2004).**

In a study going back to 1985 Nyquist et al. subjected human tibias to static and dynamic three-point-bending tests. The applied loads were directed from the anterior to posterior or from lateral to medial and sustained fracture at or near mid-span. The maximum bending moments for seven male cadavers with a lateral load applied at impact speeds between 2,9 and 4,2 m/s were between 224 and 431 Nm with an average of 312 Nm. As a result, an injury threshold of 350 Nm for the maximum tibia bending moment was proposed by the Japanese Automobile Research Institute (Ishikawa, 2004).

For tests on real cars with the Flex PLI version GTα Konosu et al. (2006) derived 50% injury risk levels for the 50<sup>th</sup> AM for the tibia and knee from the reviewed literature (Table 1).

**Table 1. Proposed 50% injury risk levels for the 50<sup>th</sup> AM (Konosu et al., 2006)**

| Leg region | 50% injury risk level for 50 <sup>th</sup> AM |
|------------|---|
| Tibia      | 312 - 350 Nm                                  |
| MCL        | 19,5 - 21,6 mm                                |
| ACL        | 11,2 mm                                       |
| PCL        | 11,2 mm                                       |

Due to the lack of an upper body mass of the FlexPLI the femur test results of the Flex-GTα were considered to be negligible and monitored only in order to check the generated strain of the bone but without any comparison with the injury risk levels derived from the previous studys. Therefore, the proposed injury risk levels are not given in Table 1 and will not be considered further within this study.

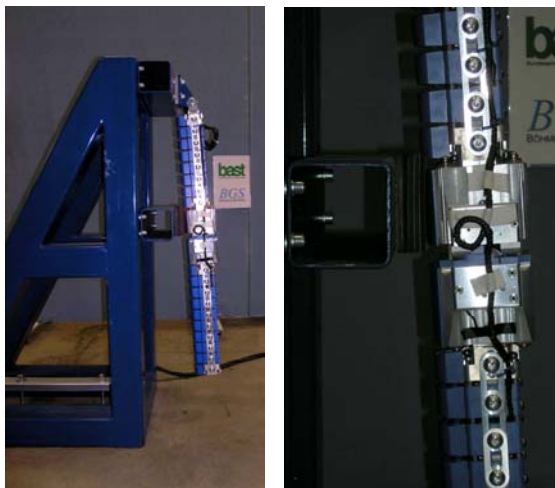
## CALIBRATION AND CERTIFICATION

### Calibration

As calibration method for tibia, femur and knee the same three point bending method as for the Flex-G has been adopted (Konosu, 2006). Only the strain gauges are calibrated, while the calibration of the sensors and the bones is still not addressed.

### Dynamic certification test

The certification procedure for the legform assembly is described in detail in an earlier study of the authors (2006). The impactor is suspended without flesh and skin over a pin joint from a fixed pendulum frame, lifted until it is 15 degrees above the horizontal and then released. A cross beam, covered with two neoprene and three rubber sheets, is fixed at a height such that it is hit by the knee joint of the released legform when reaching the vertical (Figures 13-15), causing bending of the bones and shearing and bending of the knee.



Figures 13, 14 and 15. Dynamic certification test.

### Dynamic certification test results

For the present study, in total 21 certification tests were performed. All ligament extensions of the Flex-GT $\alpha$  (medial collateral ligament MCL, anterior cruciate ligament ACL and posterior cruciate ligament PCL) were within the measurement range. (Figures 16 and 17).

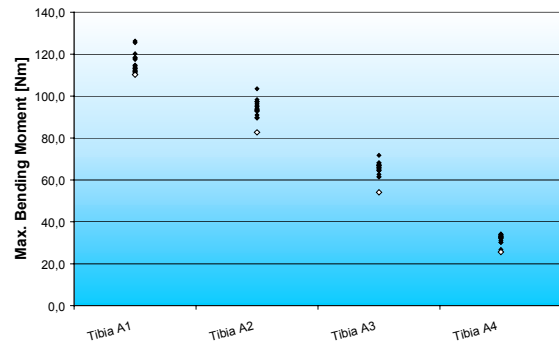


Figure 16. Certification results of the tibia section ( $\diamond$ : full assembly test).

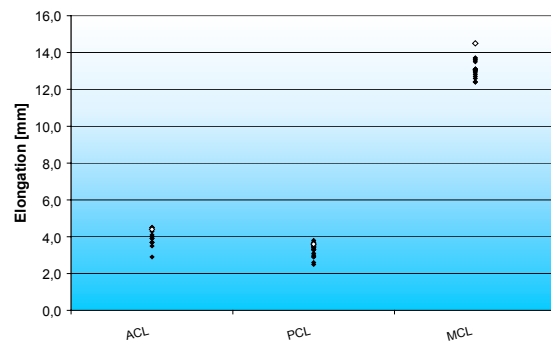
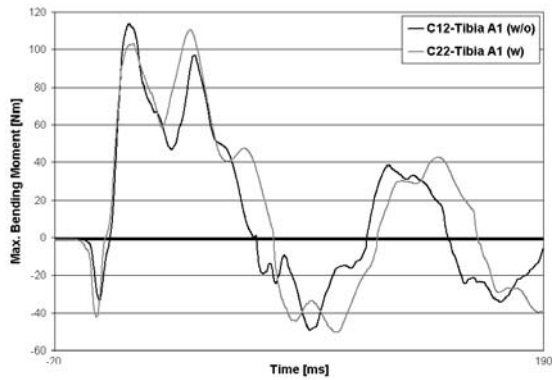
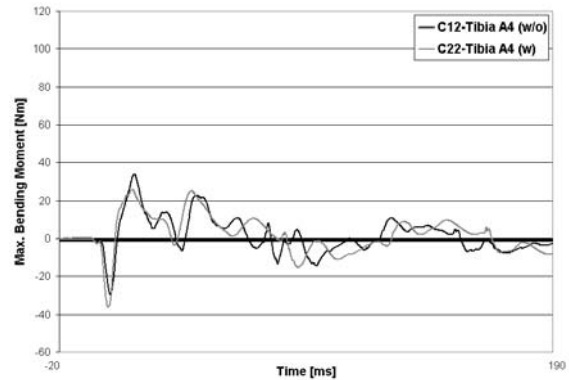


Figure 17. Certification results of the knee ligaments ( $\diamond$ : full assembly test).

In addition, one full assembly dynamic certification test was performed, i.e. that the legform impactor was used as during the real car tests, covered with all neoprene and rubber layers while those layers were removed from the cross beam. As it can be seen in Figures 16 and 17, the results for the maximum bending moments and ligament elongations showed quite similar results. While the maximum bending moments for the tibia segments were the lowest ones from all tests, the ligament peak elongations were comparatively high. Figures 18-21 compare the traces for the tibia bending moments.



**Figure 18.** Comparison of the bending moments of the tibia A1 segment with (w) and without (w/o) flesh and skin.



**Figure 21.** Comparison of the bending moments of the tibia A4 segment with (w) and without (w/o) flesh and skin.

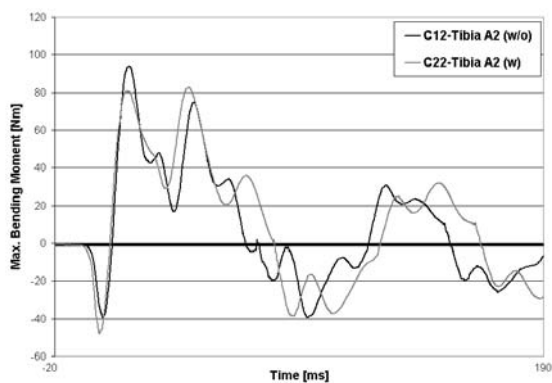


**Figure 19.** Comparison of the bending moments of the tibia A2 segment with (w) and without (w/o) flesh and skin.

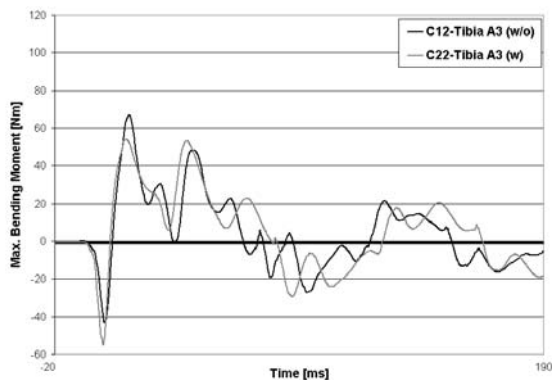


**Figure 20.** Comparison of the bending moments of the tibia A3 segment with (w) and without (w/o) flesh and skin.

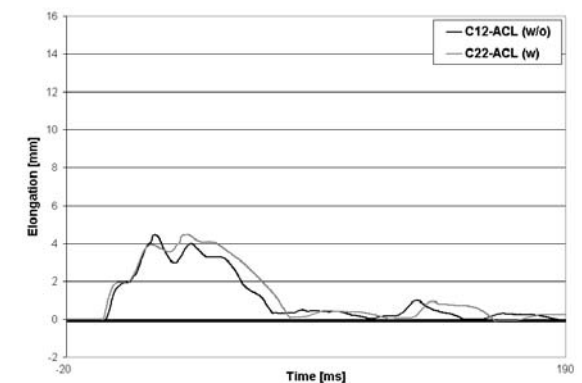


**Figure 22.** Comparison of the ACL elongations with (w) and without (w/o) flesh and skin.

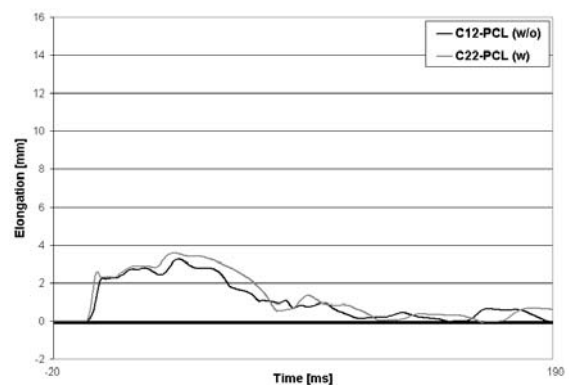


**Figure 23.** Comparison of the PCL elongations with (w) and without (w/o) flesh and skin.

As it can be seen, the legform showed a comparatively similar behaviour for the bending moments. Anyway, within the first peak all tibia segments showed a higher bending moment in the currently proposed certification test (without flesh and skin), while the second peak was higher within the full assembly test.

Figures 22-24 compare the traces of the knee ligament elongations measured within the currently proposed certification test and the full assembly certification test.

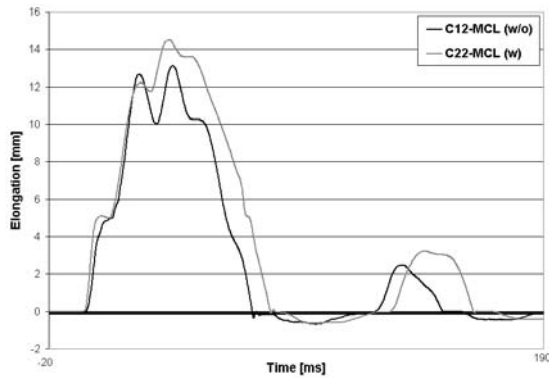


**Figure 24. Comparison of the MCL elongations with (w) and without (w/o) flesh and skin.**

Also the knee ligaments showed a quite similar behaviour with and without flesh and skin. In general, the knee of the fully assembled impactor (with flesh and skin) gave higher results. This phenomenon can be explained by a higher knee stiffness due to the rubber sheets applied over the whole impactor length and therefore a different energy application.

The standard deviation S of the certification results (tests 1-21) was assessed according to the dummy requirements described by Mertz (2004). The results are given in Table 2.

**Table 2. Repeatability of the certification results**

| Dynamic certification |                                     |      |      |      |                 |       |      |
|-----------------------|-------------------------------------|------|------|------|-----------------|-------|------|
|                       | Max. bending moment [Nm]<br>- Tibia |      |      |      | Elongation [mm] |       |      |
|                       | A1                                  | A2   | A3   | A4   | ACL             | PCL   | MCL  |
| SD                    | 4,41                                | 3,33 | 2,33 | 2,16 | 0,43            | 0,34  | 0,41 |
| [%]                   | 3,82                                | 3,53 | 3,53 | 6,75 | 10,44           | 10,48 | 3,14 |
| Ass.                  | A                                   | A    | A    | A    | N               | N     | A    |

G: good, A: acceptable, M: marginal, N: not acceptable

The leg showed acceptable results for the MCL elongation and all bending moments of the tibia. As for the ACL and PCL elongation the certification tests gave unacceptable results.

## REAL CAR TESTS

Two cars with pedestrian friendly bumpers according to the EEVC test procedure and limits, a Mercedes A-Class with a Euro NCAP rated green lower leg area, and a VW Golf V with borderline results to a green bumper area were tested with the Flex-G impactor by the authors of this study. (2006). As the test results with reduced impact speeds (24 km/h) already exceeded partially the measuring range for the bending moment as well as for the elongation of the leg, the series production cars were modified by removing the bumper padding and adding a padding at the lower outer

contour of the car front. As the Flex-GT $\alpha$  with a significantly higher bending stiffness and a knee bending limitation increased by 30% was expected to deliver usable results with series production cars even at the European regulatory test speed of 40 km/h, the same cars were tested in their unmodified versions at 40 km/h. For comparability reasons an identical impact height of 25 mm above ground level according to the proposed GTR was chosen. An extension of the test series was made to include a car representing the SUV category with a green lower leg test area (Audi Q7) and a car representing the sedan category and designed for compliance with phase 1 of the European Directive. Both cars were tested at an impact height of 75 mm above ground level as this height was used within latest simulations by JARI and resulted in a better knee injury assessment ability.

## VW Golf V test results

The impact points to be tested with the Flex-GT $\alpha$  on the VW Golf V were located identically to two green / borderline rated Euro NCAP test points (Figure 25).



L1b: three tests / L3a: one test  
(bumper vertical bracing rib)  
Euro NCAP: -136,5 g / -2,4 mm / 15,7°  
L2b: three tests  
(manufacturers' emblem)  
Euro NCAP: -135,6 g / -2,7 mm / 13,4°

**Figure 25. Golf V Euro NCAP impact locations to be tested with the Flex-GT $\alpha$ .**

Test point L3a as a symmetrical identical point to L1b according to Euro NCAP was tested one time in order to validate this assumption made by the test laboratory and the sensitivity of the Flex-GT $\alpha$  on mirrored test point.

In total, seven tests at three different impact locations were performed with the Flex-GT $\alpha$  on the Golf V. The results are shown in Figures 26 and 27.

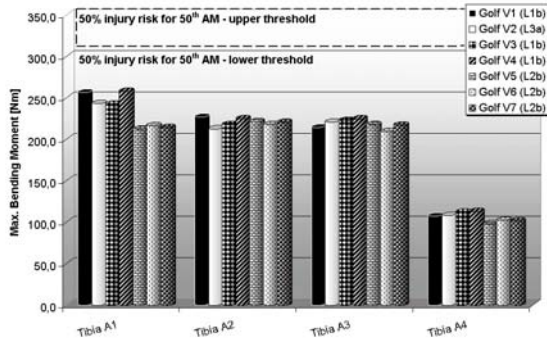


Figure 26. Golf V test results for the tibia segments.

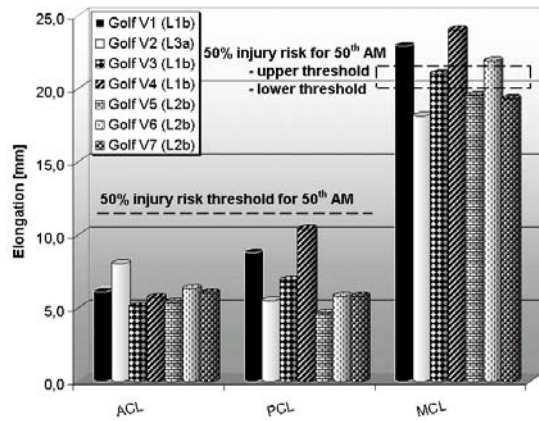


Figure 27. Golf V test results for the knee ligaments.

As it can be seen from the diagrams all three impact locations met the proposed tibia and ACL and PCL knee injury criteria. Only the MCL ligament exceeded the thresholds in half of the tests. Test V2 was performed on a location symmetrical identical to tests V1, V3 and V4, where the PCL peak elongation was permanently higher than the ACL peak elongation. Therefore, the lower PCL than ACL elongation in test V2 initially seemed to confirm the symmetric. However, the ACL peak elongation in test V2 occurred at a completely different time and was significantly higher than in the symmetrical identical tests V1, V3 and V4 (Figure 28).

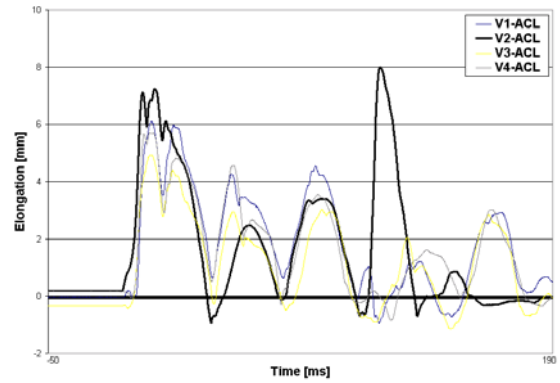


Figure 28. ACL elongations in the Golf V tests (1-4) - examination of the symmetric.

Besides, also the lower result for the MCL ligament in test V2 could lead to the conclusion of a high knee sensitivity towards structures assumed to be similar. Nevertheless, quite similar characteristics of the MCL elongation traces within the tests 1-4 can be stated, as shown in Figure 29.

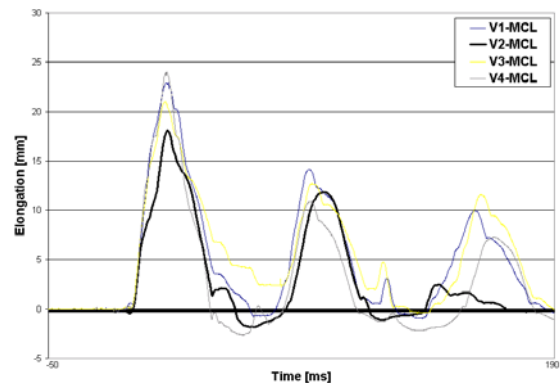


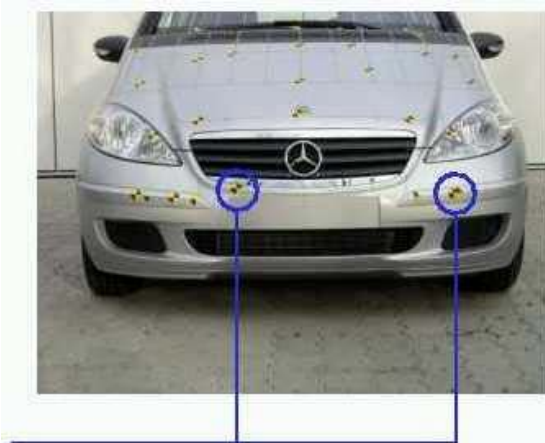
Figure 29. MCL elongations in the Golf V tests (1-4) - examination of the symmetric.

For the tibia bending moments, all traces of tests 1-4 showed similar tendencies. The tibia section did not show a high sensitivity towards mirrored test points.

In three of the tests the proposed requirements were all met, two of them on a Euro NCAP green rated test point with a knee bending angle of 13,4° in the corresponding Euro NCAP test.

### Mercedes A-Class test results

As on the Golf V, also the impact points to be tested with the Flex-GT $\alpha$  on the Mercedes A-Class were located on two green Euro NCAP rated test points (Figure 30).



L2a: three tests / L2b: one test  
 (left / right end of number plate area)  
 Euro NCAP: -113,0 g / -2,7 mm / 11,5°  
 L3b: three tests  
 (left part of headlamp area)  
 Euro NCAP: -143,0 g / -3,7 mm / 8,4°

**Figure 30. A-Class Euro NCAP impact locations to be tested with the Flex-GTα.**

Test point L2b as a symmetrical identical point to L2a according to Euro NCAP was tested one time for validation purposes and in order to analyse the sensitivity of the Flex-GTα towards mirrored test point.

Seven tests at three different impact locations were performed. The results for the tibia and knee are shown in Figures 31 and 32.

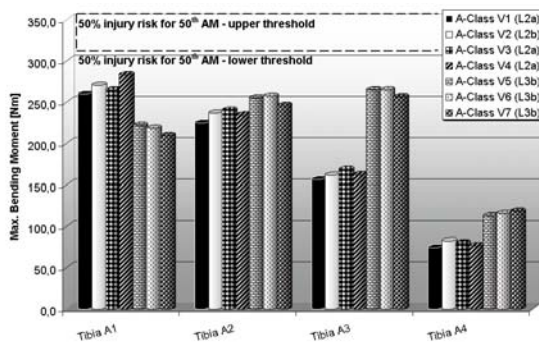


**Figure 31. A-Class test results for the tibia segments.**

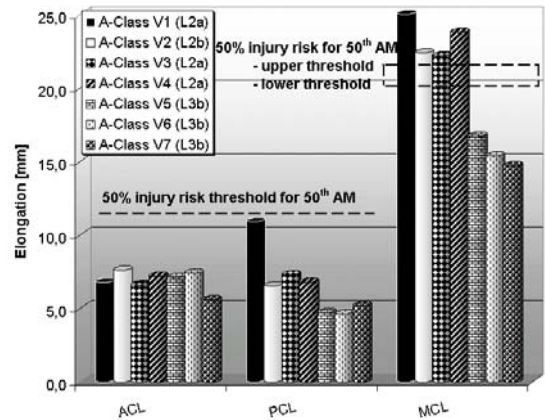


**Figure 32. A-Class test results for the knee ligaments.**

Again, all three impact locations on the Mercedes A-Class met the proposed tibia and ACL and PCL injury risk thresholds. The MCL ligament exceeded the elongation thresholds at the first and second impact location (Tests V1-V4). Impact point V2 that was mirrored to V1 did not show the tendency of the Golf tests where the ACL and PCL results were the other way around compared to the first impact location. This might also be the case because no clear tendency for the ACL/PCL results of the first impact point can be observed. No tendency can be seen either regarding the MCL sensitivity on mirrored impact points. Despite the quite similar characteristics of the knee elongation traces, test V1 shows quite different peak values and a different behaviour especially for the PCL elongation. Here, also the symmetrical identical point V2 behaves differently (Figure 33).

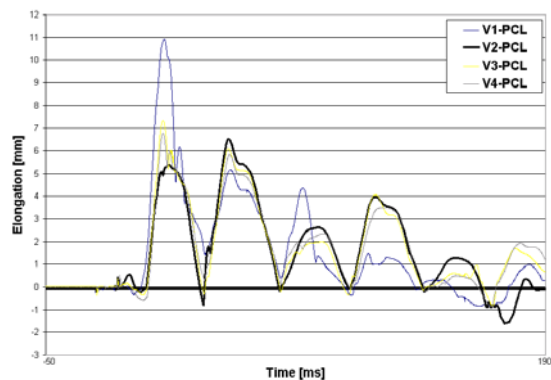


**Figure 33. PCL elongations in the A-Class tests (1-4) - examination of the symmetric.**

The traces for the tibia bending moments in tests 1-4 confirmed the Golf V results. Therefore, no sensitivity of the tibia towards mirrored test points could be observed.

The third impact location (L3b) met in all three tests the proposed requirements clearly. Euro NCAP rated this point green and measured a bending angle of 8,4°.

### Audi Q7 test results

On the Audi Q7 representing the SUV car category two tests were performed at two different impact locations that were both rated green according to Euro NCAP (Figure 34).

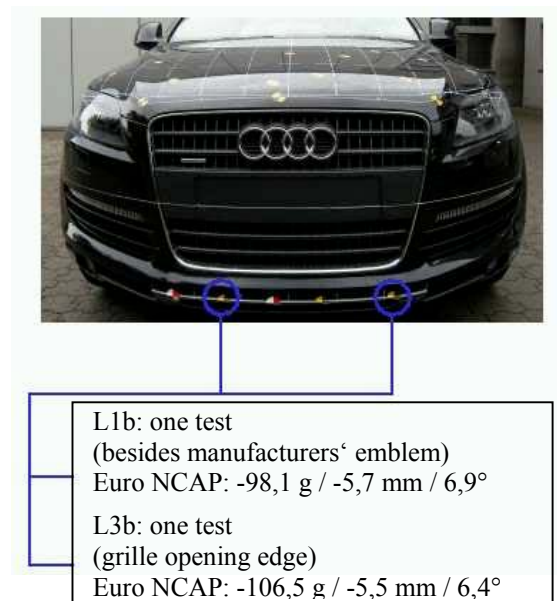


Figure 34. Q7 Euro NCAP impact locations to be tested with the Flex-GTα.

As impact height 75 mm above ground level were chosen. The tibia and knee results are shown in Figures 35 and 36.

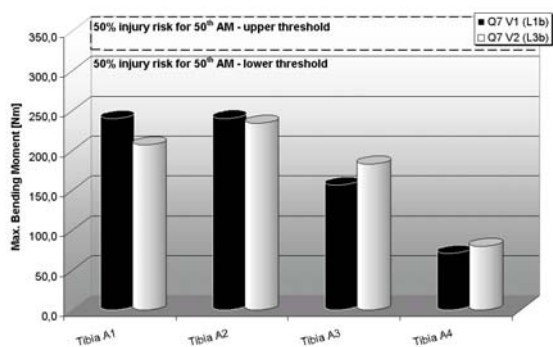


Figure 35. Q7 test results for the tibia segments.

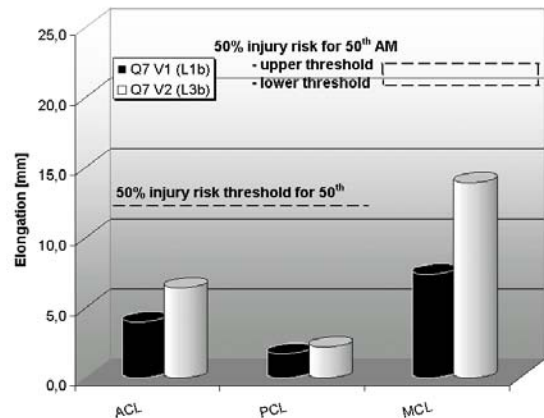


Figure 36. Q7 test results for the knee ligaments.

Both impact locations met all proposed test requirements clearly, whereas the MCL load measured in the second test was significantly higher than that of the first test. This does not confirm the Euro NCAP results where the bending angle of the second test was slightly lower than that of the first test.

### Sedan test results

The last car to be tested within this study, a sedan type car MY 2007, has been type approved according to the European Directive on pedestrian protection, i.e. that the bumper area homogeneously met the requirements of phase 1 which are 200 g for the tibia acceleration, 6 mm for the shearing displacement and 21° for the knee bending angle. Three points on the bumper have been tested at an impact height of 75 mm above ground level. The results are given in Figures 37 and 38.

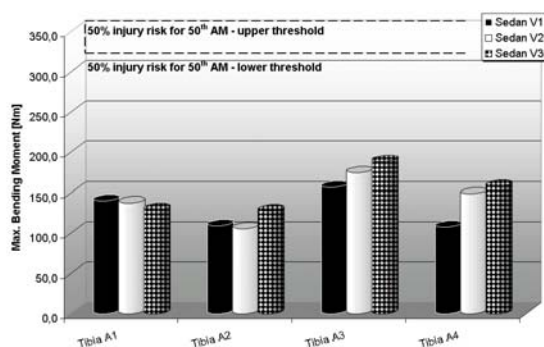
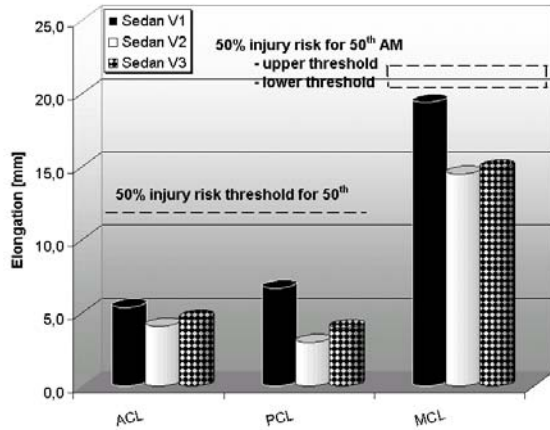


Figure 37. Sedan test results for the tibia segments.



**Figure 38. Sedan test results for the knee ligaments.**

All three impact locations met the proposed injury criteria clearly. The load on the MCL ligament in the first test was higher than in the following ones but still slightly below the currently proposed lower 50% injury risk threshold of 19,5 mm. These results fully confirm those of the homologation tests where the first test showed the highest bending angle of the rigid WG 17 impactor while the following two tests have met all legform to bumper criteria even of the current phase 2.

**REPEATABILITY**

**Real car tests**

For the determination of the repeatability of test results with the Flex-GT $\alpha$  impactor the test values of each of the four impact points being tested three times were taken for the calculation of the standard deviation (SD). Based on the requirements for dummies (Mertz, 2004) the repeatability of the real car tests was assessed according to Table 3.

**Table 3. Repeatability of the real car test results**

| Golf V  |                                  |      |      |      |                 |       |      |
|---------|----------------------------------|------|------|------|-----------------|-------|------|
| L1b     | Max. bending moment [Nm] - Tibia |      |      |      | Elongation [mm] |       |      |
|         | A1                               | A2   | A3   | A4   | ACL             | PCL   | MCL  |
| SD      | 8,42                             | 4,98 | 5,39 | 3,06 | 0,5             | 1,75  | 1,52 |
| [%]     | 3,34                             | 2,23 | 2,44 | 2,76 | 8,93            | 20,14 | 6,71 |
| Ass.    | A                                | G    | G    | G    | M               | N     | A    |
| L2b     |                                  |      |      |      |                 |       |      |
| L2b     | Max. bending moment [Nm] - Tibia |      |      |      | Elongation [mm] |       |      |
|         | A1                               | A2   | A3   | A4   | ACL             | PCL   | MCL  |
| SD      | 1,95                             | 2,07 | 4,87 | 2,19 | 0,46            | 0,69  | 1,45 |
| [%]     | 0,91                             | 0,94 | 2,27 | 2,17 | 7,77            | 12,83 | 7,15 |
| Ass.    | G                                | G    | G    | G    | M               | N     | M    |
| A-Class |                                  |      |      |      |                 |       |      |
| L2a     | Max. bending moment [Nm] - Tibia |      |      |      | Elongation [mm] |       |      |
|         | A1                               | A2   | A3   | A4   | ACL             | PCL   | MCL  |
| SD      | 12,00                            | 7,81 | 6,20 | 2,64 | 0,31            | 2,24  | 1,45 |

| [%]  | 4,45                             | 3,35 | 3,81 | 3,43 | 4,45            | 26,84 | 6,13 |
|------|----------------------------------|------|------|------|-----------------|-------|------|
| Ass. | A                                | A    | A    | A    | A               | N     | A    |
| L3b  | Max. bending moment [Nm] - Tibia |      |      |      | Elongation [mm] |       |      |
|      | A1                               | A2   | A3   | A4   | ACL             | PCL   | MCL  |
| SD   | 6,53                             | 5,82 | 4,71 | 2,80 | 0,96            | 0,32  | 1,01 |
| [%]  | 3,01                             | 2,30 | 1,80 | 2,41 | 14,39           | 6,65  | 6,51 |
| Ass. | A                                | G    | G    | G    | N               | A     | A    |

G: good, A: acceptable, M: marginal, N: not acceptable

The calculations for the standard deviation state a repeatability between good and acceptable for all maximum tibia bending moments at all of the four impact locations, while the repeatability results for the knee elongation are in less than half of the cases still acceptable. Here, the PCL ligament shows the highest sensitivity and not acceptable repeatability results at three impact locations. The repeatability of the MCL ligament test results is at least at three impact locations still acceptable. In total, four measurement locations showed unacceptable repeatability results (Figure 39).

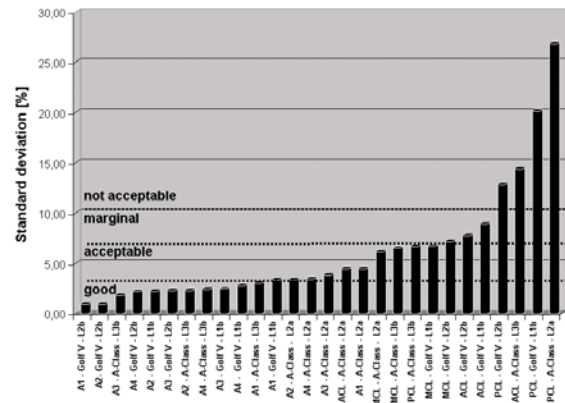


**Figure 39. Sensitivity of the measurement locations depending on the impact location.**

**Inverse tests**

In order to obtain more detailed information about the factors causing scatter in the knee elongation test results, three additional tests under idealised test conditions were performed. Therefore, the Flex-GT $\alpha$  legform was impacted by a linearly guided honeycomb impactor with a mass of 8,1 kg at an impact speed of 39 km/h (Zander et al., 2005). During the impact the honeycomb impactor hit the knee center with its upper edge. The test results are given in Figures 40 and 41.

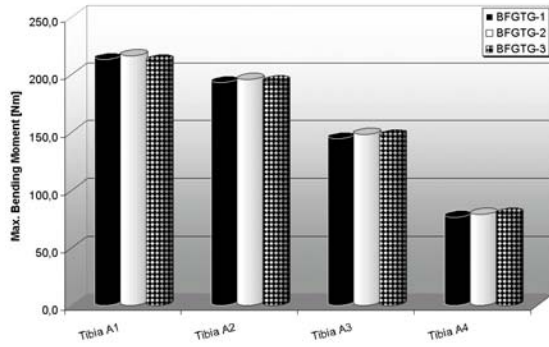


**Figure 40. Inverse test results for the tibia segments.**

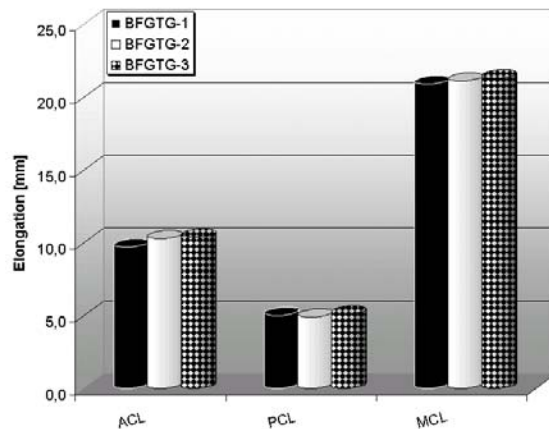


**Figure 41. Inverse test results for the knee ligaments.**

For the assessment of the repeatability of the test results the standard deviation was calculated and the results compared with the dummy requirement criteria (Table 4).

**Table 4. Repeatability of the inverse test results**

| Al honeycomb |                                     |      |      |      |                 |      |      |
|--------------|-------------------------------------|------|------|------|-----------------|------|------|
|              | Max. bending moment [Nm]<br>- Tibia |      |      |      | Elongation [mm] |      |      |
|              | A1                                  | A2   | A3   | A4   | ACL             | PCL  | MCL  |
| SD           | 2,57                                | 1,42 | 1,76 | 1,27 | 0,38            | 0,10 | 0,20 |
| [%]          | 1,20                                | 0,73 | 1,20 | 1,62 | 3,74            | 2,00 | 0,95 |
| Ass.         | G                                   | G    | G    | G    | A               | G    | G    |

G: good, A: acceptable, M: marginal, N: not acceptable

The standard deviation that was between good and acceptable for the maximum tibia bending moments obtained during the real car tests could be confirmed by the inverse tests. Here, all test results showed a high repeatability for all tibia segments and the PCL and MCL ligament. Only the repeatability of the ACL ligament was assessed not better than acceptable.

The results of the tests under idealised impact conditions reveal the sensitivity of the Flex-GT $\alpha$

towards marginally changed impact parameters as impact height and x,y and z-rotation. When eliminating these parameters the Flex-GT $\alpha$ -impactor itself shows a very high repeatability. A study on the variation of different impact parameters under otherwise constant impact conditions could be carried out to obtain a conclusion about the influence on the test results with the aim to define tolerances within a test procedure to be drafted.

## DISCUSSION

Several improvements have been incorporated within the development of the Flex-GT $\alpha$  impactor. It is now robust enough to be tested at a regular impact speed of 40 km/h on cars with modern front shapes without any modification. In general, good test results according to Euro NCAP could be confirmed by tests with the Flex-GT $\alpha$  on real cars. Only the MCL ligaments exceeded partly the currently proposed 50% injury risk thresholds for the 50<sup>th</sup> AM. However, it has to be stressed that newest developments of cars with modern front shapes tested in this study like the Audi Q7 or being designed for the european type approval like the sedan type car met all test requirements clearly. On the other hand, good test results with the FlexPLI have already been confirmed by tests with the rigid EEVC WG 17 legform impactor in an earlier study of the authors (Zander et al., 2006). In case of the parallel introduction of the Flex PLI as a test tool within regulations on pedestrian protection this might give car manufacturers a certain reliability which is imperatively needed during the car design and development process.

In real car tests, the Flex-GT $\alpha$  shows a good to acceptable repeatability of the maximum bending moment results, whereas the knee seems to be very sensitive towards car front modifications and different impact parameters like impact height or the impactor rotation. This can be stated by tests under idealised impact conditions, where the impactor shows a high repeatability of test results also for the knee ligaments. A study on the variation of impact parameters should be carried out and impact tolerances should be defined.

Regarding the knee elongations the Flex-GT $\alpha$  sometimes reveals a high sensitivity towards mirrored test points. Therefore, the question on symmetrical identical car front structures needs to be analysed in detail.

Like previous versions of the FlexPLI also the Flex-GT $\alpha$  is lacking an upper body mass. Therefore, test results of the femur loadings have not been considered within this study. Further research on the influence of an upper body mass on

femur loads during collisions of pedestrians with car fronts is needed.

The handling and usability of the Flex-GT $\alpha$  legform impactor are good. No expendables like foam or ligaments are needed. No changes were made within the calibration procedure of the strain gauges which therefore still needs to be re-defined, as it is influenced by mechanical aspects.

The dynamic certification test is still performed without flesh and skin. A full assembly dynamic certification test that was additionally performed showed quite similar peak results, even though the traces show some differences regarding the knee stiffnesses and peak value times. Therefore it currently seems to be the more appropriate certification procedure.

For the ACL and PCL ligament the dynamic certification test showed an unacceptable repeatability. These results were likely being influenced by a rotation of the impactor around its vertical axis due to the suspension method at the pendulum frame as well as the existing clearance of the knee. Therefore, the certification procedure still requires a revision.

## CONCLUSIONS

Even though tests with the current version of the FlexPLI and the EEVC WG 17 legform impactor are still not comparable in a full extent, good test results with the rigid WG 17 impactor according to the EEVC limits could be confirmed by the results with the biofidelic Flex-GT $\alpha$  according to the currently proposed injury thresholds. Furthermore, good results with the FlexPLI were confirmed by WG 17 results in an earlier development level already. It can be concluded that on the one hand former car front developments for meeting the EEVC criteria were already beneficial for the protection of pedestrians, and that on the other hand the introduction of the new biofidelic impactor would not necessarily have an influence on the design of already started developments. These aspects might give car manufacturers a reliability regarding their design and development process.

The comparatively lower repeatability of the knee test results within real car tests especially for the ACL and PCL ligament reveals the high sensitivity of the knee towards even minor modifications of the car front as well as a variation of impact parameters like impact height and impactor rotation. Further research in this field is needed. Nevertheless, the information obtained by the FlexPLI on the protection potential of car fronts can help to show a broader variation of possible

design changes needed to meet the requirements of the biofidelic impactor and herewith to improve the protection of pedestrians and other vulnerable road users during a collision with a modern car front.

## REFERENCES

Bose D., Bhalla K., Rooij L., Millington S., Studley A., Crandall J. 2004. „Response of the knee joint to the pedestrian impact loading environment.“ SAE World Congress, SAE paper no. 2004-01-1608.

Bhalla K., Bose D., Madeley N., Kerrigan J., Crandall J. 2003. „Evaluation of the response of mechanical pedestrian knee joint impactors in bending and shear loading.“ Paper no. 429 of ESV conference proceedings 2003.

EEVC Working Group 17. 2002. „Improved test methods to evaluate pedestrian protection afforded by passenger cars.“ December 1998 report with September 2002 updates.

European Union. 2003. „Directive 2003/102/EC of the European Parliament and of the Council of 17 November 2003 relating to the protection of pedestrians and other vulnerable road users before and in the event of a collision with a motor vehicle and amending Council Directive 70/156/EEC.“ Official Journal of the European Union, 06.12.2003.

Imaizumi, I: “Report on Flex-G car test results.” 2<sup>nd</sup> Meeting of GRSP technical evaluation group. Bergisch Gladbach, Germany, 2005.

Ishikawa H. 2004. „Discussion on injury thresholds for pedestrian legform test.“ 6<sup>th</sup> Meeting of GRSP informal group on pedestrian safety. Paris, France, 2004.

Ivarsson J., Lessley D., Kerrigan J., Bhalla K., Bose D., Crandall J., Kent R. 2004. „Dynamic response corridors and injury thresholds of the pedestrian lower extremities.“ IRCOBI conference proceedings 2004.

Kajzer J., Matsui Y., Ishikawa H., Schroeder G., Bosch U. 1997. „Shearing and bending effects at the knee joint at high speed lateral loading.“ Proceedings of the 41<sup>st</sup> Stapp Car Crash Conference, SAE paper no. 973326.

Kerrigan J., Bhalla K., Madeley N., Funk J., Bose D., Crandall J. 2003. „Experiments for establishing pedestrian-impact lower limb injury criteria.“ SAE World Congress, SAE paper no. 2003-01-0895

Konosu A., Ishikawa H., Tanahashi M. 2001. „Reconsideration of injury criteria for pedestrian

subsystem legform test - problems of rigid legform impactor -.“ Paper no. 01-S8-O-263 of ESV conference proceedings 2003.

Konosu A., Issiki T., Tanahashi M. 2005. „Development of a pedestrian lower extremity protection car using a biofidelic flexible pedestrian legform impactor.“ Paper no. 05-0106 of ESV conference proceedings 2005.

Konosu A. 2006. „Information on the flexible pedestrian legform impactor GT alpha (Flex-GT $\alpha$ ).“ 3<sup>rd</sup> Meeting of GRSP technical evaluation group. Bergisch Gladbach, Germany, 2006.

Konosu A. 2006. „Evaluation activities on injury assessment ability of the flexible pedestrian legform impactor GT alpha (Flex-GT $\alpha$ ).“ 3<sup>rd</sup> Meeting of GRSP technical evaluation group. Bergisch Gladbach, Germany, 2006.

Mertz, H. 2004.: “Calculation methods & acceptance levels for assessing repeatability and reproducibility (R & R).” ISO/TC22/SC12/WG5 Document N751.

Nakahira Y., Furukawa K., Niimi H., Ishihara T., Miki K., Matsuoka F. 2000. “A combined evaluation method and a modified maximum likelihood method for injury risk curves.” IRCOBI conference proceedings 2000.

Nyquist G., Cheng R., El-Bohy A., King A. 1985. “Tibia bending: strength and response.” Proceedings of the 29<sup>th</sup> Stapp Car Crash Conference, SAE paper no. 851728.

United Nations Economic Commission for Europe. 2006. “Proposal for a global technical regulation on uniform provisions concerning the approval of vehicles with regard to their construction in order to improve the protection and mitigate the severity of injuries to pedestrians and other vulnerable road users in the event of a collision.” ECE/TRANS/WP.29/GRSP/2006/2. 3 March 2006.

Zander O., Lorenz B., Leßmann P., Gehring D. 2005. “The pedestrian legform impactor according to EEVC WG 17 - results of an actual research and possibilities for the implementation within regulations on pedestrian protection.” IRCOBI conference proceedings 2005.

Zander O., Lorenz B. 2006. “ Assessment of the flexible pedestrian legform impactor (FlexPLI-G) as a test tool for legislation on pedestrian protection.” IRCOBI conference proceedings 2006.

# PEDESTRIAN RECONSTRUCTION USING MULTIBODY MADYMO SIMULATION AND THE POLAR-II DUMMY: A COMPARISON OF HEAD KINEMATICS

**RWG Anderson**

**LD Streeter**

**G Ponte**

**AJ McLean**

Centre for Automotive Safety Research, University of Adelaide

AUSTRALIA

Paper number 07-0273

## ABSTRACT

The aim of this study was to reconstruct three pedestrian collisions with multi-body simulations using the computer program MADYMO and the Polar-II dummy. In this paper, we compare the head kinematics of the computer simulation and the Polar-II test with reference to the vehicle-pedestrian contacts in the actual cases. We also discuss aspects of the reconstructions made using these different tools, especially findings on the velocity trajectory of the head. The cases selected for reconstruction were ones in which the pedestrian's height and weight were close to the 50th percentile adult human male, and where the accident investigation provided good estimates of impact speed and complete injury data. The cases were investigated to estimate the speed of the vehicle at impact and the position of the pedestrian relative to the vehicle. Contact points between the vehicle and pedestrian were recorded. From this information MADYMO simulations were made to estimate the kinematics of the pedestrian during the collision. We then reconstructed each case using the Polar-II full-scale pedestrian dummy. Results showed that some aspects of the head kinematics were in good agreement but, generally, Polar-II head impact angles were steeper and the head impact location was more forward than the location suggested by the simulations and the cases themselves. Leg kinematics were noticeably different, with the Polar-II legs remaining engaged with the front of the vehicle for a longer period of the collision. In contrast to the simulations, the Polar-II legs were in some instances still engaged as the head struck the vehicle.

## INTRODUCTION

Subsystem pedestrian tests form the basis of regulation and consumer tests related to pedestrian safety (for a reference, see EEVC, 2002). From a vehicle development point of view, subsystem tests are useful for certain aspects of passive safety development and in the improvement of the vehicle

design against the benchmark of regulatory standards. They are of more limited value for rigorous testing of advanced active and passive safety devices and do not reveal unintended interactions between aspects of vehicle design. Therefore, a valid pedestrian dummy would provide an important and useful tool to study the interaction between the vehicle and the human body in a collision.

For example, it would be counterproductive if the velocity of the head were increased on impact by designing a vehicle to protect the knee from a rupture to the medial ligament (a relatively rare occurrence). As such, interactions between contacts in pedestrian collisions are important. Also, some devices that are being developed to protect pedestrians use sensing to trigger them (Fredriksson et al., 2001) and must also bear the load of the torso as well as the head in the collision. The development and refinement of such safety interventions will benefit from an adequate pedestrian dummy. Computer simulation can reveal many important interactions in pedestrian tests, and simulation is being used more-or-less successfully to reconstruct actual pedestrian crashes (eg. Konosu, 2002; Depriester et al., 2005; Yang, 2003; Yang et al., 2005; Anderson et al, 2002; Anderson et al., 2003). These simulations are difficult to validate, but the performance of the model against PMHS tests and a correspondence between contact points in the actual case and in the simulation can provide a guide. Usually, the pattern of contact between pedestrian and vehicle can be explained with such simulations and so we have tended to view such tools as reliable when used carefully. However, these tools do not negate the value of an adequate pedestrian dummy for testing the design of vehicles.

Polar-II is a pedestrian dummy developed by Honda R&D Ltd., in conjunction with GESAC Inc. The development of this dummy is described in Akiyama et al. (2001). Experience with the use and evaluation of this dummy is being used to guide the

development of an SAE pedestrian dummy standard.

Ultimately, the requirement of any simulation or test tool is the same – to represent a pedestrian in a collision, to allow the measurement of the response of the structure being hit, and a measure of the risk of injury that the impact produces. Obviously, there should be some relationship between the results of tests with a pedestrian surrogate and the consequences in an actual accident. And given the parallel roles of sub-system tests and any future work in which a pedestrian dummy might be used, we are interested in examining how the results of sub-system tests compare with the results of dummy tests, and how each of these compare with injuries actually suffered in accidents. We have previously reported on the ability of the subsystem tests to discriminate injurious pedestrian impacts (Anderson et al., 2002 and 2003).

Some recent papers have reported on the performance of the Polar-II dummy in simulated pedestrian collisions. Kerrigan et al (2005a; 2005b) compare the kinematics of the dummy with PMHS tests in collisions with a small sedan (Kerrigan et al., 2005a) and with a sports utility vehicle (Kerrigan et al., 2005b). While Kerrigan et al. concluded that the biofidelity of the Polar-II was good overall, the comparisons showed some trends:

- The wrap-around-distance for the head strike was 15- 20% shorter in Polar-II tests on the small sedan. This difference was smaller in the SUV tests - around 5-10%.
- In sedan tests, the head velocity profile of Polar-II did not match the cadaver velocity profiles: The dummy head achieved higher peak speeds but the speed of the head was lower on impact than the cadaver head speeds. In SUV tests, the velocity profiles matched more closely.
- The velocity of the Polar-II head exhibited a larger vertical component on impact in all tests
- In sedan tests, the head of the Polar-II struck the vehicle surface earlier than the PMHS subjects. The average timing of head strike in PMHS tests was 140 ms after first contact, and 126-131 ms in Polar-II tests. In SUV tests, timing was almost identical.

In 2003, we had an opportunity to replicate, with Polar-II, reconstructions of crashes that we had investigated at the scene and reconstructed using our multi-body pedestrian model and subsystem impact laboratory. These cases were well documented with good injury data and so they were useful candidate cases to reconstruct with Polar-II,

the output of which could be compared with the injury.

In this paper, we compare the kinematics of Polar-II with our multi-body simulations (in MADYMO) and the evidence of contact in the crash. We intend to report more fully on the comparison of the kinetics of the Polar-II collision and the injuries in these cases in a subsequent publication.

## AIM

The aim of this study was to compare the head kinematics of actual pedestrian collisions with reconstruction using MADYMO multi-body simulation, and from Polar-II reconstructions.

## MATERIALS AND METHODS

### Accident data

The three cases used for this study were pedestrian accidents investigated by the Centre for Automotive Safety Research (formerly known as the Road Accident Research Unit). The cases had been studied as part of a research program that includes the study of brain injuries in automotive accidents and studies that were designed to characterize injuries to pedestrians more generally. This program has collected data on over 500 pedestrian accidents since the late 1970s.

We selected cases for this study using the following criteria:

- The size and weight of the pedestrian were close to the 50<sup>th</sup> percentile human male. This was to ensure that the Polar-II dummy could adequately represent the stature of the pedestrian in the reconstruction.
- The physical evidence (dents and scrapes on the car, injuries to the pedestrian) clearly revealed the kinematic trajectory of the pedestrian. This was to ensure that the MADYMO simulation could be verified, and hence the head impact speed in the sub-system test and the initial position and trajectory of the Polar-II dummy.
- The vehicle was the substantial cause of any head injury suffered by the pedestrian.
- The speed of the vehicle could be estimated. This was used as an initial condition in the MADYMO simulation and the Polar-II test.

The accidents are summarized in Table 1.

**Table 1 Details of cases reconstructed for this study**

| Case   | Vehicle Details |                     |                           | Pedestrian details |     |        |        |
|--------|-----------------|---------------------|---------------------------|--------------------|-----|--------|--------|
|        | Year            | Model               | Impact Speed <sup>1</sup> | Age                | Sex | Weight | Height |
| Case 1 | 1992            | Ford Fairmont       | 33 km/h                   | 52                 | M   | 75 kg  | 178 cm |
| Case 2 | 1973            | Holden Torana       | 55 km/h                   | 75                 | M   | 75 kg  | 175 cm |
| Case 3 | 1983            | Holden VK Commodore | 60 km/h                   | 35                 | M   | 81 kg  | 178 cm |

<sup>1</sup>Speed used in the simulation and the Polar-II test

In cases we investigate, the scene of the accident is surveyed, and the lengths of any skid-marks left by the vehicle are measured, and the location of the impact point and final position of the pedestrian, scuff marks on the road, debris, and any other feature of relevance are noted. The speed of the striking vehicle is estimated from the evidence left by the braking vehicle and the trajectory of the pedestrian.

If the pedestrian is fatally injured, a member of the crash investigation team records injuries at autopsy, and their height, weight, and the dimensions of various body segments are measured.

In cases where the pedestrian's injuries are not lethal, the pedestrian is interviewed and asked to describe their injuries and the circumstances of the collision. Further information on the pedestrian's injuries is obtained from their hospital medical record. The South Australian Trauma Registry is also consulted in cases where data on the pedestrian's injuries are not complete.

The crash investigators inspect the striking vehicle for signs of contact with the pedestrian, such as dents, scratches and scuffs on the surface of the vehicle. The location of the head contact is identified by a dent in a panel or cracks in the windscreen, and often by the presence of hair on the contact area. The location of each contact is measured from defined datum points, replicable in the laboratory later. In the three cases reported here, these records were used to check the simulation of the collision with the MADYMO model and the Polar-II.

The following sections give an overview of the simulation, and Polar-II reconstructions and the methods used to evaluate the results.

### Computer simulation

Each of the three cases was simulated by computer using a MADYMO model that represents the 50<sup>th</sup> percentile human male. (Adjustments were made to the model to reflect actual anthropometry using a tool based on GEBOD; Baughman et al., 1983) The model was described by Garrett (1996; 1998), and has been used for simulating accidents from data collected during accident investigation (Anderson

et al., 2000; Anderson et al., 2002; Anderson et al., 2003).

The model as a whole has been validated using the results of cadaver tests (Garret, 1998). Recently, the neck of the model has been improved to better represent the response of the neck in frontal and lateral directions reported by Thunnissen et al. (1995) and Wismans et al. (1986).

### Implementation of the model in the simulation of the accidents

Vehicles identical to the make, model and series of those involved in the cases were obtained, and the geometry of the cars were measured using a digital theodolite using a process we have described before (Anderson et al., 2003) and the measured geometry was used as a basis of the vehicle model in MADYMO. The geometry was then approximated by a series of planes, elliptical cylinders, and ellipsoids. Contact stiffnesses for the vehicle were based on Ishikawa et al. (1993).

In setting the initial posture of the pedestrian, we ignored both the walking velocity and the velocity of the limbs during locomotion. The orientation of the pedestrian can often be estimated either from statements from the pedestrian themselves or from drivers, witnesses, and/or marks on the body. The impression of the bumper or other component often indicates the orientation of the pedestrian, and the alignment of marks often indicated the position of limbs and torso as they were struck. Sometimes, it is not possible to determine the exact posture of the pedestrian, so simulations are made that cover the possible range of postures in the accident, or using postures covering a human gait cycle (Anderson et al., 2005). However, for this study, after performing simulations representing the gait cycle, a single simulation was designed that was subjectively judged by the authors to represent the accident most closely, based on the match between contact locations and marks left on the vehicle. This was necessary, as the Polar-II reconstruction would be set up to match the initial conditions set in the simulation. Variations in head impact conditions due to changes in gait are described in Anderson et al. (2005).

## Polar-II reconstructions

The tests were conducted at the Japan Automobile Research Institute (JARI) in Tsukuba, Japan and at the Honda R&D crash test facility in Tochigi, Japan. We are very grateful to the staff of both organisations in making their facilities available and performing the tests on our behalf, and providing data from each test.

In each test, the dummy was set in a posture that matched the initial position of the pedestrian in the simulation. Data on joint angles and segment positions relative to the front of vehicle were provided to the test engineers. Because the dummy was designed to be struck on the left-hand side, the dummy positioning was the mirror image of the crash in two cases where the pedestrian was struck on the right.

Coordinated high speed film, shot in the three principal orthogonal planes, provided estimates of the velocity of the dummy and its component parts, and 44 channels of data were collected on loads and accelerations to various parts of the dummy.

The Polar-II head trajectory was calculated from video analyses of the test: the displacement of the centre-of-gravity and the vehicle was tracked using high speed video which was taken from three orthogonal views giving the three components of displacement. The velocity of the head and the vehicle was estimated using a Simpson's rule method and then subjected to centred five-point smoothing. The vehicle velocity was then subtracted from the Polar-II head velocity to produce an estimate of the time varying velocity of the dummy head relative to the vehicle. Corresponding data from the simulations were extracted from the model results.

We report the head velocity data in two ways: head speed versus time and head speed versus the angle of the relative velocity to the horizontal. Typical figures are shown in Figure 1 and Figure 2. The annotations in Figure 2 correspond to typical phases in the trajectory of the head: (a) as the car strikes, the relative velocity is equal to the velocity of the car. The relative speed of the head is nearly constant, and only the angle of the velocity is changing for a period after the initial contact. (b) As the upper body of the pedestrian is put under tension, the head accelerates rapidly. After this acceleration, the centre of gravity of the head moves in a circular motion toward the upper surface of the car, slowing slightly just before contact (c). This point is marked on the plot with an "o". After the initial contact the head rapidly loses all vertical speed, and hence the velocity's

locus rapidly returns to the horizontal before the head rebounds. The angular position of the impact point in Figure 2 reveals the contribution of horizontal and vertical components in the impact velocity.

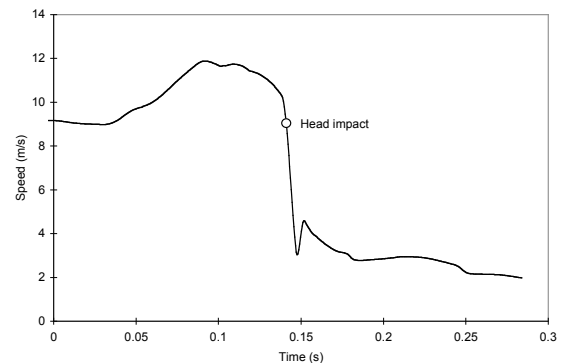


**Figure 1** An example of head speed over the duration of a pedestrian impact.

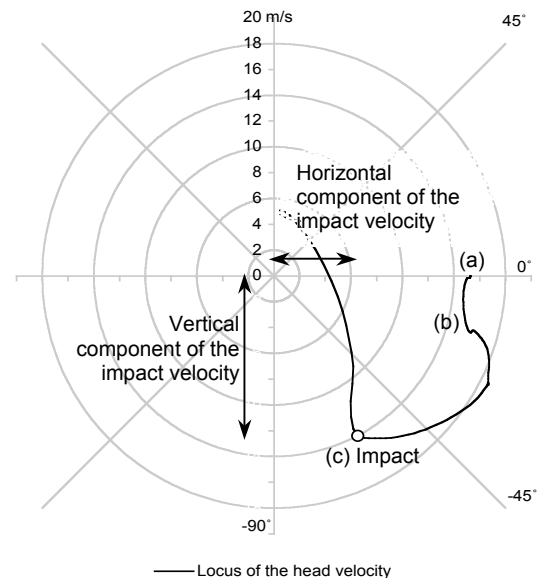


**Figure 2** The locus (speed and angle) of the velocity of a pedestrian's head in a collision with a car.

Finally, we can compare the trajectory of the head relative to the vehicle produced by the simulation with the trajectory of the Polar-II head. A common way to present this is a plot of the vertical position against the horizontal position of the head. Trajectory data in Polar-II tests were calculated relative to the vehicle using the system described by Kerrigan et al. (2005a and b) with one difference – the origin of the vehicle coordinate system was centred on the ground, with the horizontal origin aligned with the most forward point on the vehicle. We wanted to ensure that trajectories were comparable with respect to the vehicle, reflecting actual head impact locations. Therefore, small differences between the

simulation and the Polar-II, in the initial horizontal position of the head relative to the vehicle, were accounted for.

## RESULTS

### Case 1: Case number PED043

The pedestrian was near the centre line of the road when he stepped backwards into the path of a vehicle travelling in the right-hand (inner) lane of a two-lane road. The pedestrian was struck by the front right-hand headlight of the vehicle and was thrown onto the bonnet, striking his head near the back of the bonnet before being thrown to the road by the impact.

The pedestrian died as a result of the collision. He experienced loss of consciousness at the scene, paramedics rating his loss of consciousness with a Glasgow Coma Score of 4-5/15. His airway and circulatory systems were also compromised. His most significant injuries were:

- A fracture to the right parietal bone and the base of the skull (open and closed),
- An extradural and subdural haematoma and other brain haemorrhages and contusions,
- A splenic laceration,
- Fractured ribs to his right side (5-7), and
- An open 30 mm laceration to the right hip and contusions to the right ankle.

The position on the road at which the pedestrian was standing when struck was identified from the presence of a scuff-mark that was caused by the twisting and sliding of the sole of the pedestrian's shoe as the vehicle struck his leg. The distance that the pedestrian was thrown implies an impact speed of approximately 33 km/h. The damage to the right front of the vehicle (Figure 5) suggests that it was these structures that caused the wounds to the pedestrian's thigh and hip. The significant depression in the right trailing edge of the bonnet was a result of the impact between the bonnet and the head of the pedestrian.

**MADYMO simulation:** An Australian 1992 Ford Fairmont was obtained for the physical reconstruction of this collision. The car was measured to obtain the geometry of the vehicle for the MADYMO simulation (Figure 3). The initial position of the pedestrian is shown in Figure 4.

Rather than simulations representing the gait cycle, two simulations were designed to represent a pedestrian taking a step backwards (left foot down and right foot down). The kinematics of the collision in these two simulations showed a significant involvement of the pedestrian's right arm in the collision. To see what effect this may

have had on the head impact velocity, two further simulations were run. In these simulations, the right arm of the pedestrian was raised slightly and positioned forward of the trunk of the body to minimise its involvement in the kinematics as the collision progressed. There was little effect on the head impact velocity, however, and so the right arm was raised slightly in the final simulation and in the Polar-II test to avoid any complications arising from arm involvement.

**Polar-II reconstruction:** The initial dummy position is shown in Figure 4. The position was set to match the initial position of the MADYMO simulation. The dummy was struck at 33 km/h

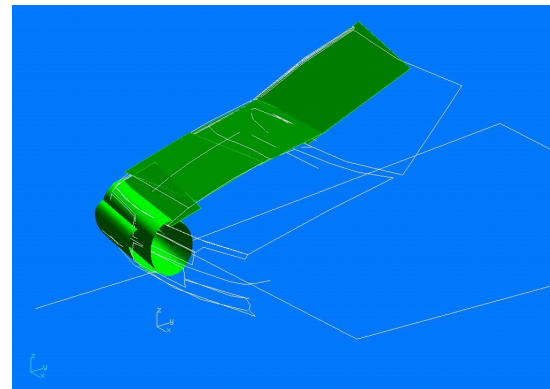


**Figure 3** Geometry of the vehicle in Case 1 (shown in white). The approximation of this geometry for the simulation is shown by the shaded geometric entities.

**MADYMO and Polar-II results:** The results of simulation and the Polar-II test are shown in Figure 5 through Figure 7. Figure 5 compares the damage caused in the actual collision with that produced in the Polar-II test. Figure 6 shows three graphs that summarise the kinematics of the head and Figure 7 shows comparisons of the positions of the simulation and Polar-II at two time points during the collision.

Several things are notable about Figure 6.

- The head impact speed in the MADYMO simulation was higher than that recorded in the Polar-II test: 12.5 m/s (138 ms after first leg contact) compared with 5 m/s (144 ms after first leg contact). The impact speed of the vehicle was 9.2 m/s.
- The difference in the head impact velocity contains differences in both the horizontal and the vertical components of the velocity.
- The angle of the head impact in the Polar-II test was slightly beyond the vertical, meaning that the head velocity has a small component toward the front of the car. Examination of the video reveals that the neck was in extension on head impact, and it appears that the tension in

the neck decelerated and rotated the head prior to impact.

- The Polar-II head trajectory and velocity were similar to the simulation for the first 100 ms. At 80 ms (Figure 7) it is apparent that, apart from a difference in the amount of sliding over the vehicle surface, the position of the dummy and the model are similar. By 120 ms, differences are becoming apparent: the dummy appears less flexible through the torso, and the neck and head appear to have realigned with the torso, something that happens only just before impact in the simulation. The difference in the amount of sliding is increasingly obvious, with the knees of the Polar-II still forward of the leading edge of the vehicle.
- The Polar-II head impact location was about 200 mm forward of the simulation head impact location, although a comparison between the damage with the case vehicle (Figure 5) shows that the location was slightly rear of the actual case impact location. Damage to the leading edge was less in the Polar-II test than in the actual case.

### Case 2: Case number H032

**Description:** The vehicle was travelling in a westerly direction on a three-lane road in the left (outer) lane. The pedestrian was crossing the road in a southerly direction. The driver said that he was travelling at no more than 55 km/hr when a vehicle following about 10 metres behind in the right hand lane distracted him. He looked in his right side rear view mirror, and it was at that point that the windscreen of his vehicle shattered. At no time prior to the accident did he see the pedestrian and did not take any evasive action.

The pedestrian died as a result of the collision. Reported movements indicate that the pedestrian would have been hit on his left side and his injuries were consistent with this. There were lacerations and bruises to the left aspect of both legs and on the left arm. The leg injuries indicate that the legs were apart at impact, with the right leg leading. The bruise on the outside of the left knee was at the same height as the front edge of the bonnet, which was noticeably dented to the left of the centre line. The head of the left femur was displaced into the acetabulum indicating a very forceful impact at that location.

Injuries to the pedestrian and damage to the vehicle indicate that the pedestrian was struck by the left front of the car and was thrown up over the bonnet, and his head struck the left side of the windscreen. As there was laceration and bruising to the occiput, he might have rotated slightly away from the car during the vault. His head also hit the dash

underlying the windscreen, where a dent was noticeable. We estimate, from the projection distance, that the impact speed was consistent with the comments of the driver: 55 km/h.

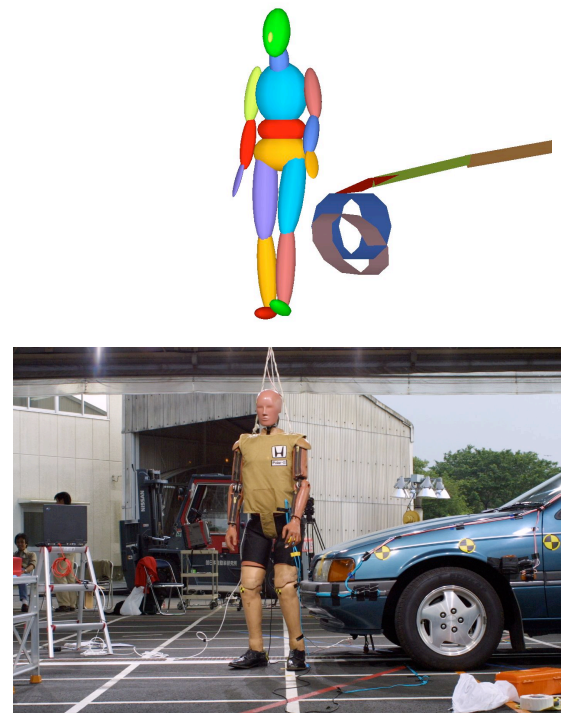


**Figure 4** Positioning of computer simulation model and Polar-II dummy in Case 1



(a)



(b)

**Figure 5** Damage to (a) the leading edge caused by the actual collision (*top*) and the Polar-II test (*bottom*), and (b) the trailing edge from the head impact in the actual case (*top*) and the Polar-II reconstruction (*bottom*) in Case 1.

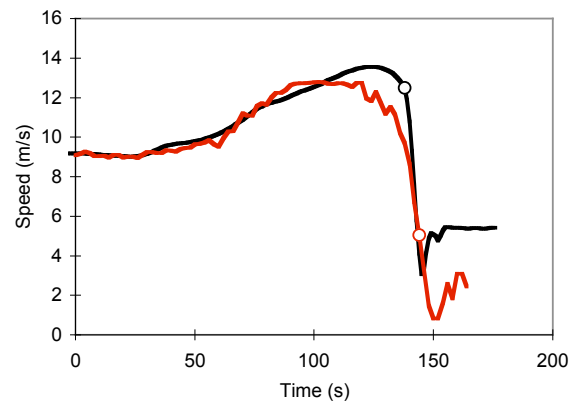
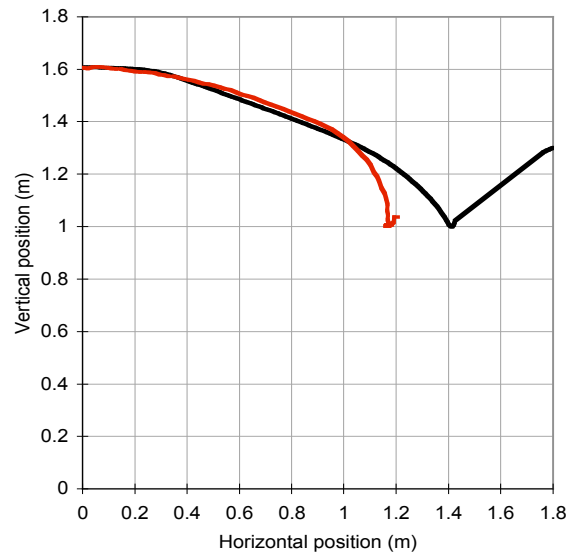
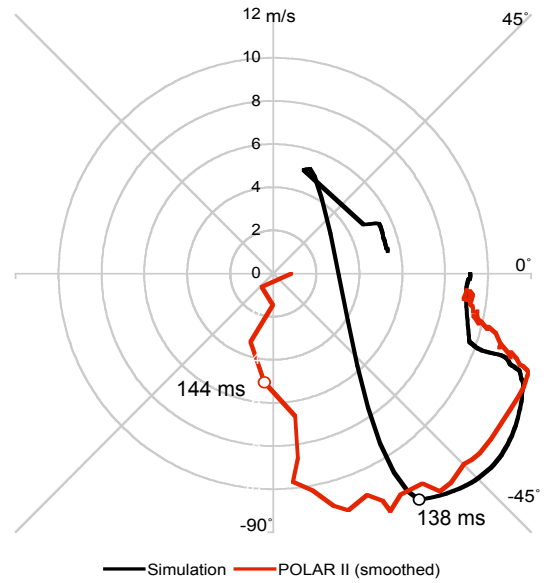
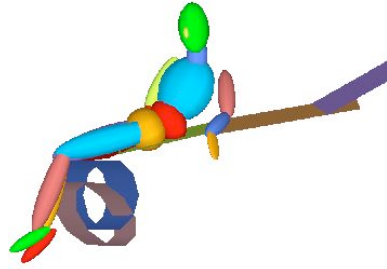
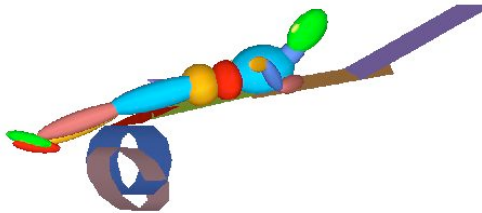


**Figure 6** (*top to bottom*) radial head velocity trajectory, head position trajectory and head velocity history for Case 1. Polar-II data are red and simulation data are black. The hollow circles represent data points associated with head impact.



(a)



(b)

**Figure 7** A comparison between the MADYMO simulation and the Polar-II test at (a) 80 ms and (b) 120 ms.

**MADYMO simulation:** A 1973 Holden Torana was obtained for the physical reconstruction of this collision. The car was measured to obtain the geometry of the vehicle for the simulation. The geometry was represented by a series of planes and elliptical cylinders, as illustrated in Figure 8.

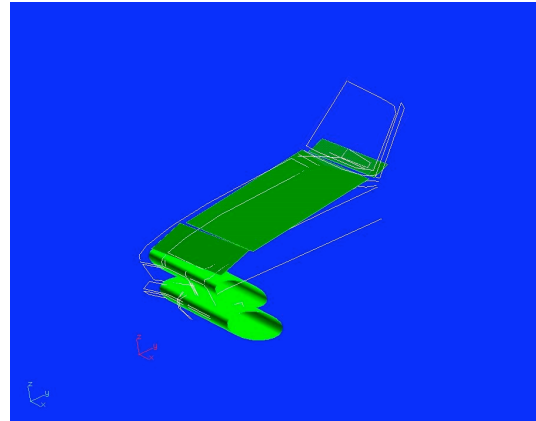


**Figure 8** Geometry of the vehicle in Case 2 (shown in white). The approximation of this geometry for the simulation is shown by the shaded geometric entities.

**Polar-II reconstruction:** The initial dummy position is shown in Figure 9. The position was set to match the initial position of the MADYMO simulation.

**Comparison of MADYMO and Polar-II results:** The results of simulation and the Polar-II test are shown in Figure 10 through Figure 12.

Several things are notable about Figure 11.

- The head speed at impact and the timing of the impact were almost identical in the Polar-II test (13.8 m/s at 100 ms) and the simulation (14.0 m/s at 103 ms).
- There were, however, differences in the components of the velocity. The Polar-II head velocity was slightly beyond vertical at impact. The radial plot of the simulation shows that the head impact velocity in the simulation included about 6 m/s in the horizontal direction.
- The Polar-II head impact location was about 400 mm forward of the simulation head impact point and the actual head impact point in the case. The Polar-II head struck the bonnet whereas the head of the pedestrian struck the windscreen and dash (Figure 10).
- The damage to the leading edge was slightly greater in the Polar-II test compared to the damage caused to the case vehicle.

Similarly to Case 1, there was significantly more sliding in the simulation than in the Polar-II test. Figure 7 shows that the Polar-II appears to become hooked on the leading edge of the vehicle – at head contact, the legs have moved over the leading edge only slightly. Unlike most modern passenger vehicles, this vehicle has a very prominent and stiff leading edge, and so this may represent an extreme case for the dummy.

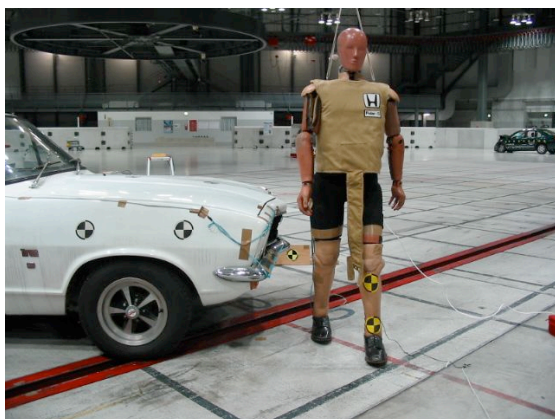
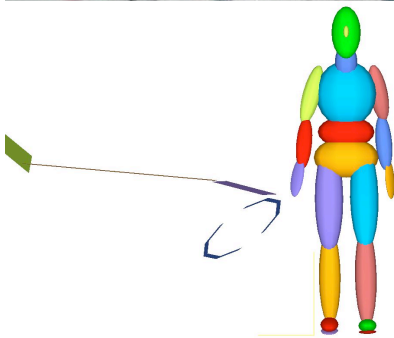


**Figure 9** Positioning of computer simulation model and Polar-II dummy in Case 2.

### Case 3: Case number PED056

**Description:** The vehicle was travelling north in the right side of a wide lane and moved to the left because another vehicle in front was turning right into a petrol station. The driver of the vehicle did

not see the pedestrian who was crossing the road from east to west, and the vehicle struck the pedestrian on its front left-hand side of the vehicle. The pedestrian was flipped up onto the bonnet, striking the windscreen before falling to the roadway.

The pedestrian was transported by ambulance to a hospital because of his injuries. He remained conscious after the accident. His most significant injuries were

- An open fracture to his left tibia and fibula - the 3 cm puncture site was 36-39 cm from ground level.
- Grazes to the left aspect of the head, behind the left ear and extending down lateral aspect of neck
- Grazing to the left shoulder, the left hand, both elbows and both knees.

The pedestrian had a clear recollection of events and from his interview we could place his initial position in an area that meant that the car had not commenced braking when he was struck. The subsequent skid marks left by the vehicle indicated that the car was travelling at 60 km/h on impact.

**MADYMO simulation:** An Australian 1983 Holden VH Commodore was obtained for the physical reconstruction of this collision. The car was measured to obtain the geometry of the vehicle for the MADYMO simulation (Figure 13). The initial position of the pedestrian is shown in Figure 14.

The pedestrian gave a detailed description of the collision, and described how his left arm slid over the bonnet before his head struck the windscreen. He described how his left forearm and hand subsequently struck the broken windscreen above his head. Each of the initial simulations produced slightly different head impact locations, and several also produced heavy impacts between the left elbow and the bonnet. The simulation that best reflected the pedestrian's description of the collision, and the head impact point in the case, was modified so that the left arm slid over the bonnet, rather than digging into it, while maintaining the correct head impact location. In this simulation, the left arm of the pedestrian went on to strike the windscreen in a manner consistent with the pedestrian's description and with the secondary damage to the windscreen.



(a)



(b)

Figure 10 Damage to (a) the leading edge caused by the actual collision (*top*) and the Polar-II test (*bottom*), and (b) the trailing edge from the head impact in the actual case (*top*) and the Polar-II reconstruction (*bottom*) in Case 2.

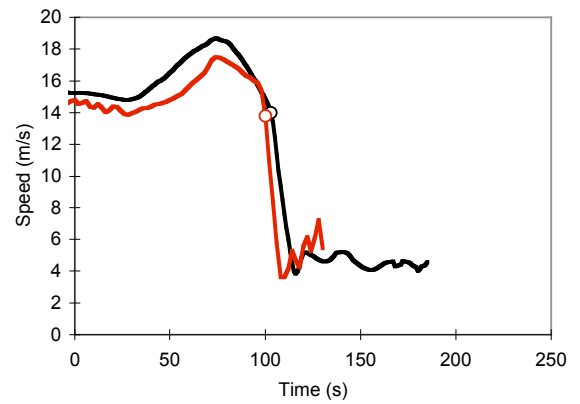
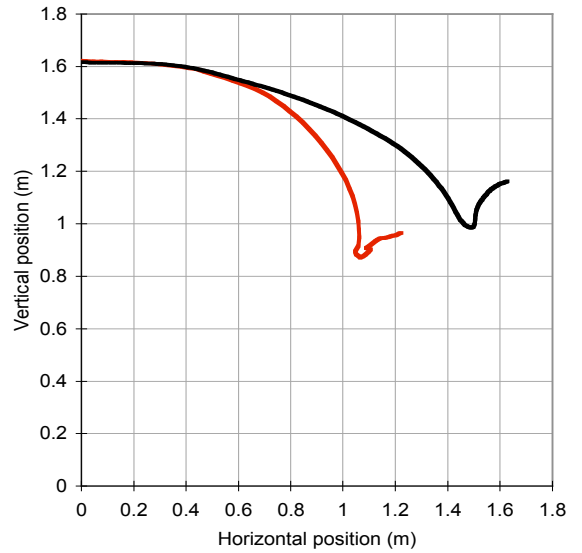
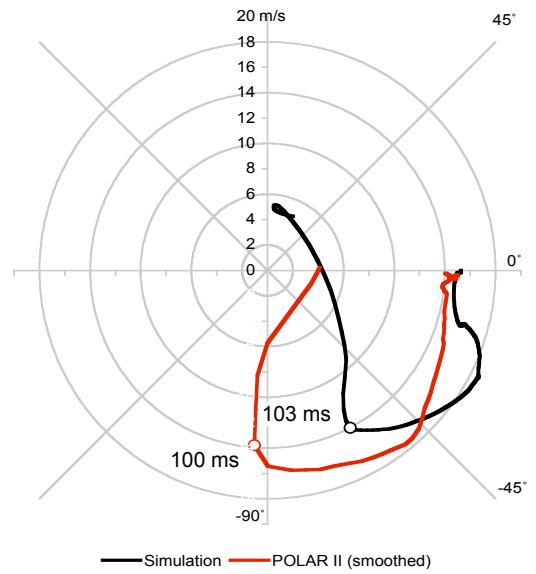
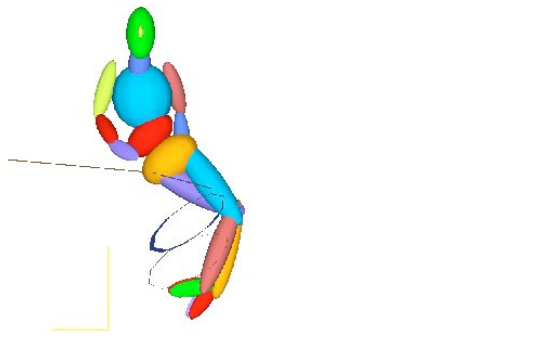
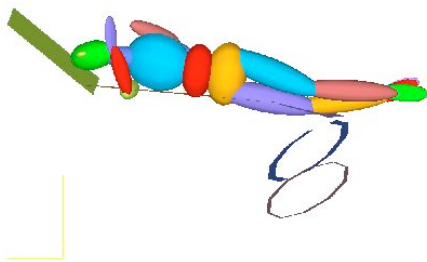


Figure 11 (*top to bottom*) Case 2 radial head velocity trajectory; head position trajectory and head velocity history. Polar-II data are red and simulation data are black. The hollow circles represent data points associated with head impact.



(a)



(b)

**Figure 12** A comparison between the MADYMO simulation and the Polar-II reconstruction of Case 2 at (a) 40 ms and (b) 100 ms.

**Polar-II reconstruction:** The initial dummy position is shown in Figure 14. The position was set to match the initial position of the MADYMO simulation.

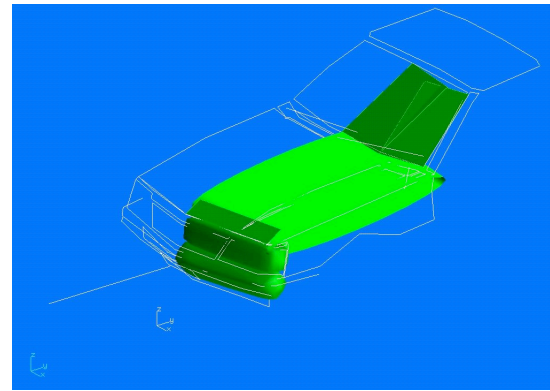


**Figure 13** Geometry of the vehicle in Case 3 (shown in white). The approximation of this geometry for the simulation is shown by the shaded geometric entities.

**MADYMO and Polar-II results for Case 3:**

Figure 15 to Figure 17 compare results of the simulation with the Polar-II test. The Polar-II test and the simulation show a pattern of similarities and differences consistent with the previous two cases. It may be noted that:

- The location of the Polar-II head strike was forward of the location in the actual case (Figure 15) and in the simulation (Figure 17).
- In early stages of the collision, the Polar-II kinematics and the simulation kinematics are similar. After 40 ms there are small differences in the amount of sliding over the bonnet, but the upper body positions are clearly similar (Figure 1 (a)). However, at 100 ms, differences in the leg kinematics have produced large differences in displacements. The simulation head impact has already occurred (Figure 16 (b)).
- The simulation head velocity reaches a higher peak level than the Polar-II (Figure 17). An examination of the components of the head velocity reveals that this difference is due to a difference in the horizontal velocity of the head. In the simulation, the head accelerates to the rear of the vehicle and then it is accelerated forward just before head impact. In the Polar-II test, the head does not significantly accelerate toward the rear of the car at any stage. This difference appears to be largely due to the differences in the amount of sliding between the lower body of the simulation pedestrian and the Polar-II.
- The head impact velocity of the Polar-II is less than in the simulation: 15.2 m/s versus 19.1 m/s. This is due to differences in the horizontal component of the velocity mentioned above, and the radial velocity plot shows this difference to be more than 8 m/s.

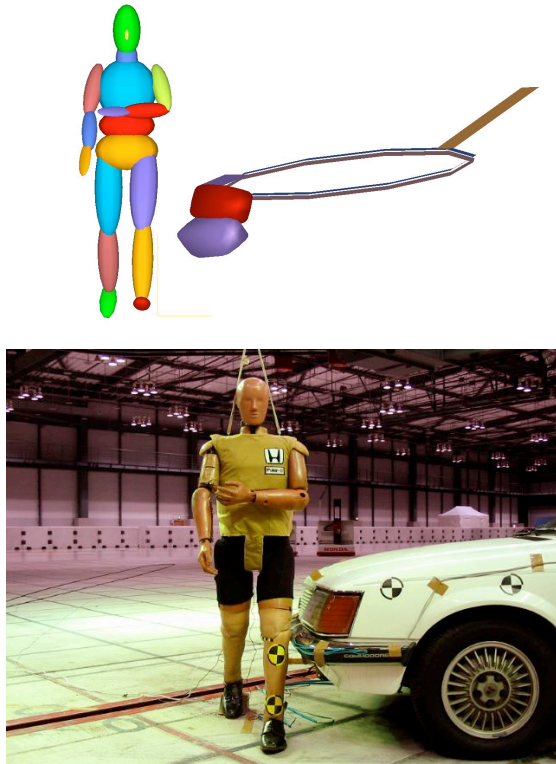


Figure 14 Positioning of computer simulation model and Polar-II dummy in Case 3.

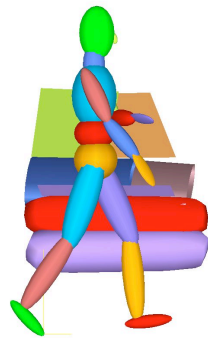
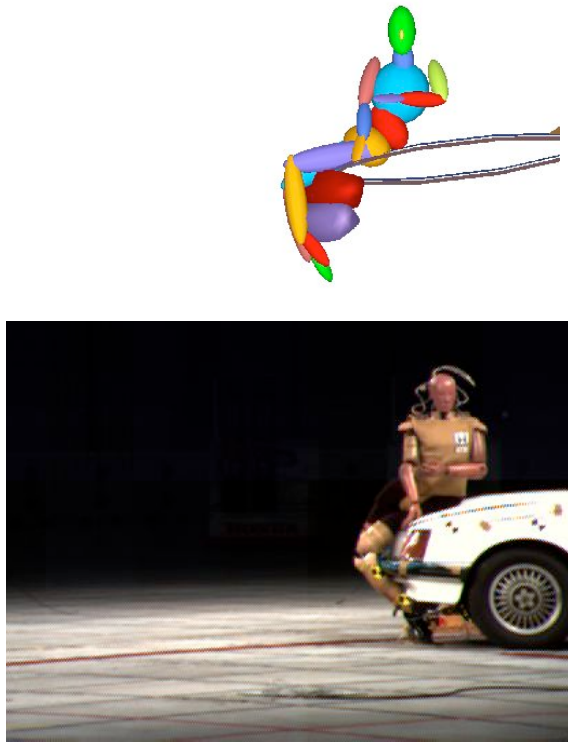


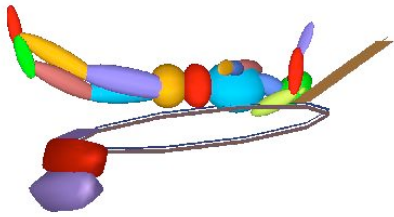
Figure 15 Damage to (a) the leading edge caused by the actual collision (top) and the Polar-II test (bottom), and (b) the trailing edge from the head impact in the actual case (top) and the Polar-II reconstruction (bottom) in Case 3.

## DISCUSSION

The purpose of this paper has been to present a comparison of the head kinematics in reconstructions of pedestrian crashes using a multi-body model of a pedestrian and reconstructions using the Polar-II pedestrian dummy. As we are mainly comparing the performance of two surrogates of actual crashes, in some respects the approach is somewhat less direct than the PMHS comparisons reported by Kerrigan et al. (2005a; 2005b). However, the reconstructions were of actual collisions, so we could relate various aspects of the performance to the evidence from the actual case. Furthermore, given the extensive use of multi-body simulations to study pedestrian kinematics, understanding the differences in the response of the Polar-II with simulation models may help to improve both pedestrian dummies and simulation techniques.



(a)



(b)

Figure 1 A comparison between the MADYMO simulation and the Polar-II reconstructions of Case 3 at (a) 40 ms and (b) 100 ms.

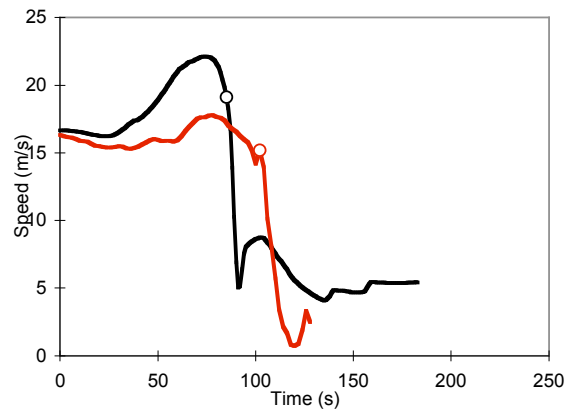
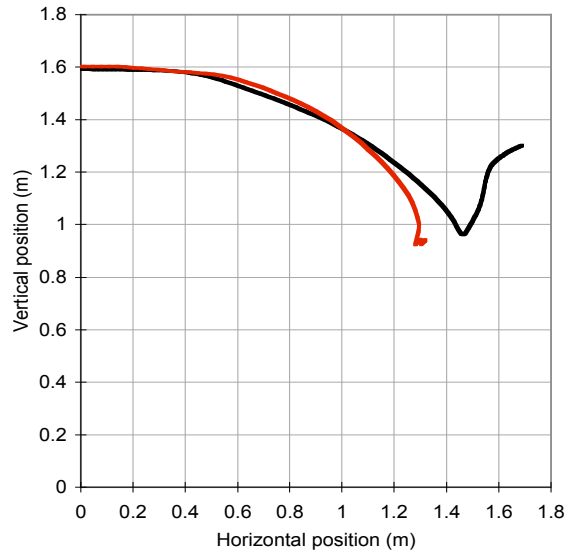
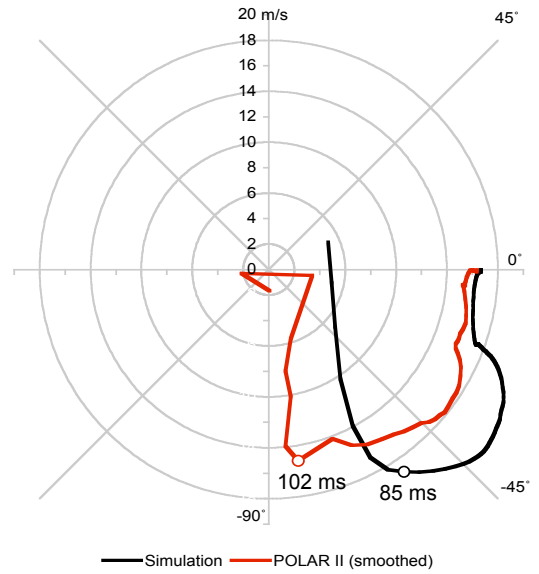


Figure 17 (top to bottom) radial head velocity trajectory; head position trajectory and head velocity history. Polar-II data are red and simulation data are black. The hollow circles represent data points associated with head impact.

In each case, we based our simulations on the physical evidence left after the crash and we could reproduce patterns of contact between the pedestrian and the vehicle in the simulation. The Polar-II reconstructions were conducted with the same make and model of vehicle, and were set up to match the initial conditions chosen for the simulation. This allowed us to compare the kinematics of the Polar-II with our simulation model, and allowed us to compare contact points produced by each surrogate with contacts in the actual case.

There were discrepancies in the head kinematics between the simulation and the Polar-II tests. Consistent across all three Polar-II tests were the following:

- Negligible horizontal velocity component in the head impact velocity, and
- Wrap-around-distances to head impact 200-400 mm shorter than the simulation results.

Both phenomena appear to be related to differences in the amount of sliding of the dummy/pedestrian model over the vehicle. There was noticeably less sliding of the Polar-II than in the simulation.

Kerrigan et al. (2005a) also noted differences in sliding between Polar-II and PMHS tests. Those authors suggested that non-biofidelic pelvic responses and different mass distribution in the dummy might contribute to the phenomenon. It should be noted that the vehicles used in the reconstructions in this paper are not contemporary designs and they might be considered relatively aggressive, and so it is possible that the apparent snagging of the dummy on the bumper/leading edge and the lack of sliding may have been worse than previously observed. In Cases 2 and 3, the radial plots suggest that this snagging might be characterised by a distinctive head velocity trajectory: an initial period of nearly vertical acceleration, followed by a period of almost horizontal deceleration relative to the car, until the horizontal component of the velocity is close to zero. The relatively steep impact velocities are also noticeable in other evaluations of Polar-II (Kerrigan et al., 2005a; Kerrigan et al., 2005b and Akiyama et al., 2001).

When we compared the Polar-II impact locations with the actual cases, the differences appeared to be greatest for the vehicle with the most aggressive leading edge (Case 2) and least with the vehicle with the least aggressive leading edge (Case 1). We suspect that the more aggressive leading edges might have caused the dummy to snag on the vehicle. This, with the pelvic response discussed by Kerrigan et al. (2005a) might explain in whole, or partly, the lack of sliding over the vehicle that was observed.

The vertical component of the impact velocity was similar in the Polar-II tests and the MADYMO simulations of Cases 2 and 3. The smaller vertical component of the velocity in Case 1 appears to be because of the oblique contact between the torso and bonnet, which appeared to rapidly decelerate the head through tension and a resistive moment in the neck.

One other aspect of the kinematics that might have affected the head velocity, and which was notably different between the Polar-II tests and simulations, was the kinematics of the legs. The legs in the MADYMO model did not remain in contact with the leading edge as long as the legs of the Polar-II, and the contact with the bumper and leading edge imparted greater kinetic energy to the legs in the simulation. We have not yet investigated the kinematics in detail, except to note that the kinematics of the legs in the simulation of PMHS tests (detailed in Ishikawa et al., 1991) fitted displacement corridors. It is possible that the greater excursion of the legs may have been partly due to the greater sliding of the pedestrian over the vehicle, the lower legs coming into greater contact with the leading edge in the simulation compared to the Polar-II tests.

In summary, the differences in the kinematics of the head of the computer model and the Polar-II seem to arise mainly as a consequence of the differences in the relative motion that occurs with respect to the vehicle, and possibly also to differences in torso/head/neck behaviour (as observed in Case 1). The behaviour of the model and/or Polar-II in these areas might be a focus of further validation and refinement.

## ACKNOWLEDGEMENTS

We thank Honda R&D and their staff for their generous support in providing the Polar-II dummy and funding all Polar-II tests. Honda R&D also paid all freight costs and travel expenses for Luke Streeter to attend the tests at JARI. Mr Yasuhiro Dokko kindly provided the dummy trajectory data and arranged and managed the tests.

The Centre for Automotive Safety Research receives sustaining funds from both the Motor Accident Commission and the South Australian Department of Transport, Energy and Infrastructure.

The views expressed in this paper are those of the authors and do not necessarily represent those of Honda R&D Ltd., the University of Adelaide or the Centre's sponsors.

## REFERENCES

- Akiyama, A., Okamoto, M., and Rangarajan, N. 2001, Development and application of the new pedestrian dummy. *Proceedings of the 17<sup>th</sup> International Conference on the Enhanced Safety of Vehicles (ESV)*, Amsterdam, The Netherlands, June 4 - 7, 2001, Paper 463.
- Anderson, R. W. G., McLean, A. J. and Dokko, Y. 2005. Determining accurate contact definitions in multi-body simulations for DOE-type reconstruction of head impacts in pedestrian accidents. *Proceedings of the 19<sup>th</sup> International Conference on the Enhanced Safety of Vehicles*, Washington, DC, June 6-9, 2005, Paper 05-0175.
- Anderson, R.W.G., McLean, A.J., Streeter, L.D., Ponte, G., Sommariva, M., Lindsay, V.L., Wundersitz, L. 2002, Severity and type of pedestrian injuries related to vehicle impact locations and results of sub-system impact reconstructions, *Proceedings of the International IRCOBI Conference on the Biomechanics of Impact*, September 18-20 2002, Munich, Germany.
- Anderson, R. W. G., Streeter, L.D., Ponte, G., Van de Griend, M., Lindsay, V.L. and Mclean, A. J. 2003, Pedestrian subsystem head impact results reflect the severity of pedestrian head injuries. *International Journal of Vehicle Design*, **31**(1/2), 1-15.
- Anderson, R. W. G., Streeter, L. D. and Mclean, A. J. 2000, Estimation of impact severity in pedestrian accidents using accident investigation, computer simulation and physical reconstruction. *Road Safety Research, Policing and Education Conference*, Brisbane.
- Baughman, L. 1983, *Development of an Interactive Program to Produce Body Description Data*, Report no. AFAMRL-TR-83-058, US Air Force Aerospace Medical Research Laboratory.
- Depriester, J-P., Perrin, C., Serre, T., Chalandon, S. 2005, Comparison of several methods for real pedestrian accident reconstruction, *Proceedings of the 19<sup>th</sup> International Conference on the Enhanced Safety of Vehicles*, Washington, DC, June 6-9, 2005, Paper 05-0333.
- EEVC 2002, EEVC Working Group 17 Report, Improved test methods to evaluate pedestrian protection afforded by passenger cars, December 1988 with September 2002 updates.
- Fredriksson, R., Haland, Y., Yang, J. 2001, Evaluation of a new pedestrian head injury protection system with a sensor in the bumper and lifting of the bonnet's rear part. *Proceedings of the 17<sup>th</sup> International Conference on the Enhanced Safety of Vehicles (ESV)*, Amsterdam, The Netherlands, June 4 - 7, 2001, Paper 131.
- Garrett, M. 1996. Head impact modelling using computer accident simulation based on cadaver records. *24th International workshop on human subjects for biomechanical research*, Albuquerque, New Mexico, US Department of Transportation. National Highways Traffic Safety Administration, 81-92.
- Garrett, M. 1998. Head impact modelling using MADYMO simulations of documented pedestrian accidents. *Conference on Pedestrian Safety*, Melbourne, Victoria, VicRoads, RACV, Federal Office of Road Safety, Australian Hotels Association, 158-168.
- Ishikawa H., Kajzer J., Schroeder G., 1993, Computer simulation of impact response of the human body in car-pedestrian accidents, *Proceedings of the Thirty-Seventh Stapp Car Crash Conference; 1993 Nov 7-8; San Antonio*, Society of Automotive Engineers, Warrendale, PA.
- Konosu, A. 2002, Reconstruction analysis for car-pedestrian accidents using a computer simulation model, *JSAE Review*, **23**, 357-363.
- Kerrigan, J.R., Murphy, D.B., Drinkwater, D.C., Kam, C.Y., Bose, D., and Crandall, J.R. 2005a, Kinematic Corridors for PMHS Tested in Full-Scale Pedestrian Impact Tests, *Proceedings of the 19th International Technical Conference on the Enhanced Safety of Vehicles*, Washington, DC, June 6-9, 2005, Paper 05-0394.
- Kerrigan, J.R., Kam, C.Y., Drinkwater, D.C., Murphy, D.B., Bose, D., Ivarsson, J., and Crandall, J.R. 2005b, Kinematic comparison of the Polar-II and PMHS in pedestrian impact tests with a sport-utility vehicle, *Proceedings of the 2005 International Conference on the Biomechanics of Impact*, 159-174.
- Thunnissen, J., Wismans, J., Ewing, C.L. and Thomas, D.J. 1995, 'Human volunteer head-neck response in frontal flexion: a new analysis', *39th Stapp Car Crash Conference, Coronado, California, November 8-10, 1995*, Paper 952721, Society of Automotive Engineers, Inc. (SAE), Warrendale PA.
- Wismans, J., Oorschot, H. and Woltring, H.J. 1986, 'Omni-directional human head-neck response', *30th Stapp Car Crash Conference*, Society of Automotive Engineers, Inc. (SAE), Warrendale PA, 313-331.
- Yang, Y., Yao, J., Otte, D. 2005, Correlation of different impact conditions to the injury severity of pedestrians in real world accidents, *Proceedings of the 19th International Technical Conference on the Enhanced Safety of Vehicles*, Washington, DC, June 6-9, 2005, Paper Number 05-0352.
- Yang, J. 2003, Pedestrian head protection from car impacts, *International Journal of Vehicle Design*, **32**(1/2), 16-27.

## PEDESTRIAN GTR TESTING OF CURRENT VEHICLES

**Ann Mallory**

Transportation Research Center Inc.

**Jason Stammen, Susan Meyerson**

National Highway Traffic Safety Administration  
United States of America

Paper No. 07-0313

### ABSTRACT

The Working Party on Passive Safety of the World Forum for Harmonization of Vehicle Regulations (WP.29) is developing a draft global technical regulation (GTR) for pedestrian safety. In order to evaluate the potential effects of the draft GTR on the U.S. fleet, NHTSA's Vehicle Research and Test Center (VRTC) conducted 88 pedestrian head impact tests on 11 vehicles selected to represent the U.S. fleet, with a focus on larger passenger vehicles. The goal was to generate an overall picture of current U.S. vehicle performance with respect to specific structures and test zones in order to better understand the potential challenges and benefits of meeting the regulation.

The peripheral areas of the head impact test zone defined in the draft GTR produced the most severe impacts, with the most challenging areas being in the rear of the test zone (in the area of the hinges, cowl, and wiper spindles) and the lateral edges of the test zone adjacent to the fenders. A smaller number of vehicles produced high-severity impacts at the front edge of the test zone. The challenging areas at the periphery of the test zone did not exceed the GTR requirements in every vehicle. Deformable hood hinges with adequate crushable space between the hood panel and fender, coverage of the cowl by the back edge of the hood, and flanges under the fender edge all resulted in significant HIC reductions from those areas in vehicles without these countermeasures.

The range of performance in the vehicles tested indicates that while there is room for improvement in current head impact protection in US vehicles, countermeasures exist to improve the worst areas of the test zone. The presence of pedestrian-friendly components in heavier and high-front vehicles shows that design modifications are not limited to smaller vehicles.

### INTRODUCTION

Nearly 1.2 million people die annually in road crashes around the world. In a comprehensive review

of epidemiological studies, the World Health Organization (WHO) estimates that between 41% and 75% of those deaths are pedestrians. Pedestrian deaths are especially prevalent in low-income and middle-income countries because of the greater variety and intensity of traffic mix and lack of separation between pedestrian and vehicle [Peden, 2004]. Although pedestrian injuries are less of an epidemic in the United States, they are still a significant problem with 4,841 pedestrians killed in 2005 alone [NHTSA, 2006]. A recent study in one U.S. urban area showed that pedestrians made up nearly half of all traffic fatalities [Nicaj, 2006]. While education, traffic design, and speed enforcement can all contribute to reducing the number of pedestrian collisions, incorporating pedestrian countermeasures into vehicle design can help to protect pedestrians from serious or fatal injuries in the event of a collision.

The Working Party on Passive Safety (GRSP) of the World Forum for Harmonization of Vehicle Regulations (WP.29) is developing a draft global technical regulation (GTR) to address pedestrian safety through vehicle design [GRSP, 2006]. This regulation includes procedures developed by the Pedestrian Safety Working Group of the International Harmonization Research Activity (IHRA) to test vehicles with child- and adult-sized headforms as well as adult-sized upper and lower legforms [Mizuno, 2005]. Because of differences in vehicle fleet composition among GRSP countries, many countries are evaluating how the GTR would affect their fleet's level of pedestrian protection.

We assume for this paper that there are four main components for evaluating the potential safety benefits of a pedestrian GTR regulation: (a) population targeted by the regulation, (b) applicable test area included in the regulation, (c) baseline performance of the vehicle fleet, and (d) injury risk reduction expected due to compliance with the regulation's performance criteria [NHTSA, 1997]. In the calculation of benefits for the pedestrian GTR, the target population is derived from accident data and vehicle statistics. The allowable test area is described

in the GTR by a procedure for laying out the boundaries of the testable area. The baseline performance is evaluated in this paper by testing a representative sample of the fleet with respect to the Head Injury Criterion (HIC) limits proposed as performance criteria in the GTR.

To calculate the safety improvements afforded by the GTR, it is assumed that non-compliant HIC values from the baseline experimental data would become compliant if the vehicle were designed to meet the GTR, leading to a reduction in HIC and a corresponding reduction in injury risk. When this potential reduction is summed for all non-compliant points, a reduced overall fatality or injury risk is estimated and this reduction, along with target population and testable area, is used to determine equivalent lives saved or injuries reduced [NHTSA, 1997].

The challenges and benefits of applying the GTR requirements to high-front vehicles are of particular interest because of the prevalence of larger vehicles in the U.S. While it has been determined that improvement to smaller passenger vehicles is feasible and cost-effective [ACEA, 2005; Lawrence, 2002; NHTSA, 2005], manufacturers have argued that higher-front vehicles present different design challenges than do passenger cars [OICA, 2006b]. The GRSP has debated the applicability of the GTR to these larger vehicles [European Commission, 2006; JAMA, 2006; OICA, 2006c]. In particular, there is concern about the feasibility of improving protection in the hood leading edge area [OICA, 2006a]. To address these concerns, test data from points within this front zone are needed to evaluate the challenges of meeting the proposed GTR in this area of the vehicle.

NHTSA's Vehicle Research and Test Center (VRTC) has conducted 88 pedestrian head impact tests on 11 vehicles selected to represent the U.S. fleet with a focus on high-front vehicles. These tests include 84 baseline tests to evaluate overall current fleet performance as well as additional testing on a vehicle known to have countermeasures designed specifically for pedestrian head impact safety. The objectives of this study were to (1) determine the current baseline performance of a key subset of the U.S. vehicle fleet for the benefit assessment, (2) identify problem areas and existing countermeasures to improve them, and (3) evaluate the difficulty of meeting the GTR requirements by estimating likely relaxation zones for each vehicle. Together, these factors were used to generate an overall picture of the current level of U.S.

vehicle performance, with respect to specific structures and test zones.

## METHODS

### Vehicles Tested

Head impact testing was performed on eleven vehicles chosen to cover a wide range of GVM (Gross Vehicle Mass) and BLE (Bonnet Leading Edge) heights (Table 1). GVM is a manufacturer-declared maximum mass for a fully-laden vehicle. The height of the leading edge is a wrap around distance (WAD) measured with a flexible tape in the vertical longitudinal plane of the vehicle. Variations in the geometry of the vehicle front end result in differences in the BLE WAD across the width of the vehicle front. Vehicles were selected to include multiple manufacturers, as well as vehicles known to have designed pedestrian countermeasures. Additional factors in the final selection of vehicles included availability of vehicles and the frequency of each model in the fleet. Efforts were made to avoid duplicate testing on vehicles that were undergoing simultaneous testing by manufacturers.

**Table 1.**  
**Vehicles tested in the current study sorted by Gross Vehicle Mass (GVM)**

| Test vehicles            | GVM (kg) | Bonnet Leading Edge WAD (mm)* |       |
|--------------------------|----------|-------------------------------|-------|
|                          |          | (Min)                         | (Max) |
| 2002 Jeep Wrangler       | 2019     | 916                           | 1111  |
| 2005 Honda CR-V          | 2020     | 880                           | 1014  |
| 2006 Volkswagen Passat   | 2020     | 840                           | 880   |
| 2006 Toyota Tacoma       | 2063     | 992                           | 1026  |
| 2003 Toyota 4Runner      | 2063     | 1030                          | 1091  |
| 1999 Dodge Dakota        | 2200     | 895                           | 995   |
| 2003 Ford Crown Victoria | 2632     | 804                           | 848   |
| 2006 Dodge Durango       | 2903     | 1088                          | 1240  |
| 2003 Hummer H2           | 3901     | 1172                          | 1196  |
| 2003 Ford E350           | 4127     | 1162                          | 1188  |
| 2005 Chevrolet Silverado | 4173     | 1210                          | 1265  |

### Impact Point Locations

The testable areas on the front structures of each vehicle were marked according to the requirements in the GTR [GRSP, 2006]. A number of GTR-defined reference lines, necessary for identification of the test zones, were drawn on each vehicle. Reference lines were drawn at wrap-around distances (WAD) of 1000 mm, 1700 mm, and 2100 mm. A bonnet leading

edge (BLE) reference line was drawn across the width of the vehicle where a straight edge at 50 degrees from the vertical, parallel to the centerline of the vehicle, contacted the front structures. Side reference lines were marked along the sides of the vehicle where a straight edge at 45 degrees from the vertical, perpendicular to the vehicle centerline, contacted the front structures of the vehicle. A bonnet rear reference line was drawn, according to GTR requirements, based on the contact location on the hood and front structures by a headform-sized sphere in contact with the windshield. The child test zone was bordered at the front by the most rearward of the 1000 mm WAD line or 82.5 mm rearward of the BLE reference line; at the sides by lines 82.5 mm inboard of the side reference lines; and at the rear by the most forward of the WAD 1700 line or 82.5 mm forward of the bonnet rear reference line. The adult zone was bordered at the front by the WAD 1700 line, at the sides by lines 82.5 mm inboard of the side reference lines, and at the rear by the most forward of the WAD 2100 line or 82.5 mm forward of the bonnet rear reference line.

For each vehicle, up to 8 baseline impact points were chosen, with up to 4 in the child zone and 4 in the adult zone (Figure 1). The Passat had a very small adult test zone and was therefore subjected to only one test in the adult zone, along with four tests in the child impact zone. A data failure in a child-zone impact in CR-V testing resulted in a total of 7 of the 8 baseline impact tests, along with four additional tests run for design comparison only. The remaining nine vehicles underwent eight tests each.

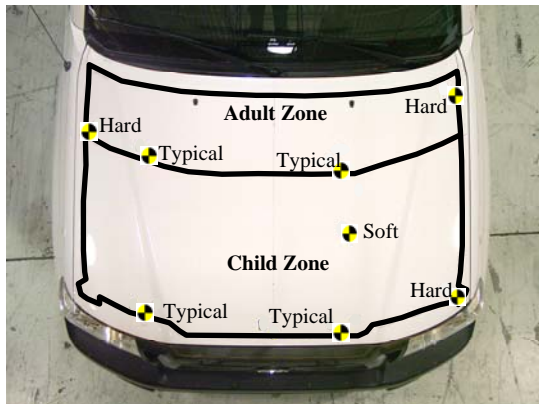


**Figure 1. Test zones and eight impact points shown for the 2006 Toyota Tacoma.**

In each zone, two points were chosen to correspond to a “typical” impact location. The WAD of these points was based on data from the Pedestrian Crash Data Study (PCDS), NHTSA’s database of pedestrian injury cases collected between 1994 and 1998. The

ratio of initial head impact WAD to pedestrian standing height was calculated for all PCDS cases where both measurements were known and impact speed was 40 km/h or less, which accounts for more than 75% of the pedestrian injured accidents according to the preamble of the draft GTR. The median WAD/standing height ratio was then calculated for each vehicle type, and multiplied by the median standing heights for a 20 year-old and a six-year old to determine the “typical” WAD for an adult head impact and a child head impact for each vehicle type (Table 2). The standing heights were 1700 mm for the adult and 1150 mm for the child, based on averaged male and female data in Centers for Disease Control growth charts [NCHS, 2000]. In each zone, one of the “typical” impacts was performed on each side of the vehicle. The lateral locations of these tests were at 1/6 and 4/6 across the total width of the testable area at that location. In this way, two unbiased points were selected across the width of the vehicle in each zone. They were located in objectively-measured locations and not selected based on the vehicle’s design. They were biased toward the passenger-side of the vehicle because of the higher frequency of pedestrian head contacts on the passenger side in PCDS data. In cases where the nominal impact location for the “typical” adult and child zones were not within the boundaries of the test zone, the point in the test zone closest to the target impact location was selected as the impact point.

**Table 2. Target WAD for “typical” head impacts (median adult and child WAD based on PCDS data and 50<sup>th</sup> percentile height of adult and six-year-old)**

|          | <b>Median WAD/Height Ratio</b> | <b>Estimated Median WAD multiplied by height of adult and child</b> |         |
|----------|--------------------------------|---|---------|
| Minivan  | 1.04                           | 1768 mm   | 1196 mm |
| Pass Car | 1.17                           | 1989 mm   | 1346 mm |
| Pickup   | 0.96                           | 1632 mm   | 1104 mm |
| SUV      | 0.94                           | 1598 mm   | 1081 mm |
| Van      | 0.86                           | 1462 mm   | 989 mm  |

The additional four tests per vehicle were targeted at locations that were the hardest and softest portions of the test zone. These tests were specific to each individual vehicle and were intended to provide points in both the best- and worst-case scenarios. The manufacturer of each vehicle was invited to contribute input on the worst-case and best-case points based on their test experience and knowledge of the design.

In addition to the baseline testing performed on all vehicles in this study, four additional tests were performed on the CR-V. The CR-V front end had features that appeared to specifically address pedestrian head safety. The four comparison-only impacts were performed as an evaluation of structures that had produced particularly severe head impacts in other vehicles. These extra tests of the CR-V pedestrian countermeasures were not included in the summary data for the 84 baseline tests because they did not follow the same guidelines as test locations for the other vehicles, but are included in this paper to better understand the potential effects of pedestrian-specific design.

### Test Procedure

Free-flight impacts were performed according to the procedure in the GTR (Figure 2). Impacts in the child zone were performed with the 3.5 kg, 165 mm diameter headform defined in section 6.3.2.1 and impacts in the adult zone were performed with the 4.5 kg, 165 mm diameter headform defined in section 6.3.2.2 [GRSP, 2006]. The impact angle was 50 degrees to the horizontal for the child headform and 65 degrees to the horizontal for the adult headform. Impact speed was  $9.7 \pm 0.2$  m/s [ $35 \pm 0.72$  km/h], for all tests except a comparison-only test (point CM-H) run on the CR-V at a speed of 9.92 m/s. The locations of first head contact for all baseline evaluation impact points were within the defined test zones. Of the four comparison-only tests performed on the CR-V, two were outside the test zone.

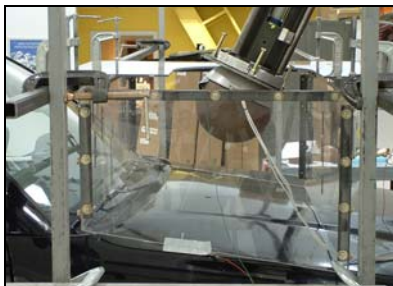


**Figure 2. Test setup for adult headform impact on Toyota 4Runner.**

Table 3 describes all the points selected for testing, including the coordinates by WAD and by lateral distance from the vehicle centerline, where positive (+) numbers are toward the driver's side of the vehicle.

The tests on each vehicle were performed on two hoods unless a significant amount of deformation was present. In cases where there was potential for

damage overlap between adjacent points, the hood was replaced and the order of remaining impacts on that vehicle was adjusted if necessary.

The headforms were instrumented with 3 uniaxial accelerometers (Endevco 7264) mounted at locations within GTR guidelines for proximity to the center of mass of the headform. Acceleration data was sampled at 20 kHz, pre-filtered at 3 kHz, then zeroed and filtered using Channel Filter Class 1000 (1650 Hz) before being used to calculate peak resultant acceleration and 15 millisecond Head Injury Criterion (HIC).

### Relaxation Zone Identification

According to the proposed GTR, manufacturers may designate up to one third of the test zone, including up to half of the child zone, as a relaxation zone. In this relaxation zone, head impacts must produce HIC measurements of less than 1700, where the remainder of test zone is limited to HIC of less than 1000.

After completion of testing, relaxation zones were proposed for each of the 11 test vehicles, by estimating the areas likely to be in the stiffest third of the test zone. These zones were selected based on proximity to supporting structures, under-hood clearance, and performance of different structures in testing. Overhead photographs of the vehicle with the hood open and closed were overlaid to help identify stiff under-hood structures within the test area (Figure 3). Zone definition involved identifying the most challenging portions of the test zone and measuring the remaining area relative to the whole test zone in overhead photographs. This process was repeated iteratively, adjusting the boundaries of the relaxation zone until it represented one third of the total test area +/- approximately 0.01 m<sup>2</sup>.



**Figure 3. Example of test zone and relaxation zone boundaries in Toyota 4Runner.**

**Table 3.**  
**Test point coordinates and descriptions**

| Vehicle  | Point | Description         | Point Type | WAD (mm) | Lateral from CL (mm) | Zone Area    |
|----------|-------|---------------------|------------|----------|----------------------|--------------|
| 4Runner  | A     | Hood Leading Edge   | T          | 1114     | -471                 | Front Child  |
| 4Runner  | B     | Hood Leading Edge   | T          | 1171     | 236                  | Front Child  |
| 4Runner  | C     | Open Area           | S          | 1472     | -385                 | Middle Child |
| 4Runner  | D     | Radiator Cap        | H          | 1280     | -377                 | Middle Child |
| 4Runner  | E     | Open Area           | T          | 1710     | -497                 | Front Adult  |
| 4Runner  | F     | Open Area           | T          | 1706     | 280                  | Front Adult  |
| 4Runner  | G     | Fender Area         | H          | 1705     | 739                  | Rear Adult   |
| 4Runner  | H     | Hinge               | H          | 1908     | -729                 | Rear Adult   |
| CrownVic | A     | Hood Ridge          | T          | 1335     | -515                 | Middle Child |
| CrownVic | B     | Open Area           | T          | 1336     | 257                  | Middle Child |
| CrownVic | C     | Battery             | H          | 1136     | -650                 | Middle Child |
| CrownVic | D     | Open Area           | S          | 1653     | 439                  | Rear Child   |
| CrownVic | E     | Open Area           | T          | 1975     | -531                 | Middle Adult |
| CrownVic | F     | Insulator Bkt       | T          | 1976     | 266                  | Middle Adult |
| CrownVic | G     | Hinge               | H          | 1972     | -775                 | Rear Adult   |
| CrownVic | H     | Engine Cover        | H          | 1874     | 24                   | Middle Adult |
| CR-V     | A     | Hood Leading Edge   | T          | 1081     | -456                 | Front Child  |
| CR-V     | B     | Hood Leading Edge   | T          | 1087     | 228                  | Front Child  |
| CR-V     | C     | Cowl Area           | T          | 1705     | -470                 | Rear Adult   |
| CR-V     | D     | Cowl Area           | T          | 1705     | 237                  | Rear Adult   |
| CR-V     | E     | Fender Area         | H          | 1399     | 692                  | Middle Child |
| CR-V     | G     | Hinge               | H          | 1704     | -701                 | Rear Adult   |
| CR-V     | H     | Hinge               | H          | 1706     | 652                  | Rear Adult   |
| Dakota   | A     | Hood Leading Edge   | T          | 1104     | -519                 | Middle Child |
| Dakota   | B     | Radiator Cap        | T          | 1104     | 260                  | Front Child  |
| Dakota   | C     | Air Intake Box Area | T          | 1705     | -514                 | Front Adult  |
| Dakota   | D     | Throttle Box        | T          | 1706     | 257                  | Front Adult  |
| Dakota   | E     | Open Area           | S          | 1308     | -284                 | Middle Child |
| Dakota   | F     | Latch               | H          | 1056     | 0                    | Front Child  |
| Dakota   | G     | Hinge               | H          | 1960     | -707                 | Rear Adult   |
| Dakota   | H     | Hinge               | H          | 1986     | 622                  | Rear Adult   |
| Durango  | A     | Hood Leading Edge   | T          | 1194     | -372                 | Front Child  |
| Durango  | B     | Hood Leading Edge   | T          | 1197     | 186                  | Front Child  |
| Durango  | C     | Battery             | T          | 1704     | -481                 | Front Adult  |
| Durango  | D     | Open Area           | T          | 1707     | 230                  | Front Adult  |
| Durango  | E     | Battery             | H          | 1493     | -590                 | Middle Child |
| Durango  | F     | Open Area           | S          | 1508     | 233                  | Middle Child |
| Durango  | G     | Cowl Area           | H          | 1900     | -120                 | Rear Adult   |
| Durango  | H     | Cowl Area           | H          | 1858     | 699                  | Rear Adult   |
| E350     | A     | Hood Leading Edge   | T          | 1264     | -547                 | Front Child  |
| E350     | B     | Hood Leading Edge   | T          | 1274     | 276                  | Front Child  |
| E350     | C     | Latch               | H          | 1278     | 0                    | Front Child  |
| E350     | D     | Open Area           | S          | 1480     | 561                  | Middle Child |
| E350     | E     | Cowl Area           | T          | 1704     | -568                 | Rear Adult   |
| E350     | F     | Cowl Area           | T          | 1706     | 282                  | Rear Adult   |
| E350     | G     | Cowl Area           | H          | 1808     | 609                  | Rear Adult   |
| E350     | H     | Hinge               | H          | 1792     | 856                  | Rear Adult   |

| Vehicle   | Point | Description       | Point Type | WAD (mm) | Lateral from CL (mm) | Zone Area    |
|-----------|-------|-------------------|------------|----------|----------------------|--------------|
| H2        | A     | Hood Leading Edge | T          | 1270     | -578                 | Front Child  |
| H2        | B     | Hood Leading Edge | T          | 1275     | 289                  | Front Child  |
| H2        | C     | Open Area         | T          | 1705     | -534                 | Front Adult  |
| H2        | D     | Handle            | T          | 1727     | 267                  | Front Adult  |
| H2        | E     | Hood Leading Edge | H          | 1328     | 382                  | Front Child  |
| H2        | F     | Hood Ridge        | H          | 1445     | 765                  | Middle Child |
| H2        | G     | Open Area         | S          | 1856     | 487                  | Middle Adult |
| H2        | H     | Latch             | H          | 2053     | 126                  | Rear Adult   |
| Passat    | A     | Open Area         | T          | 1346     | -480                 | Middle Child |
| Passat    | B     | Open Area         | T          | 1346     | 240                  | Middle Child |
| Passat    | F     | Open Area         | S          | 1174     | 435                  | Middle Child |
| Passat    | G     | Hinge             | H          | 1501     | -683                 | Rear Child   |
| Passat    | H     | Cowl Area         | T          | 1698     | 0                    | Middle Adult |
| Silverado | 1     | Open Area         | T          | 1705     | 320                  | Front Adult  |
| Silverado | 2     | Open Area         | S          | 2030     | -310                 | Rear Adult   |
| Silverado | 3     | Hood Leading Edge | T          | 1335     | -580                 | Front Child  |
| Silverado | 4     | Fender Area       | H          | 1337     | 750                  | Front Child  |
| Silverado | 5     | Fluid Cap         | T          | 1705     | -632                 | Front Adult  |
| Silverado | 6     | Hinge             | H          | 2095     | 779                  | Rear Adult   |
| Silverado | 7     | Latch             | H          | 1340     | 0                    | Front Child  |
| Silverado | 8     | Hood Leading Edge | T          | 1342     | 291                  | Front Child  |
| Tacoma    | A     | Hood Leading Edge | T          | 1110     | -487                 | Front Child  |
| Tacoma    | B     | Hood Leading Edge | T          | 1100     | 243                  | Front Child  |
| Tacoma    | C     | Open Area         | T          | 1710     | -487                 | Front Adult  |
| Tacoma    | D     | Open Area         | T          | 1710     | 243                  | Front Adult  |
| Tacoma    | E     | Hood Leading Edge | H          | 1103     | 693                  | Front Child  |
| Tacoma    | F     | Open Area         | S          | 1462     | 275                  | Middle Child |
| Tacoma    | G     | Fender Area       | H          | 1706     | -726                 | Middle Adult |
| Tacoma    | H     | Hinge             | H          | 1942     | 716                  | Rear Adult   |
| Wrangler  | A     | Hood Leading Edge | T          | 1153     | -501                 | Front Child  |
| Wrangler  | B     | Hood Leading Edge | T          | 1168     | 250                  | Front Child  |
| Wrangler  | C     | Hood Ridge        | T          | 1705     | -389                 | Front Adult  |
| Wrangler  | D     | Open Area         | T          | 1705     | 195                  | Front Adult  |
| Wrangler  | E     | Open Area         | S          | 1599     | -246                 | Rear Child   |
| Wrangler  | F     | Latch             | H          | 1072     | 603                  | Front Child  |
| Wrangler  | H     | Cowl Area         | H          | 2014     | 534                  | Rear Adult   |
| Wrangler  | I     | Hinge             | H          | 2071     | 350                  | Rear Adult   |
|           |       |                   |            |          |                      |              |
| CRV       | CM-L  | Latch Area        | CM         | 1072     | 3                    | Front Child  |
| CR-V      | CM-W  | Wiper Base        | CM         | 1822     | 76                   | Outside Zone |
| CR-V      | CM-H  | Headlight Area    | CM         | 1050     | -634                 | Front Child  |
| CR-V      | CM-C  | Cowl Area         | CM         | 1810     | -292                 | Outside Zone |

T Typical  
S Soft  
H Hard  
CM Countermeasure comparison test

## RESULTS

For the baseline 84 tests, Figures 4 through 14 show the location of impact points relative to the estimated relaxation zones that were identified after testing was complete, along with the 15-millisecond HIC result from each test. The test zones are outlined in black, with the outer, lighter (yellow) zone representing the relaxation zone and the inner, darker (green) zone representing the remaining two thirds of the test zone. The child and adult zone boundary is a dashed line. The relaxation zones represent approximately one third of the total allowable test area. The relaxation zones on each vehicle met the GTR requirement that the relaxation zone not exceed one half of the child zone. Removing that requirement, however, would not have had any effect on the relaxation zones estimated for this set of vehicles.

The results of an additional four tests performed on the CR-V for comparison purposes only are shown in Figure 15.

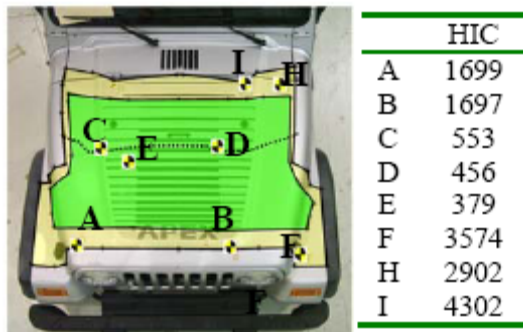


Figure 4. 2002 Jeep Wrangler results.

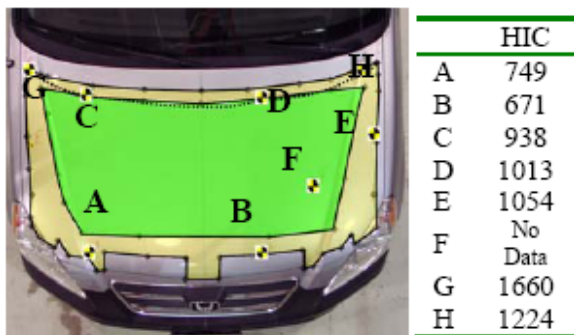


Figure 5. 2005 Honda CR-V results (baseline).

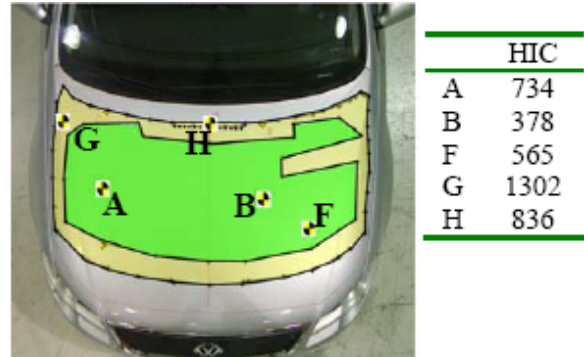


Figure 6. 2006 Volkswagen Passat results.

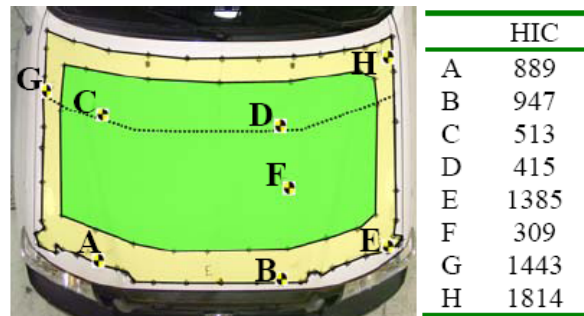


Figure 7. 2006 Toyota Tacoma results.

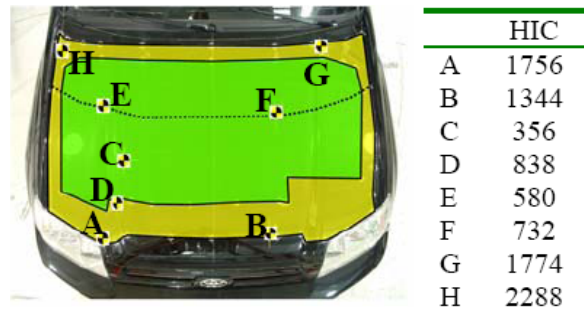


Figure 8. 2003 Toyota 4Runner results.

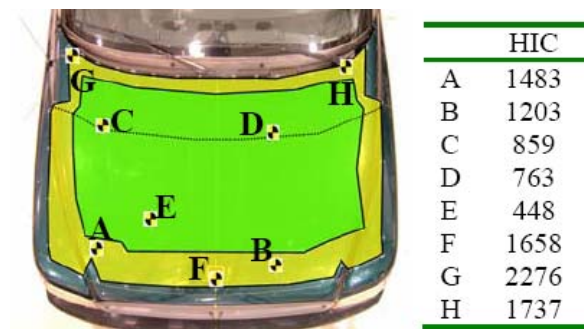


Figure 9. 1999 Dodge Dakota results.

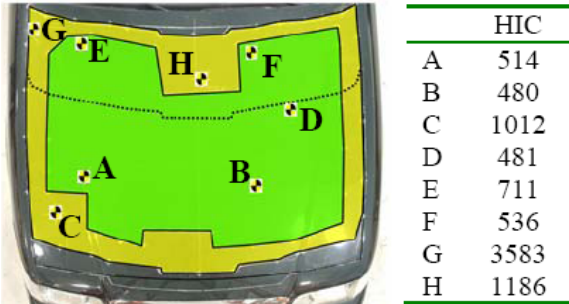


Figure 10. 2003 Ford Crown Victoria results.

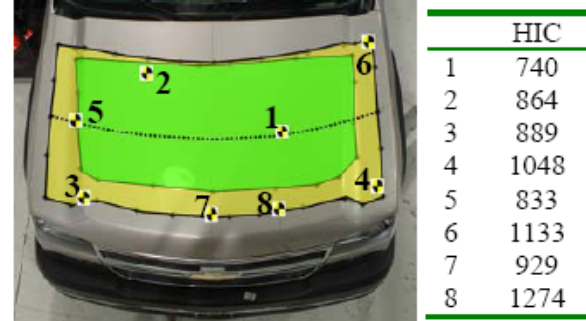


Figure 14. 2005 Chevrolet Silverado results.

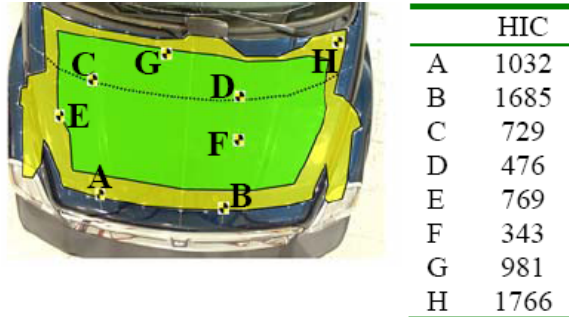


Figure 11. 2006 Dodge Durango results.

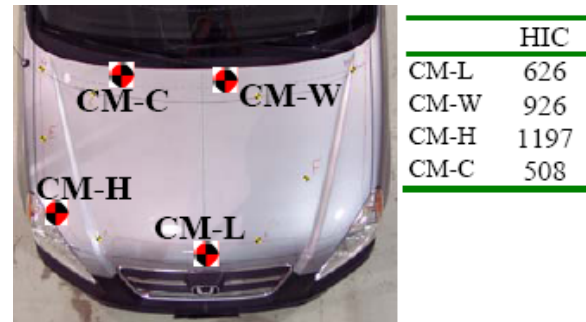


Figure 15. 2005 Honda CR-V counter-measure impacts for comparison only.

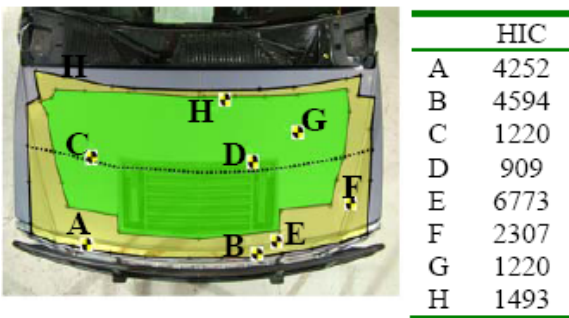


Figure 12. 2003 Hummer H2 results.

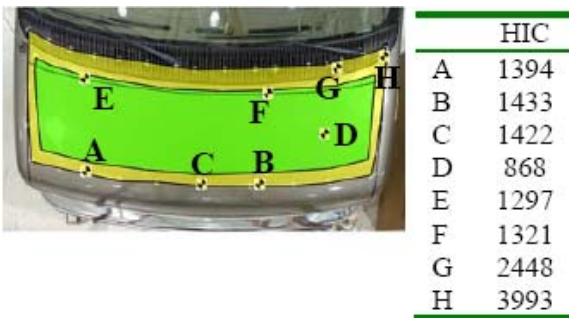


Figure 13. 2003 Ford E350 results.

Table 4 summarizes statistics from the 84 baseline test results grouped by location within each test zone. The child and adult zones were each divided into a front, middle, and rear region, where the front and rear regions were within approximately one head radius (82.5 mm) from the front and rear boundaries of the test zone respectively. The pass/fail status is indicated by the number of impacts with HIC below 1000, which would pass at any location in the test zone and the number of impacts with HIC above 1700, which would fail at any location in the test zone. Also listed is the number of impacts between HIC 1000 and HIC 1700, which would pass only if located within a manufacturer-defined relaxation zone.

Table 5 summarizes the baseline test data by vehicle. The Silverado, Passat, and CR-V had no “failing” impacts. Although all three vehicles had impacts with HIC between 1000 and 1700, these points were all within the estimated relaxation zones for these vehicles. The H2 and the E350 had failing impacts over 1700, as well as points between 1000 and 1700 that were *not* in the estimated relaxation zone. The remaining six vehicles had failing points over 1700, but all tested points between 1000 and 1700 fell in the estimated relaxation zone.

Sixteen of the 17 points with HIC above 1700 were in the peripheral areas of the test zone. Table 6

shows the relative severity of impacts near various structures in the test zone. The five highest average HIC values by impacted structure were obtained for

components along the front, rear, and side of the hood. The only central structure having a HIC above 1700 was the hood ridge of the H2.

**Table 4.**  
**Summary of HIC results by location within test zone**

| Zone         | Avg HIC | Std Dev | Min | Max  | N  | Pass (<1000) | Pass only if in relaxation zone (1000-1700) | Fail (>1700) |
|--------------|---------|---------|-----|------|----|--------------|---|--------------|
| Rear Adult   | 1943    | 1005    | 864 | 4302 | 21 | 3            | 7   | 11           |
| Middle Adult | 989     | 348     | 536 | 1443 | 6  | 3            | 3   | 0            |
| Front Adult  | 698     | 220     | 415 | 1220 | 14 | 13           | 1   | 0            |
| Rear Child   | 721     | 506     | 379 | 1302 | 3  | 2            | 1   | 0            |
| Middle Child | 779     | 519     | 309 | 2307 | 16 | 12           | 3   | 1            |
| Front Child  | 1846    | 1472    | 671 | 6773 | 24 | 6            | 13  | 5            |
| Adult        | 1378    | 942     | 415 | 4302 | 41 | 19           | 11  | 11           |
| Child        | 1205    | 1134    | 309 | 6773 | 43 | 20           | 17  | 6            |
| Total        | 1374    | 1110    | 309 | 6773 | 84 | 39           | 28  | 17           |

**Table 5.**  
**Summary of results by vehicle, in descending order by average HIC**

| Vehicle             | Avg HIC | Std Dev | Min | Max  | N | Pass (<1000) | Pass only if in relaxation zone (1000-1700) | Fail (>1700) |
|---------------------|---------|---------|-----|------|---|--------------|---|--------------|
| Hummer H2           | 2846    | 2125    | 909 | 6773 | 8 | 1            | 3 (none in estimated relax zone)            | 4            |
| Jeep Wrangler       | 1945    | 1505    | 379 | 4302 | 8 | 3            | 2   | 3            |
| Ford E350           | 1772    | 1001    | 868 | 3993 | 8 | 1            | 5 (3 in estimated relax zone)               | 2            |
| Dodge Dakota        | 1303    | 600     | 448 | 2276 | 8 | 3            | 3   | 2            |
| Toyota 4Runner      | 1208    | 685     | 356 | 2288 | 8 | 4            | 1   | 3            |
| Ford Crown Victoria | 1063    | 1052    | 481 | 3583 | 8 | 5            | 2   | 1            |
| Honda CR-V          | 1044    | 329     | 671 | 1660 | 7 | 3            | 4   | 0            |
| Dodge Durango       | 973     | 519     | 343 | 1766 | 8 | 5            | 2   | 1            |
| Chevrolet Silverado | 964     | 176     | 740 | 1274 | 8 | 5            | 3   | 0            |
| Toyota Tacoma       | 964     | 544     | 309 | 1814 | 8 | 5            | 2   | 1            |
| Volkswagen Passat   | 763     | 348     | 378 | 1302 | 5 | 4            | 1   | 0            |

**Table 6.**  
**Summary of results by impacted structure, in descending order by average HIC**

|            | Impacted Structure  | Avg HIC | Std Dev | Min  | Max  | N  | Pass (<1000) | Pass only if in relaxation zone (1000-1700) | Fail (>1700) |
|------------|---------------------|---------|---------|------|------|----|--------------|---|--------------|
| Peripheral | Hinge               | 2301    | 1140    | 1133 | 4302 | 11 | 0            | 4   | 7            |
|            | Hood Leading Edge   | 1892    | 1578    | 671  | 6773 | 19 | 5            | 10  | 4            |
|            | Latch               | 1815    | 1020    | 929  | 3574 | 5  | 1            | 3   | 1            |
|            | Cowl Area           | 1500    | 731     | 836  | 2902 | 9  | 3            | 3   | 3            |
|            | Fender Area         | 1330    | 349     | 1048 | 1774 | 4  | 0            | 3   | 1            |
| Central    | Engine Cover        | 1186    | NA      | 1186 | 1186 | 1  | 0            | 1   | 0            |
|            | Hood Ridge          | 1125    | 1024    | 514  | 2307 | 3  | 2            | 0   | 1            |
|            | Radiator Cap        | 1020    | 258     | 838  | 1203 | 2  | 1            | 1   | 0            |
|            | Handle              | 909     | NA      | 909  | 909  | 1  | 1            | 0   | 0            |
|            | Air Intake Box Area | 859     | NA      | 859  | 859  | 1  | 1            | 0   | 0            |
|            | Battery             | 837     | 153     | 729  | 859  | 3  | 2            | 1   | 0            |
|            | Fluid Cap           | 833     | NA      | 833  | 833  | 1  | 1            | 0   | 0            |
|            | Throttle Box        | 763     | NA      | 763  | 763  | 1  | 1            | 0   | 0            |
|            | Open Area           | 603     | 260     | 309  | 1220 | 22 | 20           | 2   | 0            |
|            | Insulator Bracket   | 536     | NA      | 536  | 536  | 1  | 1            | 0   | 0            |

**DISCUSSION**

The results of the GTR head testing on eleven US vehicles did not show a clear connection between vehicle size and performance in head testing. Although two of the three vehicles with the highest average HIC were among the heaviest and highest-front vehicles (the H2 and the E350), the Jeep Wrangler also showed high average HIC, in spite of being one of the lighter vehicles with moderate front-end height. Conversely, the Silverado was the

heaviest, highest-front vehicle in the test series, but had an average HIC below 1000 and had no failing impacts. Location within the test zone and hood material selection appeared to have more effect on impact severity than did vehicle size. Figure 16 shows that HIC values measured centrally on the hood tended to be lower than those measured peripherally at the rear, sides, and front of the test area.

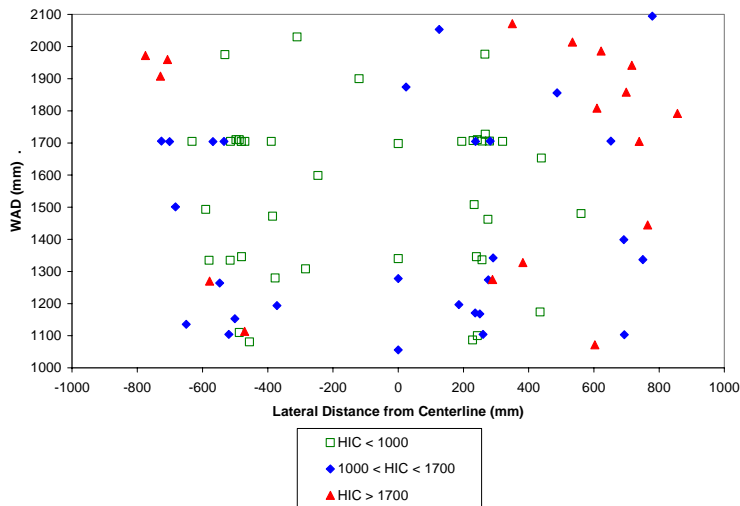


**Figure 16. Two-Dimensional Locations of Impacts.**

The hood hinge location had the highest average HIC value of all impacted areas with a HIC value over 1000 in every case. The hood hinge was selected as a potential hard point on nine of the eleven test vehicles. On two of those vehicles, two locations on the hinge were tested for a total of eleven hinge impacts. Hinge impacts that were particularly severe (over HIC 1700) tended to produce less damage and be shorter duration impacts while those that were under 1700 tended to produce more deformation and be longer in duration (Figure 17).

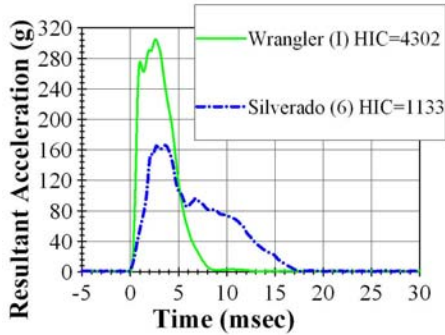


**Figure 17. Resultant acceleration of most severe hinge impact (Wrangler, green solid) and least severe hinge impact (Silverado, blue dashed), showing difference in impact duration.**

The hinge is a difficult area to design for pedestrians because of the strength required to support the hood and the necessary lack of clearance due to its location. The two vehicles that did worst were the two with an exposed hinge with no hood covering (E350 and Wrangler) to dissipate energy before direct contact (Figure 18).

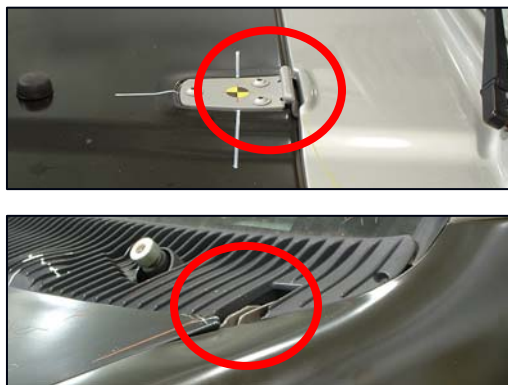


**Figure 18. Wrangler (Top) & E350 Hinges.**

The more compliant hinge designs on the Passat, Silverado, and CR-V appeared to be a deformable hinge, combined with an overlaid layer of crushable hood space (Figure 19).



**Figure 19. Passat hinge with low-profile deformable hinge and crush space over hinge.**

Even apart from the hinges, the entire area on or adjacent to the cowl, including over the wiper spindles, appeared to be challenging for pedestrian design. The worst performers in the cowl area did not have hood overhang over the cowl, and in fact the E350 had an exposed cowl that allowed direct contact by the headform (Figure 20). Vehicles that did best in the cowl area were those whose rear hood edge extended over the cowl, leaving a crush space between the hood and the structures below and preventing direct exposure of the head to the cowl (Figure 21).



**Figure 20. Exposed Cowl on E350.**



**Figure 21. Hood Coverage of the Cowl (Durango).**

The test zone markup procedure at the rear hood appeared to be effective at keeping likely impact areas in the zone and unlikely impact areas out of the zone. The test zone boundary at the rear of the hood was the most forward of the WAD 2100 line or 82.5 mm forward of the bonnet rear reference line. The bonnet rear reference line was located at the point of contact between a headform-sized sphere and the hood, cowl or other front structure when the sphere is traversed across the vehicle while maintaining contact with the vehicle. Therefore, if the geometry of the windshield and rear edge of the hood prevented the headform from contacting the cowl, the cowl was not included in the test zone. Since the headform

represents the size of a typical adult head, a cowl that was not in the test zone seemed unlikely to be contacted by a human pedestrian while a cowl that was in the test zone appeared that it could be contacted by a pedestrian head.

The area of the test zone adjacent to the fender appears to be another difficult area for many vehicles. Although there was only one failure (HIC 1774 on 4Runner), none of the four fender area impacts in the series had HIC under 1000. The solutions that work at the rear (such as overhanging hood to allow crush space at the edge) simply would not work with a standard side hood edge, supported laterally by the fender. The best performer in a fender-adjacent impact was the CR-V, which has deformable flanges under the fender-hood junction as well built-in crush space in adjacent areas of the hood reinforcement (Figure 22).

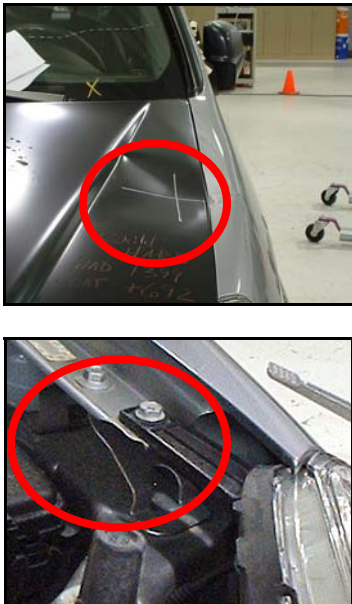


**Figure 22. CR-V Countermeasures at Fender.**

In the hood leading edge and latch area, eight of eleven vehicles passed the HIC requirements, based on the assumption that this area would be in the relaxation zone. Although the average HIC of the latch and hood leading edge areas were more severe than all other areas except for the hinge (Table 6), these high average values were a result of a small number of very severe impacts (HIC > 3000) on two vehicles. Nineteen of 24 impacts in this area were below the relaxation zone limit of 1700 HIC, and six were below 1000.

The vehicles that did best in hood leading edge impacts tended to have high, rounded front hood

areas like those on the Silverado, Durango, and CR-V, allowing plenty of crush space to shield stiffer underlying components including the front structural support, latch components, and underhood components (Figure 23). Those that failed the HIC < 1700 requirement in this area tended to have specific design features that presented unique risks for pedestrians. Three of those failures were in the H2, whose stiff composite hood was shaped into a very harsh corner at the front edge, resulting in HIC values of 4252, 4594, and 6773. A fourth failure was at the external latch on the Jeep Wrangler, which produced a HIC of 3574. These two designs are unlike any others tested; thus the countermeasures that worked well for the Silverado and Durango would not necessarily address these problems. The Wrangler's latch and the stiff front area of the H2 both represent pedestrian design challenges that may require unique solutions. A fifth failure in a 4Runner test adjacent to a headlamp may be a more typical issue for US large vehicles. An impact performed adjacent to the CR-V's headlamp for comparison, produced a HIC of 1197. The CR-V showed more deformation to hood area adjacent to the headlamp than the 4Runner did, indicating more crush space available at the edge of the CR-V hood.



**Figure 23. Sloped Hood at Leading Edge (Silverado and Durango shown here).**

As shown in Table 6 and Figure 16, HIC values measured in central hood impacts were low, compared to the peripheral areas of the test zones at the fender, cowl area, and hood leading edge. Of 36 central-area tests, only one test exceeded HIC 1700 and only five others were above 1000. It may be that the larger vehicles tested in this series had larger than average engine compartments, allowing sufficient clearance over stiff engine compartment components, and avoiding the engine compartment clearance issues faced by designers of small cars. As a result of this large amount of clearance, dynamic deformation was very high in most central hood cases.

The relaxation zones approximated in the current study indicate that there is enough relaxation area available such that most failing vehicles would be able to pass the GTR requirements by focusing on redesign of the specific peripheral areas that produced greater than 1700 HIC. Six of the eight vehicles with failing points had no points between 1000 and 1700 outside the estimated relaxation zone. This pass rate suggests that most vehicles will require improvement to only the very stiffest structures to meet the requirements of the proposed GTR. Only the H2 and the E350 had failing impacts (>1000 HIC) that were outside the relaxation zone. These may represent vehicles in the fleet that will require more widespread design modifications. These two vehicles were the only vehicles in the study that had hoods made of a composite material, rather than steel or aluminum. Impacts to these hoods resulted in little damage or evidence of deformation, particularly in impacts around the periphery, suggesting that hood material changes may be required for these vehicles to meet the GTR in and out of the relaxation zone.

Test results indicate that many areas around the periphery of the hood present design challenges for manufacturers. Of the three vehicles that had no “failing” impacts (Table 5), the CR-V and the Passat appeared to have pedestrian countermeasures designed specifically to address these challenges as described earlier in this discussion. In contrast, the third vehicle with no failing impacts (Silverado) did not appear to have design countermeasures such as those identified on the CR-V and the Passat, or other structures that appeared to be designed specifically for pedestrians. The performance of these three vehicles shows that design problems introduced by the proposed requirements, though challenging, can be solved.

A limitation of the current study is that a relatively small sample of vehicles and points were tested. This study’s focus on larger vehicles in the US fleet also limits the conclusions that may be drawn regarding the benefit of the regulation for the entire US fleet.

## CONCLUSIONS

The results of this series of head impact tests show that design improvements would be required in order for many vehicles in the US fleet to meet the proposed pedestrian GTR. These improvements would be expected, in turn, to reduce pedestrian fatalities and injuries. An estimate of the magnitude of these benefits will require additional test data and assessment.

Based on the relaxation zones estimated for each test vehicle, three of the eleven vehicles in this test series had no failing test points. Six of the eleven vehicles tested would likely require design improvements to specific structures around the periphery of the test zone to bring HIC in these areas below 1700. Two of the vehicles are expected to require more widespread design changes to reduce HIC in the relaxation zone below 1700 and to reduce HIC outside the relaxation zone to below 1000.

Head impact performance in pedestrian GTR testing does not appear to depend on vehicle size. For example, the large Silverado was one of the best performers, while the small Wrangler was among the worst performers in this series of tests.

For the vehicles tested, the hinges and impact locations adjacent to the cowl and fender appeared to be the most challenging areas of the GTR test zone. However, the ability of several vehicles to limit the impact severity in these areas to passing levels suggests that pedestrian-friendly design is possible in these areas, even for larger vehicles.

A smaller number of vehicles showed high-severity impacts toward the front of the test zone, adjacent to the hood leading edge. These results represented unique design features that were particularly aggressive toward pedestrians. The majority of the vehicles in this test series were able to limit HIC in this area to less than 1700, in some cases without any obvious pedestrian-specific design countermeasures.

## ACKNOWLEDGEMENTS

The authors thank David Hyder and Patrick Biondillo of the Transportation Research Center Inc for their technical expertise in setting up and performing the tests.

## REFERENCES

ACEA. 2005. “Proposal for new criteria for headform impactor to bonnet tests and justification” Ninth Meeting of the Informal Group on Pedestrian Safety, Working Party on Passive Safety (GRSP), INF GR PS/158, December 2005, Geneva, Switzerland.

European Commission. 2006. “Proposal for draft amendments to draft global technical regulation on pedestrian protection.” Thirty-Ninth Meeting of the Working Party on Passive Safety (GRSP), GRSP-39-12, May 2006.

GRSP (WP.29). 2006. "Proposal for a Global Technical Regulation on Uniform Provisions Concerning the Approval of Vehicles with Regard to their Construction in Order to Improve the Protection and Mitigate the Severity of Injuries to Pedestrians and Other Vulnerable Road Users in the Event of a Collision." TRANS/WP.29/GRSP/2006/2.

JAMA. 2006. "Proposal for draft amendments to draft global technical regulation [GTR] on pedestrian safety." Thirty-Ninth Meeting of the Working Party on Passive Safety (GRSP), GRSP-39-16-rev.1, May 2006.

Lawrence, G.J.L., Hardy, B.J. and Donaldson W.M.S. 2002. "Costs and Effectiveness of the Honda Civic's Pedestrian Protection, and Benefits of the EEVC and ACEA Test Proposals." TRL Limited, Report prepared for the Vehicle Standards and Engineering Division, Department for Transport, Local Government and the Regions, PR/SE/445/02 S222C/VF.

Mizuno Y. 2005. "Summary of IHRA Pedestrian Safety WG Activities (2005) – Proposed Test Methods to Evaluate Pedestrian Protection Afforded by Passenger Cars." Proceedings of the 19<sup>th</sup> International Technical Conference on the Enhanced Safety of Vehicles (ESV), Paper No. 05-0138.

NCHS (National Center for Health Statistics). 2000. "2 to 20 years: Girls Stature-for-age and Weight-for-age percentiles" and "2 to 20 years: Boys Stature-for-age and Weight-for-age percentiles." <http://www.cdc.gov/growthcharts>.

NHTSA (National Highway Traffic Safety Administration). 1997. "Preliminary Regulatory Evaluation, Head-Impact Energy Absorbing Dynamic Systems (HEADS), Amendments to FMVSS No. 201, Upper Interior Head Protection." Office of Regulatory Analysis, Plans and Policy.

NHTSA. 2005. "Relaxation zone and GVWR application for US" Ninth Meeting of the Informal Group on Pedestrian Safety, Working Party on Passive Safety (GRSP), INF GR PS/166, December 2005, Geneva, Switzerland.

NHTSA. 2006. "Traffic Safety Facts 2005, Pedestrians." NCSA, DOT HS 810 624.

Nicaj, L., Wilt, S., and Henning, K. 2006. "Motor vehicle crash pedestrian deaths in New York City: the plight of the older pedestrian." Injury Prevention; 12(6): 414-6.

OICA. 2006a. "OICA position on keeping the size of the exemption zone in the bonnet leading edge area." Tenth Meeting of the Informal Group on Pedestrian Safety, Working Party on Passive Safety (GRSP), INF GR PS/183, January 2006, Washington DC.

OICA. 2006b. "Headform Tests Data" Tenth Meeting of the Informal Group on Pedestrian Safety, Working Party on Passive Safety (GRSP), INF GR PS/176, January 2006, Washington DC.

OICA. 2006c. "OICA comments on document GRSP/2006/7 presented by the USA." Thirty-Ninth Meeting of the Working Party on Passive Safety (GRSP), GRSP-39-5, May 2006.

Peden, M. et al., eds. 2004. "World Report on Road Traffic Injury Prevention." World Health Organization.

# PEDESTRIAN KINEMATICS INVESTIGATION WITH FINITE ELEMENT DUMMY MODELS BASED ON ANTHROPOMETRY SCALING METHOD

**Costin Untaroiu**

**Jaeho Shin**

**Johan Ivarsson**

**Jeff Crandall**

Center of Applied Biomechanics, University of Virginia,  
United States

**Yukou Takahashi**

**Akihiko Akiyama**

**Yuji Kikuchi**

Honda R&D Co., Ltd.

Japan

Paper Number 07-0328

## ABSTRACT

Pedestrian-vehicle impact experiments using cadavers have shown that factors such as vehicle shape and pedestrian anthropometry can influence pedestrian kinematics and injury mechanisms. While a parametric study examining these factors could elucidate the complex relationships that govern pedestrian kinematics, it would be impractical with cadaver tests due to the relative expense involved in performing numerous experiments on subjects with varying anthropometry. On the other hand, finite element (FE) modeling represents a more feasible approach since numerous experiments can be conducted for a fraction of the expense. The current study examined the relationship between pedestrian anthropometry and front shape of a mid-size sedan using a PAM-CRASH model of the 50th percentile male (50th) Polar-II pedestrian dummy extensively validated against experimental data. In order to evaluate the influence of pedestrian anthropometry on response kinematics, scaled dummy models were developed based on the weight and height of the 5th percentile female (5<sup>th</sup> F) and 95th percentile male (95<sup>th</sup> M). Simulations of the 5<sup>th</sup> F, 50<sup>th</sup> F, 50<sup>th</sup> M, and 95th Polar-II FE models struck at 40 km/h by a mid-size sedan were used to generate trajectories of the head, upper thorax, mid-thorax, and pelvis. In an effort to assess the validity of scaling techniques when interpreting trajectory data from vehicle-pedestrian crashes, the trajectories of the 5<sup>th</sup> F, 50<sup>th</sup> F and 95<sup>th</sup> M model were scaled to the 50<sup>th</sup> M and compared to those generated with the 50th model. The results demonstrated nonlinear behavior of dummy kinematics that could not be accounted for with traditional linear scaling techniques.

## INTRODUCTION

The pedestrian is one of the most vulnerable road users and comprise about 65 percent of the 1.17 million annual traffic related fatalities in the world (World Bank, 2007). The probability for a pedestrian to be injured or killed is much higher than that for a vehicle occupant. In 2005, 8.7% of vehicle-pedestrian impacts in the US were fatal, whereas the corresponding fatality rate for occupants in crashes only was 1.3% (NHTSA, 2007).

Protection of pedestrians in car-to-pedestrian collisions (CPC) has recently generated increased attention with regulations implemented or proposed in Europe (EEVC, 2002), Korea (Youn et al., 2005), and Japan. While subsystem experiments are currently being used as the basis of evaluations for these regulations, car-to-pedestrian dummy impact tests or car-to-human/dummy impact simulations provide complimentary data that better describe the complete vehicle-pedestrian interaction.

An advanced pedestrian dummy, called Polar-II, has been developed and continuously improved by Honda R&D, GESAC, and the Japan Automobile Research Institute (JARI) (Akiyama et al., 1999, 2001; Okamoto et al., 2001, Takahashi et al., 2005, Crandall et al., 2005). While the dummy incorporates advanced instrumentation in the head, neck, chest, pelvis, and lower limbs (Akiyama et al. 2001), the primary purpose of the Polar-II dummy was reproducing pedestrian kinematics in a collision with a vehicle. Kerrigan et al. (2005a, b) performed vehicle impact tests on the Polar-II and post mortem human surrogates (PMHS) in identical conditions and showed that the Polar-II dummy generally replicates the complex kinematics of the PMHS. However, the

Polar-II dummy has the general characteristics of the 50<sup>th</sup> percentile male and can therefore not predict kinematics for all statures of pedestrians.

A FE model of the Polar-II dummy has been developed, validated in component tests (Shin et al. 2006), and verified at the full scale level against kinematic data (Shin et al. 2006, 2007) recorded during the vehicle-dummy impact experiments performed by Kerrigan et al. (2005). The Polar-II FE model was developed using Hypermesh (Altair Engineering) and Generis (ESI) as pre-processors and PAM-CRASH/PAM-SAFE FE solver (version 2001, ESI) was used for impact simulations. The model contains 27,880 elements that represent the head, neck, thorax, abdomen, pelvis, upper arms, forearms, hands, thighs, knees, legs, and feet and has a total mass and height close to that of the 50<sup>th</sup> percentile male.

It is believed that pedestrian kinematics is highly influenced by vehicle geometry and pedestrian anthropometry (Mizuno, 2005). While the dependence of pedestrian kinematics on vehicle geometry has been previously shown (Kerrigan et al 2005 a, b), there have been few studies presenting the influence of the pedestrian adult anthropometry (Shin et al 2007). Thus vehicle-pedestrian simulations were performed with a mid-size sedan vehicle model and a family of dummies corresponding to peaks and extremes of the adult population (Figures 1 and 2), and the trajectories of several upper body locations were calculated. Additionally, a traditional height scaling technique of PMHS trajectories to those corresponding to the 50<sup>th</sup> percentile male has been evaluated using the kinematic response of scaled dummies.

## METHODOLOGY

### Pedestrian Anthropometric Data

The development of pedestrian dummies requires the anthropometric data of subjects in standing posture. Most anthropometric data have been gathered for subjects in a typical semi-reclined seated posture for design of occupant dummies (e.g. Schneider et al. 1985, Seidl 1997). A few studies (e.g. Gordon et al. 1998, Anthropometric Source Book 1978) also considered anthropometric characteristics of the standing posture. The Anthropometric Survey (ANSUR) of U.S. Army Personnel conducted during the two-year period from 1987 to 1988 (Gordon et al. 1989) includes over 132 anthropometric measurements collected for 9,000 subjects in standing and sitting postures. This database showed symmetric distributions of height and mass around average values, those considered to

correspond to the 50<sup>th</sup> percentile of anthropometric subjects (Figures 1 and 2). To study the influence of anthropometry on pedestrian kinematics in lateral car-to-pedestrian impacts, four dummy models were created:

- a 50<sup>th</sup> M and a 50<sup>th</sup> F which represent the adult population peaks
- a 5<sup>th</sup> F and a 95<sup>th</sup> M which represent extreme subjects of the adult population

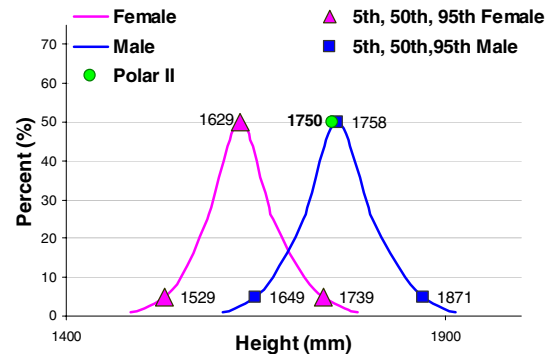


Figure 1: Height Distribution

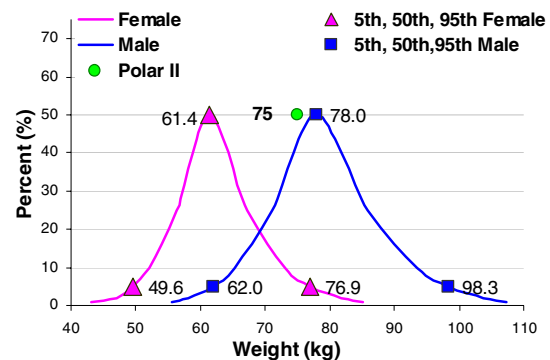


Figure 2: Weight Distribution

The Polar-II FE model (Shin et al 2006) was used to represent the 50<sup>th</sup> percentile male because it closely approximated the anthropometric characteristics (Figures 1 and 2). The other three models were derived by scaling this model according to the methodology presented in the next section.

### Scaling of the Polar-II FE Model

#### Scaling of Dummy Geometry

A preliminary study of the ANSUR anthropometric data revealed non-proportional variations in all anatomical directions of body measurements for all anthropometric subjects under study (5<sup>th</sup> F, 50<sup>th</sup> F, 50<sup>th</sup> M, and 95<sup>th</sup> M) which make scaling a challenging task. For the purpose of the

current study, we selected mass and height as the most important anthropometric characteristics to match with the corresponding data of ANSUR subjects. Therefore, the scaling of each model was performed in two steps:

- scaling in vertical direction (z-axis) – to match the stature(height)

$$\lambda_{z,subject} = \frac{H_{subject}}{H_{Polar-II}} \quad (1)$$

- scaling in the transverse plane (x-y plane) – to match the total mass

$$\lambda_{x,subject} = \lambda_{y,subject} = \sqrt{\frac{m_{subject}}{m_{Polar-II} \lambda_{z,subject}}} \quad (2)$$

To verify the scaled dummy models obtained according to this methodology: 5<sup>th</sup> percentile female (5F-S), 50<sup>th</sup> percentile female (50F-S), and 95<sup>th</sup> percentile male (95M-S), several specific anthropometric dimensions of the scaled models and the Polar-II model were compared with the corresponding data of the ANSUR subjects. These specific dimensions in all anatomical directions (Figure 3) are: cervical height (1), iliacristale height (2), vertical thumbtip reach down (3), knee height (4), menton-top of head (5), head breadth (6), bideltoid breadth (7), waist breadth (8), chest depth (9), and buttock depth (10).

### Scaling of Inertial Properties

The components of the Polar-II model can be classified as either deformable or rigid parts. Using the mass densities of each component, that was assumed constant between the Polar-II FE model and scaled dummy models, the inertial properties (mass and the components of the inertia tensor) of the deformable parts were calculated from their meshes. The inertial properties of rigid bodies, which usually have simplified meshes, were defined in the input file of the model based on measurement data. As a consequence, an algorithm for obtaining the mass and components of the inertia tensor relative to new centers of gravity of scaled rigid models was developed (see Appendix) and applied for all scaled dummy models. The same factors used to scale the dummy geometry were also used to scale inertia properties of rigid parts.

### Scaling of Joint Properties

Several components of the dummy are connected by defined joint models for which the joint stiffness is characterized by a moment-angle curve. Based on the principles of dimensional analysis (Langhaar, 1951), the moment of a scaled entity can

be expressed as a function of the length scale factors (Ivarsson et al. 2004):

$$M_{scaled} = \lambda_x \lambda_y \lambda_z M_{Polar-II} \quad (3)$$

As a result, all moment-angle curves of the scaled dummy models were scaled using this equation.

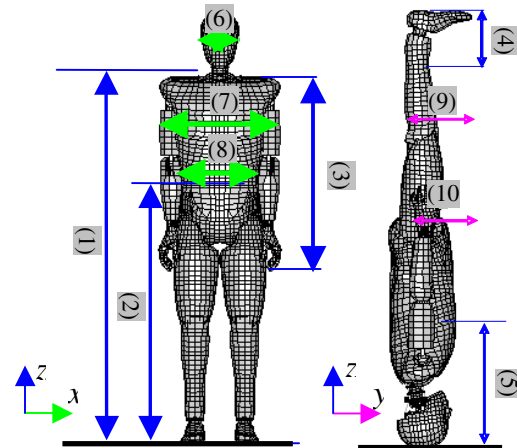


**Figure 3:** Anthropometric dimensions used to compare scaled dummy models with corresponding ANSUR data (Gordon et al. 1989)

### Vehicle-Pedestrian Simulations

Four full-scale pedestrian impact simulations were performed using the Polar-II dummy model and scaled dummy models. The methodology used to perform these simulations was similar to that used in previous verification studies presented by Shin et al. (2006, 2007). The Polar-II dummy model was positioned laterally at the vehicle-centerline in a mid-stance gait with the left lower extremity in the leading position and the right lower extremity closest to the vehicle (a mid-size sedan). To promote repeatability and reduce test-to-test variability, the upper extremities were bound at the wrist with the left wrist closer to the abdomen. A plane simulating the ground level was specified and a pre-impact preload was applied just before impact through an initial feet-ground penetration corresponding to the dummy weight. The front-end of the vehicle model included all exterior structures that could contact the dummy as well as the stiff underlying structures (e.g., engine components) that could be loaded by the exterior vehicle structures during the impact. The mass of the simplified vehicle model was adjusted to the mass of the vehicle sled buck by adding the mass differential to the vehicle CG. A 40 km/h initial velocity in the impact direction (towards the pedestrian) was applied to the vehicle model at the beginning of the simulations. Kinematic trajectories of the head center of gravity (CG), T1

(i.e., top of thoracic spine), T8 (i.e., mid-thoracic spine) and pelvis CG (locations of the photo targets used in the full scale PMHS tests by Kerrigan et al., 2005 a, b) were calculated to allow for comparison with body segment trajectories of four different dummy models (Figure 4). Additionally, the wrap around distance (WAD) to head contact was calculated in all simulations.

To provide a basis for validation of the pedestrian dummy against the PMHS data, the PMHS kinematic response was linearly scaled to the 50<sup>th</sup> percentile male's response using a length scale factor. Thus, the original PMHS trajectories for  $x(t)$  and  $z(t)$  together with time were scaled using the height ratio of the PHMS relative to the 50<sup>th</sup> percentile male (Kerrigan et al. 2005 a, b). In order to verify the validity of this method, all trajectories of the dummy models (5F-S, 50F-S, and 95M-S) were scaled to Polar-II (50<sup>th</sup> percentile male model) data using the same methodology. The percentage error between scaled trajectories and the corresponding Polar-II trajectories were calculated according to (4).

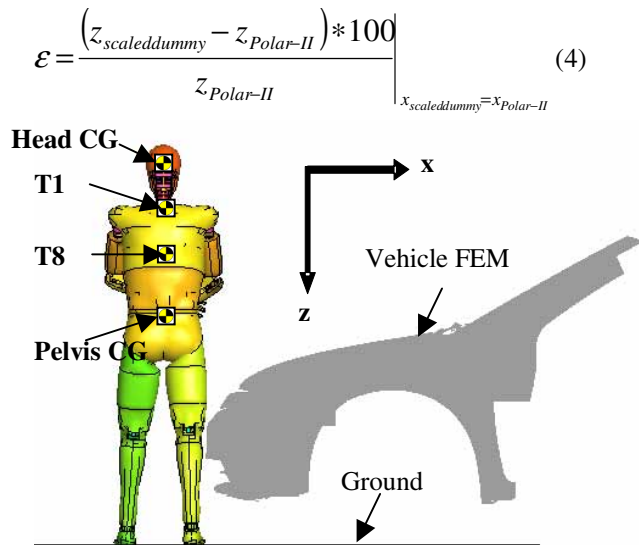


**Figure 4:** Node set of the pedestrian dummy model used in the kinematics analysis.

## RESULTS

### Polar-II Scaled Dummy Models

Three new dummy FE models -5F-S, 50F-S, and 95M-S (Figure 5)- were obtained by scaling the Polar-II model with the factors calculated using equations 1 and 2 and listed in Table 1. While the scaling of 5<sup>th</sup> and 50<sup>th</sup> percentile female dummy models involved almost uniform scaling (under 1 %

variation between  $\lambda_z$  and  $\lambda_x=\lambda_y$  scaling factors), a substantial variation (3.4 %) was observed between scaling factors in the x-y plane and the z-direction of the 95<sup>th</sup> percentile male model.

The specific body measurements (Figure 3) of each dummy model exhibit good agreement with the corresponding data of the ANSUR subjects. Polar-II dimensions are similar ( $\pm 2\%$ ) in all directions with the corresponding dimensions of the ANSUR 50<sup>th</sup> percentile male. While specific dimensions of the scaled dummy models in the z-direction (Figure 6) are close to corresponding values of the ANSUR subjects ( $\pm 2\%$ ), several variations ( $\pm 6\%$ ) in the x-y plane were recorded (Figure 7). All scaled dummy models have the same height and mass as their corresponding ANSUR subjects (5<sup>th</sup> female, 50<sup>th</sup> female and 95<sup>th</sup> male).

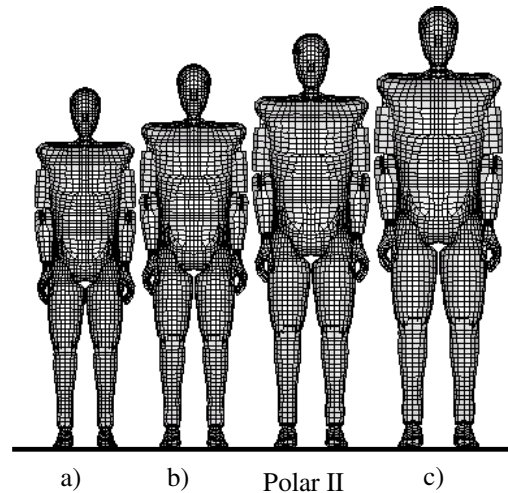


**Figure 5:** Polar II FE model and its scaled models: 5<sup>th</sup> female (5F-S) (a), 50<sup>th</sup> female (50F-S) (b), and 95<sup>th</sup> male (95M-S) (c).

**Table 1.** The factors used to obtain dummy FE models by scaling the Polar-II FE model (50<sup>th</sup> percentile male)

| Dummy Model                        | Scale Factors |                       |
|------------------------------------|---------------|-----------------------|
|                                    | $\lambda_z$   | $\lambda_x=\lambda_y$ |
| 5 <sup>th</sup> percentile female  | 0.873         | 0.871                 |
| 50 <sup>th</sup> percentile female | 0.93          | 0.938                 |
| 95 <sup>th</sup> percentile male   | 1.069         | 1.107                 |

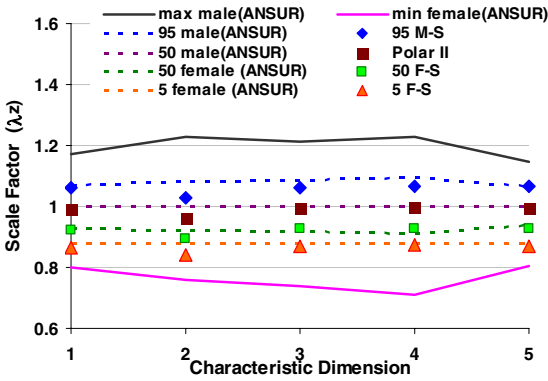


**Figure 6:** Specific dimensions (vertical direction) normalized to corresponding dimensions of the 50<sup>th</sup> percentile ANSUR male (Gordon et al. 1989). Comparison between Polar-II scaled models and ANSUR data

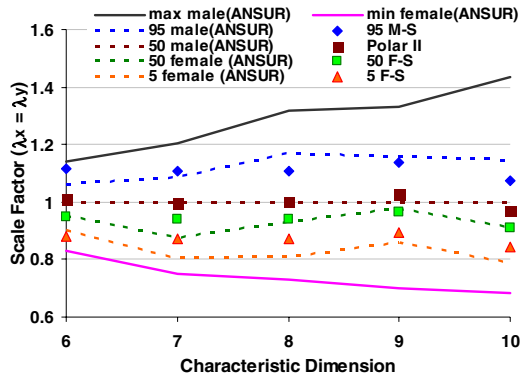


**Figure 7:** Specific dimensions (transversal plane) normalized to corresponding dimensions of the 50<sup>th</sup> percentile ANSUR male (Gordon et al. 1989). Comparison between Polar-II scaled models and ANSUR data

### Vehicle-Dummy Lateral Impact Simulations

Dummy posture relative to the vehicle at the time of head impact for the original Polar-II (50<sup>th</sup> male) dummy and the scaled dummy models are illustrated in Figure 8. In all cases, the car-pedestrian dummy head impacts occurred in the windshield region, except for the 5<sup>th</sup> female dummy model for which the vehicle-head impact took place in the cowl region. The Polar-II 50<sup>th</sup> male WAD to head contact obtained from the simulation (1959 mm) was within the range of Polar-II experimental test data (1947 ±21 mm) suggesting good kinematic predictability of the FE dummy model (Figure 9). A linear variation of WAD to head contact with respect to dummy height was observed in both simulations using FE dummy models ( $R^2=0.996$ ) and PMHS tests ( $R^2=0.899$ )

(Kerrigan et al. 2005a). However, the dummy WAD obtained from simulations and Polar-II test data (Kerrigan et al., 2005) were lower than that of the corresponding value of the PMHS data (Figure 9).

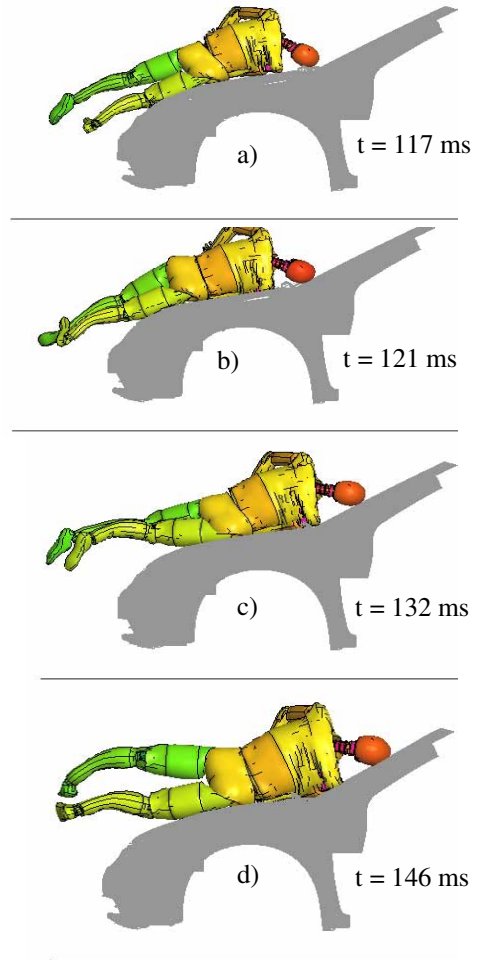


**Figure 8:** 5F-S (a), 50F-S (b) Polar-II (50<sup>th</sup> percentile male) (c), and 95M-S dummy models at the pedestrian head strike time.

Kinematic trajectories of the head CG, T1, T8 and pelvis CG together with their trajectory corridor (area bordered by the extreme trajectories) are illustrated in Figures 10, 11, 12, and 13. All trajectory curves were calculated until head strike in a system fixed with respect to the vehicle's motion, which was called the Vehicle Coordinate System (VCS). The origin of the VCS system is defined by the intersection of the vertical line (z-axis) passing through the initial position of the dummy head CG and the horizontal line (x-axis) of the ground level (Kerrigan et al. 2005). A linear variation of upper body trajectories are observed between the time the bumper strikes the legs and the time the dummy pelvis flesh starts to interact with the leading edge of

the hood. However, after that point, a strong non-linearity was observed in all pelvis CG trajectories. Kerrigan et al. (2007) have indicated that this may be a function of the pelvis sliding over, penetrating into, or bouncing off the hood depending on the extent of pelvic interaction with the leading edge of the vehicle. The largest pelvis bounce was observed in the 5F-S dummy model for which some of the upper body trajectories (pelvis CG, T1, and T8) were closer or even slightly higher than the corresponding trajectories of a taller dummy model – 50 F-S dummy.

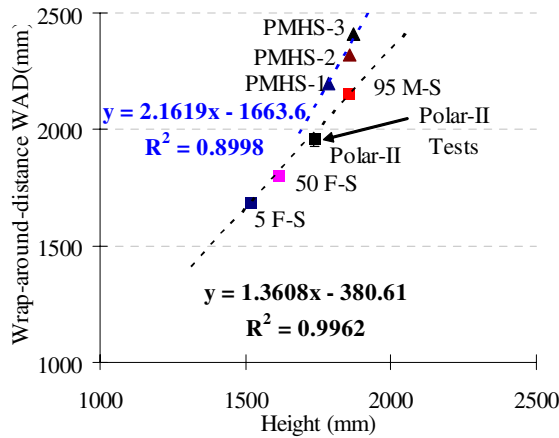


**Figure 9:** WAD to head contact vs. height curves. Comparison between Polar-II and dummy results and PMHS data (Kerrigan et al 2005a)

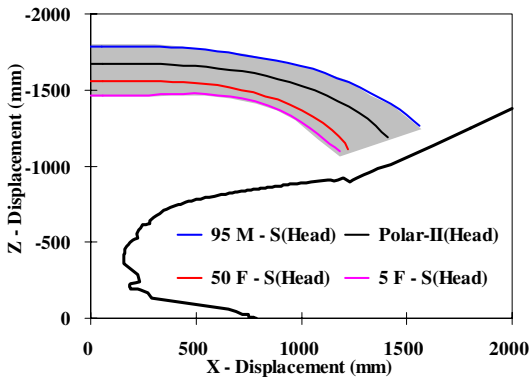


**Figure 10:** Head- Center of gravity (CG) trajectory corridor and comparisons between the Polar-II and scaled dummy models

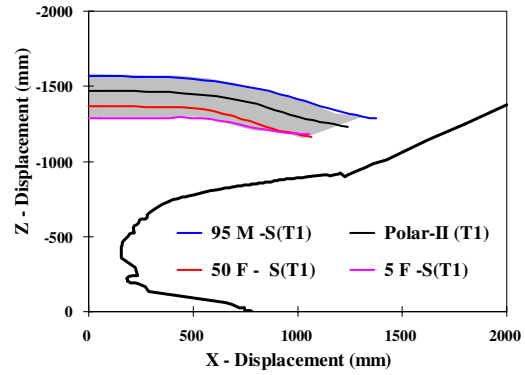


**Figure 11:** T1 trajectory corridor and comparisons between the Polar-II and scaled dummy models

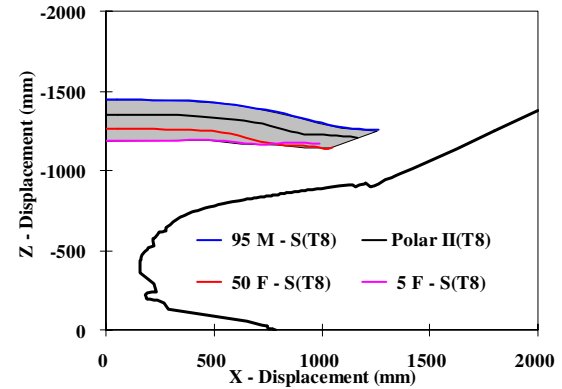


**Figure 12:** T8 trajectory corridor and comparisons between the Polar-II and scaled dummy models

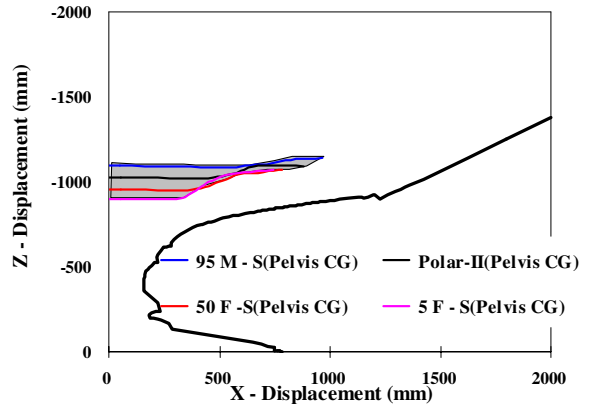


**Figure 13:** Pelvis CG trajectory corridor and comparisons between the Polar-II and scaled dummy models

Upper body trajectories of the 5 F-S, 50 F-S and 95 M-S scaled to the corresponding data of

Polar-II (50<sup>th</sup> percentile male) are illustrated in Figures 14 and 15. These scaled curves have two portions delimited by specific events: 1) after bumper-leg contact but before pelvis flesh-leading edge contact and 2) after pelvis flesh-leading edge contact but before head strike. As expected, in the first part, scaled trajectories matched very well the corresponding trajectories of the Polar-II (50<sup>th</sup> percentile male). However, significant differences between scaled trajectories and corresponding 50<sup>th</sup> percentile trajectories appear in the second region, especially close to the time of head strike. The maximum error between these trajectories calculated as the percentage difference between vertical displacements at the same horizontal level are illustrated in Figure 16. As can be observed, the scaled trajectories of the 5F – S dummy overestimate the corresponding Polar-II trajectories for all recorded upper body segments, with the error decreasing from pelvis to head region. A similar trend is also observed for scaled trajectories of the other dummy that is smaller than the Polar-II (50F-S). However, while the pelvis CG/T8 scaled trajectories overestimate the corresponding Polar-II (50<sup>th</sup> male) trajectories, T1/head CG scaled trajectories underestimate the corresponding Polar-II trajectories. In case of the largest dummy- 95M-S, the maximum error of upper body scaled trajectories shows an opposite trend. While the pelvis CG, T8, and T1 underestimate the corresponding 50<sup>th</sup> male trajectories, an overestimation is recorded in scaled trajectory of the head CG. Overall, the maximum error of all scaled trajectories varies from -12 % (50<sup>th</sup> female head CG) to +11.6% (5<sup>th</sup> female pelvis CG).

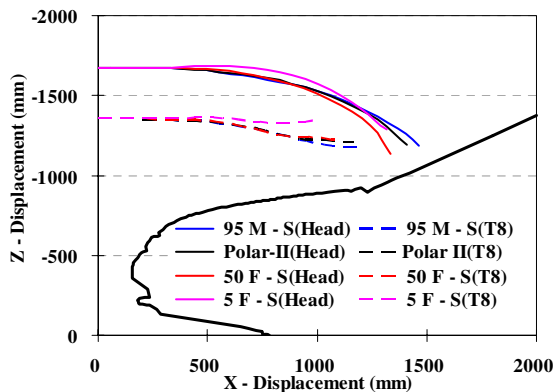


**Figure 14:** Scaled Head CG and T8 trajectory comparisons between the Polar-II and scaled dummy models

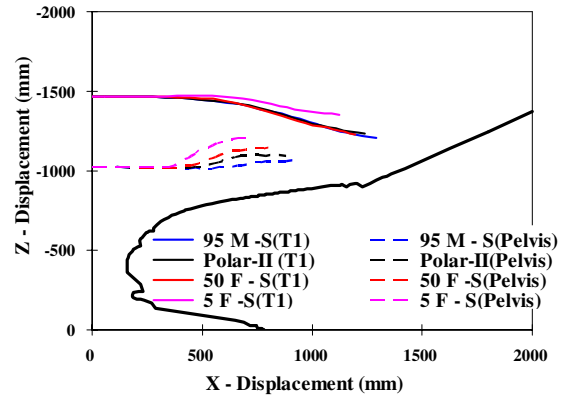


**Figure 15:** T1 and pelvis CG trajectory comparisons between the Polar-II and scaled dummy models

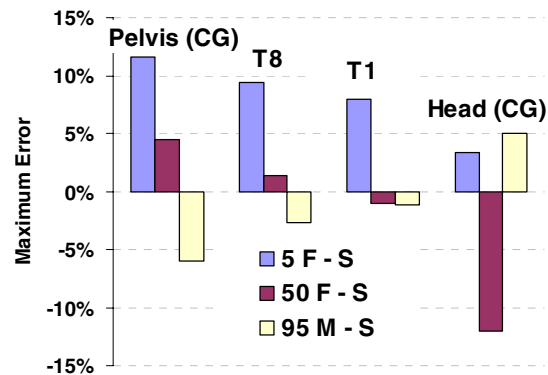


**Figure 16.** The maximum error (%) of the scaled pedestrian trajectories

## DISCUSSION

Three new FE pedestrian dummy models were obtained using the validated FE Polar-II dummy model as reference (Shin et al. 2006, 2007). Uniform scaling in the vertical direction and transverse plane was used to obtain FE dummy models corresponding to three representative ANSUR subjects (5<sup>th</sup> female, 50<sup>th</sup> female, and 95<sup>th</sup> male). While several differences between specific dimensions of scaled models and anthropometric data (maximum 7% in transversal plane) were observed, global dummy characteristics (height and mass), which may have a major role in pedestrian kinematics during a vehicle impact, were matched by this scaling technique. In addition, specific vertical dimensions of scaled dummies, which may have a significant influence on the vehicle-pedestrian interaction due to joint positions, showed minor differences (under 2%)

relative to anthropometric data. The scaling method used in the current study to obtain new dummy models with different anthropometry from a reference model shows easy implementation and relatively good results. While differences between all specific dimensions of dummy and anthropometric data may be reduced by using more complex scaling techniques (c.f., Kriging method used for scaling a pelvis FE model by Besnault et al., 1998) with specific scaling factors for each body segments, the effort to connect scaled body parts into the whole dummy scaled model will increase considerably. Due to lack of test data between joint properties and anthropometry, joint stiffness properties of the new dummy models were obtained by scaling Polar-II stiffness curves (Langhaar, 1951). Therefore, when this data will be available in literature, an update of joint stiffness curves for all scaled models is recommended.

A complex variation of pedestrian upper body trajectories was observed in simulations of vehicle-pedestrian lateral impacts with different sized dummies and the same vehicle model having a 40km/h initial velocity. Dummy trajectory corridors, defined as the surface which covers all dummy trajectories, are uniform during the initial phase of impact but demonstrate different behavior after pelvic interaction with the hood leading edge and before head strike. While the pelvis CG corridor narrows after the pelvis flesh starts to interact with leading edge, a significant extension of the head CG corridor is recorded for the same period. Trajectory corridors with almost constant widths are recorded for T1 and T8 trajectory corridors before head strike event

In dummy simulations as in PMHS tests (Kerrigan et al. 2005) linear relationships were observed between WAD and pedestrian height. However, the dummy models predict lower WADs than the PMHS tests. A potential cause of these kinematic differences between dummies and PMHSs could be the musculature effects in the neck, spine and chest which have been incorporated in the dummy models (Crandall et al., 2005).

Linear scaling of dummy upper body trajectories to the corresponding responses of the 50<sup>th</sup> male with respect to dummy height showed important limitations. A consistent error pattern in terms of vertical displacement for a certain horizontal displacement was identified between the scaled dummy trajectories based on dummy size and the location of recorded targets. The scaled trajectories of smaller dummies tended to overestimate the corresponding response of the 50<sup>th</sup> male model in regions close to pelvis and to underestimate (or in the case of the 5<sup>th</sup> female, to overestimate) the regions

close to the head. The opposite pattern was observed for the taller dummy model (95<sup>th</sup> male). While the current study is limited to only one vehicle type, one vehicle speed, and one pedestrian orientation, these observations suggest that the linear scaling of upper body trajectories must be used cautiously with an awareness of the inherent assumptions and limitations. Ultimately, the results suggest that an advanced non-linear approach must be developed to predict the correct kinematics. Alternatively, a complete family of physical and/or computational dummy models will be required to describe the complexity of the pedestrian-vehicle interaction as a function of their relative geometry.

## CONCLUSIONS

Three finite element dummy models of different anthropometry were obtained by scaling the Polar-II dummy – a pedestrian dummy previously validated in pedestrian impact conditions. All dummy models, which were intended to represent the anthropometric breadth of the general adult population, have similar mass and height characteristics as equivalent subjects obtained from an anthropometric database. In addition to stature and mass, several specific body measurements also showed agreement with the corresponding anthropometric data. The dummy models were used to study the influence of pedestrian anthropometry on kinematic responses in vehicle-pedestrian impact simulations. While the WAD to head contact demonstrated a linear relationship with the dummy height, upper body trajectories appeared to be influenced by the target location and dummy size. Thus linear scaling of PMHS trajectories to the corresponding 50<sup>th</sup> percentile male trajectories has potentially significant limitations in terms of reproducing the correct kinematics.

## REFERENCES

- [1] Akiyama A., Yoshida S., Matsushashi T., Moss S., Salloum M., Ishikawa H., Konosu A. (1999) Development of Human-like Pedestrian Dummy, Paper 9934546, Japanese Society of Automotive Engineers, Chiyoda-Ku, Tokyo, Japan.
- [2] Akiyama A., Okamoto M., N. Rangarajan (2001) Development and Application of the New Pedestrian Dummy, Paper 463, Proceedings of the 17<sup>th</sup> International Technical Conference on the Enhanced Safety of Vehicles (ESV), Amsterdam, The Netherlands.

[3] Besnault B., Guillemot H., Robin S., Lavaste F., Le Coz J.Y. (1998) A parametric finite element model of the human pelvis. 42nd Stapp Car Crash Conference. 1998.

[4] Crandall J., Wiley K., Longhitano D., Akiyama A. (2005) Development of Performance Specifications for a Pedestrian Research Dummy, Paper 05-0389, Proceedings of the 19<sup>th</sup> International Technical Conference on the Enhanced Safety of Vehicles (ESV), Washington DC, United States.

[5] European Enhanced Vehicle-Safety Committee, EEVC Working Group 17 Report—Improved Test Methods to Evaluate Pedestrian Protection Afforded by Passenger Cars, [www.eevc.org](http://www.eevc.org), (December 1998 with September 2002 updates).

[6] Gordon, C.C., Churchill, T., Clauser, C.E., Bradtmiller, B., McConville, J.T., Tebbetts, I., Walker, R.A. (1989). 1988 Anthropometric Survey of U.S. Army Personnel: Methods and Summary Statistics. Final Report (NATICK/TR-89/027) U.S. Army Natick Research Development and Engineering Center, Natick, Massachusetts.

[7] Ivarsson B.J., Crandall J., Longhitano D., Okamoto M. (2004) Lateral Injury Criteria for the 6-year-old Pedestrian – Part I: Criteria for the Head, Thorax, Neck, Thotax, Abdomen and Pelvis, Paper 2004-01-0323, Society of Automotive Engineers.

[8] Kerrigan J., Murphy D., Drinkwater C., Kam C. Y., Bose D., Crandall J. (2005a) Kinematic Corridors for PMHS Tested in Full-Scale Pedestrian Impact Tests, Paper 05-0394, Proceedings of the 19<sup>th</sup> International Technical Conference on the Enhanced Safety of Vehicles (ESV), Washington DC, United States.

[9] Kerrigan J., Kam C., Drinkwater C., Murphy D., Bose D., Ivarsson J., Crandall J. (2005b) Kinematic Comparison of the Polar-II and PMHS in Pedestrian Impact Tests with a Sport-Utility Vehicle, Proceedings of the 2005 International Research Council on the Biomechanics of Impact (IRCOBI), Prague, Czech Republic.

[10] Kerrigan J., Crandall J., Deng B. (2007) Pedestrian Kinematic Response to Mid-sized Vehicle Impact, International Journal of Vehicle Safety, in press

[11] Langhaar, H. L. (1951) Dimensional Analysis and Theory of Models. John Wiley & Sons, Inc., New York.

[12] Mizuno Y. (2005) Summary of IHRA pedestrian Safety WG Activities (2005) – Proposed Test Methods to Evaluate Pedestrian Protection Affordable by Passenger Cars

[13] NASA. Anthropometric Sourcebook (1978). NASA Reference Publication No. 1024, Houston TX

[14] National Highway Traffic Safety Administration (NHTSA), (2007) <http://www-nrd.nhtsa.dot.gov/Pubs/overviewtsf05.pdf>

[15] Okamoto Y., Akiyama A., Okamoto M., Kikuchi Y. (2001) A Study of the Upper Leg Component Tests Compared with Pedestrian Dummy Tests, Paper 380, Proceedings of the 17<sup>th</sup> International Technical Conference on the Enhanced Safety of Vehicles (ESV), Amsterdam, The Netherlands.

[16] Pam System International, (2004) PAM-CRASH / PAM-SAFE REFERENCE MANUAL, Version 2004.

[17] Seidl, A., ‘RAMSIS – A New CAD Tool for Ergonomic Analysis of Vehicles Developed for the German Automotive Industry’. Tecmath GmbH, SAE Paper 970088.

[18] Schneider, L.W., Robbins, D.H., Pflüg, M.A., and Snyder, R.G., (1985) ‘Development of an Anthropometrically based Design Specifications for an Advanced Adult Anthropomorphic Dummy Family’. Volumes 1-3, Final Report DOT-HS-806-715. National Highway Traffic Safety Administration U.S. Department of Transportation, Washington D.C.

[19] Shin J., Lee S., Kerrigan J., Darvish K., Crandall J., Akiyama A., Takahashi Y., Okamoto M., Kikuchi Y. (2006) Development and Validation of a Finite Element Model for the Polar-II Upper Body, Paper 2006-01-0684, Society of Automotive Engineers.

[20] Shin J., Untaroiu C., Kerrigan J., Crandall J., Subit D., Takahashi Y., Akiyama A., Kikuchi Y., Longitano D. (2007) Investigating Pedestrian Kinematics with the Polar-II Finite Element Model, Paper 2007-01-0756 Society of Automotive Engineers.

[21] Takahashi Y., Kikuchi Y., Okamoto M., Akiyama A., Ivarsson J., Bose D., Subit D., Shin J., Crandall J. (2005) Biofidelity Evaluation for the Knee and Leg of the Polar Pedestrian Dummy, Paper 05-0280, Proceedings of the 19<sup>th</sup> International Technical Conference on the Enhanced Safety of Vehicles (ESV), Washington DC, United States.

[22] Youn Y., Kim S., Oh C., Shin M., Lee C. (2005) Research and Rule-Making Activities on Pedestrian Protection in Korea, Paper 05-0117, Proceedings of the 19<sup>th</sup> International Technical Conference on the Enhanced Safety of Vehicles (ESV), Washington DC, United States.

[23] World Bank Group: Road Safety, (2007). <http://www.worldbank.org/html/fpd/transport/roads/safety.htm> (accessed February 6 2007).

## APPENDIX

### Scaling of Rigid Parts

A rigid part is usually defined in a FE model by its mass  $m$  and the components of the mass moment of inertia tensor  $I$  with respect to a local coordinate system with the origin at the rigid body center of gravity (CG). To find a relationship between the inertial properties of a rigid body obtained by scaling and its initial inertial properties (in original configuration) the following theorem will be used.

#### Theorem

Assume a rigid body with the mass  $m$  and the mass moment of inertia tensor  $I$  with respect to a local coordinate system  $oxyz$  (the direction of the local axes parallel to the global axes), and  $o(x,y,z)$  – the center of gravity (Figure A1).

(A.1)

Assume a linear transformation (scaling) with respect to the global coordinate system  $O_1x_1y_1z_1$  with scale factors  $\lambda_x, \lambda_y, \lambda_z$  and a constant mass density between models. Thus, the mass of the scaled model will be:

$$M = m\lambda_x\lambda_y\lambda_z \quad (A.2)$$

and the components of the inertia tensor with respect to the new local coordinate system  $O(\lambda_x x_o, \lambda_y y_o, \lambda_z z_o)$  will be:

$$I_{xx} = \lambda_x\lambda_y\lambda_z(\lambda_y^2 J_y + \lambda_z^2 J_z) \quad (A.3)$$

$$I_{yy} = \lambda_x\lambda_y\lambda_z(\lambda_x^2 J_x + \lambda_z^2 J_z)$$

$$I_{zz} = \lambda_x\lambda_y\lambda_z(\lambda_x^2 J_x + \lambda_y^2 J_y)$$

(A.4)

where

$$I_{xy} = \lambda_x^2\lambda_y^2\lambda_z I_{xy}$$

$$I_{xz} = \lambda_x^2\lambda_y\lambda_z^2 I_{xz}$$

$$J_x = (I_{yy} + I_{zz} - I_{xx})/2$$

$$J_y = (I_{zz} + I_{xx} - I_{yy})/2 \quad (A.5)$$

$$J_z = (I_{yy} + I_{xx} - I_{zz})/2$$

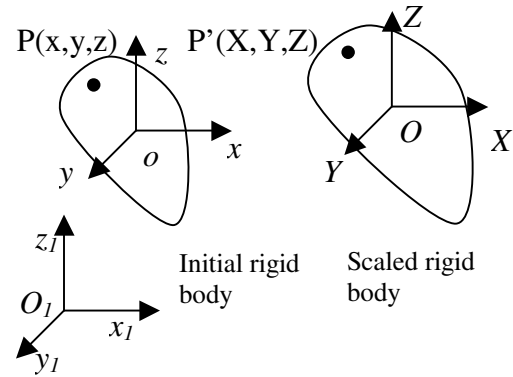


**Figure A1:** Rigid body in initial and scaled configurations; A particular case - the axes of local system are parallel to those of the global system.

#### Proof

Linear scaling (transformation) with respect to the global system  $O_1x_1y_1z_1$  will move each point  $P$  of the original body ( $\Omega$ ) which has a coordinate  $(x,y,z)$  with respect to the system  $oxyz$  and coordinate  $(x_1,y_1,z_1)$  with respect to the system  $O_1x_1y_1z_1$  into the point  $P'$  of scaled body ( $\Omega'$ ) which has coordinate  $(X,Y,Z)$  with respect to the system  $OXYZ$  and coordinate  $(X_1,Y_1,Z_1)$  with respect to the system  $O_1x_1y_1z_1$  (Figure A1).

$$X_1 = \lambda_x x_1 = \lambda_x x + \lambda_x x_{o1} = \lambda_x x + x_o$$

$$\text{Thus, } X = \lambda_x x$$

Similarly it can be shown that

$$Y = \lambda_y y \quad Z = \lambda_z z$$

Thus, the scaled diagonal components of inertia tensor will be:

$$I_{xx} = \int_{\Omega'} (Y^2 + Z^2) \rho dV = \int_{\Omega} (\lambda_y^2 y^2 + \lambda_z^2 z^2) \rho \lambda_x \lambda_y \lambda_z dv$$

$$= \lambda_x \lambda_y \lambda_z (\lambda_y^2 J_y + \lambda_z^2 J_z)$$

Similar it can be shown that

$$I_{yy} = \lambda_x \lambda_y \lambda_z (\lambda_x^2 J_x + \lambda_z^2 J_z)$$

$$I_{zz} = \lambda_x \lambda_y \lambda_z (\lambda_x^2 J_x + \lambda_y^2 J_y)$$

The scaled off-diagonal components of inertia tensor will be

$$I_{xy} = \int_{\Omega'} YZ \rho dV = \int_{\Omega} \lambda_x \lambda_y xy \rho \lambda_x \lambda_y \lambda_z dv$$

$$= \lambda_x^2 \lambda_y^2 \lambda_z J_{xy}$$

Similarly it can be shown that

When the axes of the local coordinate system are not parallel to corresponding axes of the global system (Figure A2), the components of mass inertia tensor in the new local system of a scaled rigid body OXYZ can be determined by according to the following procedure:

1. Obtain the inertia tensor  $i'$  with respect to a system  $ox'y'z'$  with axes parallel to the global coordinate system  $O_1x_1y_1z_1$  from the mass inertia tensor  $i$  from the initial coordinate system  $oxyz$ .

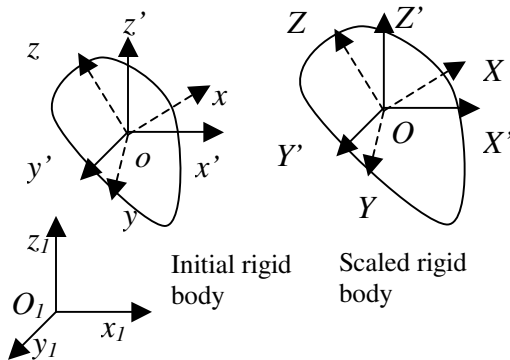


**Figure A2:** Rigid body in initial and scaled configurations; general case

The inertia tensor  $i'$  will be:

$$i' = Q i Q^T \quad (A.6)$$

where  $Q$  is the transformation matrix (orthogonal matrix) between  $oxyz$  and  $ox'y'z'$ .

2. Obtain the inertia tensor  $I'$  of the scaled rigid body with respect to a system  $OX'Y'Z'$  (with the axes parallel to the global system axes) using [A.3 – A.4] equations.
3. Obtain the inertia tensor  $I$  with respect to a system  $OXYZ$  with axes parallel to the initial local coordinate system  $oxyz$

Thus, the inertia tensor  $I$  will be:

$$I = Q^T I' Q \quad (A.7)$$

# INJURY MITIGATION IN SUV-TO-PEDESTRIAN IMPACTS

**Rikard Fredriksson, Erik Flink, Ola Boström**

Autoliv Research  
Sweden

**Kenneth Backman**

Autoliv Sweden  
Sweden  
Paper number 07-0380

## ABSTRACT

In passenger car-to-pedestrian impacts head and leg injuries account for the largest number of severe injuries (AIS 3+). US data from 2005 confirmed this but when studying LTV (Light Truck Vehicle) type of vehicles; thorax injuries replaced leg injuries at 2<sup>nd</sup> place for AIS 3+ injuries. For passenger cars the hood edge contributed to very few injuries, while in the LTV vehicles it was the main contributor for both lower extremity as well as thorax injuries. It is likely that the lower extremity injuries mainly consist of pelvic injuries, and that the hood edge (also called bonnet leading edge or BLE) of large Sport Utility Vehicles (SUV) produce more thorax injuries while lower SUV hood edges produce more pelvic injuries.

The recent development of pre-crash sensors has opened up new possibilities for pedestrian protection. Reversible solutions can be used as well as airbags in the very front of the car, where time is too short when using a bumper contact sensor.

In this study a bonnet leading edge airbag was developed to mitigate pelvis and thorax injuries for an SUV. The airbag was designed using mathematical simulations with the goal to decrease the upper legform requirements below the threshold levels of EuroNCAP. A physical prototype was produced which was tested and further developed using side impact dummies at a test speed of 40 km/h where pelvic and thoracic loadings were in focus. To do this a dummy test method was developed based on field data. The field data showed that the injury pattern of car occupants in near-side crashes is similar to that of pedestrians impacted by SUVs.

In simulations the BLE airbag proved able to pass the tough EuroNCAP requirements with the upper legform impactor. In full-scale tests the airbag decreased the risk of chest and pelvis injuries considerably, with the largest reductions in the chest and abdomen area.

## INTRODUCTION

The upper legform test has been discussed and criticized during many years. The test method was

developed as part of EEVC Working Group 10 (EEVC 1994) during the 80's and early 90's, when cars were box-shaped and caused rather many pelvis and femur injuries. Today's passenger cars are considerably more stream-lined and the EEVC working group 17 showed in their report a large decrease of these injuries from 1980 to 1990 cars (EEVC 1998). Therefore when the EU pedestrian directive (2003/102/EC) was finally enforced 2005, this test had been changed to a "monitoring test". A monitoring test means that a test is performed and the data is recorded and saved for the future, but no requirement is set. This is a way for regulators to keep track of the car fleet if it becomes more aggressive in this area of the car.

However, in the USA the Sports Utility Vehicle (SUV) has become very popular and now makes up around 50% of the total sales (Summers et al 2003). This car type has a more box-shaped front and it is also significantly higher in the front than today's passenger cars. Lefler and Gabler (2004) reported that the fatality risk is increased with more than 2.5 times for SUVs compared to cars. Head injuries are the most frequent cause of severe injury for LTVs, as well as for cars. According to Longhitano et al (2005-1), chest injuries are in 2<sup>nd</sup> place for AIS3+ injuries for the so called Light Trucks and Vans (LTV). For passenger cars lower extremity injuries take the 2<sup>nd</sup> place

In a second study, Longhitano et al (2005-2) reports that the most common torso AIS 3+ injury locations in SUV impacts are ribcage at 23% and lung at 21%, followed by aorta at 11%. For AIS 4+ injuries, ribcage still leads, now shared with aorta, at 23 %. Spleen follows at 14%.

Longhitano et al (2005-1) also studied the car impact location. The most frequent AIS 3+ torso injury causing part of the LTV was the hood edge with the hood in second place.

The pedestrian test methods consist of sub-system test methods or pedestrian dummy tests. The sub-system test methods include legform, upper legform and headform test methods. The upper legform is developed to mitigate femur or pelvis injuries for passenger cars.

The dummy test method standard (SAE 2006) is limited in measuring requirements in the chest and

abdomen region. Only chest acceleration is required, while chest displacement is recommended. For abdomen there is no requirement or recommendation.

The Polar II dummy was developed for pedestrian impacts (Akiyama et al 2001), with a focus in the development on leg impact, dummy kinematics and head impact. It has measuring capabilities for chest deflection with a so called “Crux” unit in one point. Okamoto et al (2001) performed crash tests with the Polar II and a utility vehicle, but the height of the bonnet leading edge was such that the BLE impact was concentrated in the pelvis region. No risk curves have been published for chest loading of a pedestrian dummy.

A pedestrian impact typically occurs when the pedestrian crosses a street. Field data shows that the pedestrian is impacted in the side in more than 2/3 of all pedestrian impacts (Kam et al 2005, Chidester and Isenberg 2001, Okamoto et al 2000, Otte 1989, Ashton 1975). The average impact velocity for severely injured (AIS 3+) pedestrians is 40 km/h (IHRA 2003). It is the impact speed on which all pedestrian test methods are based.

The aim of this study is to develop a bonnet leading edge airbag which can mitigate not only pelvis and femur injuries, but also thorax injuries, depending on the height of the car and the pedestrian.

## METHOD

### Simulations

To save development time and costs, a finite element (FE) simulation model was used to determine the basic characteristics of the bonnet leading edge airbag. A Ford Explorer MY 1997 FE model was downloaded from the NCAC website (NCAC 2006). NCAC is a collaborative effort between National Highway Traffic Safety Administration (NHTSA), Federal Highway Administration (FHWA) and George Washington University. An FE upper legform model was used as impactor (Ove Arup upper legform model V3). The setup can be seen in Figure 1.

EXPLORER - MBJ - NCAP  
Time = 32

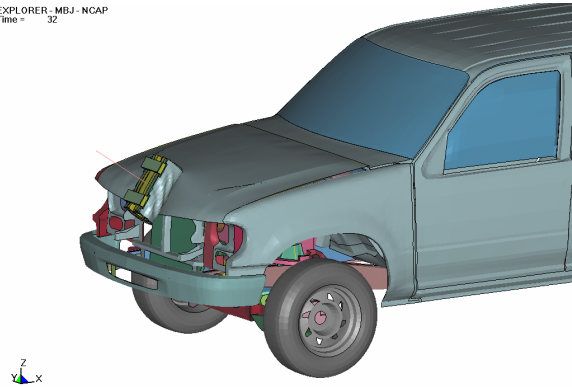


**Figure 1. SUV and upper legform FE model.**

The upper legform is currently used in EuroNCAP and the test specifications were taken from there. To determine impactor angle and mass and test impact speed, geometric measurements are taken from the car regarding bonnet leading edge height and bumper lead. For the vehicle in this study, specifications gave a test speed of 40 km/h, impactor mass of 11.4 kg, and an impact angle of 27 degrees.

To decrease calculation times in the FE model, the car model was reduced in such a way that parts, that were not believed to influence the pedestrian impact, were removed. Comparative simulations were then performed with the original and the reduced model. They showed almost identical results. (See the graph for upper legform force in Appendix Figure 9.) Bending moment showed very similar results.

When studying the upper legform force and bending moment it was found that the model gave rather low values. When comparing with a real vehicle it was found that the lock latch was missing in the model. It is a rather stiff and heavy part just designed for locking the hood/bonnet. Geometric measurements were taken from the real vehicle and introduced into the model. To find the right stiffness EuroNCAP data was used. In EuroNCAP, tested vehicles in the “large offroader” category in average had an upper legform force of 9.2 kN and a bending moment of 577 Nm, while “small off-roaders” had 8.6 kN and 535 Nm. It was also decided to include an “overload” case which reflected the highest values found in EuroNCAP tested “large off-roaders”. The chosen new reference model resulted in an upper legform force of 9.6 kN and a bending moment of 560 Nm, while the overload model resulted in a force of 15.5 kN, and a bending moment of 980 Nm. This is shown in Appendix Figure 10 and Figure 11.

Next step was to introduce an airbag. The airbag was tuned to give resulting force and bending moment below the EuroNCAP requirements for the upper legform. The EuroNCAP higher level requirements are 300 Nm

in bending moment and 5 kN in force. This is estimated to correspond to a risk of 18-20% for pelvis and femur fracture. The prototype airbag can be seen in Figure 2.

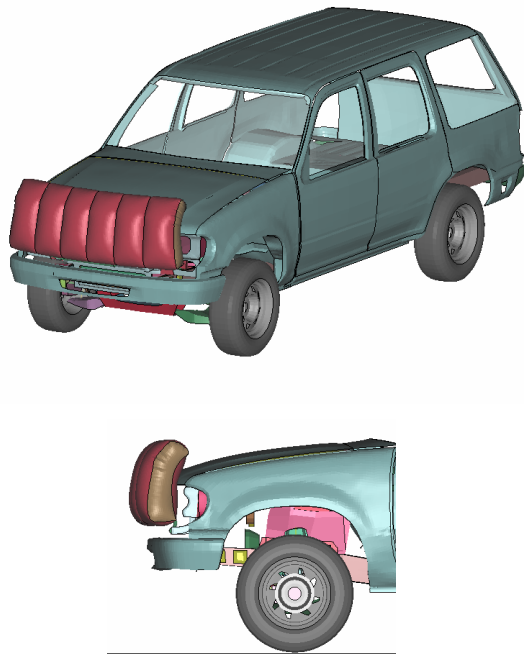


**Figure 2. Bonnet leading edge (BLE) airbag.**

**Field data**

A field data study of side impacts was performed, to compare with the Longhitano data of chest injuries for pedestrian to SUV impacts. NASS data from 1994-2005 was studied. In total 208 crashes were studied, where the occupant was hit from the near-side with an impact direction between 2-4 o'clock or 8-10 o'clock. Age of the occupant was between 19 and 50 years old, all younger and older were excluded. In total 208 occupants were included, where the impact vehicle was in 84 cases a passenger car and in 124 cases a LTV. AIS 3+ chest and abdomen injuries were selected for study. In total 386 injuries were included. This makes it comparable to Longhitano's data for pedestrians. The analysis was done both for unweighted and truncated weighted data. The truncation was done to give less importance to cases with very high weight factors. The truncation was set so that 98% of the cases kept its weight factor, while the weight factor was reduced to a certain limit for those cases above the limit. For the truncated weighted data the 208 crashes corresponded to 5602 car impacts and 7781 LTV impacts.

Skeletal injuries (ribcage) placed first for both target vehicles and both weight methods, between

32.6 to 40.7% in near-side data as well as for the pedestrians. Lungs placed second in all cases with values between 23.3 to 27.3%. In third place it was quite close between arteries/veins, spleen and liver in all cases. The unweighted near-side data is compared below with the pedestrian injury data for cars in Figure 3 and the LTV comparison is shown in Figure 4. Although the two databases do not use identical terminology it is quite similar so general comparisons are possible.

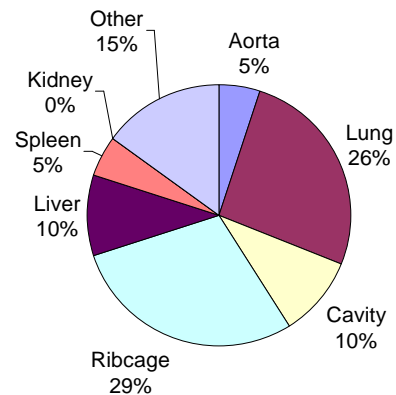
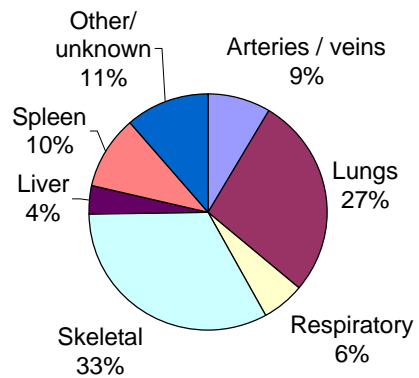


**Figure 3. Chest/abdomen AIS3+ injury distribution for near-side car occupants (top) compared to pedestrians (bottom) (Longhitano et al 2005-2), both impacted by cars.**

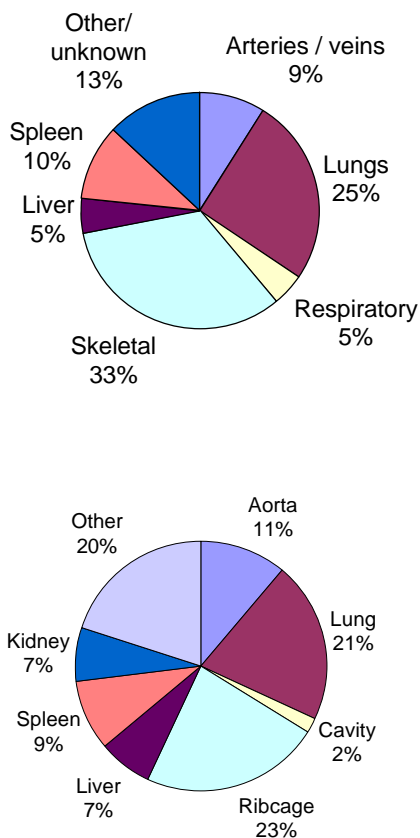


**Figure 4. Chest/abdomen AIS3+ injury distribution for near-side car occupants (top) compared to pedestrians (bottom) (Longhitano et al 2005-2), both impacted by LTVs.**

### Full-scale crash tests

No test method exists to evaluate pedestrian chest injuries in impacts with high front-end cars. The standard pedestrian dummy test method has a limited measuring capability in the chest region, and with a high front end car the risk of running over the dummy will largely increase. The chest contact with SUVs occur early in the event, when not much upper body bending has occurred. Therefore it was believed relevant to use side impact dummies for this test method.

**Sled** – A physical airbag was designed according with the mathematical BLE airbag. The BLE bag was mounted to a car buck of a Ford Explorer, 1997 model year. The car buck was cut behind the A-pillars and was mounted on a sled. In front of the car buck a low friction bench was placed. This bench was adjustable to different heights. The dummy was placed on the bench approximately 500 mm from the car front. The sled

pulse was chosen so that the sled had come to a full stop when the dummy first impacted the car. In this way it was possible to simulate a car impact to dummy at 40 km/h impact speed, all done on a sled but still a full-scale test. This eliminated the risk of the car driving over the dummy after first impact.

The hood edge height of the Ford Explorer 1997 was measured to 1017 mm above the ground, and the bench was adjusted so that the different percentile dummies would impact at the correct height corresponding to its respective body height. The test setup with the adjustable bench is shown in Figure 5, and in the left part of Figure 6 and Figure 7 the test vehicle is shown with the two percentile pedestrians.

It was also found that a 2006 model year Ford Explorer was considerably higher with a BLE height of 1168 mm. Since only the 1997 model year was available as test vehicle this was simulated by lifting the 1997 model car buck to match the BLE height of the 2006 model Ford Explorer. This could also be seen as an attempt to include a larger part of the SUV fleet. As a result, the test series consisted of four different impact heights.



**Figure 5. Sled setup with dummy on bench and car buck.**



**Figure 6. Ford Explorer 1997 model (left) and 2006 model (right), and pedestrian scaled to 5<sup>th</sup> percentile female.**



**Figure 7.** Ford Explorer 1997 model (left) and 2006 model (right), and pedestrian scaled to 50<sup>th</sup> percentile male.

It was decided to exclude all dummy loading that came from contact with the bumper.

**Dummy** – Two dummies were chosen due to their good measuring capabilities in the chest area, the SIDII 5<sup>th</sup> percentile female and the EuroSIDII 50<sup>th</sup> percentile male. The dummies differ slightly in instrumentation but in common they had head, T1, T12, pelvis and rib acceleration, rib displacement and forces in neck and pubic symphysis. Injury parameters used in the study were viscous criterion (VC), chest compression, abdomen and pelvis force.

The idea of the tests was to simulate impact with a standing pedestrian but with a seated dummy. Because these dummies are seated the hip point (H-point) height above the ground for a standing situation is not given. This was determined with Madymo to 813 mm for the 5<sup>th</sup> percentile and 936 mm for the 50<sup>th</sup> percentile. These values were used for the dummies in the study.

In the “high SUV” test the 5% dummy the dummy pelvis impacted the bumper. In all other tests the pelvis contact was above the bumper. It was decided to exclude dummy loading that came from contact with the bumper.

**Film** – Three high speed digital cameras were used, filming at 1000 fps from the top, side and from the side with an angle.

**Impact conditions** – All tests were run at 40 km/h. The dummy was impacted on the right hand side with the torso in a vertical position and the thighs in a horizontal position. The arms were placed in a 35 degree position from the vertical.

**Test plan** – Seven tests were planned and performed according to the test plan in Table 1. Due to lack of replacement parts, a reference test for the 5<sup>th</sup> percentile impacting the SUV with high BLE was not possible to perform.

**Table 1. Test plan for full-scale tests**

| SUV height | Dummy     | Bag |
|------------|-----------|-----|
| Low        | 5% female | Bag |
|            |           | Ref |
|            | 50% male  | Bag |
|            |           | Ref |
| High       | 5% female | Bag |
|            | 50% male  | Bag |
|            |           | Ref |

### **Injury criteria and risk curves**

No injury criteria exist for a pedestrian chest impact. Due to the similar nature of the impact and the input from field data, a survey of the injury criteria for side impact for car occupants was performed.

The SID-IIs is a 5<sup>th</sup> percentile dummy. Injury criteria values are shown below from three sources using the SID-IIs: 1) a technical working group for side airbag out-of-position testing (a joint project of Alliance, AIAM, AORC and IIHS), 2) Insurance Institute of Highway Safety (IIHS) side impact test program and 3) a proposed FMVSS 214 upgrade in Table 2.

**Table 2. Injury criteria and IARV for SID-IIs**

| SID-IIs                    |            |             |        |                    |
|----------------------------|------------|-------------|--------|--------------------|
|                            | TWG SIDIIs | IIHS SIDIIs |        | FMVSS 214 proposed |
|                            |            | Good        | Accept |                    |
| Chest VC                   | NA         | 1.0         | 1.2    | NA                 |
| Chest D (mm)               | 34         | 34          | 42     | NA                 |
| Abdomen F (kN)             | NA         | NA          | NA     | NA                 |
| Pelvis Acetab f            | NA         | 4.0         | 4.8    | NA                 |
| Pelvis Iliac F (kN)        | NA         | 4.0         | 4.8    | NA                 |
| Pelvis Acet + Iliac F (kN) | NA         | 5.1         | 6.1    | 5.1                |

Injury criteria thresholds for the EU regulatory test using EuroSID-1, as well as EuroNCAP tests using EuroSID-2 and a proposal for FMVSS 214 are shown in Table 3.

**Table 3. Injury criteria and IARV for EuroSID2-re**

| ES-2re                         |     |           |     |                    |
|--------------------------------|-----|-----------|-----|--------------------|
|                                | EU* | Euro NCAP |     | FMVSS 214 proposed |
|                                |     | High      | Low |                    |
| Chest VC                       | 1.0 | 0.32      | 1.0 | NA                 |
| Chest D (mm)                   | 42  | 22        | 42  | 35-44              |
| Abdomen F (kN)                 | 2.5 | 1.0       | 2.5 | 2.4-2.8            |
| Pelvis Pubic F (kN)            | 6.0 | 3.0       | 6.0 | 6.0                |
| *EU requirements for EuroSID-1 |     |           |     |                    |

In a NHTSA NPRM, injury risk curves for the side impact dummies SID-II<sub>s</sub> and ES-2re are presented. Injury risk curves for SID-II<sub>s</sub> and EuroSID2-re were developed using cadaver sled test data and corresponding sled tests with the two dummies (Kuppa 2004 and Kuppa et al 2003). For the SID-II<sub>s</sub>, risk curves were developed for thoracic and abdominal rib deflection, and a pelvic force which adds the measurements of acetabular and iliac force. For the EuroSIDII risk curves were developed for thoracic rib deflection, abdomen force and pubic symphysis force.

ISO developed thoracic injury risk curves for AIS3+ injuries using the Eurosid-1 (ISO 2005). Since no risk curves for VC, and the dummies used in this study, could be found in literature; it was decided to use the risk curves for Eurosid-1.

## RESULTS

### Simulations

The two significantly different hood edge stiffness cases resulted in very similar output values with the airbag (see Appendix Figure 12 and Figure 13). The force value is slightly above the EuroNCAP requirement while the bending moment value is well below the required level.

### Full-scale crash tests

The thoracic, abdomen and pelvis injury values were evaluated. The injury values used were Viscous Criterion (VC), Chest Compression and pelvis force. For the ES-2, abdominal force also was evaluated. The SIDII-s 5<sup>th</sup> percentile female dummy has three thoracic ribs and two abdominal ribs, and the maximum VC and compression values were taken for the thoracic respectively the

abdomen ribs. These values were calculated into an injury risk value using risk curves. (See Table 4) In the same way the risk values were calculated for the EuroSID-II 50<sup>th</sup> percentile tests. (See Table 5)

Highest chest values were found for the 5<sup>th</sup> percentile female impacting the low SUV, while abdominal force had the highest value in the 50<sup>th</sup> percentile “high SUV” test. When using both VC and chest compression as criteria there was a risk greater than 90% of an AIS3+ injury. These values were reduced considerably with the airbag. The maximum value was then chest compression at 46%. All risk values, except for the risk values already below 1%, decreased considerably with the airbag. The “5%F/high SUV” test was not possible to compare to a reference test, but it had risk values in line with the “5%/low SUV” bag test.

**Table 4. Chest/abdomen injury risk values from the SID-II<sub>s</sub> (5%-F) crash tests**

|                 |     | VC          |             | Compression |            |
|-----------------|-----|-------------|-------------|-------------|------------|
|                 |     | Th Ribs     | Abd Ribs    | Th Ribs     | Abd Ribs   |
|                 |     | Risk* AIS3+ | Risk* AIS3+ | Risk AIS3+  | Risk AIS4+ |
| <b>Low SUV</b>  | Bag | 23%         | 8%          | 46%         | 0.6%       |
|                 | Ref | 99%         | 77%         | 91%         | 0.7%       |
| <b>High SUV</b> | Bag | 30%         | 6%          | 30%         | 0.1%       |

\*Note. VC risk values taken from risk curves for Eurosid-1.

**Table 5. Chest/abdomen injury risk values from the ES-2 (50% M) crash tests**

|                 |     | VC*         | Compression | Abdomen Force addition |
|-----------------|-----|-------------|-------------|------------------------|
|                 |     | Risk* AIS3+ | Risk AIS3+  | Risk AIS3+             |
| <b>Low SUV</b>  | Bag | 1%          | 12%         | 1.3%                   |
|                 | Ref | 28%         | 31%         | 3.7%                   |
| <b>High SUV</b> | Bag | 29%         | 33%         | 3.4%                   |
|                 | Ref | 66%         | 57%         | 99%                    |

\*Note. VC risk values taken from risk curves for Eurosid-1.

Pelvic injury risks were rather low already in the reference tests, with a maximum risk value of 11% in the “50%M/low SUV” reference test. The pelvis then hits at the height of the hood edge. This value was reduced to 1.7% risk of pelvic injury with the airbag. See Table 6 and Table 7.

**Table 6. Pelvic injury risk values from the 5%F crash tests**

|                |     | Iliac +Acet F |
|----------------|-----|---------------|
|                |     | Risk AIS2+    |
| <b>Low SUV</b> | Bag | 2.7%          |
|                | Ref | 4.2%          |
| <b>High</b>    | Bag | N/A           |

**Table 7. Pelvic injury risk values from the 50%M crash tests**

|                 |     | Pubic symph. F |
|-----------------|-----|----------------|
|                 |     | Risk AIS3+     |
| <b>Low SUV</b>  | Bag | 1.7%           |
|                 | Ref | 10.6%          |
| <b>High SUV</b> | Bag | 0.6%           |
|                 | Ref | 0.7%           |

The maximum AIS3+ risk values for each test were selected, taken from the body part showing the largest risk in each test configuration. See Table 8. Most values come from thoracic rib compression. For the “50%M/high SUV” reference test, abdomen force resulted in the highest risk of injury. For the “5%F/low SUV” reference test the highest risk value was found in the chest region using the VC criterion. But since the risk values, using the VC criterion, were based on Eurosid-1 this value was put into parenthesis.

**Table 8. Maximum risk values in each test (different body parts)**

|              |                 |     | Max risk value | Body part |
|--------------|-----------------|-----|----------------|-----------|
|              |                 |     | Risk AIS3+     |           |
| <b>5% F</b>  | <b>Low SUV</b>  | Bag | 46%            | Thor.     |
|              |                 | Ref | 91% (*99%)     | Thor.     |
|              | <b>High SUV</b> | Bag | 30%            | Thor.     |
|              |                 | Ref | N/A            | Thor.     |
| <b>50% M</b> | <b>Low SUV</b>  | Bag | 12%            | Thor.     |
|              |                 | Ref | 31%            | Thor.     |
|              | <b>High SUV</b> | Bag | 33%            | Thor.     |
|              |                 | Ref | 99%            | Abd.      |

\* Value in parenthesis from using VC criterion (based on ES-1 risk curve)

## DISCUSSION

In the simulations two significantly different BLE stiffnesses were used to cover a range of vehicles. However, it was found as a result almost identical upper legform loadings when adding the airbag. This is indicating that the airbag design is not so sensitive to bonnet leading edge stiffness, making it easier to design it for different SUVs.

When studying the risk values from the tests it can be seen that the highest risk values for each test configuration is found at the body part that is situated at the height of the hood edge in the impact. This indicates that the presented test method reflects the injuries found in the field, where chest injures can be linked to high bonnet leading edge heights.

The so-called “high SUV” tests were introduced to try to study the influence of a higher bonnet leading edge on the pedestrian torso loading. Since a test vehicle with this bonnet leading edge height was not available, this was simulated by lifting the car buck to match the hood edge height of the higher SUV. This means that the bumper of the SUV will be positioned higher than it would have been on the higher SUV. Therefore it was considered relevant to exclude dummy loadings that resulted from bumper contact.

The test configuration used in this study with side impact dummies leads to an impact in a seated position. It is likely not to influence the thorax and abdomen impact with the car front, but in the pelvis impact it is possible that the load is spread over a larger area of pelvis and femur instead of the pelvis only. Therefore it is likely that the pelvic forces should be somewhat higher with a standing dummy.

In three test configurations both tests with and without the BLE airbag were performed. In these three test configurations risk reductions can be calculated, using the different criteria (see Figure 8). The risk was reduced in the identified critical injurious loadings between 42 and 97% with the BLE airbag. The three loadings with lower risk reduction have already very low risk values without the airbag. These specific risk values are all below 4% injury risk in the reference tests.

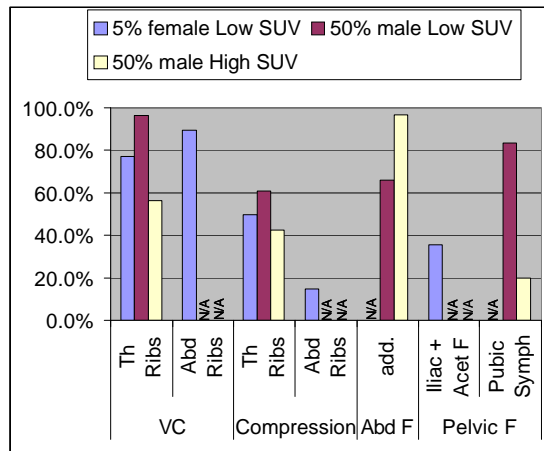


**Figure 8. Risk reduction with the BLE airbag for different injury values.**

From earlier full-scale tests it has been found that the head impact speed of a pedestrian dummy was decreased with a car with less stiff hood edge compared to a car with a stiffer bonnet leading edge. Therefore as a next step, the BLE airbag effect of reducing head impact speed of a pedestrian dummy could be studied.

## CONCLUSIONS

A new test method, for evaluation of pedestrian impacts to the bonnet leading edge of high front end cars, such as SUVs, has been developed in this study. The front design of SUVs leads to an early impact to the torso of pedestrians with not much upper body bending. This lead to the conclusion that side impact dummies could be used for this evaluation. The benefit of using side impact dummies is the good measurement capabilities for the chest and abdomen area. The field data showed a similar injury distribution in near-side car occupant injuries and pedestrian injuries which led to the conclusion that side impact injury criteria and injury risk curves could be used.

An airbag system was developed to mitigate injuries caused by the pedestrian impact to the bonnet leading edge of SUVs. The initial design was developed using finite element simulations. In simulations the airbag proved able to pass the tough EuroNCAP requirements with the upper legform impactor. In full-scale tests the airbag decreased the risk of chest and pelvis injuries considerably, with the largest reductions in the chest and abdomen area. For example the chest compression was reduced more than 40% with the airbag in all test configurations. The airbag system seems to be a good candidate to mitigate torso injuries in a pedestrian-to-SUV impact.

## REFERENCES

Akiyama A, Okamoto M, Rangarajan N (2001); "Development and application of the new pedestrian dummy", International Technical Conference of Enhanced Safety of Vehicles (ESV) paper no. 463, Amsterdam, Netherlands.

Ashton SJ (1975); "The cause and nature of head injuries sustained by pedestrians", Proc. Of the 2<sup>nd</sup> International Conference on Biomechanics of Serious Trauma, Birmingham, pp 101-113, September 9-11, IRCOBI, Bron, France.

European Experimental Vehicles Committee (1994); "Proposals for methods to evaluate pedestrian protection for passenger cars", EECV Working Group 10 report.

European Experimental Vehicles Committee (1998); "Improved test methods to evaluate pedestrian protection afforded by passenger cars", EECV Working Group 17 Report, December 1998.

IHRA (2003); "INF GR PS 31 IHRA PS WG Pedestrian accident data", GTR Informal Group of Pedestrian Safety.

International Standard Organization TC22/SC12/WG6 (2005); "Road vehicles – Injury risk curves to evaluated occupant protection in side impact", TR12350:2005.

Kuppa S, Eppinger R, McKoy F, Nguyen T, Pintar F, Yoganandan N (2003); "Development of side impact thoracic injury criteria and their application to the modified ES-2 dummy with rib extensions (ES-2re)", Stapp Car Crash Journal, Vol. 47, pp 189-210.

Kuppa (2004); "Injury Criteria for Side Impact Dummies", FMVSS No. 214 NPRM docket: NHTSA-2004-17694 submission, <http://www-nrd.nhtsa.dot.gov/departments/nrd-51/BiomechanicsTrauma.html>, NHTSA, USA.

Lefler DE, Gabler HC (2004); "The fatality and injury risk of light truck impacts with pedestrians in the United States", Accident Analysis and Prevention 36, pp 295-304.

Longhitano D, Henary B, Bhalla K, Ivarsson J, Crandall J (2005-1); "Influence of vehicle body type on pedestrian injury distribution", SAE World Congress, paper no 2005-01-1876, Detroit, USA, 2005.

Longhitano D, Ivarsson J, Henary B, Crandall J (2005-2); “Torso injury trends for pedestrians struck by cars and LTVs”, 19<sup>th</sup> ESV Conference proceedings, paper no 05-0411, Washington DC, USA.

National Crash Analysis Center (NCAC) website; <http://www.ncac.gwu.edu/vml/models.html>

Okamoto Y, Akiyama A, Okamoto M, Kikuchi; “A study of the upper leg component tests compared with pedestrian dummy tests”, International Technical Conference of Enhanced Safety of Vehicles (ESV) paper no. 380, Amsterdam, Netherlands, 2001.

Otte D (1989); “Influence of vehicle front geometry on the injury situation of injured pedestrians”, Road traffic accident research, Medical University of Hannover.

SAE International, Surface Recommended Practice (2006); “Performance specifications for a 50th percentile male pedestrian research dummy”, SAE Pedestrian Dummy Task Group, TG N36 Rev 38\_20060328.

Summers S, Hollowell T, Prasad A (2003); “NHTSA’s Research Program for Vehicle Compatibility”, Proceeding of the Eighteenth Conference on Enhanced Safety of Vehicles, Nagoya, Japan, 2003.

## APPENDIX

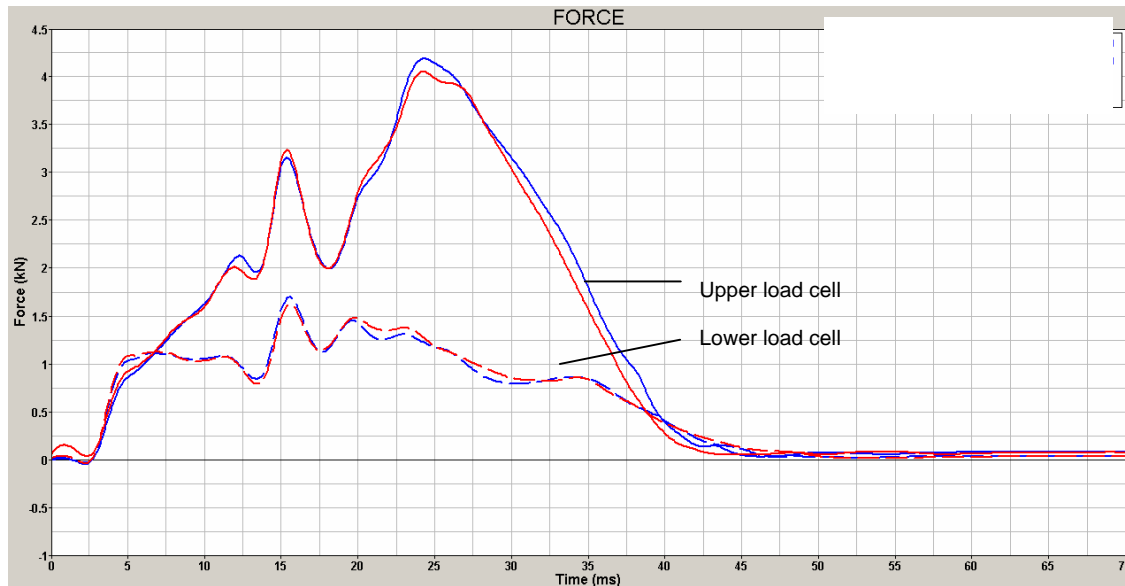
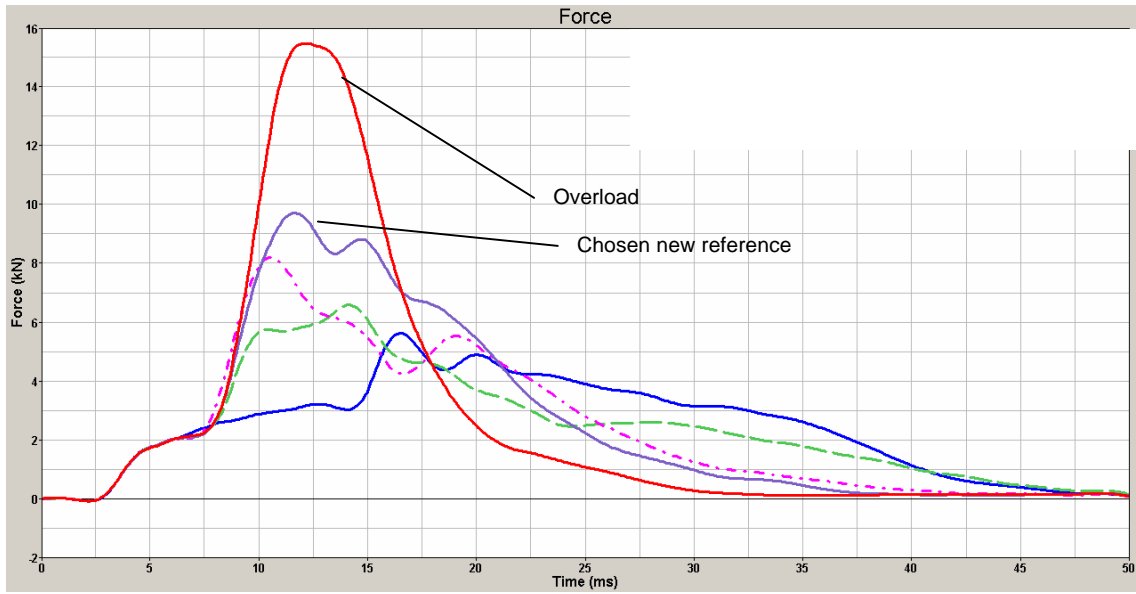
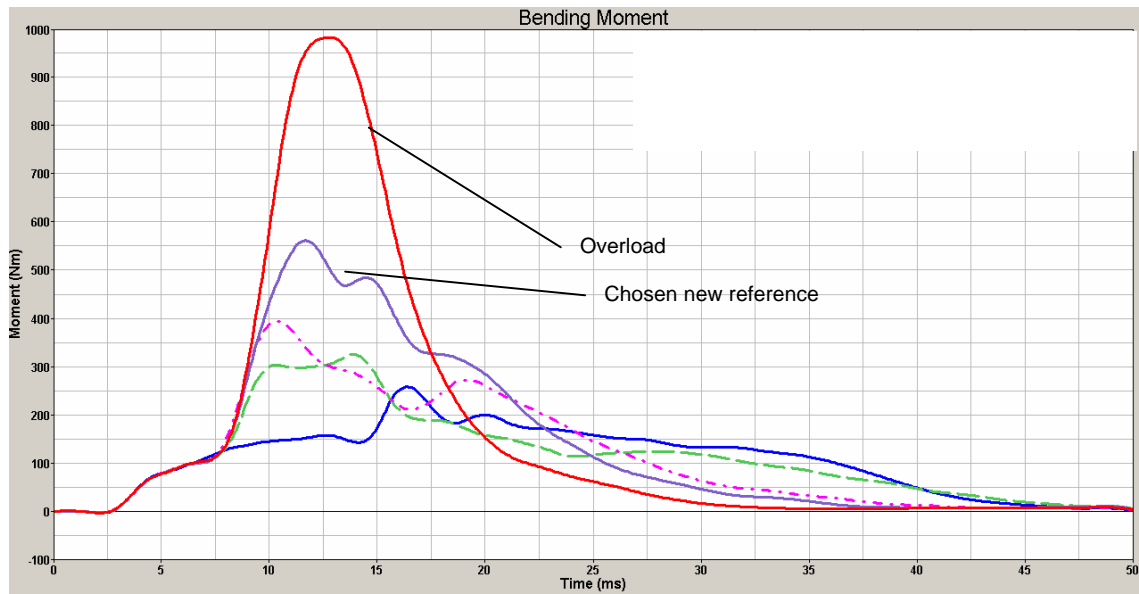


Figure 9. Comparison of original and reduced model, upper legform forces.



**Figure 10. Determination of BLE stiffness in car model, upper legform force.**



**Figure 11. Determination of BLE stiffness in car model, upper legform bending moment.**

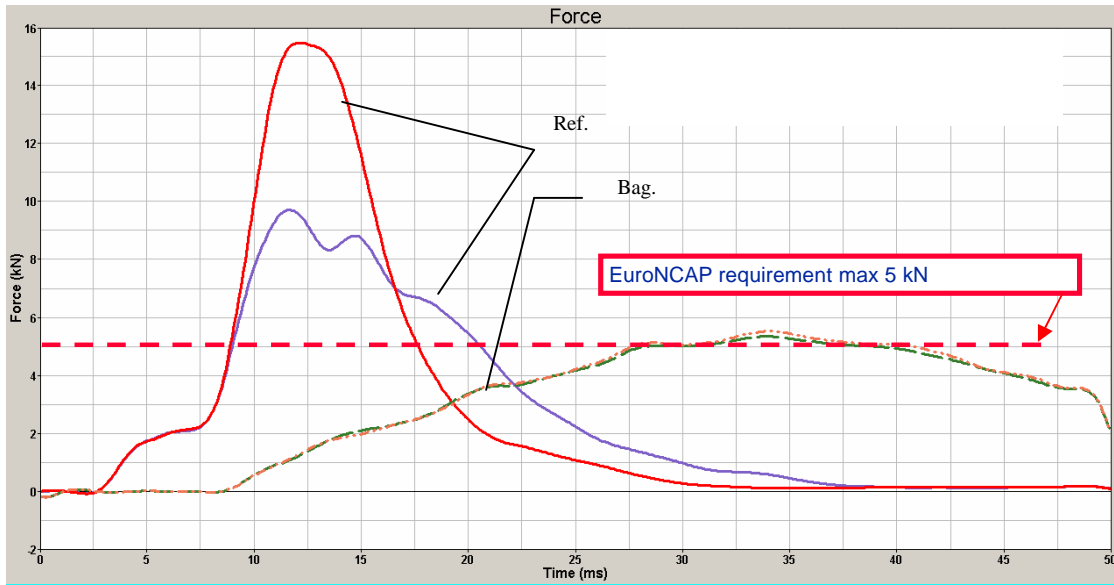


Figure 12. Upper legform force with and without BLE airbag. EuroNCAP threshold in dashed red.

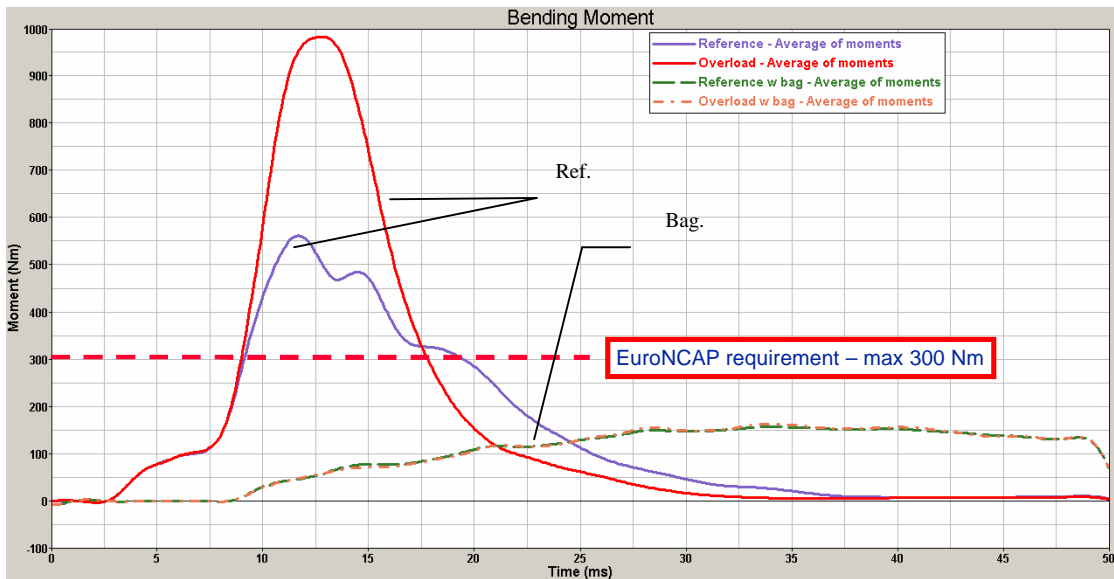


Figure 13. Upper legform bending moment with and without BLE airbag. EuroNCAP threshold in dashed red.

The injury IARV values from all tests are listed in Table 9. They are compared to the IIHS side impact threshold levels for the tests using the SIDII-s dummy (5<sup>th</sup> percentilen female), and EuroNCAP side impact threshold levels when using the EuroSID-II dummy (50<sup>th</sup> percentile male).

**Table 9. Test data from all tests with colour marking and threshold limits using IIHS and EuroNCAP protocols**

|                       |          |       |         | VC      |          | Compression |          | Abdomen        | Pelvis         |               |
|-----------------------|----------|-------|---------|---------|----------|-------------|----------|----------------|----------------|---------------|
|                       |          |       |         | Th Ribs | Abd Ribs | Th Ribs     | Abd Ribs | Force addition | Iliac + Acet F | Pubic Symph F |
| Vehicle               | Bag?     | Dummy | m/s     | m/s     | mm       | mm          | kN       | kN             | kN             |               |
| 5%F                   | Low SUV  | Bag   | SID-IIs | 0.38    | 0.18     | 36.50       | 29.00    | N/A            | 2.72           | N/A           |
|                       |          | Ref   | SID-IIs | 1.76    | 0.78     | 52.80       | 30.20    | N/A            | 3.17           | N/A           |
|                       | High SUV | Bag   | SID-IIs | 0.44    | 0.13     | 32.00       | 17.80    | N/A            | 5.49           | N/A           |
| IIHS "Good" limit     |          |       |         | 1       | 1        | 34          |          |                | 5.1            |               |
| IIHS "Accept" limit   |          |       |         | 1.2     | 1.2      | 42          |          |                | 6.1            |               |
| 50%M                  | Low SUV  | Bag   | ES-2    | 0.01    | N/A      | 2.6         | N/A      | 0.80           | N/A            | 3.24          |
|                       |          | Ref   | ES-2    | 0.32    | N/A      | 27.1        | N/A      | 1.31           | N/A            | 4.97          |
|                       | High SUV | Bag   | ES-2    | 0.33    | N/A      | 28.4        | N/A      | 1.26           | N/A            | 2.22          |
|                       |          | Ref   | ES-2    | 0.70    | N/A      | 49.0        | N/A      | 6.18           | N/A            | 2.42          |
| EuroNCAP higher limit |          |       |         | 0.32    |          | 22          |          | 1              |                | 3             |
| EuroNCAP lower limit  |          |       |         | 1       |          | 42          |          | 2.5            |                | 6             |

# A COMPARISON STUDY ON VEHICLE TRAFFIC ACCIDENT AND INJURIES OF VULNERABLE ROAD USERS IN CHINA AND GERMANY

**Jikuang Yang**

Hunan University, Changsha  
China

**Dietmar Otte**

Hannover Medical University  
Germany  
Paper Number 07-0417

## ABSTRACT

The vehicle traffic accidents have been widely studied in different countries, but the difference of nature of traffic accidents in different countries was not adequately investigated for set suitable protective strategy in different area. This study aimed to identify the occurrence, type and mechanisms of the traumatic injuries of the vulnerable road users (VRUs) in vehicle collisions in China and Germany.

The accident data (in the years 2000 to 2005) were collected from traffic police and hospital in Changsha, China as well as from GIDAS database documented in Medical University Hannover, respectively. An in-depth study was carried out based on the collected data by using approaches of statistics analysis and virtual reconstructions. The results from analysis of Chinese data were compared with results from analysis of German data.

The injury severities were determined using AIS code and ISS values. The results were presented in terms of cause of injuries, injury distributions, injury patterns, injury severity. The VRUs accidents were identified as vital issue in urban traffic safety and therefore a high priority should be given to this road user group in research of safe urban transportation.

It was discussed with regard to accident data collection, accident sampling and injury distributions, the factors influenced the injury outcomes etc.

The data sources reflects the real situations of vulnerable road users in traffic accidents in Changsha and Hannover and may not in the whole countries of China and Germany.

This study will contribute to the determination of different nature of vehicle traffic accidents between motorized and motorizing areas, which will form a firm background for making safety counter-measures.

## INTRODUCTION

In 2005, total of 98,738 road users were killed and 469,911 are injured in China, resulting in substantial economic losses due to fatalities and long-term

consequences [1]. The vulnerable road users (VRUs) form a large proportion of the total fatalities. The safety issue of the VRUs is therefore to be a priority in the research of vehicle traffic safety in China. Knowledge from in-depth accident investigations will be valuable for improving VRU safety. It demonstrates an urgent demand for preventive measures.

In Germany 440,000 road users were injured in 2004, the half of these were aged between 25 to 65 years old, 5800 fatalities could be registered in that year, 14% were pedestrians[2].

Pedestrians are one of the most vulnerable road users in city traffic. They represent a high risk population since they are unprotected in vehicle impacts. About 25,000 pedestrians are killed in the traffic accidents each year in China [3]. In the European Union (EU) 7,000 pedestrians are killed each year, 5,000 in the USA, about 3,000 in Japan. Within the EU countries, the relative frequency of the pedestrian fatalities varies remarkably from 14% in Sweden to 32% in UK. Pedestrian protection is therefore a priority item in traffic safety strategies of nearly all countries worldwide [4].

The objective of this study is to identify the occurrence and type of the traumatic injuries of the relatively unprotected vulnerable road users especially the situation of the pedestrians in vehicle collisions, and to investigate the correlation of traffic injuries with human factor and engineering, environment factors, by using valid and reliable materials collected from local hospital and traffic administration authorities. The knowledge from the study is a prerequisite for developing guidelines to improve pedestrian safety and with this perhaps the safety for all other kind of vulnerable road users.

## METHOD AND MATERIALS

Vehicle accident data were collected from Changsha in China. The Changsha is a capital city of Hunan

Province, which is located in south middle of China, with a population 2,060,000 in the city center, 6,133,000 including residents in suburb and registered vehicles 255,599 in 2000.



Figure 1. The urban area of Changsha, the capital of Hunan Province located in south middle of China.

In the present study, a general statistic analysis was carried out in terms of occurrence and type of the accidents of the unprotected vulnerable road users, especially the situation of the pedestrians in vehicle collisions. A preliminary analysis was also carried out to identify the type of pedestrian accidents in terms of involved vehicles.

Analysis of pedestrian injuries was carried out using collected data from hospital in terms of cause of injuries, injury distributions, injury patterns, and injury severity.

Pedestrian accident cases collected from the accident database GIDAS (German In-Depth Accident Study) were used for an in-depth analysis of pedestrian injuries.

A comparison was carried out in terms of analysis results based on accident data from Changsha and Hannover. The factors influenced the injury outcomes were proposed and discussed in terms of vehicle transport environment and road users. The results were discussed with regard to accident data collection, accident sampling and injury distributions etc.

Finally, accident reconstructions are conducted using mathematical models to study the impact dynamics and injury biomechanics in pedestrian traffic accidents.

### Accident data from Changsha

The accident data from Changsha consist of two parts: one part of the data was collected from Traffic Police Section, another part of the data was collected from Wujing Hospital. The hospital admits the patients with

traffic trauma in the urban area of Changsha.

### Police data

There are total 19,323 accident cases in traffic police database registered from 2001-01-01 to 2005-12-31. Total of 42998 victims involved in the accidents. Among 19,323 accidents, 3603 cases were pedestrian accidents, accounted for 18.7% of all reported accidents, 1473 cyclist cases, 7.6%, 1447 motorcyclist cases, 7.5%.

Table 1: Distribution of vulnerable road user accidents

|              | Accidents | %     |
|--------------|-----------|-------|
| Pedestrian   | 3603      | 18.7% |
| Cyclist      | 1473      | 7.6%  |
| Motorcyclist | 1447      | 7.5%  |
| Others       | 12800     | 66.2% |
| Total        | 19323     | 100%  |

Of 42998 victims, 4% were killed, 5% were severely injured, 36% were slightly injured, and 55% had no injuries.

Table 2: Comparison of proportions of injury severity

|                   | Victims | %    |
|-------------------|---------|------|
| Fatalities        | 1934    | 4%   |
| Seriously injured | 2003    | 5%   |
| Slightly injured  | 15325   | 36%  |
| No injuries       | 23736   | 55%  |
| Total             | 42998   | 100% |

This police database has total 3,603 pedestrian victims, of which 16% victims were killed, 11% were severely injured, 72% were slightly injured, and 1% pedestrians had no injuries.

This police database has total 1,496 cyclist victims. Among those victims, 9% cyclists were killed, 11% were severely injured, 77% were slightly injured, and 1% had no injuries.

### Hospital data

An in-depth study on the hospital clinical records for 622 traffic injury patients was carried out in cooperation between researchers and medical doctors. In total of 403 cases were collected based on the study of the clinical report from 2000 to 2005. The hospital data are summarized according to accident date, patient age, gender, and available information about injury pattern, injury severities, as well as type of accident vehicles. Pedestrian accident data were also collected from traffic administration authorities with information about accident sites and vehicles based on accident report. 72 cases of the pedestrian patients were selected with detailed injury descriptions for determination of the injury severities and analysis of pedestrian injuries using AIS [5] code and ISS value. The situation of

treatment period and heal was studied based on hospital documentations to identify the consequence of accident.

### GIDAS accident data from Hannover Medical University

In the district of Hannover a representative sampling of accidents was carried out by the order of German Government (Federal Highway Research Institute BAST) in cooperation with the car manufactures FAT since the year 1999 (Otte et al, 2003). In the area of Hannover nearly 1000 accidents with injured person are collected there annually in a continued and representative way. These accident cases were documented in the accident database GIDAS by Accident Research Unit at Medical University of Hanover. The collected cases in the GIDAS database contain very detailed information about pedestrian victims on age, gender, height/weight, injuries, speed determination and details of the accident cars as well as the accident scene issues.

Altogether 407 vehicle-to-pedestrian accident cases from the GIDAS database were collected based on the following standards: (1) the pedestrian should sustain at least an AIS 1 injury; and (2) the accident occurred during the period from 2000 to 2005.

### Accident Reconstructions

In passenger car-to-adult pedestrian accidents, the head injuries attract particular attention due to the severe or fatal consequences. Many studies have been carried out in this area but the injury mechanisms and the tolerances of brain remain controversial. This study presents an approach (Figure 2) to investigate the skull-brain injury mechanisms by using a MBS pedestrian model and a head FE model. Furthermore, the acquired knowledge will be used for assessment of the risks of head brain injuries, and improvement of the car safety design for protection of pedestrian head injuries.

A FE model of human body head (HBM-head) was developed[6, 7] based on anatomical features of a 50th percentile male adult head with mass 4.4 kg (Figure 2). The HBM head model consists of scalp, skull with dura, falx cerebri, tentorium, falx cerebelli, pia, cerebrum, cerebellum, brain stem and ventricles. The properties of brain soft tissues exhibit incompressible behavior, which were defined using visco-elastic material model. The HBM-head FE model was validated in terms of the intracranial and ventricular pressure with two load pulses from cadaver impact tests at speeds of 9.94 and 6.80 m/s.

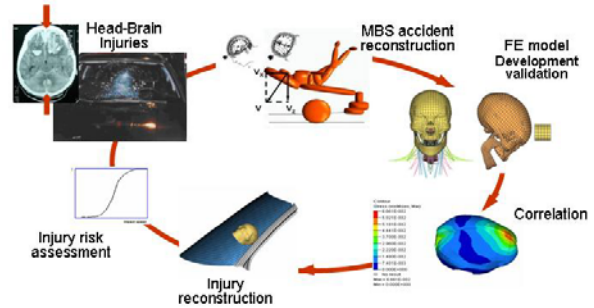


**Figure 2:** An approach to study pedestrian skull-brain injuries using MBS and FE models.

A passenger car-to-pedestrian crash was carried out using multi-body system (MBS) models to acquire the head impact conditions for the head impact velocity, head position, and head orientation (Figure 3a).

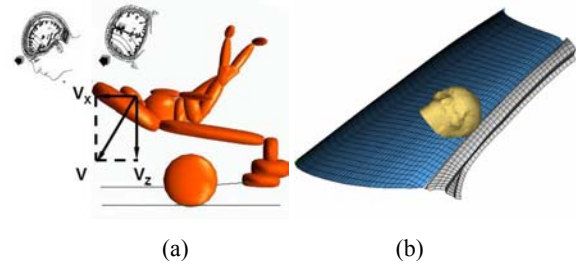


**Figure 3:** (a) A multi-body dynamic model of a car to pedestrian impact, (b) HBM-head FE model impact to windscreen and A-pillar.

The HBM-head FE model was used for reconstruction of skull fracture and brain injuries via a virtual test of head impact against windscreen and A-pillar (Figure 3b). A stress analysis was conducted to determine the correlation of the stress and pressure distributions of the brain model with the injuries observed in the head-windscreen collisions.

## RESULTS AND ANALYSIS

### **Involvement of vehicles**

Considering vehicle types involved in accidents in Changsha, the pedestrians were struck most frequently by passenger car and motorcycle. Figure 4a shows approximately 52 % of the accidents are passenger cars, and 22 % motorcycle-pedestrian collisions, 16 % truck, and 3.5 % bicycle. Compared to the China's situation for Germany there can be registered mainly car involvement in pedestrian collisions (80.6%) (Figure 4b).

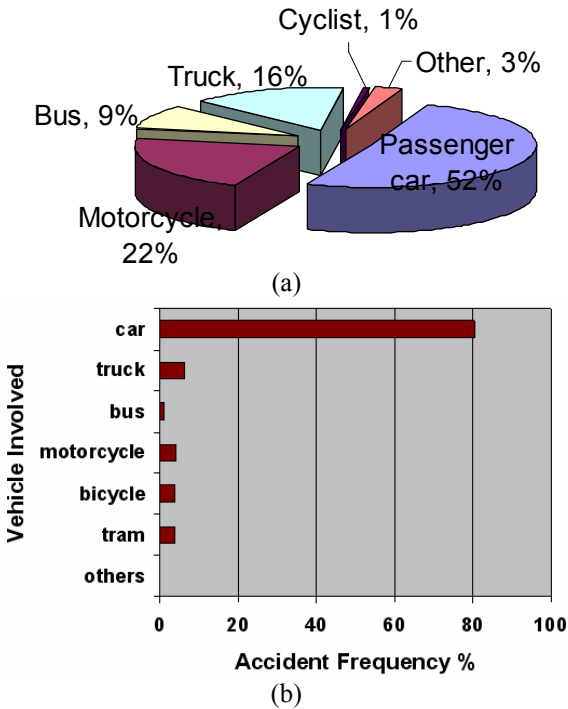


Figure 4. Frequency distribution of vehicle type in pedestrian accident: (a) 3603 cases from Changsha Traffic Police Station, (b) 407 cases from GIDAS Hannover.

### Frequency of Pedestrian Accidents

An analysis of frequency of pedestrian accidents was conducted with the collected data in terms of age groups, gender and injured body parts.

### Age distribution in pedestrian accidents

Figure 5a illustrates the age distribution in pedestrian accidents for Changsha. 7.9% of injured pedestrians are children under 15 years old. The pedestrians under 20 years old accounted for 18.1%. 71.9% of pedestrians involved in an accident were adults from 21 to 60 years old and formed the big group. Elderly pedestrians 60 years old above accounted for 9.9% of all injured pedestrians.

Figure 5b illustrates the distribution in pedestrian accidents for Hannover in different age groups: 32,5% for child pedestrians under 15 years old, 42,3% for pedestrian under 20 years old, 36,4% for 21-60 age group, and 21,4% for older pedestrians >60 age group.

It can be seen that in Germany the highest risk existing for young and old pedestrians, compared to this in China the adult group of 20 to 50 years old is injured mainly.

### Gender distribution in pedestrian accidents

Table 3A and 3B (Appendix) present the results for the

age distribution of injured pedestrians in terms of gender. Of the Changsha pedestrians, 67 % of the pedestrians are male and 33 % are female. Of the Hannover pedestrians, 51.9 % are male and 48.1 % are female. We noted that the male pedestrians encounter in both countries for higher risks than that for females in vehicle accidents.

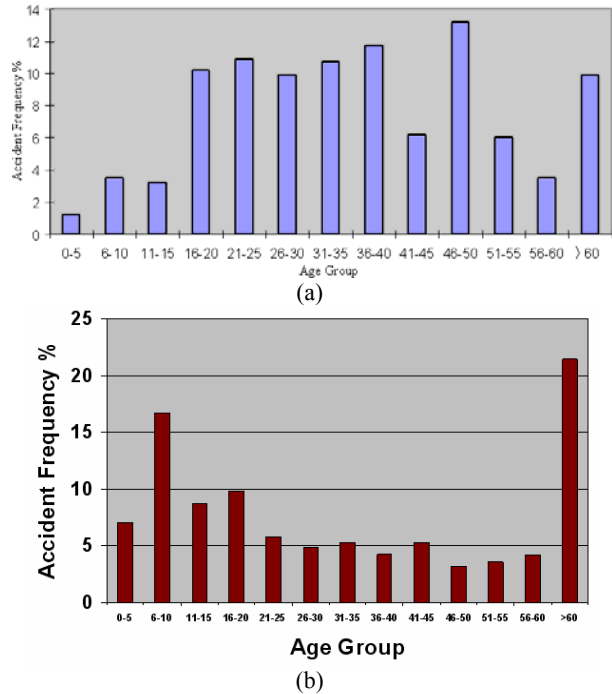


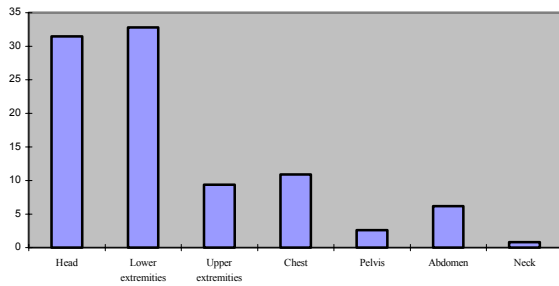
Figure 5 Frequency distribution of age group in pedestrian accident (a) 403 cases from Changsha Wujing hospital, and (b) 206 cases from GIDAS Hannover

### Distribution of injury frequency by body parts

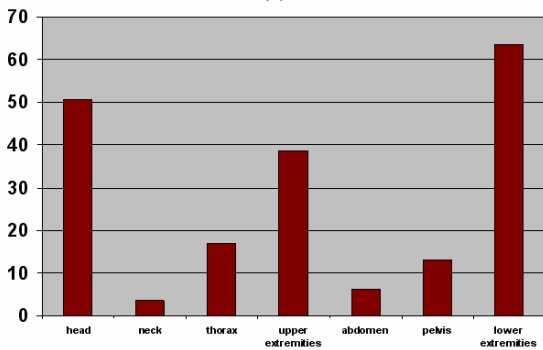
Figure 6a presents the results for the distribution of injured body parts from Changsha cases. The head and lower extremities were found to be the most frequently injured[4]. Of the total pedestrian patients, 31.5% suffered head injuries. The lower extremity injuries accounted for 32.8%, and upper extremities 9.4%. In pedestrian accidents chest and pelvis injuries also took a significant proportion of 13.5 % of all injuries. Abdominal injuries were found in 6.2%, and the neck injuries were relatively rare, in 0.8%.

Figure 6b presents the distribution of injured body parts for Hannover GIDAS data. 50.7% suffered head injuries. The lower extremity injuries accounted for 63.5%, and upper extremities 38.7%. In pedestrian accidents chest and pelvis injuries also took a significant proportion of 17.1 % for the thorax and 13.0% for the pelvis. Abdominal injuries were found in 6.3%, and the neck injuries were relatively rare, in 3.6%. The injury distribution is similar between China and Germany, the head and the legs are the major

exposed injured body parts, in Germany a higher injury risk of the arms can be seen in the diagrams.



(a)



(b)

Figure 6. Distribution of injury by body regions pedestrian (a) Changsha, and (b) GIDAS Hannover

### Severity and distribution of pedestrian injuries

For an in-depth study of pedestrian injuries Changsha 72 cases were selected from the Wujing Hospital with a sampling defined as follows: (1) the injuries were described with very detailed information which can be used to determine the injury severity with AIS code; (2) the pedestrian should sustain at least an AIS 1 injury; and (3) accident occurred during the period from 2000 to 2005.

### AIS coding and analysis

The severity of injury sustained by individual body area is given in Table 4. The percentage is that the number of body segment injuries refer to the total number of registered injuries by injury severity. With the detailed information of 72 cases from Wujing hospital, the injuries are rated on the AIS scale[5]. The overall injury severity classified with AIS code is summarized in Table 4A. 59.7 % of the cases with AIS 1 and 2 minor/moderate injuries, and 25 % with serious injuries, the severe and critically injured pedestrians are 9.7% and 5.6 %, respectively. It was found that head and lower extremities were, again, the body parts most frequently injured. From the clinical documentation in Wujing hospital we noted that the head injury patterns

are skull fractures and brain injuries, including cerebral concussion, lacerations, contusion, and intracranial hematoma. The common thorax injury patterns are rib fractures with hemoth and pneumoth. The leg injuries are more frequent than upper thigh fractures including the toe, tibia, fibula fracture. The pelvis injuries are parenchyma contusion.

With the detailed information of GIDAS Hannover, the overall injury severity classified with AIS code is summarized in Table 4B. 90.8% of the cases with MAIS 1 and 2 minor/moderate injuries, and 6.2% with MAIS 3 serious injuries. The severe and critically injured pedestrians (MAIS 5/6) are 2.1%.

Table 4A: Injury severity of pedestrians in selected 72 cases (Changsha)

| Injury Severity | MAIS | Number | %    |
|-----------------|------|--------|------|
| Minor           | 1    | 3      | 4.2  |
| Moderate        | 2    | 40     | 55.5 |
| Serious         | 3    | 18     | 25.0 |
| Severe          | 4    | 7      | 9.7  |
| Critical        | 5    | 4      | 5.6  |
| Fatal           | 6    | 0      | 0    |
| Total           | -    | 72     | 100  |

Table 4B: Injury severity of pedestrians in collected 206 cases (GIDAS Hannover)

| Injury Severity | MAIS | Number | %    |
|-----------------|------|--------|------|
| Minor           | 1    | 231    | 68.3 |
| Moderate        | 2    | 116    | 22.5 |
| Serious         | 3    | 36     | 6.2  |
| Severe          | 4    | 7      | 1.0  |
| Critical        | 5    | 13     | 1.6  |
| Fatal           | 6    | 4      | 0.5  |
| Total           | -    | 407    | 100  |

The compared injury distribution between Changsha /Hannover are shown the different sampling criteria, the data of Hannover consider the whole injury distribution in a statistical manner (minor to fatal). Changsha cases are representing the situation of a hospital, therefore directly died persons at the scene (MAIS 6) are not included.

### ISS value and analysis

The ISS value was calculated for the selected 72 cases from Changsha and 206 cases from GIDAS. Table 5 (Appendix) presented the calculated ISS values.

The injury severity grade ISS is a good predictor for the whole severity of the injured body related to the complexity of treatment and the outcome of survival. It can be seen that the german injured pedestrians has a better injury outcome, 91.7% suffered ISS<10. A polytraumatized victim with risky treatment starts at

ISS values above 15. In Germany those cases can be seen in 3.3% compared to China in 16.6%.

### **Analysis of injury severity by body regions in age groups**

Table 6 (Appendix) presented distribution of injury severity by pedestrian body regions, and Table 7 (Appendix) presented Distribution of injury severity by age group.

In all age groups the injury risk is very high for the China situation compared to the German situation. Nearly three-quarter of the Hannover pedestrians suffered injury severity grades MAIS 1 only, except the older age group of >60 years old ( 54.8%). 26.0% were MAIS 3+ injured. Compared to this 62.5% of the greater 60 years old pedestrians were MAIS 3+ injured in Changsha. A very low number of minor injured pedestrians could be registered there in all age groups.

### **Correlation of skull-brain injuries with physical parameters**

From head-windscreen impact, the received contact force of the HBM-head model is 4.4kN and the intracranial pressure maximum 250kPa. From head-A-pillar impact, the received contact force of the HBM-head model is average 16kN and the intracranial pressure maximum 815kPa.

The skull fracture appeared in an A-pillar impact, and there is lower risk of skull fracture in windscreen impact. The intracranial pressure maximum 250kPa from windscreen impact could correlate with minor coup/countercoup injuries. The intracranial pressure maximum 815kPa from A-pillar impact could predict severe coup/countercoup injuries.

The simulation of head-brain impacts indicated that coup/countercoup pressure, Von Mises and shear stress were important physical parameters to evaluate the brain injury risk.

The correlation of skull fracture with the predicted physical parameters can be determined. Thereby, we can finally obtain reasonable advices to improve safety design of car frontal structure for minimizing the risk of pedestrian head injuries.

## **DISCUSSION**

### **Causation of Injuries**

The vehicle traffic accidents steeply increased in the past decade worldwide therefore in China as well as in Germany. But the injury situation related to traffic accidents seems to have different pictures for Germany and China. The annually fatalities in the reported

accidents of China increased from 49,271 in 1990 to 107,000 in 2004. The road traffic authority made large efforts to control incidence of the accidents, but the tendency of the accident growth is still a critical issue in China. Particularly, the fatalities of vulnerable road users formed a main proportion of all reported fatalities in traffic accidents. For instance about 12,500 pedestrians were killed in 1990, and 26,000 in 2001, which accounted for about 26% of all traffic fatalities annually. Compared to this, for Germany the number of casualties could be reduced over the last 30 years continuously to a total number of currently 5361 in 2005. The percentage of fatal pedestrians built 13% on that total number.

The present study is based upon an analysis of 403 accidents in urban area of Changsha in China and the area of Hannover in Germany. The evaluation method was described and the available accident data were analyzed. The used samples are small, but as a preliminary study the presented methodology for an in comparison of different in-depth accident studies could be used for comparison of the injury risk and injury outcome for different countries. Such methodology can be used for further studies with new collection of accident data in the area and special research issues.

It was found that the present results are quite comparable with results from studies by other researchers. For instance, the pedestrian accident is a common problem in both motorized countries and motorizing countries, which occur frequently in city build up area, but the injury risk for pedestrians in Germany can be seen as much less danger as in China. On the other hand the combined results of the in-depth analysis of the two different areas of China and Germany are shown major resources for further countermeasures on car safety developments, i.e. young and old pedestrians needs to focus in Germany, adult pedestrians 20 to 50 years old needs to protect more in China. The finding of the frequency in age distribution is quite different from that in other motorized countries. Child pedestrian accidents accounted for 25.3% in the USA, 33.1% in Europe, and 34.2 in Japan. A further study is needed to identify the factors which affect the different results.

Pedestrian accident analyses have been conducted worldwide in the past four decades[8-11]. Pedestrian impact conditions and injury outcomes were identified from these studies. The findings of the distribution of pedestrian injuries to different body segments are compared between the results from this study and results from published studies by other researchers worldwide as presented in Table 6, showing the distribution of injured body regions (100%). As a common tendency, the head and the lower extremities

have been found to be the most frequently injured body regions.

The analysis of pedestrian accidents in Changsha indicated that motorcycles and passenger cars are most frequently involved in vehicle pedestrian accidents compared to Germany where the major collision partner of a pedestrian is a car (80.6%). 43.9 % of the accidents in Changsha are motorcycle-pedestrian collisions, and 30.3 %, passenger cars. In the EU countries, the number of pedestrian struck by passenger cars is around 60% to 85% of the reported vehicle pedestrian accidents[6], and 56% of the reported pedestrian accidents are caused by passenger cars in the USA. Due to the difference of involved vehicles from country to country, the priority of safety countermeasures should be given considering the frequency of involved vehicles [13-16].

### Counter-measures

Even that for Germany a good reduction of the number of fatalities and severe injured pedestrians can be registered over the last decade further measurements for safety can be seen as important, the head injury risk and the risk of lower extremities should be focussed in the future.

There is great potential of reduction of the accidents and fatalities in China by enhancing safety consciousness of all road users, improving the traffic administration, and strictly implementing traffic laws.

It is necessary to point out that a large amount of the accidents resulted from people's mistake. The accidents and accident casualties mainly attributed to the causation factors. This study considered not the aspects of causation, but in-depth-analysis could be also a good tool for such research in different countries.

### Limitations

It is also noticed that the limitations existed in this study. The data sources partly reflects the real situations of pedestrians in traffic accidents in Changsha and Hannover and not in the whole countries of China and Germany. On the other hand, the used samples are influenced by their specific sampling criteria being different for Changsha and Hannover. For Changsha in some cases the medical records were not complete due to that the injured pedestrians left the hospital without the continual cure and the reports could not point out whether they have healed and in the sample not those fatalities were included which died directly on the scene. Another problem existed in Changsha on the medical records provided comprehensive data on the injuries, they seldom provided exact details of the locations and extent of the injuries, and it bring up a

difficulty to classify the injuries according to the AIS code. Compared to this the data of GIDAS Hannover are comprehensive and give information on every issue of accident and injury details [6].

## 5 CONCLUSIONS

Pedestrian accidents represent a group of vulnerable road users with high risk of unprotection, and in relation with the importance of pedestrians within the traffic of a country therefore a high priority should be given to this road user group in research of safe urban transportation.

About over two thirds of injured pedestrians are male pedestrians. The exposure of injury risks to elderly people is much higher than that to younger pedestrians. This seems to be relevant for the German situation where the major injured pedestrians could be seen. In Changsha the main focus has to be given to the adults in the age of 20 to 50 years of age. In urban area of Changsha motorcycles and passenger cars are most frequently involved in vehicle pedestrian accidents.

The head and lower extremity injuries are the predominant types of pedestrian injuries. Chest and pelvis were frequent injured, then followed by abdomen injuries, whereas injuries to upper extremities and neck were relatively infrequent. It is necessary to give the priority of injury prevention to the head and lower extremities. Meanwhile in China many European Cars are driven, therefore it can be expected that in some years the same safety standard and injury risk will be approached. Further in-depth studies may identify this common approach.

## 6 ACKNOWLEDGMENT

This study is sponsored by the Natural Science Foundation of China (NSFC 10472031). The authors would like to thank Mr. Zhimin Liu, Mr. Chao Zhang, the Officer of Traffic Police in Changsha, and Prof. Dietmar Otte, Hannover Medical University, for provided accident data.

## REFERENCE

- [1] Statistics of Road Traffic Accidents in P.R. of China. Traffic Administration, the Ministry of Public Security, 2005.
- [2] Statistcal Data of the Statistical Bureau Germany, Wiesbaden 2005.
- [3] Wang Z G. 'Mechanisms for Occurrence of Road Traffic Injuries'. *Chinese Journal of Traumatology*. 1999. 15 : 85-86.

- [4] Yang J K. (1997). ‘Injury Biomechanics in Car–Pedestrian Collisions: Development, Validation and Application of Human–Body Mathematical Models’. Thesis for the Degree of Doctor of Philosophy. Department of Injury Prevention Chalmers University of Technology, Gothenburg, Sweden.
- [5] AAAM (1998). ‘Abbreviated Injury Scale – 1990 Revision’. Association for the Advancement of Automotive Medicine, Des Plaines, IL, USA.
- [6] Yang, JK, Yao, JF, Wan, X, Xu, W (2004) ‘Simulation of Human Neck Responses to Dynamic Load Associated with Car Collisions Using a Head-Neck FE Model’, *The 2<sup>nd</sup> World Congress of Chinese Biomedical Engineers (WCCBME)*, 27-29 September 2004, Beijing China.
- [7] Yang, J.K., Xu, W., Wan, X.M. Development and Validation of a Head2Neck Finite Element Model for the Study of Neck Dynamic Responses in Car Impact. *Journal of Hunan University (Natural Sciences)*, Vol. 32, No. 2, 2005, pp. 6-12.
- [8] Otte D, Krettek C, Brunner H, Zwipp H. (2003) ‘Scientific Approach and Methodology of a New In-Depth-Investigation Study in Germany so called GIDAS’, *Proceedings of the 18th ESV Conference*, Nagoya, Japan, Paper No. 161.
- [9] Otte D. (1999) ‘Severity and Mechanism of Head Impacts in Car to Pedestrian Accidents’, *Proceedings of International IRCOBI Conference on Biomechanics Impacts*, Barcelona, Spain, pp. 329-341.
- [10] D Otte, T Pohlemann. (2001) ‘Analysis and Load Assessment of Secondary Impact to Adult Pedestrians after Car Collisions on Roads’, *Proceedings of the International IRCOBI Conference on the Biomechanics of Impacts*, Isle of Man, United Kingdom, pp. 143-157.
- [11] Y Mizuno, H Ishikawa. (2001). ‘Summary of IHRA Pedestrian Safety WG Activities-Proposed Test Methods to Evaluate Pedestrian Protection Afforded by Passenger Cars’. The 17<sup>th</sup> ESV Conference, June 4-7, 2001, Amsterdam, The Netherlands.
- [12] Danner M, Langwieder K. and Wachter W. Injuries to Pedestrians in Real Accidents and Their Relation to Collision and Car Characteristics’. Department of Automotive Engineering Association of German Automobile Insurerans.
- [13] Li L, Yang J K, Li W Q, FANG H F. ‘A Study of Pedestrian Injuries in Traffic Accidents in Changsha of China’. *Journal of Hunan University*.2002.Vol.29:15-23.
- [14] NHTSA (1999) ‘Traffic safety facts - pedestrian, Report, National Highway Traffic Safety Administration’, Department of Transportation, Washington DC, U.S.A.
- [15] EEVC (1994). ‘Proposals for Methods to Evaluate Pedestrian Protection for Passenger Cars’. Report, European Experimental Vehicle Committee, working group 10.
- [16] ETSC (1997). ‘A Strategic Road Safety Plan for the European Union’. *European Transport Safety Council*, Brussels.

## APPENDIX

Table 3A: Distribution of pedestrian age and gender in traffic accidents (Changsha)

| Age \ Gender | 0-15yr |      | 16-60yr |      | >60yr  |      | Total  |      |
|--------------|--------|------|---------|------|--------|------|--------|------|
|              | Number | %    | Number  | %    | Number | %    | Number | %    |
| Female       | 13     | 40.6 | 101     | 30.5 | 19     | 47.5 | 133    | 33.0 |
| Male         | 19     | 59.4 | 230     | 69.5 | 21     | 52.5 | 270    | 67.0 |
| Total        | 32     | 100  | 331     | 100  | 40     | 100  | 403    | 100  |

Table 3B: Distribution of pedestrian age and gender in traffic accidents (GIDAS Hannover)

| Age \ Gender | 0-15yr |      | 16-60yr |      | >60yr  |      | Total  |      |
|--------------|--------|------|---------|------|--------|------|--------|------|
|              | Number | %    | Number  | %    | Number | %    | Number | %    |
| Female       | 49     | 38.3 | 89      | 48.7 | 56     | 61.6 | 194    | 48.1 |
| Male         | 79     | 61.7 | 97      | 51.3 | 37     | 38.4 | 213    | 51.9 |
| Total        | 128    | 100  | 186     | 100  | 93     | 100  | 407    | 100  |

Table 5: Correlation of injury severity with ISS value

| ISS   | Changsha data |      | GIDAS data |      | Severity |
|-------|---------------|------|------------|------|----------|
|       | N             | %    | N          | %    |          |
| < 10  | 53            | 73.6 | 350        | 91.7 | Minor    |
| 10-15 | 7             | 9.7  | 28         | 5.0  | Moderate |
| 16-19 | 7             | 9.7  | 5          | 0.8  | Serious  |
| 20-39 | 5             | 6.9  | 11         | 1.4  | Severe   |
| 40-66 | 0             | 0    | 5          | 0.6  | Critical |
| 75    | 0             | 0    | 4          | 0.5  | Fatal    |
| Sum   | 72            | 100  | 403        | 100  | -        |

Table 6A: Distribution of injury severity by pedestrian body regions (Changsha)

| Injury severity<br>Body segment | Slight, AIS<3<br>(N= 43 ) |      | Serious, AIS=3<br>(N= 18 ) |      | Fatal, AIS>3<br>(N= 11 ) |      | Total<br>(N= 72 ) |     |
|---------------------------------|---------------------------|------|----------------------------|------|--------------------------|------|-------------------|-----|
|                                 | Injury                    | %    | Injury                     | %    | Injury                   | %    | Injury            | %   |
| Head                            | 23                        | 67.6 | 2                          | 5.9  | 9                        | 26.5 | 34                | 100 |
| Face                            | 9                         | 100  | 0                          | 0    | 0                        | 0    | 9                 | 100 |
| Lower extremities               | 24                        | 66.7 | 12                         | 33.3 | 0                        | 0    | 36                | 100 |
| Upper extremities               | 3                         | 100  | 0                          | 0    | 0                        | 0    | 3                 | 100 |
| Chest                           | 6                         | 66.7 | 3                          | 33.3 | 0                        | 0    | 9                 | 100 |
| Pelvis                          | 3                         | 100  | 0                          | 0    | 0                        | 0    | 3                 | 100 |
| Abdomen                         | 3                         | 60   | 2                          | 40   | 0                        | 0    | 5                 | 100 |
| Neck                            | 0                         | 0    | 0                          | 0    | 0                        | 0    | 0                 | 0   |

Table 6B: Distribution of injury severity by pedestrian body regions (GIDAS Hannover)

| Injury severity<br>Body segment | Slight, AIS<3<br>(N= 347 ) |      | Serious, AIS=3<br>(N=36 ) |     | Fatal, AIS>3<br>(N=24) |      | Total<br>(N= 407) |     |
|---------------------------------|----------------------------|------|---------------------------|-----|------------------------|------|-------------------|-----|
|                                 | Number                     | %    | Number                    | %   | Number                 | %    | Number            | %   |
| Head                            | 192                        | 94.0 | 7                         | 1.9 | 15                     | 3.1  | 214               | 100 |
| Lower extremities               | 232                        | 92.2 | 30                        | 7.5 | 1                      | 0.3  | 263               | 100 |
| Upper extremities               | 144                        | 97.5 | 6                         | 2.5 | 0                      | 0    | 150               | 100 |
| Chest                           | 62                         | 85.8 | 6                         | 5.2 | 13                     | 9.0  | 81                | 100 |
| Pelvis                          | 54                         | 97.7 | 1                         | 0.4 | 2                      | 1.9  | 57                | 100 |
| Abdomen                         | 24                         | 91.7 | 1                         | 1.0 | 3                      | 7.3  | 28                | 100 |
| Neck                            | 15                         | 87.4 | 0                         | 0   | 3                      | 12.6 | 18                | 100 |

Table 7A: Distribution of injury severity by age group (Changsha)

| MAIS  | Age | 0-15yr |      | 16-60 yr |      | >60 yr |      | Total  |      |
|-------|-----|--------|------|----------|------|--------|------|--------|------|
|       |     | Number | %    | Number   | %    | Number | %    | Number | %    |
| 1     |     | 1      | 16.7 | 2        | 3.4  | 0      | 0    | 3      | 4.2  |
| 2     |     | 1      | 16.7 | 35       | 60.3 | 3      | 37.5 | 39     | 54.2 |
| 3     |     | 1      | 16.7 | 12       | 20.7 | 5      | 62.5 | 18     | 25   |
| 4     |     | 2      | 33.3 | 6        | 10.3 | 0      | 0    | 8      | 11.1 |
| 5     |     | 1      | 16.7 | 3        | 5.2  | 0      | 0    | 4      | 5.6  |
| 6     |     | -      | -    | -        | -    | -      | -    | -      | -    |
| Total |     | 6      | 100  | 58       | 100  | 8      | 100  | 72     | 100  |

Table 7B: Distribution of injury severity by age group (GIDAS Hannover)

| Age<br>MAIS | 0-15yr |      | 16-60  |      | >60    |      | 总计     |      |
|-------------|--------|------|--------|------|--------|------|--------|------|
|             | Number | %    | Number | %    | Number | %    | Number | %    |
| 1           | 81     | 72.4 | 110    | 71.6 | 40     | 54.8 | 231    | 68.3 |
| 2           | 40     | 23.2 | 47     | 18.8 | 29     | 29.3 | 116    | 22.5 |
| 3           | 6      | 4.0  | 17     | 6.0  | 13     | 10.0 | 36     | 6.2  |
| 4           | 0      | 0    | 3      | 0.9  | 4      | 2.6  | 7      | 1.0  |
| 5           | 1      | 0.4  | 7      | 2.1  | 5      | 2.3  | 13     | 1.6  |
| 6           | 0      | 0    | 2      | 0.5  | 2      | 1.1  | 4      | 0.5  |
| Total       | 128    | 100  | 186    | 100  | 93     | 100  | 407    | 100  |

Table 8: Comparison of percentage distribution of pedestrian injuries by body region

| Body region       | China<br>(Changsha)(%) | GIDAS<br>(%) | Europe<br>(%) | Australia<br>(%) | Japan<br>(%) | USA<br>(%) |
|-------------------|------------------------|--------------|---------------|------------------|--------------|------------|
| Head              | 31.5                   | 26,4         | 29.8          | 39.3             | 28.6         | 32.7       |
| Face*             | 5.8                    | -            | 5.3           | 3.7              | 2.4          | 3.7        |
| Neck              | 0.8                    | 2,2          | 1.8           | 3.1              | 4.5          | 0.0        |
| Chest             | 10.9                   | 10,0         | 11.6          | 10.4             | 8.5          | 9.5        |
| Abdomen           | 6.2                    | 3,5          | 3.8           | 4.9              | 4.8          | 7.7        |
| Pelvis            | 2.6                    | 7,0          | 7.9           | 4.9              | 4.5          | 5.3        |
| Upper extremities | 9.4                    | 18,5         | 8.1           | 8.0              | 9.0          | 7.9        |
| Lower extremities | 32.8                   | 32,4         | 31.3          | 25.8             | 37.2         | 33.3       |
| Unkown            | 0.0                    | -            | 0.5           | 0.0              | 2.1          | 0.0        |
| Total             | 100                    | 100          | 100           | 100              | 100          | 100        |

\* not distinguished from head injuries.

## PEDESTRIAN SAFETY ENHANCEMENT USING NUMERICAL METHODS

**Daniel Baumgartner**

**Daniel Marjoux**

**Remy Willinger**

ULP – University Louis Pasteur of Strasbourg  
France

**Emma Carter**

**Clive Neal-Sturgess**

BASC – University of Birmingham  
United Kingdom

**Luis Guerra**

**Luis Martinez**

INSIA – Institute for Automobile Research  
Spain

**Roger Hardy**

CIC – Cranfield Impact Centre  
United Kingdom

Paper Number 07-0426

### ABSTRACT

This study aims at investigating head injury mechanisms for brain injuries, subdural or subarachnoidal haematoma (SDH or SAH) and skull fractures in adult pedestrian real world accidents by in-depth accident analysis and accident numerical reconstruction. Nine accident cases were carried out using a multi-body system pedestrian and cars' models to acquire the head impact conditions such as head impact velocity, position and orientation against the car's bonnet or windscreen. These impact conditions were then imposed on a head, car's windscreen and bonnet finite element model in order to calculate different mechanical parameters that are sustained by each victim during the impact. These calculated head stresses, strains and energies were then correlated with the observed injury patterns and compared to existing and available head injury mechanisms and tolerance limits. The accident investigation reports and pedestrian kinematics before the head impact came from the University of Birmingham (United Kingdom), INSIA (Spain) and DaimlerChrysler (Germany). They were worked out in the framework of an FP6 Integrated Project on Advanced Protection Systems (APROSYS). The head, the bonnet and the windscreen FEM, the injury mechanisms and tolerance limits have been developed at the University of Strasbourg (France) in a recent past. The reconstruction results show that the numerical tools employed predicted the observed injuries well. Nevertheless, it should be pointed out that the numerical tools used can only predict injuries reliably if both the pedestrian and vehicle side are modelled appropriately, i.e. with detailed finite element structures with well validated material and contact stiffness data. Brain

neurological injuries were well correlated with brain Von Mises stress. Brain contusions occurred through high brain pressures. Skull fractures and SDH or SAH were well correlated with the global strain energy of the skull and of the brain/skull interface respectively. It has been concluded that these results showed that such numerical models are good tools to predict human head injuries. They will therefore be useful to improve the head protection devices i.e. the design, the conception, the evaluation and the optimization of cars' windscreens and bonnets against well defined injury criteria.

### INTRODUCTION

In road traffic accidents involving cars and pedestrians, head injuries are one of the most common injury types and the main cause of severe fatalities. Therefore, a particular attention has to be paid to the pedestrians' head protection in road traffic in order to reduce these severe fatalities. Among others, efforts can be done to improve the protection ability of the cars' windscreens and bonnets. The following described methodology, that has been led during an Integrated Project of the 6<sup>th</sup> Framework (Advanced Protective Systems: APROSYS), was designed to provide human head injuries numerical prediction tools.

### METHODOLOGY

After having replicated the pedestrian's body kinematics for different real world accident cases by using MADYMO software, it will be focused in that work on the head impact against the considered part of the striking car (i.e. car's windscreen or bonnet). For that purpose we will use a finite element model (FEM) of the human head as well as one of the car's windscreen and bonnet. These different real world accidents numerical reconstructions will allow us to calculate a great deal of mechanical parameters the victims will sustain. These calculated mechanical parameters will then be compared to existing human head injury mechanisms and tolerance limits. Indeed, it will be showed that such numerical models are able to predict head injuries. In fact, it will be interesting to compare the predicted injuries to the observed injuries in order to demonstrate the ability of such numerical models to predict injuries. More generally, it will be shown how powerful such numerical tools can be in order to design, to evaluate, to validate and to optimise car structures against physiopathological injury criteria.

## **MATERIALS**

### **FEM of the human head**

The FEM of the human head that will be used in that part the study is the one developed at the University Louis Pasteur of Strasbourg in the past few years. That model is detailed in [KAN 97] in its first version as well as is in [WIL 03] in its more updated version. It is usually called the ULP FEM of the human head. A much more detailed description is proposed below. Such numerical methods and models have been largely used in the past few years by [LOV 75], [GEN 85], [THI 90], [MEN 92], [ZHO 96], [AND 00], [KIN 03] and [TAK 03]. The ULP FEM of the head is three dimensional with a continuous mesh. The meshing of the model has been achieved by using the HYPERMESH software. It contains 13208 elements divided in 10395 brick elements and 2813 shell elements and it weights 4800 g. This FEM includes the main anatomical components of the head which are illustrated in terms of mesh properties and mechanical behaviour in Table 1: the falx of the brain and the tentorium of the cerebellum, the brain/skull interface, the brain and the cerebellum, the skull, the face and the surrounding skin. The Table 1 gives also an illustration of each anatomical component which is modelled. The ULP FEM of the head is validated against experimental data from [NAH 77] and [TRO 92] in terms of brain accelerations and pressures and against experimental data from [YOG 94] regarding skull bones fractures. The ULP FEM of the head is especially validated in case of long duration high dampened impacts that last more than 15 ms and that usually reveal an important rotational acceleration component. This validation is refined by [BAU 01] who modelled the cerebral spinal fluid flow through the brain/skull interface and the lateral ventricles by introducing into the FEM a fluid solid coupling behaviour thanks to an arbitrary Eulerian Lagrangian formulation. That model has been developed by using the RADIOSS CRASH software. Of particular importance and rarely modelled, it must be underlined that the ULP FEM of the human head is able to predict skull fracture thanks to a Tsai Wu criterion. Such a criterion is based on the maximal tension and compression stresses that are sustained in shell elements. In terms of finite elements, if an element reaches the allowed maximal values, it is deleted. This means that it is taken out of the model from the next time step. That failure criterion is also detailed in Table 1.

### **FEM of the car's windscreen**

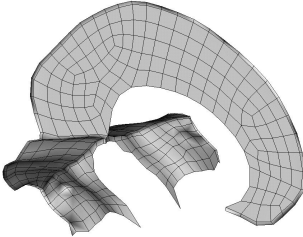
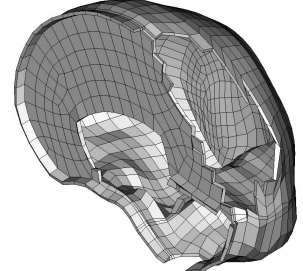
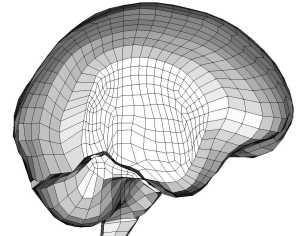
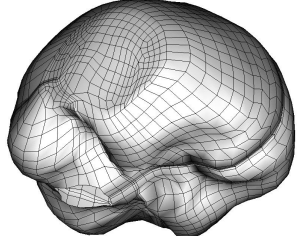
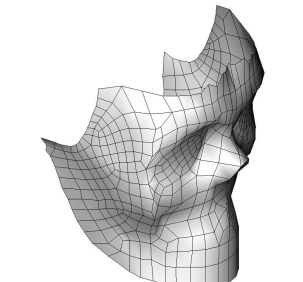
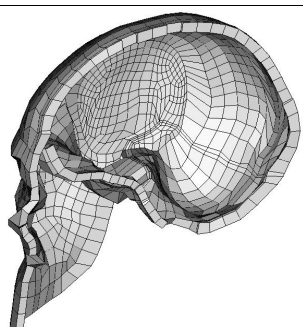
In order to represent a car's windscreen a (1200 mm x 800 mm) rectangular surface is regularly

meshed by using 1536 three layered composite shell elements. Both external laminated glass layers which have a thickness of 2.2 mm are linked together through an internal poly vinyl butyl membrane which has a thickness of 1 mm. The three layered composite shell elements of the windscreen's border are fixed to a rigid frame in order to represent the car's mass and inertia. These border elements are free to translate but they are fixed in their three rotational degrees of freedom. Eventually added masses are set on these border elements of the windscreen in order to represent the mass and the inertia of the car. Nevertheless, that added mass has no significant influence on the dynamic response of the head during the impact as shown in a recent internal study. The mechanical behaviour adopted for both external laminated glass layers of the windscreen is an elastic plastic brittle law that allows rupture. The linking plastic membrane's mechanical behaviour is assumed to be linear elastic. Both mechanical behaviours rely on the experimental data determined by [HAV 75] and detailed in Table 2. The validation of the windscreen FEM is based on a comparison between the damages which are observed and predicted by the FEM in a specific and standard head impact configuration. This windscreen FEM relies on the one developed by [MUK 00].

### **FEM of the car's bonnet**

In order to model a car's bonnet, a (1200 mm x 1500 mm) rectangular surface has been regularly meshed by using 4500 shell elements. The thickness of each element is set to 1 mm. These shell elements' border are fixed to a rigid frame in order to represent the car's mass and inertia as it has been done for the windscreen. These border elements are free to translate but they are fixed in their three rotational degrees of freedom. Eventually added masses are set on these border elements of the car's bonnet in order to represent the mass and the inertia of the car. Nevertheless, that added mass has no significant influence on the dynamic response of the head during the impact as for the windscreen. The mechanical behaviour adopted for the car's bonnet shell elements is elastic plastic (Johnson Cook mechanical behaviour law) as detailed in Table 3 for one case. It must be underlined that the contact stiffness characteristics between the pedestrian head and the vehicle at the head impact spot were not available and were therefore roughly estimated through EuroNCAP test data on alternative impact points. Furthermore, the EuroNCAP impactor test data has not been available for the vehicles involved in the accidents GP001 and GP002 for example such that the test data of a similar vehicle was used in these cases – VW Audi A3 instead of VW Golf 3 and VW Polo respectively.

**Table 1.**  
**ULP FEM of the human head. Mesh properties and mechanical behaviour.**

| Anatomical Segment                                | Illustration  | Mesh  | Mechanical Behaviour    | Mechanical Characteristics  | Mechanical Characteristics   |
|---|---|---|-------------------------|---|--|
| Falx of the Brain and Tentorium of the Cerebellum |    | 471 shell elements                          | Linear Elastic          | e = 1 mm<br>$\rho = 1140 \text{ kg/m}^3$<br>$E = 31.5 \text{ MPa}$<br>$\nu = 0.45$  | /  |
| Brain/skull Interface                             |    | 2591 brick elements                         | Linear Elastic          | $\rho = 1040 \text{ kg/m}^3$<br>$E = 0.012 \text{ MPa}$<br>$\nu = 0.49$   | /  |
| Brain and Cerebellum                              |   | 5508 brick elements                         | Elastic Plastic         | $\rho = 1040 \text{ kg/m}^3$<br>$K = 1125 \text{ MPa}$<br>$G_0 = 0.049 \text{ MPa}$<br>$G_{inf} = 0.0167$<br>$\beta = 145 \text{ s}^{-1}$   | /  |
| Skull   |  | 1813 three layered composite shell elements | Elastic Plastic Brittle | <b>Cortical</b><br>e = 2 mm<br>$\rho = 1900 \text{ kg/m}^3$<br>$E = 15000 \text{ MPa}$<br>$\nu = 0.21$<br>$K = 6200 \text{ MPa}$<br>$UTS = 90 \text{ MPa}$<br>$UTC = 145 \text{ MPa}$ | <b>Trabecular</b><br>e = 3mm<br>$\rho = 1500 \text{ kg/m}^3$<br>$E = 4600 \text{ MPa}$<br>$\nu = 0.05$<br>$K = 2300 \text{ MPa}$<br>$UTS = 35 \text{ MPa}$<br>$UTC = 28 \text{ MPa}$ |
| Face  |  | 529 shell elements                          | Linear Elastic          | e = 10 mm<br>$\rho = 2500 \text{ kg/m}^3$<br>$E = 5000 \text{ MPa}$<br>$\nu = 0.23$   | /  |
| Skin  |  | 2296 brick elements                         | Linear Elastic          | $\rho = 1000 \text{ kg/m}^3$<br>$E = 16.7 \text{ MPa}$<br>$\nu = 0.42$  | /  |

**Table 2.**  
**FEM of the car's windscreen. Mechanical behaviour.**

| Structure | $\rho$<br>[kg/m <sup>3</sup> ] | E<br>[mm] | E<br>[GPa] | $\nu$ | $\epsilon_{rt}$ | $\epsilon_{mt}$ | $\sigma_{el}$<br>[MPa] |
|-----------|--------------------------------|-----------|------------|-------|-----------------|-----------------|------------------------|
| Glass     | 2400                           | 2.2       | 65         | 0.22  | 0.000615        | 0.00123         | 3.8                    |
| PVB       | 950                            | 1         | 50000      | 0.22  | /               | /               | /                      |

**Table 3.**  
**FEM of the car's bonnet example. Mechanical behaviour.**

| Structure | $\rho$<br>[kg/m <sup>3</sup> ] | E<br>[mm] | E<br>[GPa] | $\nu$ | a   | b   | n     | $\sigma_{max}$<br>[MPa] |
|-----------|--------------------------------|-----------|------------|-------|-----|-----|-------|-------------------------|
| Bonnet    | 2700                           | 1         | 69         | 0.3   | 120 | 567 | 0.623 | 345                     |

## Human head injury mechanisms and tolerance limits

### Introduction

A first step would be to define the injury types. Even this classification is not definitive due to terminology differences which may exist. The second step will be to define the injury parameters, i.e. the mechanical parameters which lead a type of injury. At this level several assumptions exist in the literature. Finally a threshold value for each injury parameter must be defined in order to become a tolerance limit to a specific injury. This difficult exercise is based either on cadaver tests, animal tests or more recently on accident reconstruction. Tolerance limits estimation on cadaver is restricted to skull fracture. Injury analysis based on animal tests is a critical issue because animal acceleration field, even scaled to the human dimension and mass will not lead to similar brain loading conditions due to the shape difference. Finally real world accident simulation is some times critical because of the lack of accident data accuracy.

### Human head injuries criteria

In order to demonstrate the ability of the previously described numerical tools to predict human head injuries, the calculated mechanical parameters can be compared to existing human head tolerance limits. In fact, human head injury mechanisms and tolerance limits can be obtained by using FEM as detailed in a great variety of past studies. In our specific study, the FEM of the human head developed at the University Louis Pasteur of Strasbourg and described previously has been used. That model has allowed us, in previous studies achieved by [WIL 03] and [WAR 80], to establish human head injury mechanisms and tolerance limits as follows:

- Brain contusions (CONT) occur when brain pressure reaches values of 200 kPa according to [WAR 80].
- Brain neurological injuries such as diffuse axonal injuries or haemorrhagic injuries (DAI) occur when brain Von Mises shearing stress

reaches values of 18 kPa (for moderate injuries (MOD DAI)) and 38 kPa (for severe injuries (SEV DAI)) according to [WIL 03].

- Subdural haematoma (SDH) or subarachnoidal haematoma (SAH) occur when the global strain energy of the brain/skull interface reaches values of 5500 mJ according to [WIL 03].
- Skull fractures (SF) occur when the global strain energy of the skull reaches values of 2200 mJ according to [WIL 03].

It must be kept in mind and strongly underlined that these injury mechanisms and tolerance limits are linked to a specific head FEM which is the one of ULP. It is common for other FEM to predict injuries thanks to other mechanical parameters like strains, displacements, or strain rates. It also usual for other FEM to use the same mechanical parameters as the ones proposed by ULP but with other values relatively to the tolerance limits. Indeed, the inferred tolerance limits are very sensible to the geometry of the model as well as to the mechanical behaviour of each anatomical feature which is modelled. The Table 4 reminds the different human head injuries mechanisms and tolerance limits. Indeed, it has been previously showed that FEM of the human head are able to predict injuries thanks to a correlation between calculated mechanical parameters on the one hand and injuries occurrence on the other hand ([WIL 03]). For each calculated mechanical parameters (which is a specific injury indicator) there exists a range of values for which:

- No specific injury is predicted.
- A specific injury is possible (but the victim can also remain uninjured).
- A specific injury is clearly predicted.

These different ranges are detailed in the Table 4. For example, if the calculated brain pressure remains under 160 kPa, no injury is predicted. If that calculated brain pressure is between 160 kPa and 240 kPa, it will not be possible to indicate if brain contusions will occur or not. Eventually, if the calculated brain pressure exceeds 240 kPa, brain contusions will be predicted without any doubt.

**Table 4.**  
**Human head tolerance limits ranges**

| <b>Calculated mechanical parameter and injury indicator</b> | <b>Injuries</b>                                   | <b>Uninjured</b> | <b>Possibly injured</b> | <b>Injured</b> |
|---|---|------------------|-------------------------|----------------|
| Brain pressure [kPa]  | Brain contusions (CONT)                           | < 160            | > 160<br>< 240          | > 240          |
| Brain Von Mises stress [kPa]                                | Brain moderate neurological injuries (MOD DAI)    | < 14             | > 14<br>< 22            | > 22           |
| Brain Von Mises stress [kPa]                                | Brain severe neurological injuries (SEV DAI)      | < 30             | > 30<br>< 46            | > 46           |
| Global strain energy of the brain/skull interface [mJ]      | Subdural or subarachnoidal haematoma (SDH or SAH) | < 4300           | > 4300<br>< 6500        | > 6500         |
| Global strain energy of the skull [mJ]                      | Skull fracture (SF)                               | < 1700           | > 1700<br>< 2700        | > 2700         |

### Real world accidents reconstruction

Nine real world accidents are considered in that study:

- One cyclist accident that has been collected and worked out at the University of Birmingham (BASC – United Kingdom) : BASC cyclist 001 (BC001). It has to be underlined that the cyclist did not wear any helmet. It is therefore possible to include such a vulnerable road user in that study and consider him as a pedestrian. In fact, from a head injury point of view, it is not critical to be a real pedestrian or another road traffic user. Nevertheless, if that cyclist would have worn a helmet, a helmet FEM would have been developed in order to reconstruct numerically that accident.
- Eight pedestrians' accidents that has been collected and worked out at the University of Birmingham (BASC – United Kingdom), DaimlerChrysler (GIDAS – Germany) and the Institute for Automobile Safety (INSIA – Spain) respectively:
  - BASC:
    - BASC pedestrian 002 (BP002)
    - BASC pedestrian 022 (BP022)
    - BASC pedestrian 023 (BP023)
  - GIDAS:
    - GIDAS pedestrian 001 (GP001)
    - GIDAS pedestrian 002 (GP002)
  - INSIA:
    - INSIA pedestrian 002 (IP002)
    - INSIA pedestrian 003 (IP003)
    - INSIA pedestrian 006 (IP006)

For each of these accident cases, one of the aims of the MADYMO software replication was to establish the relative position and velocity between the head and the windscreen or the bonnet of the striking car at the time of the head impact. The ULP FEM of the head is then positioned towards the windscreen or the bonnet in respect to the MADYMO software calculated position just before the head impact. The initial relative velocity between the head and the windscreen or the bonnet is then set on the nodes of the head on the hand and on the nodes of the windscreen or the bonnet on the other hand. That numerical analysis is done thanks to the RADIOSS CRASH finite element code. The pre processing and the post processing is achieved on a SUN SUNBLADE 150 workstation. The engine is running on a DEC ALPHA SERVER. Each accident case is run over a duration of thirty milliseconds. Such a running duration corresponds to a CPU time of eight hours approximately. The different mechanical parameters that are calculated during the head impact are the following:

- Brain pressure.
- Brain Von Mises shearing stress.
- Global strain energy of the brain/skull interface.
- Global strain energy of the skull.
- Deleted elements of the skull (in order to check the ability of the model to predict skull fractures).

It is important to notice that for some of these cases, a secondary ground impact occurred (BP002, BP022, BP023, GP001 and GP002). It is possible for that secondary ground impact to generate injuries too. In the undergoing study, that impact is

not presented. It remains a perspective for ongoing studies. Thus, an observed injury that may not be predicted by the numerical tools that are developed in that study may occur in the secondary ground impact. This has obviously to be checked in future studies and compared to the first impact on the vehicle's windscreen or bonnet.

## RESULTS

### Introduction

For each accident case, a table shows the calculated mechanical parameters that lead to the predicted injuries as well as the observed injuries. If the observed injury is indeed predicted, a green square appears. And if the observed is not predicted, a red square appears. Moreover, if a star appears in the predicted injury column, this means that it is not really possible to decide whether or not the injury is predicted: there could be an injury but there could also not be an injury

### BASC cyclist 001 (BC001)

**Table 5.**  
**BC001 numerical simulation results.**

| Calculated mechanical parameter                        | Maximal value | Observed injury | Predicted injury |
|--|---------------|-----------------|------------------|
| Brain pressure [kPa]                                   | 150           | NO CONT         | NO CONT          |
| Brain Von Mises stress [kPa]                           | 55            | SEV DAI         | SEV DAI          |
| Global strain energy of the brain/skull interface [mJ] | 2923          | SAH             | NO SAH           |
| Global strain energy of the skull [mJ]                 | 790           | SF              | NO SF            |

The Table 5 shows the results of the numerical accident reconstruction of case BC001. In that cyclist accident case, the numerical model predicts well the brain neurological injuries (which are severe) but is unable to predict the subarachnoidal haematoma as well as the skull fracture. Both these injuries can not occur in the secondary ground impact since such an impact is not mentioned in the accident report. Moreover, the model represents well the absence of injuries as brain contusion in that case.

### BASC Pedestrian 002 (BP002)

**Table 6.**  
**BP002 numerical simulation results.**

| Calculated mechanical parameter                        | Maximal value | Observed injury | Predicted injury |
|--|---------------|-----------------|------------------|
| Brain pressure [kPa]                                   | 130           | CONT            | NO CONT          |
| Brain Von Mises stress [kPa]                           | 25            | SEV DAI         | MOD DAI          |
| Global strain energy of the brain/skull interface [mJ] | 2261          | SAH             | NO SAH           |
| Global strain energy of the skull [mJ]                 | 2167          | SF              | SF*              |

The Table 6 shows the results of the numerical accident reconstruction of case BP002. In that pedestrian accident case, it seems that the brain contusions and severe neurological injuries as well as the subarachnoidal haematoma are linked to the secondary ground impact since the first impact simulation does not predict these injuries. In fact, such a secondary ground impact is mentioned in the accident report. Nevertheless, the observed skull fracture is well predicted by the simulation even if it could be possible for the victim not to sustain skull fractures according to the prediction criterion.

### BASC pedestrian 022 (BP022)

The Table 7 shows the results of the numerical accident reconstruction of case BP022. In that pedestrian accident case, the victim sustained brain contusions, brain severe neurological injuries, a subdural haematoma and a skull fracture. Nevertheless, none of these injuries is predicted by the model. Brain moderate neurological injuries are possible but not sure. Therefore, it seems clear that the whole injuries sustained by that victim may be linked to the secondary ground impact which is mentioned in the accident report. Another hypothesis could be that the complete accident reconstruction process is wrong and led to wrong inputs for the FEM of the human head, the car's windscreen and the car's bonnet. In fact, wrong data may have been collected on the accident scene or badly interpreted.

**Table 7.**  
**BP022 numerical simulation results.**

| Calculated mechanical parameter                        | Maximal value | Observed injury | Predicted injury |
|--|---------------|-----------------|------------------|
| Brain pressure [kPa]                                   | 110           | CONT            | NO CONT          |
| Brain Von Mises stress [kPa]                           | 18            | SEV DAI         | MOD DAI*         |
| Global strain energy of the brain/skull interface [mJ] | 1601          | SDH             | NO SDH           |
| Global strain energy of the skull [mJ]                 | 461           | SF              | NO SF            |

**BASC pedestrian 023 (BP023)**

**Table 8.**  
**BP023 numerical simulation results.**

| Calculated Mechanical parameter                        | Maximal value | Observed injury | Predicted injury |
|--|---------------|-----------------|------------------|
| Brain pressure [kPa]                                   | 1590          | CONT            | CONT             |
| Brain Von Mises stress [kPa]                           | 80            | SEV DAI         | SEV DAI          |
| Global strain energy of the brain/skull interface [mJ] | 21737         | NO SDH          | SDH              |
| Global strain energy of the skull [mJ]                 | 25642         | SF              | SF               |

The Table 8 shows the results of the numerical accident reconstruction of case BP023. In that pedestrian accident case, each specific observed injury is predicted by the simulation shall it be brain contusions, severe brain neurological injuries or skull fractures. Besides, the model predicts a subarachnoidal or subdural haematoma whereas such a vascular injury is not observed.

**GIDAS pedestrian 001 (GP001)**

**Table 9.**  
**GP001 numerical simulation results.**

| Calculated mechanical parameter                        | Maximal value | Observed injury | Predicted injury |
|--|---------------|-----------------|------------------|
| Brain pressure [kPa]                                   | 65            | NO CONT         | NO CONT          |
| Brain Von Mises stress [kPa]                           | 10            | NO DAI          | NO DAI           |
| Global strain energy of the brain/skull interface [mJ] | 651           | NO SDH          | NO SDH           |
| Global strain energy of the skull [mJ]                 | 1618          | NO SF           | NO SF            |

The Table 9 shows the results of the numerical accident reconstruction of case GP001. In that pedestrian accident case, no injuries are observed. That fact is well represented by the impact simulation. It has to be noticed that a secondary ground impact is mentioned in the accident report. It will therefore be important to check whether or not that secondary ground impact generates injuries even if the victim did not sustain any injury.

**GIDAS pedestrian 002 (GP002)**

**Table 10.**  
**GP002 numerical simulation results.**

| Calculated mechanical parameter                        | Maximal value | Observed injury | Predicted injury |
|--|---------------|-----------------|------------------|
| Brain pressure [kPa]                                   | 126           | NO CONT         | NO CONT          |
| Brain Von Mises stress [kPa]                           | 16            | MOD DAI         | MOD DAI*         |
| Global strain energy of the brain/skull interface [mJ] | 2305          | NO SDH          | NO SDH           |
| Global strain energy of the skull [mJ]                 | 4818          | NO SF           | SF               |

The Table 10 shows the results of the numerical accident reconstruction of case GP002. In that pedestrian accident case, the model predicts well the absence of brain contusions and subarachnoidal or subdural haematoma. None skull fracture is observed but this is not predicted in the impact simulation since the impact simulation predicts a skull fracture which is not observed in reality. Moreover, the moderate brain neurological injuries are well predicted by the simulation even if it could be possible for the victim to not sustain such an injury.

**INSIA pedestrian 002 (IP002)**

**Table 11.**  
**IP002 numerical simulation results.**

| Calculated mechanical parameter                        | Maximal value | Observed injury | Predicted injury |
|--|---------------|-----------------|------------------|
| Brain pressure [kPa]                                   | 100           | NO CONT         | NO CONT          |
| Brain Von Mises stress [kPa]                           | 18            | MOD DAI         | MOD DAI*         |
| Global strain energy of the brain/skull interface [mJ] | 225           | NO SDH          | NO SDH           |
| Global strain energy of the skull [mJ]                 | 1258          | NO SF           | NO SF            |

The Table 11 shows the results of the numerical accident reconstruction of case IP002. In that pedestrian accident case, the only injury that is sustained by the victim (i.e. moderate brain neurological injuries) is well predicted by the model. Moreover, the model predicts well the absence of brain contusions, subarachnoidal or subdural haematoma as well as skull fractures. None secondary ground impact is mentioned in the accident report.

**INSIA pedestrian 003 (IP003)**

The Table 12 shows the results of the numerical accident reconstruction of case IP003. In that pedestrian accident case, the only injury that is sustained by the victim (i.e. moderate brain neurological injuries) is predicted by the model but is only predicted in a severe range (which is possible but not yet sure). Moreover, the model predicts well the absence of brain contusions, subarachnoidal or subdural haematoma as well as

skull fractures. None secondary ground impact is mentioned in the accident report.

**Table 12.**  
**IP003 numerical simulation results.**

| Calculated mechanical parameter                        | Maximal value | Observed injury | Predicted injury |
|--|---------------|-----------------|------------------|
| Brain pressure [kPa]                                   | 88            | NO CONT         | NO CONT          |
| Brain Von Mises stress [kPa]                           | 35            | MOD DAI         | SEV DAI*         |
| Global strain energy of the brain/skull interface [mJ] | 1176          | NO SDH          | NO SDH           |
| Global strain energy of the skull [mJ]                 | 233           | NO SF           | NO SF            |

**INSIA pedestrian 006 (IP006)**

**Table 13.**  
**IP006 numerical simulation results.**

| Calculated mechanical parameter                        | Maximal value | Observed injury | Predicted injury |
|--|---------------|-----------------|------------------|
| Brain pressure [kPa]                                   | 110           | NO CONT         | NO CONT          |
| Brain Von Mises stress [kPa]                           | 15            | MOD DAI         | MOD DAI*         |
| Global strain energy of the brain/skull interface [mJ] | 1270          | NO SDH          | NO SDH           |
| Global strain energy of the skull [mJ]                 | 530           | NO SF           | NO SF            |

The Table 13 shows the results of the numerical accident reconstruction of case IP006. In that pedestrian accident case, the only injury that is sustained by the victim (i.e. moderate neurological injuries) is well predicted by the model. The prediction is possible but not yet sure. Moreover, the model predicts well the absence of brain contusions, subarachnoidal or subdural haematoma

as well as skull fractures. None secondary ground impact is mentioned in the accident report.

## **DISCUSSION**

### **Brain contusions**

Three accident victims sustained brain contusions. One of these contusions was well predicted by the accident numerical simulation whereas two of them were not predicted. Nevertheless in both cases where the simulation did not predict brain injuries, a secondary ground impact occurred. It is therefore possible that the secondary ground impact was responsible for that kind of injury. Besides, six victims did not suffer from brain contusions and this was very well predicted by the accident numerical reconstruction for each of these six cases.

### **Brain neurological injuries**

Only one victim did not suffer from brain neurological injuries shall they be moderate or severe. The accident numerical reconstruction predicted well the lack of injury in that specific case. Four accident victims sustained some moderate brain neurological injuries. For all these cases, the accident numerical reconstruction predicted moderate brain neurological injuries. Four victims suffered from brain severe neurological injuries. For two of them the model predicted well the injury patterns. Nevertheless for both remaining victims, the accident numerical simulation predicted brain moderate neurological injuries. Thus, the right injury pattern was predicted but not in the right range.

### **Subdural or subarachnoidal haematoma**

Three victims sustained a subarachnoidal or a subdural haematoma consecutively to their accident. For all these three accident cases, the model was not able to predict that specific injury. Nevertheless, in two cases the accident report mentioned a secondary ground impact that may be responsible for the observed injury. Besides, six accident victims did not sustain any subarachnoidal or subdural haematoma. Only for of these six victims the accident numerical reconstruction predicted such an injury. Thus, for the five other accident cases, none subarachnoidal or subdural haematoma was predicted.

### **Skull fractures**

Four accident victims revealed a skull fracture. For two of them, the model predicted well that specific injury. Nevertheless, for the two remaining victims, the accident numerical reconstruction was not able to predict any skull fracture. It can be noticed that

for one of these two cases, the accident report mentioned a secondary ground impact that might be responsible for that observed injury. Moreover, five victims did not suffer from skull fractures. The model predicted that none occurrence of injury well for four victims. Thus the model predicted a skull fracture only for one victim that did not reveal any skull fracture.

## **CONCLUSIONS AND PERSPECTIVES**

From an injury prediction point of view it can be concluded that the numerical tools that have used to reconstruct the real world accident cases under study are pretty good (i.e. the FEM of the human head, of the car's windscreen and bonnet). Moreover, they are much more powerful to predict the absence of injury. It has to be underlined that statistical results have not been derived from that study since the number of accidents considered is too low at that level. Nevertheless, in some cases, the observed injuries were not predicted at all. But in the majority of these accident cases, a secondary ground impact was mentioned in the accident report. It is therefore desirable to reconstruct numerically the second part of the accident in order to evaluate the mechanical field parameters that are sustained by each victim at that level. It could therefore be useful to compare the outcomes of both impact numerical reconstructions to infer which impact is responsible for which injury. A further step would be to increase the numbers of accident cases in the database. In fact, the numerical reconstruction of a great number of different cases would allow leading a statistical approach in that framework. Another perspective lies in the improvement of the numerical models that are used for the reconstructions. In fact, efforts have still to be made to access to more accurate geometries as well as mechanical behaviour of the car's bonnet and windscreen and of the human head. Nevertheless, even if models are powerful and reliable, the complete accident reconstruction process has to be controlled very accurately. Indeed, the initial conditions of the head impact against the striking structure have to be known with a great precision if conclusions should be inferred from such numerical tools. Therefore the kinematics of the whole pedestrians – and thus the whole pedestrian and car model – have to be calculated with a high accuracy. This has been possible in the framework of that cooperation work between different European Institutes but asked for tremendous efforts. It can be concluded that these results showed that such numerical models are good tools to predict human head injuries. However, the numerical tools used can only predict injuries reliably if both the pedestrian and vehicle side are modelled appropriately, i.e. with detailed FE structures with well validated material and contact

stiffness data. They will therefore be useful to improve the head protection devices i.e. the design, the conception, the evaluation and the optimization of cars' windscreens and bonnets against well defined injury criteria.

## REFERENCES

[KAN 1997] Validation of a 3D anatomic human head model and replication of head impact in motorcycle accident by finite element modelling, Proc. of the 41<sup>st</sup> Stapp Car Crash Conf., pp. 329-338, Kang H.S., Willinger R., Diaw B., Chinn B., 1997.

[WIL 2003] Human head tolerance limits to specific injury mechanisms, Int. J. of Crashworthiness, vol. 8, n°6, pp. 605-617, Willinger R., D. Baumgartner, 2003.

[LOV 1975] Brain susceptibility to velocity changes – Relative and absolute limits for brain tissue tolerance to trauma and their relation to actual traumatic situations, Proc. of the International Interdisciplinary Symposium on Traffic Speed and Causalities, Funen, Lövenhielm P., 1975.

[GEN 1985] The state of the art of head injury biomechanics – A review, 29<sup>th</sup> Conf. of the American Association for Automotive Medicine, pp. 447-463, Gennarelli T.A., 1985.

[THI 1990] The strain dependent pathophysiological consequences of inertial loading on central nervous system tissue, Proc. of the IRCOBI Conf., pp. 191-202, Thibault L., Gennarelli T., Margulies S., 1990.

[MEN 1992] Finite element modelling of the brain to establish diffuse axonal injury criteria, PhD Dissert., Ohio State University, Mendis K., 1992.

[ZHO 1996] Head injury assessment of a real world crash by finite element modelling, Proc. of the AGARD Conf., Zhou C., Kahlil T.B., Dragovic L.J., 1996.

[AND 2000] A study of the biomechanics of axonal injury, PhD Dissert., University of Adelaide, South Australia, Anderson R., 2000.

[KIN 2003] Is head injury caused by linear or angular acceleration? , Proc. of the IRCOBI Conf. 2003, pp. 1-12, King A., Yang K., Zhang L., Hardy W., 2003.

[TAK 2003] On the development of the SIMon finite element head model, Proc. of the 47<sup>th</sup> Stapp

Car Crash Conf., pp.107-133, Takhounts E., Eppinger R., 2003.

[NAH 1977] Intracranial pressure dynamics during head impact, Proc. of the 21<sup>st</sup> Stapp Car Crash Conf., pp. 339-366, Nahum A.M., Smith R., Ward C.C., 1977.

[TRO 1992] Development of a FEM of the human head according to a specific test protocol, SAE n° 922527, Trosseille X., Tarrière C., Lavaste F., Guillon F., Domont A., 1992.

[YOG 1994] Biomechanics of skull fracture, Proc. of the Head Injury Symposium, Washington DC, pp. 227-236, Yoganandan N, Pintar F.A., Sances A., Walsh P.R., Ewing C.L., Snyder T., Snyder R.G., 1994.

[HAV 1975] Strength of plastics and glass, Cleaver Hume Press, New York, Haward R.N., 1975.

[MUK 2000] Modelling of head impact on laminated glass windshields, Proc. of the IRCOBI Conf., pp. 323-334, Mukherjee S., Chawla A., Mahajan P., Mohan D., Mane N., Singh M., Sakurai M., Tamura Y., 2000.

[WAR 1980] Intracranial pressure: a brain injury criterion, Proc. of the 24<sup>th</sup> Stapp Car Crash Conf., SAE Paper n°801304, Ward C.C., Chan M., Nahum A.M., 1980.

# A COMPARATIVE STUDY BETWEEN SUBSYSTEM AND GLOBAL APPROACHES FOR THE PEDESTRIAN IMPACT

**Sophie Chalandon**

Faurecia  
France

**Thierry Serre**

**Catherine Masson**

French National Institute for Transport and Safety Research (INRETS)  
France

**François Minne**

Union Technique de l'Automobile, du Motocycle et du Cycle (UTAC)  
France

**Pierre-Jean Arnoux**

**Christophe Perrin**

French National Institute for Transport and Safety Research (INRETS)  
France

**Patrick Borde**

**Christian Cotte**

Faurecia  
France

**Christian Brunet**

**Dominique Cesari**

French National Institute for Transport and Safety Research (INRETS)  
France  
Paper Number 07-0429

## ABSTRACT

In order to improve the pedestrian safety during an impact with a vehicle, subsystem tests have been defined to evaluate the aggressiveness of the front-end of cars. These subsystems tests have to be reproducible and are representative of the three decomposed impacts of the pedestrian with the car: lower leg on the bumper, upper leg on the hood, head on the hood or the windscreen. The velocity, angle and mass of the adult headform impactor and its impact area are invariable parameters. Upper legform impactor parameters are determined by vehicle characteristics. Lower legform impactor parameters are invariable (velocity and positioning). Nevertheless, these decoupled tests do not take into account the influence of the whole body on impacts. Therefore, it appears important to compare these subsystem tests with global conditions observed in real accidents. The objective of this paper is to perform this work on two French vehicles. Concerning the global conditions, four full-scale experimental tests with PMHS and the associating multibody numerical simulations were performed in classical (lateral impact for the pedestrian, centred for the vehicle) and real configurations.

In that way, two real accidents have been chosen in this impact configuration with a velocity value close to 40 km/h. Each reconstruction of accidents is based on In-Depth Accident Investigation first.

Then, a parametric study using multibody models, validated with an experimental test, gives a hypothetic initial configuration of the accident. This configuration is used to put on an experimental reconstruction. Then, results from numerical and experimental studies are compared for the adult headform, the upper legform and the lower legform impacts. Finally, a global comparison is analysed more specifically on injuries not include on the subsystem approach. These injuries are also compared to Accidental Database to know whether their proportion is important or not.

## INTRODUCTION

From 1980 to 2001, pedestrian accident proportion decreased in France. Since 2001, this tendency has been reversed and from 2004, pedestrian accident proportion has increased up to 16% of total French road accidents [ONISR, 2007].

The standard pedestrian accident configuration is characterised by a vehicle frontal Impact (67%), a pedestrian lateral Impact (80-90%) and velocities lower to 50 km/h (85 %) [Robertson et al., 1966, Ravani and al., 1981, EEVC, 1982 and 1998, IHRA, 2001].

In 1998, the EEVC (European Enhanced Vehicle-safety Committee) published a pedestrian protection evaluation report [EEVC, 1998]. This

document led to a European directive (2003/102/EC) applied in October [EC-OJ, 2003]. The objective was to improve the pedestrian safety by reducing the aggressiveness of the front end of the cars regarding pedestrians. This regulation is decomposed in two phases. The phase one is already in application while the phase two is carried out. Moreover, EEVC report led to consumerist tests. In Europe, Euro NCAP tests are performed in order to defend consumers.

Four subsystem tests reproduce and represent the three decomposed pedestrian impacts with the car: lower leg, upper leg, adult head and child head. Test protocols are based on a specific impact configuration which corresponds to the standard one, with about 30-40 km/h vehicle velocity.

From existing data in the field of accident statistics, biomechanics and test results of EEVC report, subsystems limitation parameters evaluate front-end vehicle aggressiveness with acceleration, HIC, force, moments, knee lateral shearing and bending HIC parameters. Head and leg subsystems tests protocols and injury criteria are independent of the vehicle. Concerning the upper leg protocol, it is dependant of the geometry vehicle.

Therefore, it appears important to compare these subsystem tests with global conditions observed in real accident. The objective is in particular to evaluate the influence of the whole body on the kinematics because it is not taken into account in subsystems tests. What can be the disparities on the different impact characteristics (lower leg, upper leg and head impact) when all the pedestrian body is considered (global configuration) and when it is decoupled in several body segments (subsystem tests)? The aim of this paper is to perform this work on two French vehicles and two global configuration types.

## METHOD

### General overview

Three types of pedestrian impact configurations were analysed and compared in this work.

The first configuration corresponded to the impact protocols defined by the subsystems tests performed in the framework of the Euro NCAP consumerist tests [Euro NCAP, 2004]. These experimental results were considered as the reference because they were compared with global conditions. However, the subsystem "Child Head" was not studied because it could not be compared with the others configurations described below (the two real accidents involved adults).

The second configuration was a global configuration corresponding to a standard accident (lateral impact on the pedestrian side and centred on the front of the vehicle). Two complementary approaches were used to study this configuration.

An experimental one based on full scale tests using PMHS subjects and then a numerical one based on the associated multibody simulation.

The third configuration concerned real accidents which have been reconstructed from an in-depth accident investigation. These real accidents have been selected close to the standard configuration. Such as for the previous global configuration, both experimental and numerical approaches have been used. But in this case, the numerical reconstruction was made firstly with multibody simulations before the experimental reconstitution [bSerre and al., 2006].

This study was applied to two different vehicles: a Peugeot 206 and a Renault Twingo.

So, in all, four full-scale experimental tests with PMHS and the corresponding multibody simulations were performed in addition to the Euro NCAP consumerist tests.

### Sub-system tests

NCAP tests procedures are effective in Europe (Euro NCAP), US (USNCAP), Japan (Japan NCAP) and Australia (ANCAP). The Euro NCAP introduced pedestrian protection since 1999. Modifications have been done in 2005 to introduce vehicle evaluation with a four stars scale. Tests methods and injury criteria are based on the 1998's EEVC report.

This method, proposed by the EEVC (Figure 1, [Davies and Clemo, 1997]) represents adult head, child head, upper leg and lower leg impacts. Four instrumented subsystems are projected on specific vehicle areas to constitute six configurations:

- **Adult head to windscreen**  
Output parameters: HPC, maximal acceleration
- **Adult head to bonnet**  
Output parameters: HPC, maximal acceleration
- **Child head to bonnet**  
Output parameters: HPC, maximal acceleration
- **Upper leg to bonnet leading edge**  
Output parameters: force and moment
- **Upper leg to bumper**  
Output parameters: force and moment
- **Lower leg to bumper**  
Output parameters: knee bending and shearing, maximal acceleration

Adult head to bonnet, child head to bonnet and upper leg to bumper were not analysed in this work. Firstly real and standard accidents included two adults. So child impact was not compared. Secondly, head impacts were located on the windscreen, so head impact to bonnet is not analysed. Thirdly, upper leg to bumper impact is used for SUV (Sport Utility Vehicle) and real accidents vehicle type is a sedan one.

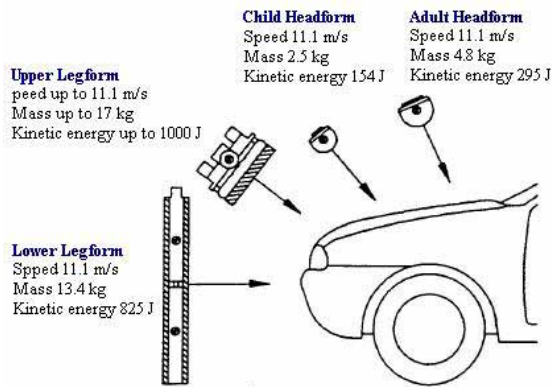


**Figure 1. Pedestrian protection test methods proposed by EVC WG10**

### Standard configuration tests

In this configuration, pedestrian had a standard posture corresponding to a walk and a road crossing. The pedestrian impact was lateral (right side) and the vehicle one was frontal, located in the centre of the front end.

About the full-scale experimental tests, they had been performed using Post Mortem Human Subjects (PMHS). They were preserved at 3°C in Winkler's preparation [Winkler, 1974]. This injection method allows to keep supple the soft tissues elasticity. Medical team checked the joint range of physiological mobility. X-Rays radiographs of the body were taken and an anatomist surgeon checked the osseous integrity in two planes (sagittal plane and frontal plane).

The subject is instrumented with accelerometers fixed on tibia, femur, pelvis, sternum, cervical vertebrae and head. (Figure 2)

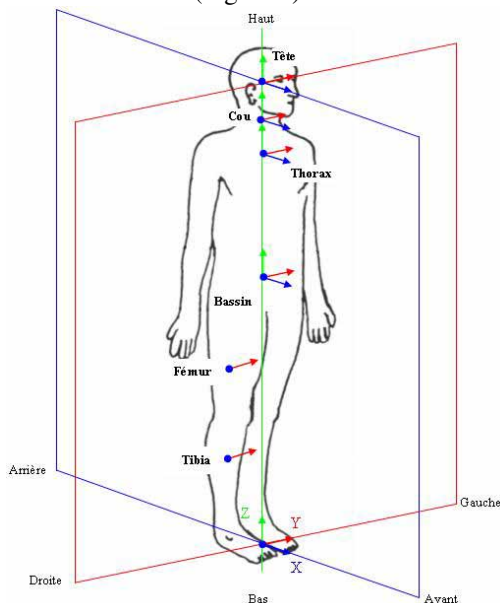


**Figure 2. PMHS sensors location**

At the beginning of tests, subject had a standing position maintained by an electromagnetic system linked to the pedestrian head (Figure 3). Ten milliseconds before impact, this system released the subject.

A horizontal catapult propelled the car. From three to seven high-speed video cameras operating at 1000 frames per second were placed in order to record the kinematics during the impact event.



**Figure 3. Experimental subject initial position**

Concerning the numerical approach, full scale crashes simulations were performed using Madymo software [Serre and al., 2006]. The pedestrian model is composed by thirty-five rigid bodies, thirty-five joints and eighty-two ellipsoids. Mechanical characteristic joints and bodies were based on biomechanical data [Yamada, 1970] [Kajzer, 1999]. The model can predict lower leg fracture and head injury criterion:

- Ten bodies connected by joints compose lower legs. Two rupture criteria are fixed, shearing force and bending moment.
- Head injuries are evaluated by the HIC criterion.

The vehicle model represents the front end of a sedan vehicle type (windscreen, bonnet, bumper and spoiler) [Glasson and al., 2000]. Fourteen parameters compose its geometry (Figure 4). Mechanical properties of the different parts of the car have been implemented from the Euro NCAP experimental tests.

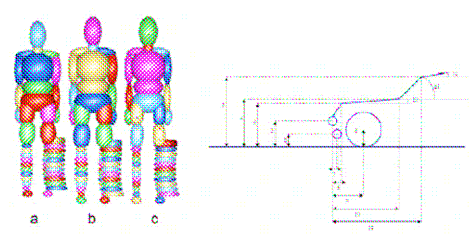


**Figure 4. Pedestrian and vehicle numerical models (Madymo®)**

Pedestrian and vehicle models were validated qualitatively and quantitatively in a pedestrian impact configuration with experimental tests comparison jointly by Chalmers University, Faurecia and Laboratory of Applied Biomechanics of INRETS [Yang et al., 1993], [Glasson et al., 2000]. These tests were realised with PMHS and several different geometric vehicles (sedan) with

impact velocity from 30 km/h to 40 km/h [Cavallero and al., 1983].

In this work, two full-scale experimental tests with PMHS and the associating multibody numerical simulations were performed in this standard configuration. Characteristics of numerical and experimental tests are resumed in Table 1.

**Table 1.**  
**Standard configuration tests characteristics**

|                         | Peugeot 206     |                 | Renault Twingo  |                 |
|-------------------------|-----------------|-----------------|-----------------|-----------------|
|                         | Exp.            | Num.            | Exp.            | Num.            |
| <b>Impact type</b>      | Frontal centred | Frontal centred | Frontal centred | Frontal centred |
| <b>Vehicle Velocity</b> | 8.9 m/s         | 8.9 m/s         | 8.9 m/s         | 8.9 m/s         |
| <b>Subject size</b>     | 1m54            | 1m54            | 1m58            | 1m60            |
| <b>Subject mass</b>     | 46 kg           | 46 kg           | 61.5 kg         | 60 kg           |
| <b>Subject age</b>      | 86 years        | -               | 86 years        | -               |

**Real accident configuration tests**

Concerning the real configuration, a global methodology has been defined in order to propose a reliable accident reconstruction [Serre and al., 2006]. This methodology gathered three complementary approaches (Figure 5). Each accident reconstruction was based on In-Depth Accident Investigation first. Then, a parametric study using multibody models gave a hypothetic initial configuration of the accident. This configuration was used to put on an experimental reconstitution and to validate the reconstruction.

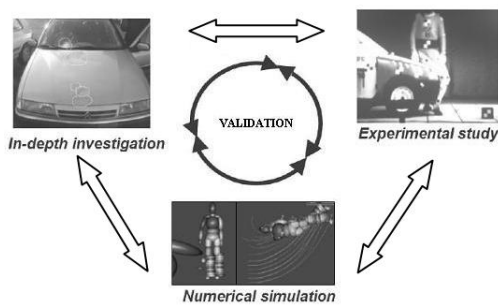


**Figure 5. Different approaches in the reconstruction method**

Accidents were chosen from an in-depth investigation performed at the laboratory Accidental Mechanism Department of INRETS [Girard, 1993]. These accidentologic data gave information to develop a first hypothetic configuration. From this, a numerical parametric study was realised to fix unknown parameters such as the vehicle velocity, its deceleration, the initial pedestrian position, etc. Each result was compared

to accidental data to be validated or not. For example, Figure 6 shows the kinematics for two different initial pedestrian postures. After iterative simulations, configuration which was closest to real accidental data was selected. Only this final reconstruction configuration is presented in this work. Finally, from this most probable numerical reconstruction, an experimental test was realised with the closest conditions.

Characteristics of numerical and experimental tests are in Table 2.

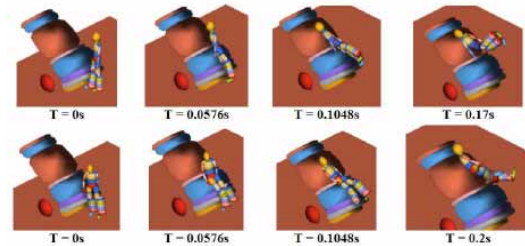


**Figure 6. Example of two different configurations**

**Table 2.**  
**Real configuration tests characteristics**

|                         | Peugeot 206   |               | Renault Twingo |               |
|-------------------------|---------------|---------------|----------------|---------------|
|                         | Exp.          | Num.          | Exp.           | Num.          |
| <b>Impact type</b>      | Frontal shift | Frontal shift | Frontal shift  | Frontal shift |
| <b>Vehicle Velocity</b> | 8.3 m/s       | 8.3 m/s       | 11.2 m/s       | 12.2 m/s      |
| <b>Subject size</b>     | 1m61          | 1m65          | 1m60           | 1m60          |
| <b>Subject mass</b>     | 44 kg         | 55 kg         | 65 kg          | 60 kg         |
| <b>Subject age</b>      | 85 years      | > 50 years    | 64 years       | > 50 years    |

**RESULTS**

**Vehicle 1: Renault Twingo**

**Head Impact**

Head impact parameters (Table 3) have been calculated in the vehicle skew for experimental and numerical results. Head angle and velocity correspond to a pre-impact time (5 ms before). Head acceleration and HIC were calculated during impact.

For all Sedan vehicles, Euro NCAP head/windscreen impact angle is 65 degrees. In both standard configuration (numerical and experimental tests), angle values are close. These values are half the Euro NCAP angle value. In real configuration, numerical (21°) and experimental (42°) head impact angle values are different.

Nevertheless, these values are lower than Euro NCAP defined angle.

For all Sedan vehicles, Euro NCAP head/windscreen impact velocity is 11.1 m/s. In standard configuration tests, velocities are lower than Euro NCAP value. In real configuration, results are close to Euro NCAP.

For the Euro NCAP Renault Twingo test, maximal impact acceleration result is 94 g and HIC is 486. In standard and real configuration, maximal impact accelerations are around 1.5 higher (up to 180) while HIC is lower. Because in the real experimental configuration case, a crash sensor record was failed, no data are provided in axe X. Acceleration resultant could not be calculated.

**Table 3.**

**Head impact parameters results for Renault Twingo**

|                       | Basic Conf. |      | Real Conf. |      | Sub System |
|-----------------------|-------------|------|------------|------|------------|
|                       | Exp.        | Num. | Exp.       | Num. |            |
| <b>Angle</b>          | 30°         | 28°  | 42°        | 21°  | 65°        |
| <b>Velocity (m/s)</b> | -           | 8.1  | 12.5       | 9.3  | 11.1       |
| <b>Acc. (g)</b>       | 153         | 154  | y:<br>z:   | 180  | 94         |
| <b>HIC</b>            | 423         | 261  | -          | 316  | 486        |

**Upper leg impact**

The upper leg impact parameters (Table 4) correspond to thigh impact. Upper leg angle represents thigh angle. Velocity corresponds to thigh impact velocity. Force represents the contact of thigh with the bonnet and the moment is the internal thigh bending moment. In experimental tests these parameters were not measured.

For Renault Twingo vehicle, Euro NCAP upper leg/bonnet impact angle is 41.3°. In standard and real configurations, numerical values are respectively 35° and 48°. Euro NCAP value is included in these results.

For Renault Twingo vehicle, Euro NCAP upper leg/bonnet impact velocity is 6.91 m/s. In both configurations, velocities are close to this defined value.

For the Euro NCAP Renault Twingo test, impact force is 5100 N and bending moment is 312 N.m. In both configurations, Forces are lower than Euro NCAP value and bending moment are close.

**Table 4.**

**Upper leg parameters results for Renault Twingo**

|                 | Numerical basic Conf. | Numerical real Conf. | Sub System |
|-----------------|-----------------------|----------------------|------------|
| <b>Angle</b>    | 35°                   | 48°                  | 41.3°      |
| <b>Velocity</b> | 6.7 m/s               | 7.4 m/s              | 6.91 m/s   |
| <b>Strain</b>   | 2370 N                | 1800 N               | 5100 N     |
| <b>Moment</b>   | 365 N.m               | 300 N.m              | 312 N.m    |

**Lower leg impact**

Knee bending and shearing in experimental tests are not calculated due to the lack of accuracy to separate the two phenomenons of translation and flexion.

For all Sedan vehicles, Euro NCAP lower leg/bumper impact velocity is 11.1 m/s. Real configuration velocity is close to Euro NCAP value while standard configuration velocity is lower.

For the Euro NCAP Renault Twingo test, maximal impact acceleration is 205 g. Standard and real configuration results vary from 190 to 320 g.

For the Euro NCAP Renault Twingo test, maximal knee bending is 33 degrees. Numerical results from both configurations are much lower.

For the Euro NCAP Renault Twingo test, maximal knee shearing is 4.2 mm. Results from both configurations are close to this value.

**Table 5.**

**Lower leg parameters results for Renault Twingo**

|                       | Basic Conf. |      | Real Conf. |      | Sub System |
|-----------------------|-------------|------|------------|------|------------|
|                       | Exp.        | Num. | Exp.       | Num. |            |
| <b>Velocity (m/s)</b> | 8.9         | 8.9  | 11.2       | 11.1 | 11.1       |
| <b>Acc. (g)</b>       | 190         | 320  | 324        | 290  | 205        |
| <b>Bending</b>        | -           | 8°   | -          | 4°   | 33°        |
| <b>Shearing (mm)</b>  | -           | 8    | -          | 6.4  | 4.2        |

## Vehicle 2: Peugeot 206

### Head Impact

The head impact parameters (Table 6) have been calculated in the same way than Renault Twingo parameters. However, the Peugeot 206 subsystem test has been done in the localisation showed in the Figure 7. This localisation is an aggressive part of the windscreen border. In the reality, the contact between pedestrian head and windscreen occurs around the centre of this vehicle part. Values can not be compared because of this difference.

Because in the standard experimental configuration case, a crash sensor record was failed, no data are provided in Y axe. Acceleration resultant could not be calculated.

For all Sedan vehicles, Euro NCAP head/windscreen impact angle and velocity are respectively 65 degrees and 11.1 m/s.

In standard configuration, numerical head angle (42°) and experimental head angle (61°) are different. In real configuration, numerical and experimental angles are equivalent (42° and 45°). These values are lower than Euro NCAP value except for the experimental standard configuration test.

In standard and real configurations, velocities are lower than Euro NCAP value.

**Table 6.**  
**Head parameters results for Peugeot 206**

|                       | Basic Conf.    |      | Real Conf. |      | Sub System |
|-----------------------|----------------|------|------------|------|------------|
|                       | Exp.           | Num. | Exp.       | Num. |            |
| <b>Angle</b>          | 61°            | 42°  | 42°        | 45°  | 65°        |
| <b>Velocity (m/s)</b> | 10.6           | 7.1  | 8.3        | 6.9  | 11.1       |
| <b>Acc. (g)</b>       | x: 74<br>z: 63 | 42.5 | 122.7      | 108  | -          |
| <b>HIC</b>            | -              | 138  | 155        | 654  | -          |

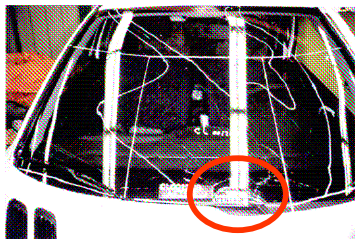


**Figure 7. Impact location of Sub-system tests for the Peugeot 206 evaluation**

### Upper leg impact

For Peugeot 206 vehicle, Euro NCAP upper leg/bonnet impact angle is 34°. In standard and real configurations, numerical values are respectively 30° and 34°, close to Euro NCAP value.

For Peugeot 206 vehicle, Euro NCAP upper leg/bonnet impact velocity is 7.9 m/s. In both configurations, velocities are lower than this defined value.

For the Euro NCAP Peugeot 206 test, impact force is 2819 N and impact bending moment is 382 N.m. In both configurations, forces are lower than Euro NCAP value. Concerning bending moment, numerical value in standard configuration is lower and in real configuration is close to Euro NCAP result.

**Table 7.**

### Upper leg parameters results for Peugeot 206

|                 | Numerical basic Conf. | Numerical real Conf. | Sub System |
|-----------------|-----------------------|----------------------|------------|
| <b>Angle</b>    | 30°                   | 30°                  | 34°        |
| <b>Velocity</b> | 5.9 m/s               | 4.8 m/s              | 7.9 m/s    |
| <b>Strain</b>   | 1950 N                | 1470 N               | 2819 N     |
| <b>Moment</b>   | 265 N.m               | 360 N.m              | 382 N.m    |

### Lower leg impact

For all Sedan vehicles, Euro NCAP lower leg/bumper impact velocity is 11.1 m/s. In both configurations, velocities are lower.

For the Euro NCAP Peugeot 206 test, maximal impact acceleration is 150 g. Standard and real configuration results vary from 100 to 360 g.

For the Euro NCAP Peugeot 206 test, maximal knee bending is 30°. Results from both configurations are close to this value.

For the Euro NCAP Peugeot 206 test, maximal knee shearing is 4 mm. Numerical results from both configurations are much higher.

**Table 8.**

### Lower leg parameters results for Peugeot 206

|                       | Basic Conf. |      | Real Conf. |      | Sub System |
|-----------------------|-------------|------|------------|------|------------|
|                       | Exp.        | Num. | Exp.       | Num. |            |
| <b>Velocity (m/s)</b> | 8.9         | 8.9  | 8.3        | 8.3  | 11.1       |
| <b>Acc. (g)</b>       | 360         | 170  | 100        | 155  | 150        |
| <b>Bending</b>        | -           | 32°  | -          | 40°  | 30°        |
| <b>Shearing (mm)</b>  | -           | 27   | -          | 32   | 4          |

## DISCUSSION

### Head impact

Impact angle values are lower than Euro NCAP value except for one case.

Angles vary with vehicle geometry and between simulations and experimental tests for some cases. Result variability between numerical and experimental tests seems to be the consequence of articular behaviour variability of PMHS and articular behaviour invariability of numerical pedestrian model.

This variability between vehicle types seem to be the consequence of geometrical vehicle parameters (windscreen angle), PMHS size, weight and articular laxity.

Impact velocities are globally lower than Euro NCAP defined value, except for Peugeot 206 tests in real configuration. In this test, vehicle velocity is close to Euro NCAP accident configuration (11.1 m/s). Euro NCAP head velocity seems to be relevant.

With impact velocities, lower than Euro NCAP one, maximum accelerations during impacts are one and half higher. In opposition, HIC is lower.

These differences can be explained by variability of parameters like impact angle, impact velocity and material behaviour used to represent pedestrian head in Euro NCAP tests.

What can be the disparities on the head impact characteristics when all the pedestrian body is considered (global configuration) and when it is decoupled in the head subsystem?

From these results, head angle seems to be overvalued while velocity seems to be relevant. Concerning head angle in Euro NCAP, it is defined with regard to a horizontal line and not to the windscreen line. It should be more adapted to fix head subsystem angle with windscreen orientation.

### Upper leg impact

Upper leg angle in standard and real configuration, for numerical and experimental tests, are close to Euro NCAP value. Moreover, angles seem to be dependant from vehicle. Euro NCAP upper leg angle value and its vehicle specificity might be relevant.

Euro NCAP Renault Twingo velocity is included between real and standard configuration thigh velocities.

About Peugeot 206 results, velocities are lower than Euro NCAP velocity. Peugeot 206 impact velocity seems to be overvalued for upper leg impact. Nevertheless, impact velocity vehicle dependence seems relevant.

Impact forces are always lower than Euro NCAP results. This test seems to overvalue this impact parameter.

Euro NCAP thigh bending moments seem to be relevant. In Renault Twingo case, Euro NCAP value is close to numerical results and in the Peugeot 206 case, Euro NCAP value is higher than results.

What can be the disparities on the upper leg impact characteristics when all the pedestrian body is considered (global configuration) and when it is decoupled in the upper leg subsystem?

From these results, vehicle velocity dependence, vehicle angle dependence and angle values seem to be relevant. About velocities parameter, it seems to be relevant for Renault Twingo vehicle and maximized for Peugeot 206 vehicle. Nevertheless, impact forces are too high in Euro NCAP configuration.

### Lower leg impact

Leg impact velocity corresponds to impact vehicle velocity. Standard tests were realised with an 8.9 m/s vehicle velocity. In real configuration, Peugeot 206 case corresponds to a crash velocity close to Euro NCAP configuration.

Between experimental and numerical tests, maximum acceleration values vary. These differences seem to come from vehicle geometry, pedestrian initial position, cadaveric rigidity and mechanical properties of numerical models.

Moreover, Euro NCAP results do not maximised real and standard configuration results. In these last configurations, it is the vehicle which impact pedestrian. In Euro NCAP protocol, it is the leg which impact the vehicle.

In the Renault Twingo case, the low lateral knee bending in standard configuration comes from knee kinematics. Indeed, the first knee kinematical movement is a lateral flexion ( $8^\circ$ ), then a posterior flexion ( $13^\circ$ ) and torsion ( $16^\circ$ ). In this case, initial pedestrian position corresponds to a right leg ahead and the impact side is on the right. During the first time of impact, pedestrian turn progressively his back to the vehicle. So, posterior flexion is maximized, lateral flexion is minimized. Knee lateral shearing is minimized too, and it is close to Euro NCAP value.

In real configuration, for Renault Twingo case, pedestrian turn back a little to the vehicle. His kinematics movement minimized lateral bending and shearing.

These cases are not critical pedestrian leg case for knee injured kinematics.

In Peugeot 206 cases, maximum of lateral knee bending are more important and reach 32° and 40°, close to Euro NCAP results. Lateral knee shearing reaches 27 and 32 mm. These kinematics are different with Renault Twingo ones. Lateral knee bending and shearing are maximised.

What can be the disparities on the lower leg impact characteristics when all the pedestrian body is considered (global configuration) and when it is decoupled in the lower leg subsystem?

From these results, Euro NCAP velocity value seems to be relevant. Lower leg sub-system seems to represent critical value in lateral bending, while it do not correspond to critical value in lateral shearing for knee.

## CONCLUSION

The aim of this work is to compare Euro NCAP subsystem protocols and results with two full-scale configurations, standard and real, in order to evaluate disparities on the different impact characteristics when all the pedestrian body is considered (global configuration) and when it is decoupled (subsystem tests). Full-scale configurations are performed on two French vehicle using two complementary approaches, numerical simulation and experimental tests.

Some differences have been observed between subsystem characteristics and body segment impacts coming from full-scale configurations.

Concerning head impact, the defined angle by Euro NCAP is globally higher and could be adapted with the vehicle geometry. The corresponding defined velocity by Euro NCAP seems to be adapted.

Concerning the upper leg impact, all Euro NCAP parameters are relevant to the global configurations except for the fixed Peugeot 206 velocity which is maximized.

Concerning lower leg impact, subsystem protocol parameters are adapted, represents knee bending critical case but does not represent knee shearing critical case.

This work has been done only on two vehicles (Renault Twingo and Peugeot 206) but will be extended to other vehicles in order to evaluate more accurately the influence of vehicle geometry, speed, etc. New vehicles which have a good evaluation in Euro NCAP will be tested in particular.

## ACKNOWLEDGEMENTS

This work is included in the framework of the APPA project (Amélioration de la Protection du Piéton lors de collision par des Automobiles).

## REFERENCES

Cavallero, C., Cesari, D., Ramet, M., Billault, P., Fariße, J., Seriat-Gautier, B., Bonnoit, J. 1983.

*Improvement of pedestrian safety: influence of shape of passenger car-front structures upon pedestrian kinematics and injuries: evaluation based on 50 cadaver tests.* SAE paper # 830624, 225-237.

Davies R.G. and Clemo K.C. 1997. *Study of research into pedestrian protection costs and benefits*, MIRA report no. 97-456502-01.

EEVC. 1982. *Pedestrian Injury Accidents*, 9<sup>th</sup> Int. Tech. Conf. on Experimental Safety Vehicles, Kyoto, Japan, US Dept. of Transportation, NHTSA, USA. Pp.638-671.

EEVC. 1998. *Improved test methods to evaluate pedestrian protection afforded by passenger cars*, Report, European Experimental Vehicle Committee, Working Group 17.

Euro NCAP. 2004. *European new car assessment program, pedestrian testing protocol*, the official site of the European New Car Assessment programme, Version 4.1. [http://www.euroncap.com/content/test\\_procedures/downloads.php?area\\_ID=3](http://www.euroncap.com/content/test_procedures/downloads.php?area_ID=3) (last visited on 2007-03-05).

Directive 2003/102/EC of the European Parliament and of the Council of 17 November 2003. *Protection of pedestrians and other vulnerable road users before and in the event of a collision with a motor vehicle and amending Directive 70/156/EEC.* OJ L 321, 6.12.2003, p. 15–25.

Girard, Y., *In-depth investigation of accidents: the experience of INRETS at Salon-de-Provence.* International congress on Safety evaluation of traffic systems: traffic conflicts and other measures, ICTCT Congress, Salzburg, Autriche, 1993.

Glasson E., Bonnoit J., Cavallero C. and Basile F., *A numerical analysis of the car front end module regarding pedestrian lower limb safety*, Vehicle Safety, C567/016/2000, pp79-91, 2000.

IHRA/PS/200, International Harmonized Research Activities, *Pedestrian Safety Working Group*, Report, 2001.

Kajzer, J., *Shearing and bending effects at the knee joint at low speed lateral loadings.* SAE paper #1999-01-0712, 1999.

ONISR, *Piétons – Grands thèmes de la sécurité routière en France*, Février 2007, <http://www.securiteroutiere.equipement.gouv.fr> (Last visited on the 03/02/2007)

Ravani B., Brougham D., Mason R.T. *Pedestrian post-impact kinematics and injury patterns*, SAE, Paper 811024, 1981.

Robertson J.S., McLean A.J. and Ryan G.A., *Traffic Accidents in Adelaide, South Australia*, Australia Road Research Board, Special Report Number 1, Canberra, 1966.

<sup>a</sup>Serre T., Masson C., Perrin C., Chalandon C., Llari M., Cavallero C., Py M., Cesari D., *Real accidents involving vulnerable road users: comparison between in-depth investigation, numerical simulation and experimental reconstitution with PMHS*, IRCOBI 2006, Madrid, September 20-22, 2006.

<sup>b</sup>Serre T., Masson C., Perrin C., Chalandon C., Llari M., Cavallero C., Py M., Cesari D., *Pedestrian and Bicyclists accidents: in-depth investigation, numerical simulation and experimental reconstitution with PMHS*, International, Crashworthiness Conference, Athens, July 4-7, 2006.

Yang, J.K., Rzymkowski, C., Kajzer, J., *Development and validation of a mathematical breakable leg model*. Proc. Int. IRCOBI Conf. Biomechanics Impacts, 175-186, 1993.

Winkler G., *Manuel d'Anatomie Topographique et Fonctionnelle*, 2nd ed. Masson, Paris, 1974.

Yamada H., *Strength of biological materials*, Ed. The Williams and Wilkins Company Baltimore: 19-49, 1970.

# **EFFECT OF VEHICLE DESIGN ON HEAD INJURY SEVERITY AND THROW DISTANCE VARIATIONS IN BICYCLE CRASHES**

**S. Mukherjee**  
**A. Chawla**  
**D. Mohan**  
**M. Singh**  
**R. Dey**

Transportation Res. and Injury Prevention program  
Indian Institute of Technology. New Delhi

## **ABSTRACT**

The variation of the throwing distance and Head Injury Criterion with car velocity, point of impact and angle of approach has been studied for bicycle impact with three different categories of vehicles- small cars, sports utility vehicles and buses. Crashes between a bicycle and the vehicles were simulated using multi body models developed in MADYMO™ with parametric variations in speed, angle of approach and point of impact. The variation in the angle of approach or point of contact causes significant changes. From the simulations, the large spread in the data reported by reconstruction is predicted to originate from variation in the impact configuration. The changes in the trends can be associated with key changes in the nature of the impact visible in the simulations (head impacting car, no impact of rider with car etc.). The kinematics of impact has significant differences in case of the bus and this leads to differences in the nature of correlations. The HIC values were found to be higher in the case of bus as compared to the SUV and the small car. The paper reinforces the hypothesis that for bicycle accident reconstruction should take into account variations in the impact configuration in addition to the throw distance recorded. The paper also gives data which when populated further could form a basis of such reconstructions.

## **INTRODUCTION**

On an average, there are about 100,000 fatalities in road accidents each year [1]. More than a million sustain serious injuries. Cyclists and pedestrians are the most vulnerable group in traffic crashes [2] and the actual number of injured cyclists and total number of crashes may be underreported. In a heterogeneous traffic situation, as it exists in India, the safety of these most vulnerable sections should be given due importance while designing motorized vehicles. Computer simulations can play an important role in understanding the phenomena of crashes. Attempts have been made to simulate impacts between cars and bicycles at different standard configurations [3]. To initiate measures to protect the vulnerable road users, it is necessary to understand the important factors and variation in phenomena for a range of vehicles. Computer simulations of crashes are through finite element analysis or multi-body dynamic simulations. Though the accuracy of finite element analysis is much higher, they are computationally expensive. Hence, multi-body simulations are often carried out for such cases using software packages such as MADYMO™ (TNO Automotive, Netherlands) have been accepted for crash safety analysis throughout the world.

The study the kinematics of impact in simulations, we redefine 'throwing distance' as the distance between the point of impact and the point at which the body first hits the ground. The car speeds were correlated with throw distance from MADYMO simulations in Mukherjee [3]. The results were then compared with experimental data in [5]. They were able to attribute the spread obtained in [5] for

frontal side impacts to the point of impact on the bicycle with the car. This paper extends their work to cover other vehicles in the traffic stream. In addition, Head Injury Criterion values calculated by MADYMO™ were compared for the cases of impacts of bicyclists with the Car, the SUV and the bus in impact of the vehicle-front with bicycle-side configuration.

## MODEL DEVELOPMENT

We need to build models for the rider, bicycle and the vehicles for these simulations and define interactions between them

### Bicycle model

The bicycle model in Mukherjee [3] and has a system of four rigid bodies: the frame, the front fork, and the two wheels. The frame and the front fork were connected by a revolute joint; for which the rotation axis is in the plane of symmetry of the bicycle. Front and rear wheel were connected by revolute joints to the front fork and the frame, respectively. Rotation axes are perpendicular to the plane of symmetry. A sketch of the bicycle with key dimensions is as shown below in Figure 1. The results reported from tests and analysis [[6], [7]] have been used to determine the mechanical properties of the wheel reproduced in Table 1. The radial stiffness of the tyre has been obtained from the stress – strain curve for the bicycle tyres [[7]]. Contacts between the road and the tyres of the car were defined using the tyre model in MADYMO™ and using internal tyre pressure, wheel diameter and wheel thickness.

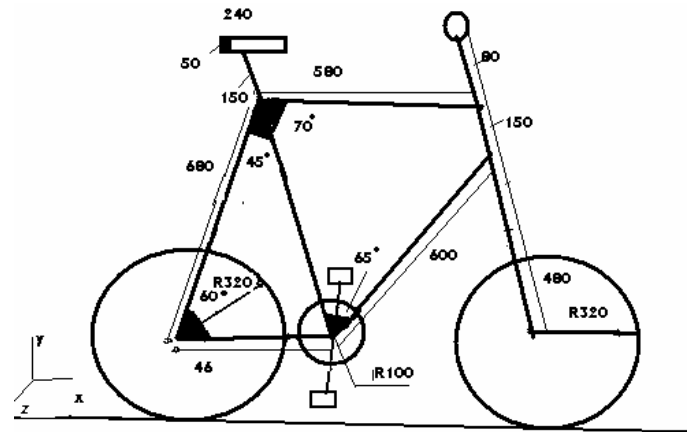


Figure 1 Dimensions of a Bicycle

Table 1 Bicycle tyre mechanical properties

| Quantity  | Value                  |
|---|------------------------|
| Outer rim radius (to centroid of rim)                                     | 309.4 mm               |
| Inner hub radius (to centre of spoke holes)                               | 18.0 mm                |
| Spoke diameter  | 2.10 mm                |
| Area of spokes in one plane   | 62.34 mm <sup>2</sup>  |
| Elastic modulus of rim  | 70 kN/mm <sup>2</sup>  |
| Elastic modulus of spokes   | 210 kN/mm <sup>2</sup> |
| Area of rim   | 138.4 mm <sup>2</sup>  |
| 2 <sup>nd</sup> moment of area of rim (for bending in the plane of wheel) | 1469 mm <sup>2</sup>   |

### Car Model

For carrying out the simulations of car-bicycle impacts, the model developed in [3] was used. For the MADYMO input file, the car frame has been modelled as a single rigid body i.e. all ellipsoids are rigidly connected to each other. The vehicle model consists of 4 multi body tree structures, representing the front left, front right, rear left, and rear right vehicle suspension.

### SUV Model

A model of a SUV was developed in a manner similar to that of the car. The vehicle was modelled as one single body, consisting of a combination of cylinders and ellipsoids. It consisted of five rigid bodies- the vehicle body and the four tyres. All the surfaces in the body of the vehicle were rigidly locked against each other. The only movable joint was between the road and the centre of gravity of the vehicle. Thus, there is only one movable part and that is the vehicle body. There is no relative movement possible between the parts. In total the model consists of 59 surfaces and 5 rigid bodies. Out of these 59 surfaces, 54 are ellipsoids while 5 are cylinders. Since from the perspective of a bicyclist, the vehicle is a very large mass, the dynamic loading effects on the SUV velocity were neglected. This allowed the usage of the same tyre properties as for the small car. The windscreen was defined using two ellipsoids while the front hood using a single ellipsoid of degree 8. The bumper was defined using 4 different ellipsoids. Due, to their size, the front headlights were modelled using two separate ellipsoids. Second degree ellipsoids were used to model the A, B C and D pillars. The suspension was also not modelled as it is sufficient to model the tyres and the centre of gravity of the vehicle.

### Bus Model

The model of the bus was developed in a manner similar to that of the SUV. The vehicle was modelled as one single body, consisting of a combination of cylinders and ellipsoids. In total the model contains 31 surfaces and 5 rigid bodies. To further analyze impacts between buses and bicycles, an alternative bus design slanting hood type of front instead of a flat-fronted design was considered.

### Contact Interactions

Multi body contact interactions were defined using the force penetration functions for the dummy with the bicycle, vehicle, pavement and road, for the bicycle with the vehicle and the road, the vehicle with the road and between dummy body parts. Head form impact test data reported in [8] for the WAGON R FX, which is similar to the WAGON R car prevalent in India was used to generate load deformation characteristics. By averaging over the bonnet and windscreen respectively, separate force – deformation characteristics were defined for the car bonnet and the windscreen. For sake of simplicity, the same deformation characteristics were used for all vehicles.

### SIMULATIONS OF CAR-BICYCLE IMPACTS

Simulations for frontal-side impacts between cars and bicycles were reported in [3] for car speeds ranging from 15 km/hr to 65 km/hr. This was extended to lower speeds of upto 2.5 km/hr. The bicycle speed was kept constant at 10km/hr. The throw distances for these simulations are plotted in Figure 2. It was observed that that for very low speeds (<10 km/hr) the spread was high and this can be expected because at such low values of throw distance, there is a significant dependence on the body part which impacts the ground. As this speed increases, the throw distances start to increase as expected.

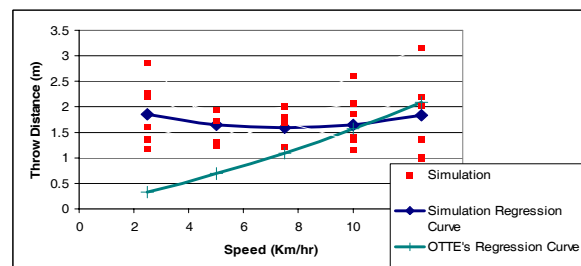


Figure 2: Throw distances for car-bicycle impacts at low speeds.

**SIMULATIONS OF SUV-BICYCLE IMPACTS**

Simulations have been performed for the SUV front impacting the bicycle Figure 3 shows a series of snapshots for the case where the SUV moving at a speed of 20 km/hr impacts with a 0.3m offset of

the bicycle pedal. Due to the characteristics of the shape of the SUV such as height and angle of inclination of the hood the phenomenon observed

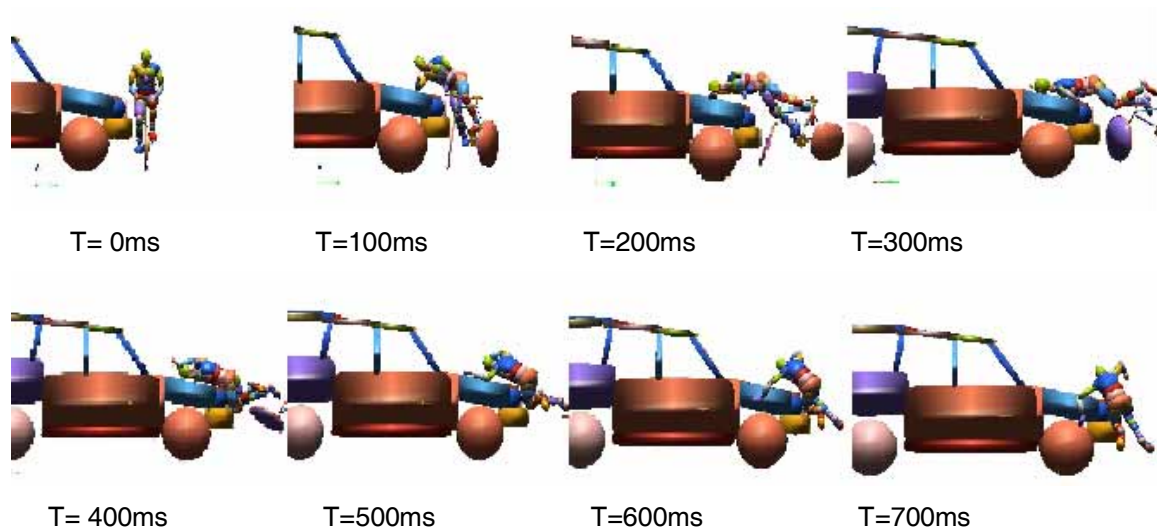


Figure 3 Motion of bicycle rider in frontal-side crash (SUV velocity = 20 km/hr, Point of impact at offset -0.3 m)

during crashes are qualitatively different. The riders do not roll up the windscreen towards the roof of the vehicle. The simulations were carried out with the speed of the cycle as 10 km/h with the impact speed of the SUV varying between 5 km/h to 65 km/h. The distance of point of impact of bicycle saddle from the vehicle centre was also varied, and is measured positive in the direction of bicycle motion as shown in Figure 4 below

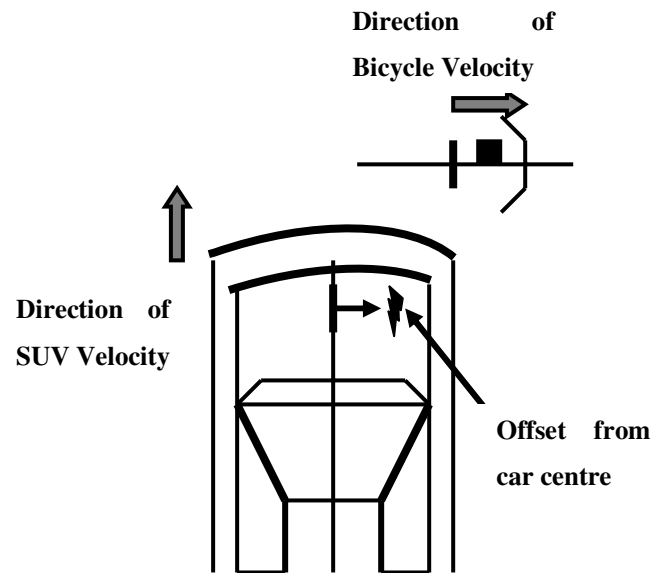


Figure 4 Frontal Side impact orientation

**Variation of throw distances with vehicle speed**

The throw distances for various speeds of the SUV are plotted in Figure 5. The results reinforce the

obvious conclusion that the throwing distance is predicted to increase as the car speed increases. The sudden changes in slopes of these otherwise monotonically varying curves can be associated with significant qualitative change in the kinematics of the bicycle rider at certain points. A qualitative change is for example the cyclist landing on the hood in the centre and instead of tumbling off, he may continue riding on the hood before rolling either in front of the vehicle or on the side. In case, the bicyclist lands in front of the vehicle, the probability of the vehicle running over is high.

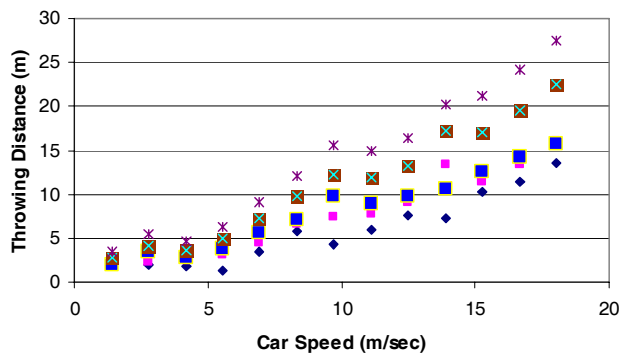


Figure 5: SUV throwing distance variation for frontal side impact

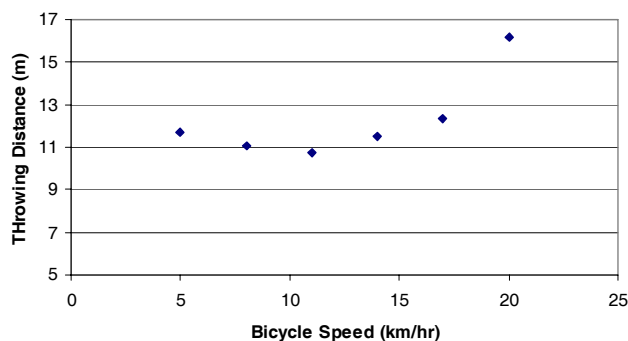


Figure 6 : Variation in throwing distance with bicycle speed at 0m offset

### Variation of throw distances with bicycle speed

The throw distances for different bicycle speeds have been plotted in Figure 6. The variation in throw distances is between 11 and 16 m for bicycle

speed variation between 5 and 25 m/s with the magnitude first decreasing then increasing. This can be attributed to the fact that as bicycle speed decreases, the drag in the direction of the bicycle motion will decrease leading to higher distances, whereas the impulse in the direction of the vehicle will decrease as the vehicle comes in contact for a lesser duration and length thus decreasing the distance.

### Variation of throw distances with vehicle speed in frontal-oblique impacts

The frontal oblique collision occurs when the bicycle front tyre hits the front of the car at an angle as shown in Figure 7. This could occur in real life when one of the vehicles turning into the path of the other vehicle. For the simulation, the angle of approach is taken as  $45^\circ$  and point of impact as car centre. The throw distances for this configuration are plotted against the vehicle speed in Figure 8. The sudden increase in throwing distance at low car speeds is attributed the change in kinematics of the bicyclist. In this situation due to low speeds, the impact does not impart a large momentum but instead the rider travels on top of the hood before rolling down in front of the vehicle. However, we again see the general trend of increase in throw distance with speed. The behavior as seen for the SUV frontal oblique crashes taking place at an angle of  $45^\circ$  is similar to those as seen in frontal crashes. The major difference is that the bicyclists rises to a higher distance and can reach the roof of the vehicle

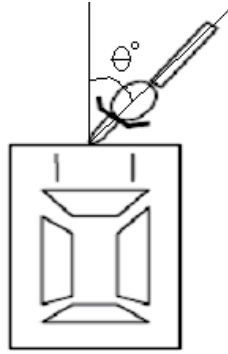


Figure 7: The frontal oblique impact configuration

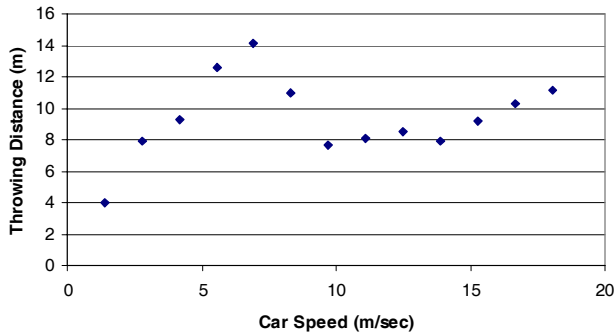


Figure 8: Variation in throwing distance with car speed in frontal oblique crashes (angle =45 degree)

**SIMULATIONS OF BUS-BICYCLE IMPACTS**

Simulations of the a flat-fronted bus front impacting a bicycle were carried out and Figure 9 shows a series of snapshots for the case where the bus moving at a speed of 50 km/hr impacts with a 0.3m offset of the bicycle pedal. The kinematics of impact of the bicyclist with the bus is quite different from that in case of the SUV and the Car. The first impact usually takes place with the leg or the saddle which is followed by the rest of the body impacting the bus front. However, due to the flat shape of the bus, bicyclist is not launched very high in the air, as was the case with SUV and the car. The flatter trajectory leads to lower throw distances.

**Variation of throw distances with vehicle speed**

The throw distances for various speeds of the bus are plotted in Figure 10. The spread in the case of the buses is much less and this can attributed to the fact the bus front is similar along its length and the impacting surface does not vary much with offset. The expected trend of monotonically increasing throw distances is observed. The magnitude of the

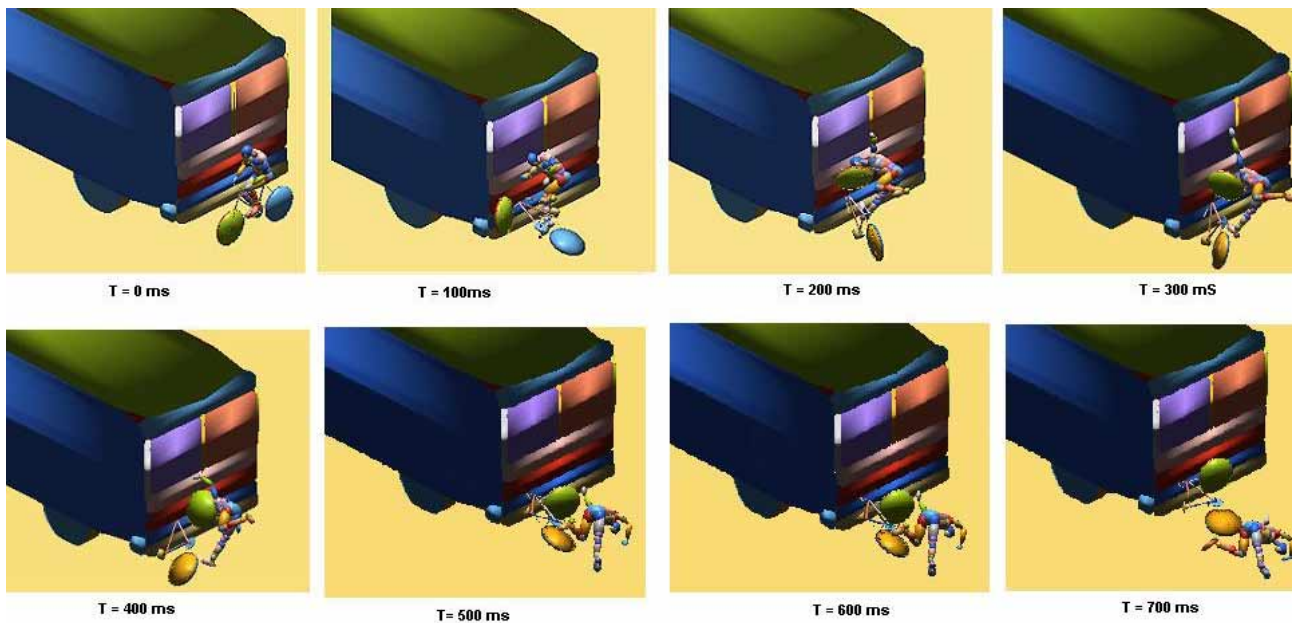


Figure 9: Motion of bicycle rider in frontal-side crash (Bus velocity = 50 km/hr, Point of impact at offset 0.0 m)

throw distances at high speeds is lower than the SUV and the car due to the difference in the crash phenomena as explained earlier. The variation in throwing distance with bicycle speed observed in simulation is not significant.

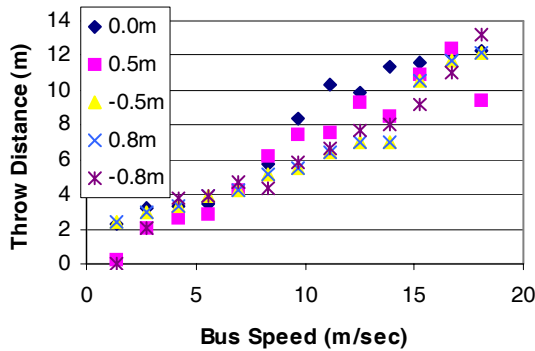


Figure 10 Throw distances in bus-bicycle impacts for different offsets

### THROW DISTANCE REGRESSION CURVES

For all the impact configurations, the nature of the curves obtained for throwing distance is similar to that seen in simulations of small cars. A comparison between the regression curves obtained from the SUV and Car simulations for frontal side impact shows similar behavior in comparison to Otte's accident reconstruction data. These regression curves were obtained by assuming a quadratic fit similar in nature to Otte's curve. The point of intersection in the case of the SUV shifts to the right as shown in Figure 12. For the frontal side impact with the SUV different kinematic situations were observed. At low speeds and negative offsets, the bicyclist lands on top of the bonnet of the vehicle and continues riding before impacting the windscreen and slowly rolling off. In some high velocity cases it was observed that the bicyclist impacts the region of the bonnet closer to the edge, thus bouncing off it without colliding with the windscreen. A completely different kinematic phenomenon is seen in case of bus-

bicycle impacts. In this case, the bicyclist is not pushed higher into the air as he impacts with a flat surface. Hence, throw distances in case of the bus-bicycle impacts are expected to be lower as compared to the SUV and the car. Looking at the coefficients of the regression curves, it can be seen that the quadratic coefficient is much smaller in case of the buses. The throw distances would thus increase slowly at higher speeds. It can be seen that at higher speeds the throw distances for the buses are less than those of the car and the SUV.

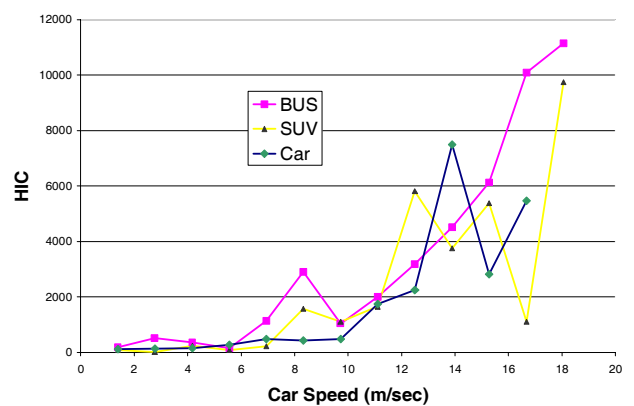


Figure 3: HIC variation with speed of vehicle

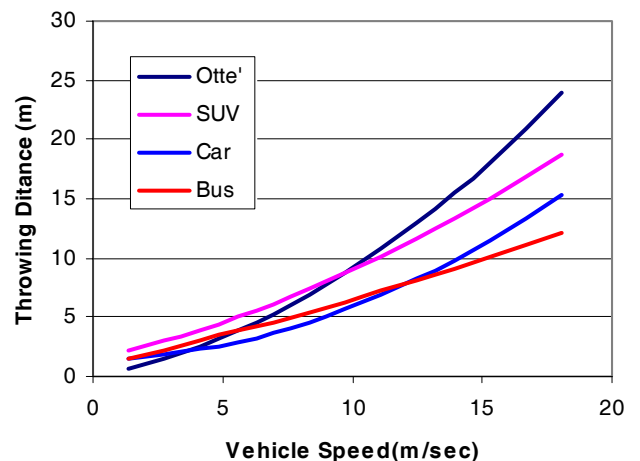


Figure 12: Throwing distance and vehicle type

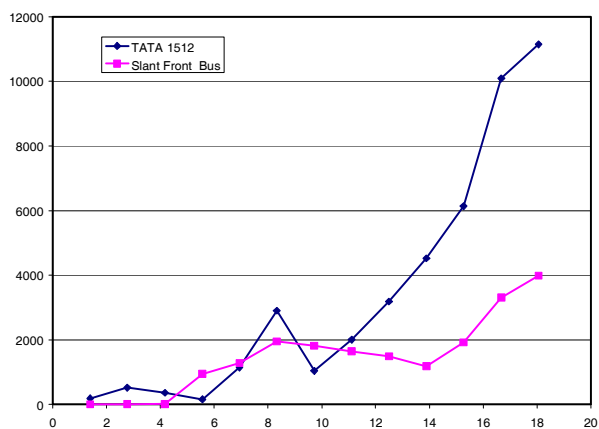
### COMPARISON OF HIC VALUES

The HIC values calculated in MADYMO™ were compared for the three cases of impacts of the bicyclists with the Car, the SUV and the Bus. The

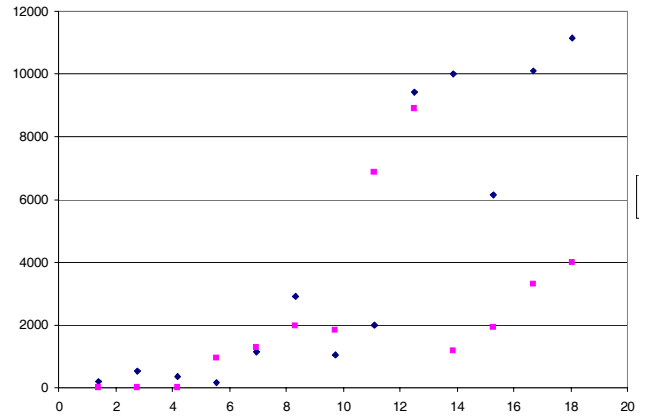
comparison was made for a central impact position in the vehicles and the variation with vehicle speed is shown in Figure 3. Unlike throw distances, the highest HIC values are generally obtained for the bus followed by the SUV. The impact of the head of the vehicle takes place immediately after the first contact in the case of the bus, leading to higher values.

### HIC Values for buses with slanting hood front

The design of the bus was modified and simulations were done with the new design in which the front of the bus has a slanting hood. The HIC values corresponding to the head impact with bus are plotted with the bus speed in Figure 17 (a). The slanted design has a lower HIC value. This is attributed to the fact that in the slanted front design the head collides with hood after it has been decelerated considerably due to the impact of the bus with the lower extremity. Figure 17 (b) below reports the overall HIC value, including the contact with the ground. The rise in HIC values is not monotonic with the speed and has a local maximum at bus velocities of about 12 m/s. At certain vehicle speeds, the bicyclist rotates in the air and impacts the ground in an orientation which leads to higher energy absorbed by the head.



(a)



(b)

Figure 5: Comparison of HIC values with speed of the vehicle

### CONCLUSION

Estimation of throwing distance for OV-bicycle crashes for four types of vehicles with parametric variation in OV speed and the point of impact have been carried out. The change in the nature of impact with change in vehicle front has been highlighted, qualitatively as well as quantitatively. There is qualitative change in the nature of impact with change in vehicle front. The contact point on the vehicle is not significant parameter for impacts with buses with uniform fronts. A flat front design leads to smaller throwing distances of the bicycle rider as the rider is not thrown up. The HIC due to the rider-bus impact is smaller in the slanted front bus. If the rider-ground contact is included, the trend of overall HIC is not so easily predicted. For the slant front bus, as the rider is thrown up, the ground contact could at times be with the head, leading to large HIC values. One of the limitation of this study is that experimental force-deformation relationships were not available for the contact interaction. The confidence in the results would be greater if experimental crash data were available.

## REFERENCES

- [1] Mohan, D.[2004], "The Road Ahead: Traffic Injuries and Fatalities in India", World Health Day, 14th April 2004, New Delhi, pp. 4-5.
- [2] Carsten, O.M.J. et al [1992], Drive Project V1031, An Intelligent Traffic System for Vulnerable Road Users. Institute for Transport Studies, University of Leeds.
- [3] S. Mukherjee, A. Chawla, D. Mohan, S. Chandrawat, V. Agarwal, "Predicting throw distance variations in bicycle crashes", International Journal of Vehicle Safety , Vol. 1, No. 4, 2006
- [4] ISO13232, (1996), Motorcycles – test and analysis procedures for research evaluation of rider crash protective devices fitted to motor cycles, International Organization of Standardization.
- [5] Otte D., Possibilities and Limitation for protective measures for injury reduction of vulnerable road users, IJCrash 2002, Vol 7 No.4, pp. 441-461.
- [6] Burgoyne, C.J. and Dilmaghanian, R. (1993) "Bicycle Wheel as Prestressed Structure." Journal of Engineering Mechanics, 119(3), pp. 439-455.
- [7] Gavin, H.P., "Bicycle Wheel Spoke Patterns and Spoke Fatigue," Journal of Engineering Mechanics, vol. 112, no. 8, (1996) pp. 736-742.
- [8] JENCAP DATA, New Car Assessment Japan, Choosing a safer car, March 2004, Ministry of Land Infra Structure and Transport and National Agency for Automotive Safety and Victim's Aid, Japan.
- [9] Otte, D. [1980], A review of different kinematics forms in two-wheel accidents—their influence on effectiveness of protective measures, SAE STAPP 801314.
- [10] Otte, D. [1989], Injury mechanism and crash kinematics of cyclists in accidents—an analysis of real accidents, SAE STAPP 892425.